GEORG-AUGUST-UNIVERSITÄT
GÖTTINGEN

Novel protein-protein interactions contribute to the regulation of cardiac excitation and Ca^{2+} handling

Dissertation
for the award of the degree
"Doctor rerum naturalium"
of the Georg-August-Universität Göttingen

within the doctoral program *Molecular Medicine (IRTG1816)*
of the Georg-August-University School of Science (GAUSS)

submitted by
Julia Menzel
from Großburgwedel

Göttingen 2020

Thesis Committee

Prof. Dr. Blanche Schwappach-Pignataro	Department of Molecular Biology University Medical Center Göttingen
Prof. Dr. Dörthe Katschinski	Institute for Cardiovascular Physiology, University Medical Center Göttingen
Prof. Dr. Stephan Lehnart	Department of Cardiology and Pneumology, University Medical Center Göttingen

Members of the Examination Board

Reviewer:	Department of Molecular Biology
Prof. Dr. Blanche Schwappach-Pignataro	University Medical Center Göttingen
2nd Reviewer:	Institute for Cardiovascular Physiology,
Prof. Dr. Dörthe Katschinski	University Medical Center Göttingen

Further Members of the Examination Board

Prof. Dr. Stephan Lehnart	Department of Cardiology and Pneumology, University Medical Center Göttingen
Prof. Dr. Michael Shattock	School of Cardiovascular Medicine and Sciences, King's College London
Prof. Dr. Michael Meinecke	Department of Cellular Biochemistry, University Medical Center Göttingen
Prof. Dr. Jürgen Wienands	Institute of Cellular and Molecular Immunology, Georg August University Göttingen

Date of oral examination: 17th July 2020

Affidavit

Herewith I declare that my doctoral thesis entitled “Novel protein-protein interactions contribute to the regulation of cardiac excitation and Ca^{2+} handling” has been written independently and with no other sources and aids than quoted.

Julia Menzel

Göttingen, June 2020

Table of Contents

List of Figures

List of Tables

List of Abbreviations

Abbreviation	Meaning
aa	amino acid sequence
ACM	arrhythmogenic cardiomyopathy
AF	atrial fibrillation
AKAP	A-kinase anchoring protein
AMPA receptor	3-hydroxy-5-methyl-4-isoxazolepropionic acid receptor
AP-2	adaptor protein complex
ARCV	right ventricular arrhythmogenic cardiomyopathy
ATP	adenosine tri-phosphate
BSA	bovine serum albumin
CaMKII	Ca2+-calmodulin-dependent protein kinase II
cAMP	cyclic AMP
Ca_v	voltage-gated calcium channel
COPI	coat protein complex I
DCM	dilated cardiomyopathy
Dlg1	Disk-large homolog 1 protein
Dlg4	Disk-large homolog 4 protein
dNTP	desoxynucleoside triphosphate
DTT	dithiothreitol
E.coli	*Escherichia coli*
EDTA	ethylenediaminetetraacetic acid
EEA1	early endosome antigen 1
EM	energy mix (ATP regeneration system)
ER	endoplasmic reticulum
ERGIC	ER-Golgi intermediated compartment
ET-1	endothelin-1
FCS	fetal bovine serum
FRET	Förster resonance energy transfer
For	forward
GAPDH	glycerinaldehyde-3-phosphate-dehydrogenase
GST	glutathione-S-transferase
G_q-coupled receptor	member of the G-protein family
G_qa-coupled receptor	G_q-receptor alpha subunit
HEK293T	human embryonic kidney 293 cells

HF	heart failure
Hsp20	small heat shock protein 20
I-1	inhibitor-1
IF	immunofluorescence
iPSC	induced pluripotent stem cells
IPTG	isopropyl-beta-D-thiogalactopyranosid
K^+ channels	potassium channel
K_{ATP}	ATP-sensitive potassium channel
K_{ir}	inward rectifier potassium channel
K_v channel	voltage-gated potassium channel
K_{2P}	two-pore domain potassium channel
kDa	kilodalton
K.O.	knock-out
LC-MS	liquid chromatography mass spectrometry
Magi-3	membrane-associated guanylate kinase WW and PDZ domain containing protein 3
MAGUK	membrane-associated guanylate kinase homolog family
MBP	maltose binding protein
MD simulations	molecular dynamic simulations
MS	mass spectrometry
MW	molecular weight
Na/K ATPase	Na^+/K^+ ATPase
NCX	Na^+/Ca^{2+} exchanger
NMR	nuclear magnetic resonance
NRCM	neonatal rat cardiomyocytes
PCR	polymerase chain reaction
pI	isoelectric point
PIP_2	phosphatidylinositol 4,5-bisphosphate
PKA	cAMP-dependent protein kinase A
PKC	protein kinase C
PLN	phospholamban
Pln$^{+/+}$	PLN WT mouse
Pln$^{-/-}$	PLN K.O. mouse model
Pln$^{+/\Delta R14}$	PLN R14del heterozygous mouse model
Pln$^{\Delta R14/\Delta R14}$	PLN R14del homozygous mouse model
PBS	phosphate-buffered saline

PMCA	plasma membrane Ca^{2+} ATPase
PMSF	phenylmethylsulfonyl fluoride
PP1	protein phosphatase 1
$PP1_C$	protein phosphatase 1 catalytic subunit
$PP1G_M$	protein phosphatase 1 regulatory subunit
PPP1R3A	protein phosphatase 1 regulatory subunit 3A
RyR	ryanodine receptor
Rev	reverse
SDS	sodium dodecyl sulfate
SERCA	sacro-(endo)plasmic reticulum Ca^{2+} ATPase
SEM	standard error of the mean
SH_3 domain	Src-homology 3 domain
SPR	surface plasmon resonance
SR	sacroplasmic reticulum
TALK	TWIK-related alkaline sensitive potassium channel
TASK	TWIK-related acid sensitive potassium channel
TBS	tris-buffered saline
TCA	trichloroacetic acid
THIK	Tandem-pore domain halothane inhibited potassium channel
TREK	TWIK-related potassium channel
TRESK	TWIK-related spinal cord potassium channel
TWIK	Two-pore domain weakly inward rectifying potassium channel
WGA	wheat germ agglutinin
WT	wild type

Abstract

Cardiac function is defined by the process of excitation and contraction. During this process, the electrical excitation of the surface membrane is coupled to Ca^{2+}-ion release at the sarcoplasmic reticulum, resulting in contraction. The small membrane-protein phospholamban (PLN) is an essential regulator of cardiac contraction by inhibiting the SR Ca^{2+}-ATPase (SERCA), which modulates the reuptake of Ca^{2+}-ions at the SR and ultimately results in cardiac relaxation. The inhibitory effect of PLN on SERCA is disrupted upon its phosphorylation by two different kinases. Beta-adrenergic stimulation activates protein kinase A (PKA), which phosphorylates PLN at S16, meanwhile increased intracellular Ca^{2+} levels stimulate Ca^{2+}-calmodulin-dependent protein kinase II (CaMKII) phosphorylation of PLN at T17, causing a longer-lasting activation of SERCA.

This study focused on the identification and characterization of novel protein-protein interactions involved in the regulation of cardiac excitation and Ca^{2+} metabolism.

Pull-down approaches from rodent and human cardiac membranes, proximity labelling in live cardiac myocytes and immunoprecipitation experiments identified the phospho-adaptor protein 14-3-3 as a novel PLN interaction partner. Pull-down experiments with monomeric or pentameric PLN demonstrated that 14-3-3 preferentially binds phosphorylated PLN pentamers. The potential 14-3-3 binding motif in PLN was further dissected with recombinant binding assays and surface plasmon resonance measurements revealing that phosphorylated S16 or T17 transform PLN into a 14-3-3 target with different binding affinity sites. In line, molecular dynamic simulations uncovered different placement of PLN, phosphorylated at either S16 or T17, in the 14-3-3 binding groove resulting in different binding energies, favoring phosphorylated T17 PLN. Functionally, upon beta-adrenergic stimulation of cardiac myocytes PKA activity was stimulated and endogenous 14-3-3 was found to be enriched in these membrane fractions. Recombinant dephosphorylation assays showed that 14-3-3 bound to phosphorylated PLN protects PLN from rapid dephosphorylation. In line, increased SERCA activity was observed upon PKA stimulation in the presence of 14-3-3 in cardiomyocytes during patch clamp analysis. The observation that CaMKII-phosphorylated PLN at T17 results in a high affinity binding of 14-3-3 suggests that 14-3-3 may regulate the less dynamic pool of PLN and raises the question of whether 14-3-3 binding is involved in the regulation of PLN disease mutations (R14del, R9C), for which PKA phosphorylation is abolished. Recombinant binding assays confirmed that 14-3-3 could still interact with PLN R9C or R14del mutants, which are associated with dilated cardiomyopathy and heart failure.

Additionally, 14-3-3 together with the coat complex COPI are well characterized regulators of the potassium ion channel family TASK, responsible for phosphorylation dependent

trafficking and cell surface expression. TASK-1 is strongly expressed in the atrium, involved in setting the resting membrane potential and associated with atrial fibrillation. Little is known about regulation and trafficking of these channels in the heart. A mass spectrometry approach and recombinant binding assays performed from cardiac membranes identified the PDZ domain containing proteins Dlg1 and Dlg4 as direct TASK-1 interactors. Further analysis of the PDZ binding site in TASK-1 confirmed the existence of a previously hypothesized PDZ-binding motif, which overlaps with the well characterized 14-3-3 binding motif located at the distal C-terminus of TASK-1. This finding suggests a phosphorylation dependent regulation of TASK-1 via 14-3-3 and PDZ domain containing proteins at the plasma membrane, yielding insight into trafficking of TASK-1 beyond the secretory pathway.

Taken together, in this study 14-3-3 was identified as a novel interaction partner of PLN. It was further demonstrated that 14-3-3 binding to PLN results in a stabilization of phosphorylated pentamers and prolonged SERCA activity, indicating a novel mechanism of PLN regulation dependent on cardiac kinase activity. In addition, the PDZ domain containing protein Dlg1 was identified as a direct interaction partner of TASK-1 in cardiac tissue. These findings expand our knowledge about the interactome and regulation of the cardiac protein PLN and the ion-channel TASK-1 underlining the importance of regulatory proteins such as 14-3-3 or Dlg1 in cellular processes like Ca^{2+} handling or protein trafficking.

1 Chapter I: Introduction

1.1 Calcium regulation by excitation-contraction coupling mechanism in the heart

Cardiac function is regulated on a beat-to-beat basis by the sympathetic and parasympathetic nervous system. The parasympathetic system lowers cardiac output by decreasing the heart rate through the neurotransmitter acetylcholine (Najafi et al., 2016). The sympathetic activation releases the catecholamines adrenaline and noradrenaline responsible for increased cardiac output (Najafi et al., 2016).

The beat-to-beat regulation allows adaption of the heart rate and blood flow based on the demands of the organism. To fulfill the function of the heart as a pump, cardiomyocytes have to rhythmically contract in a coordinated or syncytium manner (Thomas et al., 2018). All process which are happening between the electrical stimulation until the contraction of cardiomyocytes is summarized under excitation-contraction coupling (Pfeiffer et al., 2014). An electrical stimulus, in form of a cardiac action potential, travels through voltage gated ion channels from the atria to the ventricle inducing cardiac contraction. The voltage gated ion channels open due to the stimulus and positive ions flow into the cardiomyocyte leading to depolarization and muscle contraction (Bartos et al., 2015).

To achieve a fast electromechanical coupling, cardiomyocytes have structural features. The sarcolemma forms the T-tubules system that allows fast electrical excitation through the cell (Walker & Spinale, 1999). Moreover, the amount of voltage-gated calcium channels (Ca_v) is high in the T-tubule (Shaw & Colecraft, 2013), which enables fast influx of Ca^{2+} ions into the cardiomyocyte after depolarization of the sarcolemma. During the plateau phase of the cardiac action potential, the $Ca_v1.2$ channels transport Ca^{2+} from the extracellular space in the cardiomyocyte (Rougier & Abriel, 2016) (Figure 1). The intracellular Ca^{2+} stores are located in each T-tubules as the sarcoplasmic reticulum (SR) (Figure 1). The rising intracellular Ca^{2+} concentration activates the ryanodine receptor (RyR) in the SR which releases large amounts of Ca^{2+} ions from the SR (Laver, 2007). The cytosolic Ca^{2+} concentration increases from 500 nM to 1 µM upon excitation (Fearnley et al., 2011). As a consequence the intracellular Ca^{2+} ions bind to troponin C which allows muscle contraction in the thin filament by actin and myosin interaction (Gomes et al., 2002).

After contraction, relaxation of cardiomyocytes is regulated by reducing the intracellular Ca^{2+} concentration (Eisner et al., 2017). Lowering the intracellular Ca^{2+} concentration is mainly performed by a combined activity of SERCA2a, plasma membrane Ca^{2+}-ATPases and Na^+/Ca^{2+} exchanger (NCX) (Calderón et al., 2014). In humans, SERCA transports more than 70% of the cytosolic Ca^{2+} back to the SR. (MacLennan & Kranias., 2003).

Thereby, SERCA is mainly responsible to mediate cardiomyocyte relaxation after a contraction (MacLennan & Kranias 2003). SERCA is inserted into the SR membrane and regulated by a small protein called phospholamban (PLN) (MacLennan & Kranias 2003) (Figure 1). PLN is the reversible inhibitor of SERCA, phosphorylation disrupts the PLN/SERCA interaction and relives the inhibitory effect resulting in enhanced cardiomyocyte relaxation (Chu et al., 2000).

Phosphorylation of PLN is regulated by the beta-adrenergic signaling pathway in parallel with the excitation-contraction pathway (Figure 1). Beta-agonists, such as catecholamines, bind a beta-adrenergic receptor which activates a G_s protein-coupled signal cascade resulting in an activated adenylate cyclase and increased intracellular cyclic AMP (cAMP) levels in cardiomyocytes. High cellular cAMP levels activate the cAMP-dependent protein kinase A (PKA) which phosphorylates several cardiac proteins including PLN (MacLennan & Kranias 2003) (Figure 1). PKA also phosphorylates phosphatases such as protein phosphates 1 (PP1) which is known to dephosphorylate PLN (Mattiazzi et al., 2005; Vafiadaki et al., 2013). Upon PKA phosphorylation PP1 is inhibited (Mattiazzi et al., 2005). PKA phosphorylation of PLN and PP1 at the time avoids fast dephosphorylation of PLN and allows SERCA to pump Ca^{2+} back into the SR. Lowered Ca^{2+} levels, due to the function of SERCA, reduces cellular cAMP levels which consequently release PP1 and dephosphorylates PLN leading to the inhibition of SERCA until a new cycle starts (MacLennan & Kranias 2003). The cardiac excitation-contraction coupling mechanism is an excellent example for how cardiac signaling pathways work together (MacLennan & Kranias 2003).

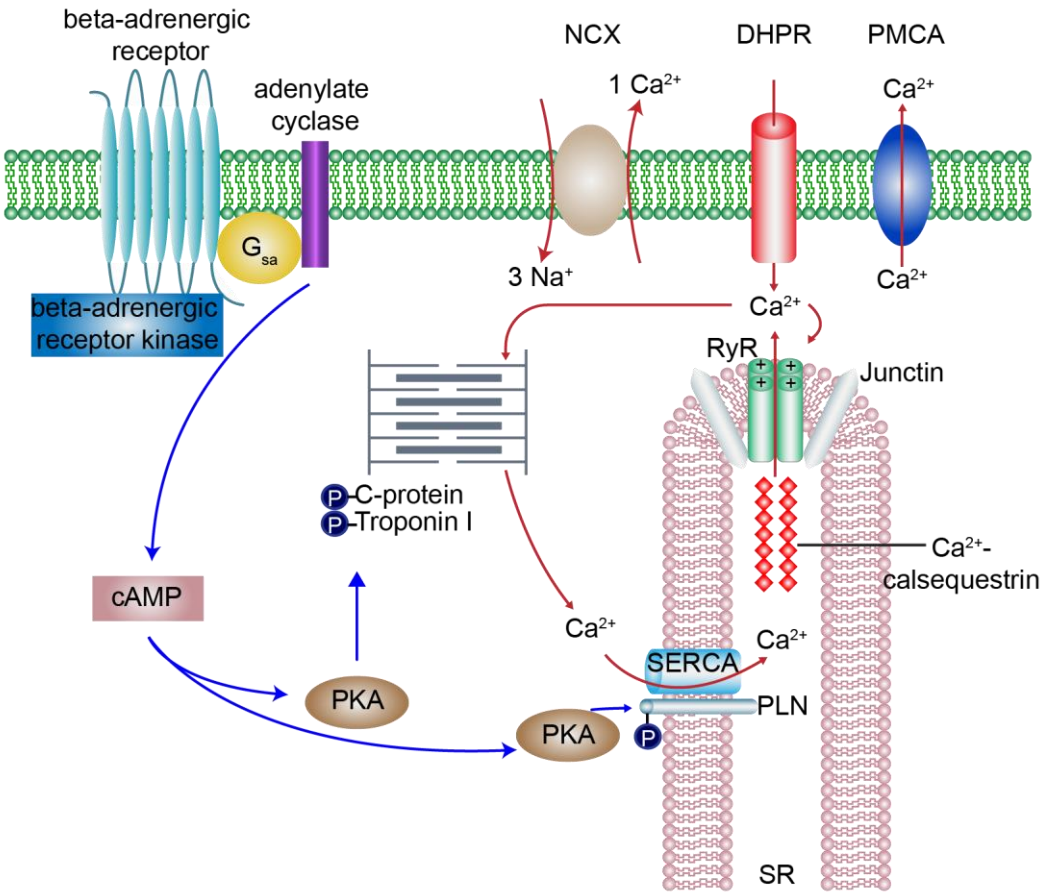

Figure 1. The cardiac-excitation-contraction coupling scheme.

Cardiomyocyte contraction and heart function is achieved by an electrical stimulus which activates voltage regulated Ca^{2+} channels (DHPR) leading to an increased cellular Ca^{2+} concentration. The Ca^{2+} ions activate ryanodine receptor (RyR) which releases large amounts of Ca^{2+} from the intracellular Ca^{2+} storages of the SR. The Ca^{2+} ions bind the myofilament and induce cardiac contraction. Relaxation of the cardiomyocyte requires removal of the Ca^{2+} ions out of the cytosol. This is done by SERCA2a, plasma membrane Ca2+ ATPase (PMCA) and the Na^{+}/Ca^{2+} transporter (NCX). Most of the Ca^{2+} is transported by SERCA which is inhibited by PLN, but the inhibition is relieved after phosphorylation of PLN. PLN is phosphorylated by cAMP or Ca^{2+} dependent kinases which are regulated over receptor mediated signal transduction. Figure adapted from (MacLennan & Kranias 2003).

1.2 Phospholamban

PLN is a small tail-anchored protein which is located in the SR. PLN is the reversible inhibitor of the cardiac isoform of SERCA and therefore important for intracellular Ca^{2+} handling and cardiac contraction (James et al., 1989). PLN is abundantly expressed in cardiac muscle and in reduced amounts also in smooth and slow skeletal muscle. In comparison to the cardiac expression, PLN is 10-50-fold less abundant in the skeletal

muscle (McTiernan et al., 1999). PLN is regulated by oligomerization and phosphorylation mediated by different kinases.

1.2.1 Structure of PLN

The PLN monomer consists of 52 amino acids (aa) which forms 4 dynamic domains: Ia (1-16 aa), the loop (17-22 aa), Ib (23-30 aa) and II (31-52 aa) (Figure 2) (Traaseth et al., 2007). The 4 dynamic regions form 3 structural and functional domains: the cytoplasmic helix Ia (1-16 aa) responsible for PLN phosphorylation and regulation, the loop (17-22 aa) which connects the cytoplasmic with the transmembrane helix, and the transmembrane helix including domain Ib and II (23-52 aa) (Figure 2) (Zamoon et al., 2003).

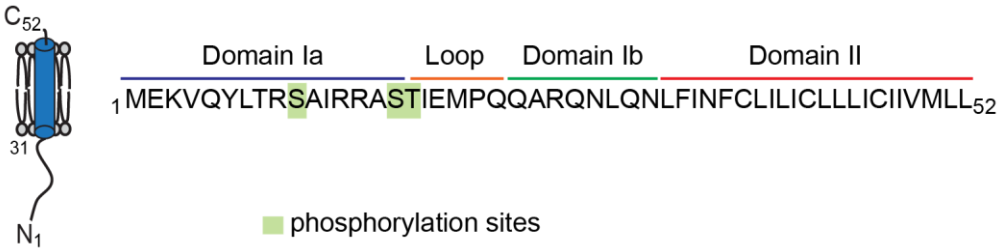

Figure 2. Schematic representation of PLN.

The 52 aa of PLN are organized in 4 dynamic domains. Domain Ia (1-16 aa) is the cytoplasmic helix which is connected via the loop (17-22 aa) with the transmembrane helix consisting of domain Ib (23-30 aa) and domain II (31-52aa).

The cytoplasmic helix domain Ia is a rigid, amphipathic alpha-helix that contains hydrophobic amino acids which allow insertion into the SR membrane facing the cytoplasm (Figure 3) (Kimura et al., 1997; Simmerman et al., 1996). The positively charged arginine residues (R9, R13, R14) bind to the negatively charged lipid head groups in the membrane and stabilize the insertion of the Ia helix (Ablorh & Thomas, 2015). Domain Ia contains a serine 16 (S16) phosphorylation site which is phosphorylated by PKA, S16 phosphorylation disrupts the PLN/SERCA interaction resulting in SERCA activation (Coyler, 1998). Phosphorylation of PLN shifts the equilibrium of domain Ia from the T-state to the R-state (Karim et al., 2006; Metcalfe et al., 2005). The structural order-to-disorder (T- to R-state) shift unwinds the cytoplasmic helix domain Ia and loosens the hydrophobic and electrostatic interactions with the SR membrane (Figure 3) (Karim et al., 2006). This was shown with nuclear magnetic resonance (NMR) residual dipolar coupling indicating a reduced number of contacts between the SR membrane and PLN cytoplasmic domain helix Ia in the disordered R-state (De Simone et al., 2013). Altogether, the cytosolic domain Ia can be present in two different conformational states: The rigid L-shaped T-state in which the cytosolic domain is helical and membrane bound, and the R-state in which the

cytosolic domain is partially unfolded and extended (Gustavsson et al., 2013). Folding and unfolding of the cytosolic domain of PLN and therefore the transition from the T-state to the R-state and vice versa happens relatively fast in the µs-ms range (Traaseth & Veglia, 2010).

The loop region in PLN (17-22 aa) connects the cytoplasmic loop with the transmembrane region and consists mostly of hydrophobic aa which allow the localization over the membrane surface (Ablorh & Thomas, 2015). The loop is the only region in PLN which is permanently exposed to the cytoplasm. The second phosphorylation site in PLN is located in the loop region and a Ca^{2+}-calmodulin-dependent protein kinase II (CaMKII) target site. Phosphorylation of the threonine 17 (T17) residue also disrupts the PLN/SERCA interaction (Mundiña-Weilenmann et al., 1996). After phosphorylation of either S16 or T17 in PLN, the loop extends and stabilizes the shift to the dynamic, unstructured R-state (Ha et al., 2012) (Figure 3).

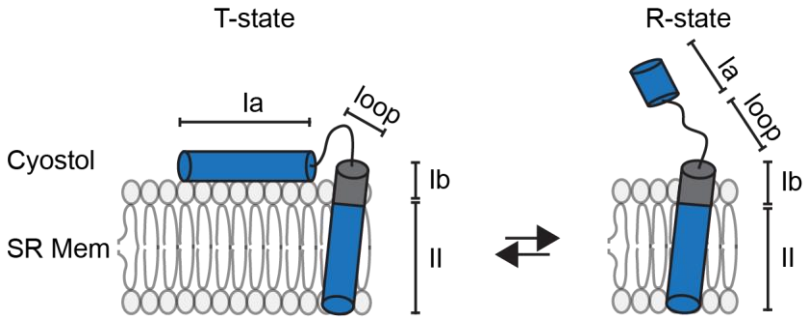

Figure 3. PLN exists in two different structural states.

The rigid T-state where domain Ia is helical and attached to the membrane or the extended and dynamic R-state, where domain Ia partially unfolds and loses contact to the SR membrane. In the T-state, PLN inhibits SERCA, but not in the R-state. The shift from T- to R-state is initiated by phosphorylation. Figure adapted from (Ablorh et al., 2015).

The transmembrane region of PLN consists of two domains Ib and II, which are both hydrophobic alpha-helices aligned on top of each other (Yu & Lorigan, 2014). The transmembrane region is important for PLN oligomerization and the interaction between PLN and SERCA (Ablorh & Thomas, 2015). The PLN transmembrane helix was found to be sufficient to fully inhibit SERCA (Kimura et al., 1997; Metcalfe et al., 2004). S16 phosphorylation in the cytosolic domain Ia shifts the PLN equilibrium towards the R-state also causing a structural change in domain Ib from an alpha-helix to an uncoiled structure which loses the alignment with domain II (Traaseth et al., 2006). This changes in the dynamics of the transmembrane domain Ib result in a decreased inhibitory effect of PLN on SERCA (Gustavsson et al., 2011; Karim et al., 2006; Traaseth et al., 2006).

Mutagenesis studies showed that the residues L31, L42 and L52 are essential for the physical PLN/SERCA interaction (Afara et al., 2006). These residues are located at one site of the domain II helix, creating a PLN/SERCA interface (Afara et al., 2006). Molecular modeling shows that the PLN residues P35, I38, I48 and V49 form a hydrophobic pocket near the SERCA N-terminus and stabilize the PLN SERCA interaction (Afara et al., 2006). The opposite face of the domain II helix is required for PLN oligomerization and pentamer formation. The residues L37, I40, L44, I47 and L51 form a leucine/isoleucine zipper which is required for pentamer formation (Simmerman et al., 1996) and stabilized by disulfide bridges formed between C36, C41 and C46 residues (Karim et al., 1998). In the PLN pentamer, the leucine/isoleucine zipper symmetrically pack and stabilize the pentamer conformation (Cornea et al., 2000; Simmerman et al., 1996). The PLN pentamer is SDS resistant and persists in a 1% SDS-PAGE (Simmerman et al., 1996). Detergent or gentle heating dissolves the PLN pentamer into the five monomers (Peuch et al., 1979; Wegener et al., 1986). On average, most PLN monomers and pentamers exist in the inhibitory T-state, the R-state population is around 16-20% in the absence of SERCA (Gustavsson et al., 2011).

1.2.2 Phosphorylation of PLN

PLN is the reversible inhibitor of SERCA2a in cardiomyocytes (Tada et al., 1975) and regulated by phosphorylation. PLN has three different phosphorylation sites present in the cytosolic Ia domain: S16 is a PKA target site, T17 is phosphorylated by CaMKII and serine 10 (S10) is a target site of protein kinase C (PKC) (Coyler, 1998). However, S10 phosphorylation by PKC was abolished *in-vivo* and no physiological effect could be identified (Edes & Kranias, 1990). Phosphorylation of S16 or T17 via beta-adrenergic stimulation resulted in positive inotropic and cardiac relaxant effects due to increased SERCA activity and Ca^{2+} uptake in the SR (Mattiazzi & Kranias, 2014). The two different phosphorylation sites in PLN, which are regulated via two different kinases, offer several possibilities of PLN regulation.

During beta-adrenergic stimulation, both S16 and T17 are phosphorylated simultaneously (Bilezikjian et al., 1981; Davis et al., 1990). Phosphorylation at T17 required increased intracellular cAMP levels to activate CaMKII kinase *in-vivo* (Kuschel et al., 1999; Lindemann et al., 1983). A study with transgenic mice expressing PLN WT, PLN S16A and PLN T17A in a PLN knockout mice background showed that phosphorylation at S16 in PLN is necessary to phosphorylate T17 (Luo et al., 1998). As a follow up, it was demonstrated that S16 can be phosphorylated without T17 phosphorylation *in vivo* and that phosphorylation of S16 alone still leads to maximal cardiac output upon beta-adrenergic stimulation (Chu et al., 2000). In addition, it was found that phosphorylation of

T17 requires higher levels of beta-adrenergic stimulation than S16. At low beta-adrenergic stimulation, just S16 is phosphorylated because the intracellular Ca^{2+} levels are not sufficient to activate CaMKII and phosphorylate T17 (Said et al., 2002). This implies that phosphorylation of S16 is also happening before T17 phosphorylation *in-vivo*. However, higher beta-adrenergic stimulation (>10 nM isoprenaline) results in a 1:1 ratio of S16 and T17 phosphorylation in PLN (Mundiña-Weilenmann et al., 1996).

In vitro S16 and T17 in PLN can be phosphorylated independently from each other (Bilezikjian et al., 1981). Under high Ca^{2+} levels and suppression of phosphatase activity, it was shown that T17 can be phosphorylated by CaMKII without prior S16 phosphorylation or beta-adrenergic stimulation (Mundiña-Weilenmann et al., 1996). This demonstrated that T17 phosphorylation mediated by CaMKII plays an important role for SERCA regulation under increased cardiac stimulation frequencies or elevated intracellular Ca^{2+} levels induced due to stress or pathophysiology conditions like ischemia-reperfusion injury or acidosis (Zhao et al., 2004; Mattiazzi, et al., 2005).

Dephosphorylation of PLN is as important as phosphorylation regarding PLN regulation. PP1 was identified to be responsible for dephosphorylation of PLN at both phosphorylation sites S16 and T17 (MacDougall et al., 1991). PP1 is a serine/threonine phosphatase which consists of two subunits, a catalytic subunit $PP1_C$ and a regulatory subunit $PP1G_M$ (Mattiazzi et al., 2005). The $PP1G_M$ subunit is responsible for the correct localization of the catalytic subunit $PP1_C$ to the SR membrane and the target protein. PKA also phosphorylates the $PP1G_M$ subunit at Ser67 upon beta-adrenergic signaling resulting in dissociation of the $PP1_C$ subunit (Mattiazzi et al., 2005). As a consequence, $PP1_C$ binds with high affinity to the regulatory proteins inhibitor 1 (I-1) and the small heat shock protein (HSP20) followed by inhibition (Vafiadaki et al., 2013) until dephosphorylation of PP1. Overall, PKA phosphorylation ensures PLN phosphorylation by simultaneous phosphorylation and inhibition of PP1 (Mattiazzi et al., 2005; Vafiadaki et al., 2013). However, in contrast to PKA, CaMKII kinase cannot phosphorylate PP1 after activation (Mattiazzi & Kranias, 2014).

1.2.3 Function of PLN monomers and pentamers

PLN exists in two different physiological conformations in the heart, the monomer and the pentamer which are in a dynamic equilibrium (Traaseth et al., 2008).

The SERCA interaction site in the PLN transmembrane domain is located on the helical face which is not required for pentamer formation, therefore pentameric PLN can theoretically interact with SERCA (Kimura et al., 1997). Whether pentameric PLN inhibits SERCA was analysed with an alanine-scanning mutagenesis and further aa substitution studies revealing that pentameric PLN has a very reduced inhibitory effect on SERCA

(Cornea et al., 2000; Kimura et al., 1996, Kimura et al., 1997). On the basis of these results, the general assumption, that PLN monomers act as an inhibitor of SERCA and the pentamers serve as a storage, were developed (Becucci et al., 2009; Kimura et al., 1997; MacLennan & Kranias 2003).

It was also found that upon beta-adrenergic stimulation and subsequent phosphorylation of PLN, the inhibitory effect on SERCA was relieved (MacLennan et al., 1998). Furthermore, it was suggested that after phosphorylation the PLN monomers are stored in the pentameric form until more PLN monomers are required (Kimura et al., 1997). Radioactive labeled PLN shifted the isoelectric point (pI) after PKA phosphorylation from basic (pI = 10) to neutral (pI = 6.7) in isoelectric focusing gels, indicating an increased size of the PLN protein after phosphorylation (Jones et al., 1985). Later the number of contacts of recombinant PLN in a phospholipid bilayer was measured with electron spin resonance experiments before and after PKA phosphorylation. The number of contacts of PLN with the lipid bilayer decreased after phosphorylation, supporting a theory that phosphorylation leads to PLN pentamer formation (Cornea et al., 1997).

However, Wittmann et al found with phosphorylation stimulation experiments that the pentamer can be directly phosphorylated by PKA even with a higher affinity for the pentamer. Phosphorylation patterns of different monomer/pentamer ratios in mammalian cells showed that PLN pentamers delay monomer phosphorylation. From this, the authors postulate a model where PLN pentamers are first phosphorylated after beta-adrenergic phosphorylation which prolongs the PLN monomer SERCA interaction and therefore the inhibitory effect of PLN on SERCA (Wittmann et al., 2015).

Despite the evidence that pentameric PLN has a very reduced effect on SERCA inhibition (Cornea et al., 2000; Kimura et al., 1996, Kimura et al., 1997), Wittmann et al pulled down both PLN monomers and pentamers in co-immunoprecipitation experiments with SERCA (Wittmann et al., 2015). Already in 1998, it was shown with transgenic mice models expressing different conformational states of PLN, that the PLN pentamers play an important role for cardiac contraction *in vivo* (Chu et al., 1998). In 2005 a first model for the interaction of PLN pentamers with SERCA was suggested (Oxenoid & Chou, 2005). With NMR analysis, it was shown that the aa which are involved in the SERCA interaction are exposed on the transmembrane segment opposite to the aa which are required for pentamer formation. A model was suggested where pentameric PLN binds a lateral binding groove in SERCA (Oxenoid & Chou, 2005). Recently, 2-D crystals show first evidence of an interaction between a PLN oligomer and the SERCA transmembrane segment M3 (Glaves et al., 2019). The binding site of PLN pentamers in SERCA is far away from the binding groove of monomeric PLN. Moreover, it was shown that the SERCA binding groove of monomeric PLN containing helix M2, M4, M6 and M9 is flexible, while the binding site

of pentameric PLN helix M3 is more rigid. The M3 helix is a stable interaction site for pentameric PLN, allowing additional SERCA regulation (Glaves et al., 2011). The physiological function of this interaction remains unknown.

1.2.4 The PLN and SERCA2a interaction

The PLN and SERCA interaction site in both proteins were analysed with mutagenesis and cross-linking experiments. It revealed that transmembrane domain II of monomeric PLN interacts with helices M2, M4, M6 and M9 of the transmembrane domain of SERCA which form a hydrophobic groove (Figure 4). The interaction is additionally stabilized by interactions of K3 and I18 of PLN and a stretch of K397 to V402 in SERCA (Figure 4) (Kimura et al., 1997; Toyofuku et al., 1994). The Ca^{2+} binding site in SERCA is on the opposite face of helix M6 (Asahi et al., 2001). The cytoplasmic domain of PLN was completely unresolved in the latest X-ray structure of PLN and SERCA (Akin et al., 2013). Interaction of the transmembrane domain of PLN to the hydrophobic cleft in SERCA occurs only in the Ca^{2+}-free E2 conformation preventing closing of the cleft during the transition of E2 to the high affinity E1 conformation (Vandecaetsbeek et al., 2011).

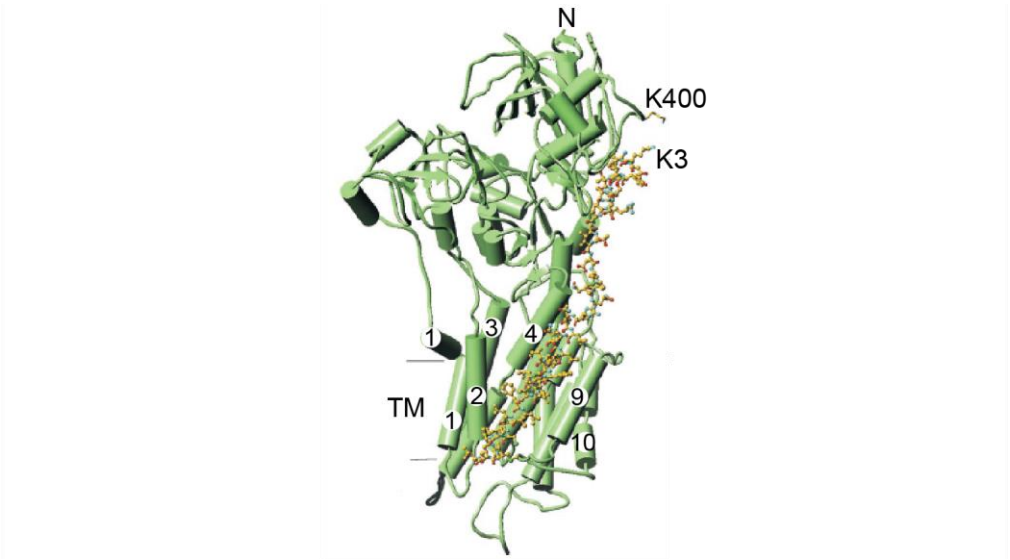

Figure 4. PLN interaction sites in the crystal structure of SERCA1a.

The transmembrane domain II of PLN binds to transmembrane domain M6 in SERCA in a groove between helices M2 and M9. The loop of PLN unfolds and stretches toward the N-terminus of SERCA and bind with the K3 residue the SERCA residues K397-V402. PLN is depicted as cyan sticks. Figure adapted from (MacLennan & Kranias 2003).

Different interaction models currently exist regarding the PLN/SERCA2a interaction. A dissociation model was postulated assuming that after phosphorylation or under high cellular Ca^{2+} concentrations the PLN monomer dissociates from SERCA which disrupts

the inhibitory effect on SERCA (Figure 5). After dissociation of PLN from SERCA, the PLN monomers are stored as pentamers. The dissociation model was developed based on cross-linking and co-immunoprecipitation experiments between SERCA and PLN (Chen et al., 2003; James et al., 1989).

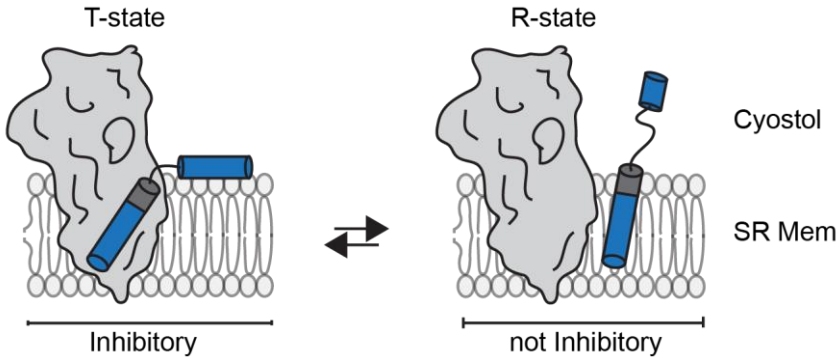

Figure 5. PLN/SERCA interaction in the dissociation model.

The PLN monomer bound to SERCA inhibits SERCA. After phosphorylation PLN dissociates from SERCA consequently SERCA is relieved from inhibition and transport Ca^{2+} ions.

The dissociation model is challenged by the subunit-model, which suggests a structural rearrangement of PLN after phosphorylation without dissociation of the PLN/SERCA construct (Dong & Thomas, 2014). Gustavsson et al identified an additional conformation of PLN called the B-state, which means bound to SERCA but not inhibitory (Gustavsson et al., 2013). The subunit model proposes a structural rearrangement of PLN after phosphorylation of PLN and does not induce dissociation of the PLN/SERCA construct (Dong & Thomas, 2014). Phosphorylation shifts the inhibitory T-state of PLN to the more flexible and non-inhibitory R-state (Gustavsson et al., 2013). In the T-state confirmation, the cytosolic domain Ia of PLN is attached to the SR membrane, phosphorylation leads to partial unfolding of the cytosolic domain which binds to the cytosolic region of SERCA (Gustavsson et al., 2013). This rearrangement of PLN in the B-state disrupts the inhibitory effect on SERCA without dissociation (Figure 6) (Gustavsson et al., 2013).

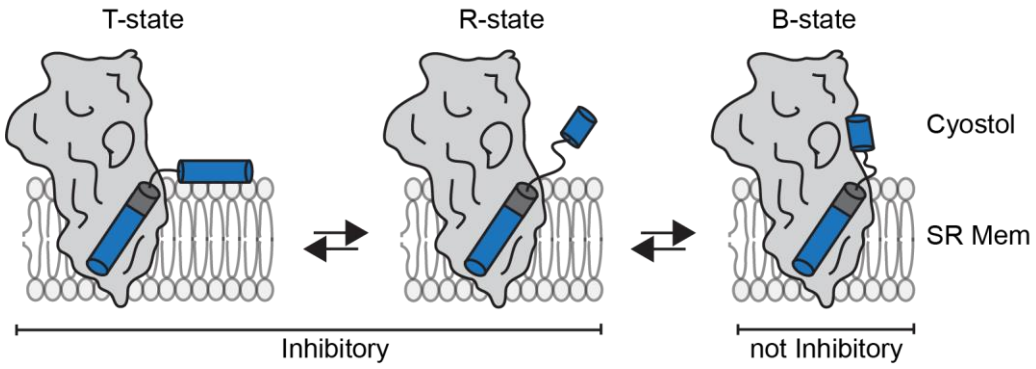

Figure 6. PLN/SERCA interaction in the subunit model.

The subunit model postulate that the inhibitory effect of PLN on SERCA depends on the confirmation of PLN and not on PLN SERCA binding. Upon phosphorylation, the cytosolic domain of PLN is partially unfolded and PLN is converted towards the R-state. In this conformation, the cytosolic domain of PLN binds the cytosolic region of SERCA and shifts the transmembrane domain of PLN and therefore loosens the SERCA/PLN interaction without dissociation. Figure adapted from (Gustavsson et al., 2013).

1.2.5 Pathophysiological relevance of PLN in the human heart

PLN is a direct inhibitor of SERCA and an important modulator of cardiac diastolic function. Consequently, decreased expression of SERCA and PLN at the RNA and protein levels were associated with cardiac dysfunction in animal models (McTiernan et al., 1999). A couple of PLN mutations in humans were identified and are usually single aa substitutions or deletions in the cytosolic domain of PLN as R9C, R9L and R14del (Young et al., 2015). The L39Stop mutation is the only human PLN mutation identified in the transmembrane domain of PLN (Haghighi et al., 2003). All mentioned mutations in the PLN gene are associated with dilated cardiomyopathy (DCM), right ventricular arrhythmogenic cardiomyopathy (ARVC) and heart failure (HF) (Young et al., 2015). DCM is associated with left ventricular contractile dysfunction due to an enlarged ventricle causing a progression to HF (van der Zwaag et al., 2012). ARVC is characterized by ventricular arrhythmias, predominantly from right ventricle leading to HF and sudden cardiac death (van der Zwaag et al., 2012). ARVC is the most-well known sub-form of arrhythmogenic cardiomyopathy (ACM) (van Opbergen et al., 2017).

The R14del mutation was identified in many patients with DCM or ACM in the Netherlands and could be traced back to originating from the north of Friesland (van der Zwaag et al., 2013). The R14del mutation disrupts the PKA binding site in PLN and therefore avoids S16 phosphorylation (Haghighi et al., 2006; te Rijdt et al., 2016). Interestingly, Haghighi et al showed that PLN R14del is a super-inhibitor of SERCA when expressed together with healthy WT PLN in mammalian cells (Haghighi et al., 2006). Later, it was also shown that

just PLN R14del expression in mammalian cells leads to mislocalisation of R14del PLN to the plasma membrane (Haghighi et al., 2012). So far just R14del heterozygous patients were identified, showing super-inhibition of SERCA which alters Ca^{2+} transport and leads to ventricular remodeling over time as well as the development of HF (Hof et al., 2019). In line, it was also shown that the R14del mutation destabilizes PLN pentamers subsequently increasing the amount of PLN R14del monomers and enhancing the super-inhibitory effect of the R14del PLN mutation (van Opbergen et al., 2017).

The L39Stop mutation was identified in heterozygous patients resulting in hypertrophy without reduced contractile performance and in homozygous patients resulting in lethal DCM (Haghighi et al., 2003; Landstrom et al., 2011). The functional consequence of the L39Stop mutation was analysed by co-expression experiments of PLN Leu39Stop and SERCA in mammalian cells resulting in no SERCA inhibition and a loss of function mutation in a homozygous background (Haghighi et al., 2003). To mimic a heterozygous model PLN, WT and PLN Leu39Stop were co-expressed with SERCA showing SERCA inhibition (Haghighi et al., 2003). Moreover, PLN carrying the L39Stop mutation was nearly absent in Western blotting and immunofluorescence (IF) experiments in mammalian cells indicating that the L39Stop mutation is either misrouted, highly unstable or fast degraded (Haghighi et al., 2003). The identification of humans carrying a homozygous L39Stopp mutation is the first natural loss-of-function PLN mutation in humans (PLN null) resulting in lethal DCM with early death (Haghighi et al., 2003). Strikingly, these findings are in strong contrast to findings of PLN ablation in mice resulting in increased cardiac function without development of HF (Hoit et al., 1995; Luo et al., 1994).

These surprising results can be explained due to differences in cardiac physiology in human and mice (Haghighi et al., 2003). Mice show a faster contraction, different Ca^{2+} transport strategies into the SR (SERCA pumps 92% of Ca^{2+} to the SR in mice) and different isoforms of motor proteins in comparison with humans (Haghighi et al., 2003; MacLennan & Kranias 2003).

The R9C mutation was also associated with early onset DCM (Schmitt et al., 2003). In the R9C mutation, a positively charged arginine residue is substituted by a reactive cysteine residue altering the hydrophobicity of the cytosolic PLN region resulting in a loss of function mutation (Schmitt et al., 2003). Until today, the R9C mutation was just identified in heterozygous patients. To mimic heterozygous conditions, equal R9C PLN and WT PLN were reconstituted in proteoliposomes together with SERCA and resulted in a dominant negative effect on SERCA (Ceholski et al., 2012). The same was true for the R9L mutation (Ceholski et al., 2012).

1.3 The phosphoadaptor protein 14-3-3

The 14-3-3 proteins are a ubiquitous class of regulatory proteins and were the first family of proteins to be regarded as phospho-serine/-threonine binding modules, regulating and influencing various phospho-proteins (Gardino et al., 2006).

First identified as a brain protein, the 14-3-3 protein family turned out to be ubiquitously expressed in all eukaryotic cells (Aitken et al., 1992). Seven different 14-3-3 isoforms were identified in mammals, two different isoforms were identified in yeast and 15 different isoforms in plants (labelled with Greek letters) (Sluchanko & Bustos, 2019).

The 14-3-3 proteins are homologous proteins and highly conserved among species (Ichimura et al., 1988; Wang & Shakes, 1996). In eukaryotic cells, 14-3-3 proteins are mostly cytosolic proteins (Mhawech, 2005) with a broad range of protein targets, like receptors, kinases, phosphatases, transcription factors and several docking or regulatory proteins, as well as oncogene products (Cau et al., 2018; Fu et al., 2000). Related to this broad spectrum of interaction partners, 14-3-3 proteins are involved in many cellular functions, such as intracellular trafficking, cell proliferation, signal transduction, apoptosis and stress response, underlining the physiological importance (Cau et al., 2018; Fu et al., 2000).

1.3.1 14-3-3 proteins in eukaryotes: Structure and function

The broad number of 14-3-3 ligands draw the idea that shared binding requirements mediate the 14-3-3 interaction (Fu et al., 2000). Early investigations of 14-3-3 interactions suggest that phosphorylated residues in the ligands are a requirement (Fu et al., 2000). The first suggested 14-3-3 consensus motif was RSX(pS/T)XP, where X represents any aa and pS/T a phosphorylated serine or threonine residue (Muslin et al., 1996; Rittinger et al., 1999). According to its proposal, this consensus motif is called mode I binding motif. Later, several additional sequences which are recognized by 14-3-3 proteins were identified, resulting in a mode II binding motif RX(F/Y)XpSXP and a mode III motif (pS/T)XCOOH (Johnson et al., 2010; Obsil et al., 2003). Mode I and II 14-3-3 binding ligands require an arginine at position -3 with respect to the phosphorylated residue and a proline residue at position +2 (Yaffe et al., 1997). Various examples showed that 14-3-3 interaction is regulated via phosphorylation of the ligand, however 14-3-3 can interact with unphosphorylated residues (Johnson et al., 2010; Obsil et al., 2003). It has been reported that unphosphorylated 14-3-3 interaction partners have several negatively charged glutamine residues in their sequence to overcome the phosphorylation residue (Wang et al., 1999).

Crystal structures from different human 14-3-3 isoforms have been resolved showing very similar structures (Gardino et al., 2006). Each monomer consists of nine antiparallel

organized alpha-helices forming an amphipathic binding grove (Stevers et al., 2018). A 14-3-3 monomer has a U-shaped conserved inner concave surface and a variable outer surface. The inner concave surface is an amphipathic groove, which contains helices 3 and 5 on one side creating a charged, polar surrounding. Meanwhile on the opposite side, helices 7 and 9 create a hydrophobic area (Figure 7) (Fu et al., 2000). The 14-3-3 binding groove is conserved among the 14-3-3 isoforms (Obsil & Obsilova, 2011; Rosenquist et al., 2000). Mutagenesis and co-crystallization experiments showed that the basic residues K49, R56 and R127 are important for the interaction with the phosphorylated 14-3-3 interaction partner (Rittinger et al., 1999). Many 14-3-3 interaction partners can bind all 14-3-3 isoforms expressed in that species, indicating the highly conserved amphipathic 14-3-3 binding groove mediates the interaction (D. Liu et al., 1995). Furthermore, it was shown with co-crystallization that the contact between 14-3-3 and a phosphorylated serine is stabilized over salt bridges to the side chains K49, R56 and R127 and a hydroxyl group in Y128 (Figure 7). Extended ligand confirmations are stabilized in the 14-3-3 binding groove by the residues K120, N173 and N224 which make contacts to the backbone groups of the +1 and -1 residue and allow the correct positioning of the phosphorylation group (Rittinger et al., 1999).

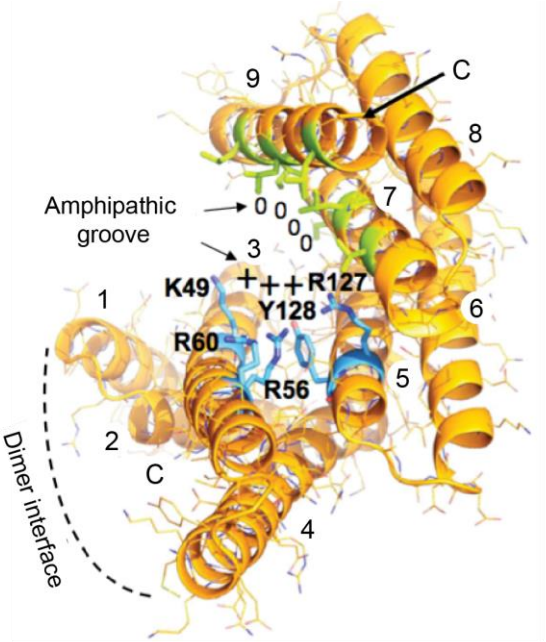

Figure 7. Crystal structure of 14-3-3 monomeric subunit.

The amphipathic groove where 14-3-3 ligand binding occurs (human zeta isoform PDB ID code 2C1). The basic residues K49, R56, R127 are required for contacting the binding partner. The residues K49, R56 and R127 and Y128 stabilize the phospho-residue through salt bridges and hydroxyl groups. The hydrophobic area of the binding groove is indicated in green (zero charges, “0”) and the polar side is shown in blue (positive charges, “+”). Figure adapted from (Sluchanko & Gusev, 2016).

Functional 14-3-3 proteins form a dimer with the N-terminus of another 14-3-3 protein (Figure 8) (Liu et al., 1995; Xiao et al., 1995). Dimerization of 14-3-3 proteins allow the formation of homo- and heterodimers (Benzinger et al., 2005; Jones et al., 1995). For the dimer formation, contacts between the alpha1 helix of one monomer and the alpha 3 as well as alpha helix 4 from the other monomer are necessary (Figure 8) (Jones et al., 1995). The dimer is stabilized by hydrophobic and electrostatic forces formed between the amino acid side chains and a highly conserved salt bridge between R18 of the alpha helix 1 and E89 of alpha helix 4 (Cau et al., 2018). Interestingly, a 14-3-3 dimer is able to bind two ligands at once (Cau et al., 2018). The ligand binding grooves in a 14-3-3 dimer is arranged in a way that they are facing in opposite directions.

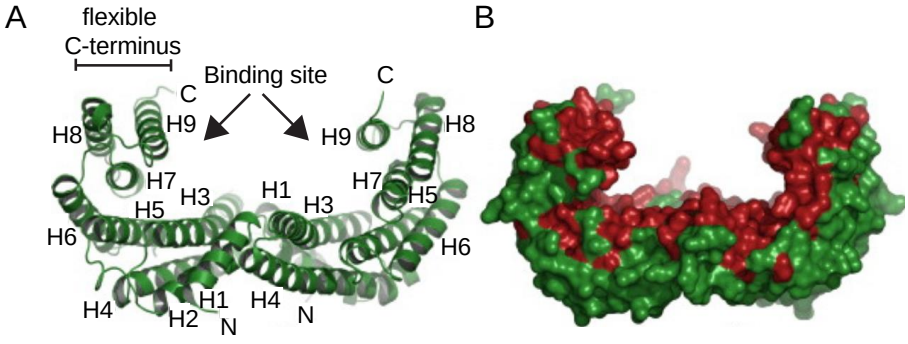

Figure 8. Crystal structure of 14-3-3 protein dimer.

(**A**) Ribbon representation of dimeric 14-3-3 showing the position of 9 alpha helixes per monomer and the contact between helix 1 of one monomer with helix 3 and 4 of the other monomer (human zeta isoform PDB ID code 1QJB). (**B**) Surface representation representing the conserved residues among all seven human isoforms in red. Within the conserved residues the conserved binding site is located. Figure adapted from (Obsil & Obsilova, 2011).

Even though the spectrum of 14-3-3 ligands is huge and 14-3-3 proteins are involved in various intracellular functions, four different modes of action have been suggested for 14-3-3 protein interactions: (1) inducing conformational changes in the target protein, (2) interference of protein-protein or DNA-protein interactions, (3) assembly of two proteins in close proximity and (4) stabilization of specific conformations (Figure 9) (Cau et al., 2018; Coblitz et al., 2006; Fu et al., 2000).

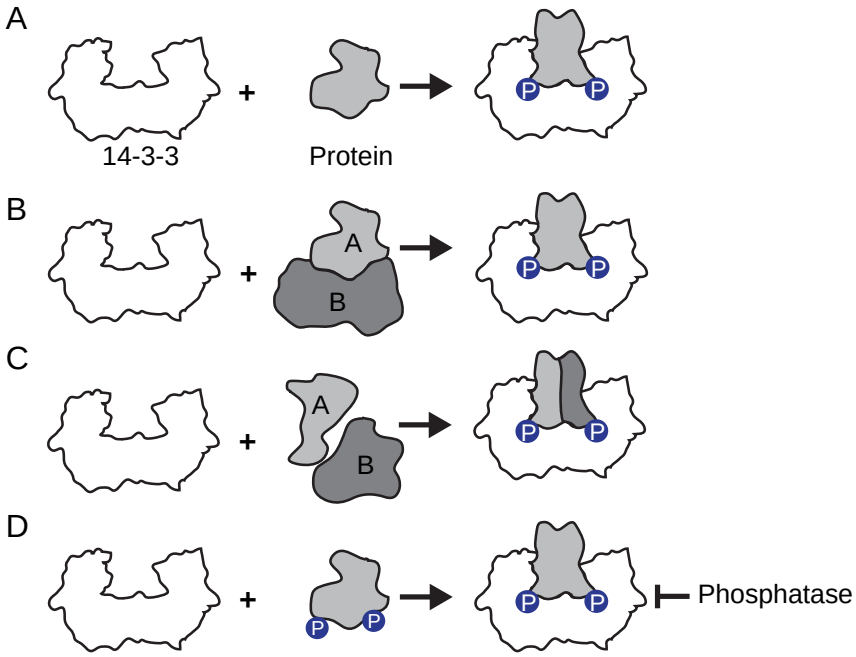

Figure 9. Different functions of the 14-3-3 protein interaction.

(**A**) Binding of 14-3-3 can change the conformation of the ligand and stabilize different conformational changes which influence the function of the ligand. (**B**) 14-3-3 can separate interacting ligands by clamping one ligand and stabilizing the separation. (**C**) The dimeric structure of the 14-3-3 protein allows to bind two ligands at the same time, bring them in close proximity and stabilize them as a complex. (**D**) 14-3-3 can stabilize proteins in a phosphorylated conformation and protect them from phosphatases. Figure adapted from (Cau et al., 2018).

1.3.2 Isoform specificity and regulation of 14-3-3 proteins

The expression of seven different 14-3-3 isoforms in mammals lead to the idea of an isoform specificity for different target proteins, introducing another possibility of fine tuning and regulation of protein-protein interactions. However, the binding groove is highly conserved among the 14-3-3 isoforms (Figure 8) (Yaffe et al., 1997), and variability is achieved with just a few residues around the ligand binding site which may create a ligand preference for different isoforms (Vincenz & Dixit, 1996). In many cases, all 14-3-3 isoforms are able to bind a phosphoresidue of a ligand with comparable affinities (Yaffe et al., 1997). Another possibility to achieve isoform specificity are posttranslational modifications of the 14-3-3 isoforms and isoform specific expression levels (Fu et al., 2000). Regarding posttranslational modifications, acetylation of lysine residues close to the 14-3-3 binding pocket, such as K49 and K120, negatively influence binding of target proteins (Choudhary et al., 2009).

During mouse embryogenesis and neuronal development different 14-3-3 isoforms show very dynamic expression patterns indicating that different 14-3-3 isoforms are required for different cellular processes (Meller et al., 1996; Watanabe et al., 1993). Moreover, in many cancer types aberrant expression of individual 14-3-3 isoforms have been identified (Hermeking, 2003). The expression of 14-3-3 zeta was found to be upregulated in many cancer cells, for example in patients with breast cancer (Neal et al., 2009). The upregulation of 14-3-3 zeta in this context was also correlated with a poor cancer prognosis of these patients (Neal et al., 2009). Interestingly, low expression of 14-3-3 isoforms gamma and theta are associated with markers for breath cancer (Song et al., 2012). In contrast, 14-3-3 sigma was reported to has a suppressive effect on cancer cell growth and tumor formation (Li et al., 2009). These are a few examples of effects caused by different expression levels of 14-3-3 isoforms implying that different expression levels may regulate 14-3-3 proteins (Cau et al., 2018).

The involvement of different 14-3-3 isoforms in cancer, as well as in neurodegenerative and other human diseases, indicate the importance of 14-3-3 modulation. The circumstances, that 14-3-3 proteins act in many cases as adaptor proteins raises interest in the use of active compounds against 14-3-3 to impact binding partners (Stevers et al., 2018). In principle two strategies are considerable, inhibition (e.g. R18) or stabilization of the interaction (e.g. fusicoccanes) (Stevers et al., 2018; Thiel et al., 2012). In both cases, small molecules can be used to either block the 14-3-3 binding groove or to stabilize the interaction. Extensive research is ongoing to identify such small protein interactors, which can help to modulate 14-3-3 protein interactions (Cau et al., 2018).

1.4 Potassium ion channels

Ion channels are integral membrane proteins which are inserted into the plasma membrane and are responsible for ion transfer over the lipid bilayer allowing cellular electrical excitability, signal transduction and muscle contraction (Bartos et al., 2015; Humphries & Dart, 2015). Potassium channels (K^+) are a large family of ion channels found in a broad spectrum of organisms like mammals, plants, bacteria and viruses (Feliciangeli et al., 2015). Several different types of potassium channels are responsible to set the membrane resting potential in many different cell types (Humphries & Dart, 2015).

The selectivity of K^+ channels is mediated by a conserved sequence (T-X-G-X-G) located in a loop between transmembrane helixes (Sansom et al., 2002). The transmembrane helixes span the lipid bilayer and form together with the selectivity filter and a cage of eight oxygen residues the pore entry (Kim & Nimigean, 2016). The oxygen residues are placed in a way that allows optimal interaction with K^+ ions to achieve selectivity (Kuang et al., 2015; MacKinnon, 2003). The interaction of the oxygen residues dehydrates the K^+ ion and allows passage through the pore (Kuang et al., 2015). The smaller Na^+ ions cannot interact with the oxygen residues around the K^+ pore and therefore do not enter the pore (Shrivastava et al., 2002).

Overall K^+ channels can be subdivided in three families: voltage gated (K_v) channels, inward rectifier (K_{ir}) channels and two-pore domain potassium (K_2P) channels (Goldstein et al., 2001; Reimann & Ashcroft, 1999) (Figure 10). K_v and K_{ir} channels form tetramers while K_2P channels dimerize in order to form a functional K^+ channel (Kuang et al., 2015). The correct assembly of the four pore domains is essential for the channel function (Sansom et al., 2002).

K_{ir} channels mostly transport K^+ ions from the outside to inside of the cell (Reimann & Ashcroft, 1999). Four different subgroups are subdivided within the K_{ir} channel family: (1) classical lipid gated K_{ir} channels, (2) G-protein gated K_{ir} channels (3) ATP gated K_{ir} channels and (4) K^+ transport channels (Hibino et al., 2010). The basic structure of K_{ir} channels contain two transmembrane segments flanking a pore forming loop (Figure 10). The transmembrane segment has cytoplasmic NH_2 and COOH termini which contain several regulatory domains and allows modulation of K_{ir} channel trafficking and function (Hibino et al., 2010). Functional K_{ir} channels can be arranged in homo- or heterotetramers (Hibino et al., 2010). Besides an oligomerization function, K_{ir} channels need phosphatidylinositol 4,5-bisphosphate (PIP_2) as a cofactor (Huang et al., 1998).

K_v channels are a very diverse group of K^+ channels including 40 K_v channels which are classified into 12 different subgroups (Gutman et al., 2005). The basic structure of a K_v channel contains six transmembrane helices spanning the lipid bilayer and a NH_2 and COOH termini. The pore forming domain is located between transmembrane domain 5

and 6, meanwhile the voltage sensor is located between transmembrane domain 4 and 5 (Figure 10). The voltage sensor membrane depolarizes via a preserved domain of positive arginine or lysine residues which consequently opens the channel (Aggarwal & MacKinnon, 1996). Further regulation of K_v channels is mediated via the amino- and carboxy termini. The amino terminus is highly conserved among the huge variety of K_v channels and contains a tetramerization domain which is required for correct channel association into homo- or heterotetramers (Bocksteins et al., 2009; Kurata et al., 2002).

K_2P channels are a relatively newly discovered K^+ channel family. The group of K_2P channels contains 15 identified channels that are grouped into six different subgroups. All K_2P channels contain four transmembrane domains, two of which are pore forming loops, one short cytoplasmic NH_2- terminus and one longer COOH terminus (Figure10) (Renigunta et al., 2015).

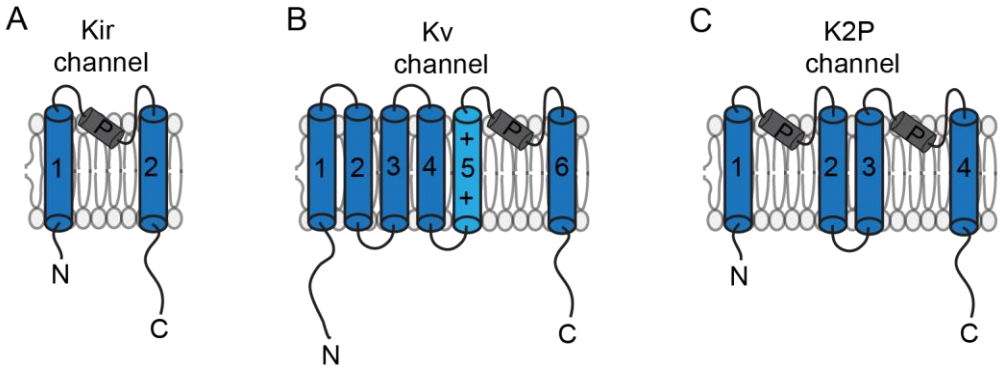

Figure 10. The K^+ channels are subdivided into three main families.

The board spectrum of K^+ channels belong to three main groups according to structure, activation stimuli or behavior. (**A**) K_{ir} channels are inwardly rectifier K^+ channels, (**B**) K_v channels are voltage sensitive channels and (**C**) two-pore domain K^+ channels (K_2P) are channels which contribute to background leak currents during an action potential and are regulated via pH changes or mechanical forces in the membrane. Functional K_{ir} and K_v channels form tetramers, whereas K_2P channels form dimers. Figure adapted from (Makino et al., 2011).

1.4.1 Two-pore potassium channels

The six subgroups of K_2P are the following: TWIK (two-pore domain weakly inward rectifying K^+ channel), TREK (TWIK-related K^+ channel), TASK (TWIK-related acid sensitive K^+ channel), TRESK (TWIK-related spinal cord K^+ channel), TALK (TWIK-related alkaline sensitive K^+ channel) and THIK (tandem-pore domain halothane inhibited K^+ channel) (Feliciangeli et al., 2015).

The K_2P channels are also called “open leak channels” because they have no voltage sensing domain and thereby are not regulated by the membrane potential (Duprat et al., 1997; F. Lesage et al., 1996). However, these channels were identified to contribute to K^+

leak currents resulting in a generation of instantaneous and non-inactivating currents over the range of membrane potential (Feliciangeli et al., 2015). This enables K_2P channels to contribute to the repolarization of the action potential and stabilize the negative resting membrane potential (Decher et al., 2011; Duprat et al., 1997; Jeevaratnam et al., 2018). In contrast, an inhibition of leak conductance leads to an increased resting membrane potential and delayed repolarization (Donner et al., 2011; Gurney & Manoury, 2009). The K_2P channels are able to adapt to the intra- or extracellular ion concentration independent from the gradient of potassium ions over the cell membrane (Thomas & Goldstein, 2009). Even though K_2P channels lack a canonical voltage sensing domain, they are able to sense voltage changes via the selectivity filter which is located in the pore (Schewe et al., 2016). Like other K^+ channels, K_2P channels are also regulated by two conserved gating mechanism. An inactivated gate with a closed selectivity filter facing the extracellular side of the lipid bilayer and an activated gate to the intracellular side (Mathie et al., 2010). Zinc and hydrogen ions regulate gating of K_2P channels by interacting with the inactivated gate in many K_2P channels (Mathie et al., 2010).

K_2P channels have been described to be regulated over various different stimuli, such as membrane stretching (Li et al., 2006), changes in extracellular pH values or by hydrophobic gating (Niemeyer et al., 2016). For example, the TRESK channel requires dephosphorylation for activation which is achieved by interaction with calcineurin. Therefore, TRESK channel activity is regulated by intracellular Ca^{2+} levels (Czirják et al., 2004). On the other hand, stimulation of G_q-protein coupled receptors show an inhibitory effect on TASK channels in the brain (Chen et al., 2006) and heart (Putzke et al., 2007). In line with TASK channels, also TREK channels are inhibited by G_q-coupled activation (Mathie, 2007).

Functional K_2P channels assemble in dimers (Figure 11). Interestingly, homo- and heterodimers between different members of the K_2P channel family were identified. Within a heterodimer each monomer contributes two-pore forming domains to form a pore with potential different affinities for stimulation or inhibition (Figure 11) (Niemeyer et al., 2016). Homo- and heterodimerization have been reported for several different K_2P family members. For example, TWIK1 form together with TASK-1 or TASK-3 heterodimers with SUMOylating sensitivity (Plant et al., 2012). Also, heterodimers between THIK2 and THIK1 were identified as an active K_2P channel (Blin et al., 2014) or heterodimers for TWIK-1 and TREK1 which are responsible for passive conductance in astrocytes (Hwang et al., 2014). A functional heterodimer formed of TASK-1 and TASK-3 could be identified in different tissues and was found to contribute to K^+ leak currents (Czirják & Enyedi, 2002; Enyedi & Czirják, 2010). Heterodimerization is a very effective way to generate channels with new or combined functions and behaviors resulting in a broad diversity.

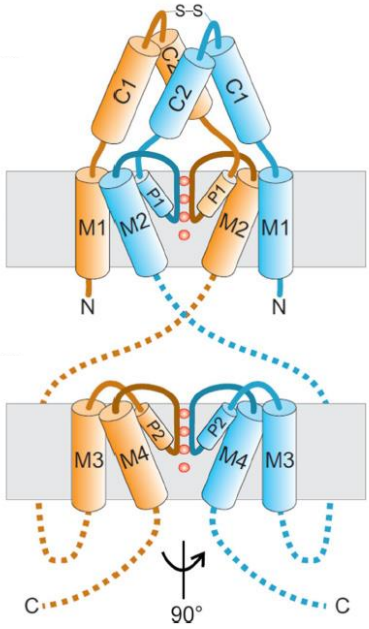

Figure 11. Structure of K_2P channel assembly.

A functional K_2P channel is a homo- or heterodimer. Each monomer (orange or blue) contributes four transmembrane domains and two-pore forming loops which are assembled into a function channel. The upper part of the representation shows the N-terminus of the channel and the lower part the C-terminus of the two subunits. Figure from (Renigunta et al., 2015).

The K_2P channels have been shown to be important regulators in various tissues with physiological and pathophysiological significances (Renigunta et al., 2015). K_2P channels were first discovered in the brain, but some channels are also expressed in smooth muscle cells and in cardiomyocytes (Gurney & Manoury, 2009). The expression of TWIK, TASK, TREK and TRAAK channels was demonstrated at mRNA levels in rat hearts, whereas only TREK-1 and TASK-1 were identified on protein level (Gurney & Manoury, 2009; Liu & Saint, 2004; Putzke et al., 2007). Interestingly, human TREK-1 and TASK-1 channels are mostly expressed in the atrium, which makes them noteworthy for the treatment of atrial fibrillation (AF) (Gurney & Manoury, 2009). The cardiac action potential has a plateau phase between depolarization and repolarization of the cell which is characteristic for cardiomyocytes (Decher et al., 2015). Knock-down or knock-out of K_2P channels in the heart results in a prolonged cardiac action potential, indicating their contribution to the plateau phase and the depolarization of cardiomyocytes (Limberg et al., 2011).

1.4.2 TASK ion channels

The TASK channel family belongs to the K_2P ion channel class and consist of three channels: TASK-1, TASK-3 and TASK-5. The TASK-1 channel was successfully cloned in 1997 (Duprat et al., 1997) and since then a lot of research was done to analyse the function of TASK channels. The sub-family of TASK channels is acid sensitive resulting in activation by alkaline pH values and inhibition due to acidosis (Duprat et al., 1997). Physiological changes in the extracellular pH can take place during hypoxia or ischemia (Duprat et al., 2007; Silver & Erecinska, 1990).

TASK channels are, as all K_2P channels, predominantly expressed in neurons and involved in the action potential generation (Renigunta et al., 2015). TASK-1 and TASK-3 were found to directly contribute to the firing rate of neurons in the thalamus and are sensitive to anesthetics, resulting in an increased firing rate (Lesage 2003; Renigunta et al., 2015). Interestingly, the TASK-5 mRNA was found to be expressed in various tissues such as pancreas, liver, kidney and heart (Ashmole et al., 2001; Hopwood & Trapp, 2005). Heterologous expression of TASK-5 failed to generate whole-cell currents (Ashmole et al., 2001; Kim & Gnatenco, 2001). TASK-5 channel distribution was found to be similar to TASK-1 in mammalian cells, but a heterodimeric TASK-1/TASK-5 channel could not be identified. It is still in question whether TASK-5 channels require other interactions partner to form a functional channel (Ashmole et al., 2001). Until know, the general assumption is, that TASK-5 channels are not functional (Lesage 2003).

For TASK-1 and TASK-3 channels, homo- as well as heterodimers were identified in Xenopus laevis oocytes (Czirják & Enyedi, 2002). TASK-1/TASK-3 heterodimers showed in many cases intermediate behavior for chemical activators or inhibitors, thereby responding to AT(1a) angiotensin II receptor stimulation with weaker inhibition as homodimeric TASK-1 channel but greater as homodimeric TASK-3 channel. The same behavior was observed for the well investigated inhibitor ruthenium red (Czirják & Enyedi, 2002). A potential heterodimerization between TASK-1 and TALK-2 was shown in pancreatic and mammalian cell lines with Förster resonance energy transfer (FRET) analysis. The sensitivity of the TASK-1/TALK-2 dimers to the extracellular pH and halothane was found to be unique for the hybrid (Suzuki et al., 2017).

1.4.2.1 Regulation of TASK channels by intracellular trafficking

TASK channels are regulated like all K_2P channels over various chemical and physical stimuli including pH changes, or by zinc and hydrogen ions. An additional way of post-translational ion channel regulation is through intracellular trafficking which ensures localization in the plasma membrane. Trafficking of TASK channels is regulated by their distal C-terminus and the two adaptor proteins 14-3-3 and coat protein complex I (COPI) (Kilisch et al., 2015). The extreme C-terminus of TASK-1 and TASK-3 contains an overlapping COPI and 14-3-3 binding mode III motif. Interaction of these two binding partners is controlled by PKA phosphorylation (Mant et al., 2011). Mutagenesis studies of the C-terminus of TASK channels identified a di-arginine motif KRR as a COPI endoplasmic reticulum (ER) retention signal in TASK-1 and TASK-3 (Zuzarte et al., 2009). COPI binds the KRR signal in the unphosphorylated TASK channel and retains the channels in the early secretory pathway until PKA phosphorylation of TASK allows 14-3-3 to bind which mediates forward trafficking (Figure 12). TASK channels were the first ion channels identified to interact with 14-3-3 (Rajan et al., 2002). With the help of mutagenesis studies, the last 40 aa of TASK channels were identified to contribute to 14-3-3 binding, whereas the last five aa were found to be essential for the interaction (Rajan et al., 2002). TASK channels with truncations in the C-terminus abolish 14-3-3 interaction and showed reduced or no currents measured by patch clamp (Rajan et al., 2002). This indicated that 14-3-3 binding to TASK channels is important to regulate forward trafficking to the cell surface and exposure of the channel (Figure 12). 14-3-3 binding to the phosphorylated TASK channel mediates forward trafficking of TASK by two effects, it prevents COPI binding due to masking the COPI interaction site and binds the channel in a conformation that induces forward transport (Schwappach, 2008; Smith et al., 2011). Consequently, trafficking of TASK channels to the cell surface is regulated by protein kinases such as PKA and the corresponding phosphatase (Kilisch et al., 2015).

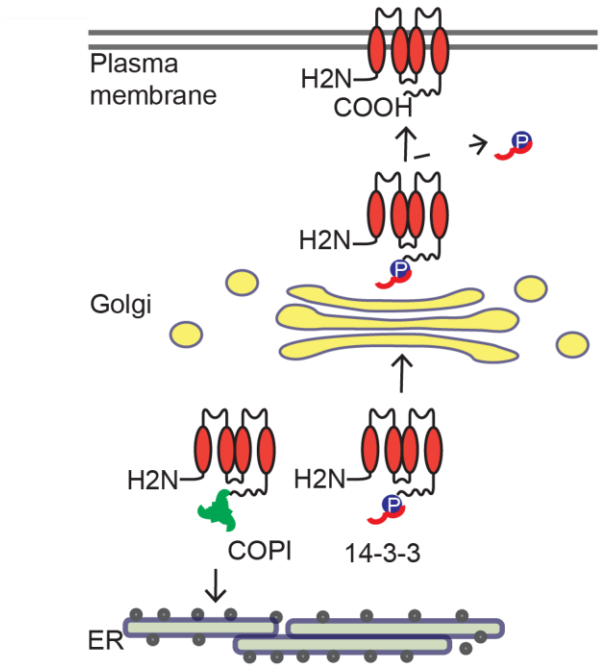

Figure 12. Regulation of TASK channel expression at the cell surface by trafficking.
Cell surface expression of TASK channels is regulated by phosphorylation dependent 14-3-3 or COPI interaction. COPI binds the unphosphorylated TASK channel and initiates retrograde trafficking to the ER. Phosphorylation of TASK allows 14-3-3 binding which is responsible for forward trafficking.

14-3-3 binding to TASK channels is mediated via phosphorylated serine residues (S393 in TASK1 and S373 in TASK-3) (Figure 13). In line with the already known 14-3-3 COPI mediated trafficking of TASK channels, mutation of these serine residues abolish phosphorylation of the trafficking control domain and reduce surface expression and currents measured for TASK channels (Rajan, Preisig-Müller, et al., 2002; Zuzarte et al., 2009). Interestingly, the TASK-1 channel contains a second PKA phosphorylatable serine residue (S392 in human TASK-1) in the extreme C-terminus (Mant et al., 2011) which is not present in TASK-3 (Figure 13).

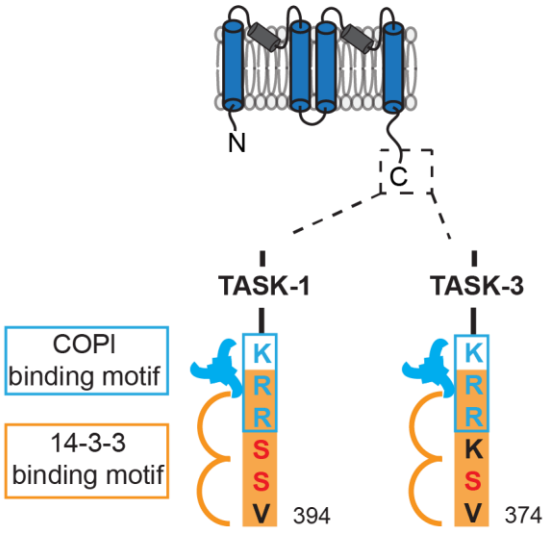

Figure 13. Schematic representation of the TASK-1 and TASK-3 extreme C-terminus.
The last 6 aa of TASK-1 and TASK-3 contain the trafficking control region with overlapping COPI and 14-3-3 binding motifs. Small sequence differences in this region cause differences in the regulation and trafficking of TASK-1 and TASK-3.

This small sequence discrepancy between TASK-1 and TASK-3 channels causes differences in the trafficking control of both channels (Kilisch et al., 2016). First of all, higher 14-3-3 binding affinity was measured for TASK-3 than for TASK-1 with fluorescent polarization titrations and surface plasmon resonance (SPR) analysis (Kilisch et al., 2016). Moreover, phosphorylation of the second serine residue in TASK-1, which is absent in TASK-3, inhibit 14-3-3 binding and prevent surface expression of TASK-1. Phosphorylation of both neighboring serine residues in TASK-1 inhibit 14-3-3 binding as well (Kilisch et al., 2016). These findings about post-translational regulation of TASK channels via trafficking implies that TASK-1 is more tightly regulated via the two phosphorylation residues.

Overall, the localization and therefore the number of TASK channels expressed at the cell surface are regulated in a complex way in different states of ion channel expression, assembly and surface presentation. At the molecular level, a reduction in the open state can be done by different chemical and physical stimuli, at the transcriptional level, up- or downregulation of protein transcription or at the posttranslational level by modulation of intracellular trafficking (Kilisch et al., 2016).

1.4.2.2 Expression of TASK-1 and TASK-3 channels in the heart

Although TASK-1 and TASK-3 channels belong to the same sub-family, just TASK-1 shows robust protein expression in rodent hearts (Kim et al., 1999; Putzke et al., 2007) and in the human atrium (Decher et al., 2011). TASK-1 is mostly expressed in the ventricle and immunostaining experiments in cardiomyocytes showed the localization at the intercalated disc and t-tubule network (Jones et al., 2002).

Putzke et al reported TASK-1 like currents in rat ventricular myocytes and suggested that TASK-1 currents contribute to the outward current during the plateau phase in the cardiac action potential and help to stabilize the resting membrane potential (Putzke et al., 2007). In line, inhibition of TASK-1 channels showed prolonged action potential (Putzke et al., 2007). The same effect was found by blocking the pore of TASK-1 channel with a TASK-1 specific inhibitor called A923 (Putzke et al., 2007). Action potential modeling and patch clamp experiments revealed that the impact of TASK-1 currents on the action potential duration is more obvious when the action potential is prolonged. This indicates that the small TASK-1 current plays a functional role in longer action potentials with a plateau shape (Putzke et al., 2007).

TASK-3 is predominantly expressed in the brain and nervous system but mRNA levels were also identified in the heart (Callahan et al., 2004; Gurney & Manoury, 2009). Interestingly, Rinné et al performed immunocytochemistry analysis of TASK-3 in right human auricles revealing TASK-3 protein expression at the cell surface (Rinné et al., 2015). However, single channel recordings in the cell-attached mode did not allow for the identification of TASK-3 homodimer channels. Instead, intermediate single channel conductance between TASK-1 and TASK-3 channels were measured indicating the presence of a heterodimer TASK-1/TASK-3 channel in cardiomyocytes (Rinné et al., 2015). The TASK-1/TASK-3 dimer was found to be expressed at the cell surface and showed a reduced affinity for TASK-1 inhibitors indicating changed pharmacologic response (Rinné et al., 2015).

1.4.2.3 TASK-1 regulation in the heart

In 2007, Putzke et al reported that TASK-1 channels are regulated via the adrenergic pathway by alpha1-adrenoreceptors. They used the selective alpha-1-adrenoceptor agonist methoxamine to block alpha-1 adrenoceptors and measured strongly reduced outward currents at pH 6 in cardiomyocytes. This experiment showed that alpha-adrenergic stimulation inhibits TASK-1 channels (Putzke et al., 2007). From rat cardiomyocytes, it is known that alpha-adrenergic stimulation prolong action potential duration by reducing outward potassium currents (Ravens et al., 1989). Even though, treatment of rat cardiomyocytes with methoxamine reduced TASK-1 like currents, it is still

an open question, how big the relative contribution of the TASK-1 currents are to the general effect of alpha-adrenergic stimulation on action potentials in rat cardiomyocytes (Decher et al., 2014).

Alpha1-adrenergic receptors are G_q-coupled receptors and upon activation they activate the phospholipase C which leads to hydrolysis of PIP_2 (Gurney & Manoury, 2009). As a consequence, the local PIP_2 levels are reduced in the plasma membrane (Stauffer et al., 1998) which is associated with ion channel activity (Baukrowitz et al., 1998; Zhang et al., 2003). PIP_2 is as a phospholipid integral part of the plasma membrane and known to be involved in several signaling pathways. (McLaughlin et al., 2002). Interestingly, PIP_2 was shown to activate TASK-1 channels and other members of the K_2P channel family (TASK-3, TREK-1, TRAAK) (Lopes et al., 2005). In line, it was shown that PIP_2 hydrolysis is responsible for inhibition of TASK channels and the strength of inhibition was determined by the level of agonist-induced inhibition (Lopes et al., 2005). The theory of PIP_2 depletion being responsible for TASK-1 inhibition was contradicted in another study, where TASK-1 currents were found to be unaltered upon PIP_2 depletion (Lindner et al., 2011). The mechanism of TASK-1 inhibition due to G_q-coupled receptors are controversial in the field (Decher et al., 2014). Contrary to the results of Lopes et al, it was shown that the G_q-receptor alpha-subunit (G_qa) directly inhibits TASK-1 (Chen et al., 2006), whereas a third study claims that phospholipase C inhibits TASK-1 (Schiekel et al., 2013).

In the brain, TASK-1 and TASK-3 were also found to be inhibited by G_qa mediated receptors (Chen et al., 2006). Receptor mediated regulation of TASK-1 was found to be controlled via the first six aa of the COOH-terminal tail (VLRFMT) (Talley & Bayliss, 2002). A detailed understanding of the suppression effect of alpha-adrenergic stimulation on TASK-1 channels remains incomplete (Decher et al., 2014).

1.4.2.4 Potential of TASK-1 in atrial fibrillation and heart failure

Endothelin-1 (ET-1) is a peptide hormone secreted by endothelia cells and functions as a vasoconstrictor regulated by two G-protein-coupled receptors (Marasciulo et al., 2006). Increased ET-1 levels are associated with HF or myocardial infarction (Becker et al., 2000). ET-1 is associated with inhibition of steady-state outward currents in rat cardiomyocytes (James et al., 2001). In line with this, Schiekel et al were able to show that ET-1 inhibited TASK-1 currents as well, suggesting that the TASK-1 channel may be involved in the arrhythmogenic effects of ET-1 (Schiekel et al., 2013).

AF is the most diagnosed form of arrhythmia with the potential of serious complications such as HF or stroke (Schmidt et al., 2011). Drugs to treat arrhythmias are not tolerant in all patients and cause side effects (Hancox et al., 2016; Schmidt et al., 2011; Wiedmann et al., 2016). It was shown that inhibition of TASK-1 channels prolonged action potential

duration (Limberg et al., 2011; Schmidt et al., 2019) and the exclusive expression in the atrium makes TASK-1 an interesting ion channel to treat AF (Limberg et al., 2011; Schmidt et al., 2014). TASK-1 mRNA and protein levels were found to be upregulated in patients suffering AF (Schmidt et al., 2015).

The finding that chronic AF is associated with increased levels of TASK-1 leading to shortened action potential duration cause increased research in identifying potential and highly selective TASK-1 blockers (Schmidt et al., 2014; Şterbuleac 2019). In 2006, Cotton at al. presented doxapram as a TASK channel inhibitor (Cotten et al., 2006). They found that doxapram inhibits the TASK-1 homodimer channel and with a strongly reduced affinity also the TASK-3 homodimer channel (Cotten et al., 2006). Interestingly, an intermediate inhibitory effect of doxapram on the TASK-1/TASK-3 heterodimer was identified (Cotten et al., 2006). In 2007, Putzke et al presented the TASK-1 channel blocker A293 (Putzke et al., 2007). In *Xenopus oocytes*, low concentrations of A293 showed a high specificity for TASK-1 channels causing an increased action potential duration (Putzke et al., 2007). Another already presented TASK-1 inhibitor is A1899, which blocks the pore of TASK-1 specifically with very high affinity (K_d in the nanomolar range) (Streit et al., 2011). Recently, the anti-arrhythmic drug ranolazine was shown to be an inhibitor of TASK-1 currents in mammalian cells and *Xenopus oocytes* (Ratte et al., 2019). This contributes to better understanding of the function of ranolazine and may help to consider ranolazine as a prototype drug (Ratte et al., 2019).

1.4.2.5 TASK channel mutations and pathogenic heart phenotypes

It was found that TASK-1 loss of function mutations cause pulmonary hypertensions (Gurney et al., 2003; Ma et al., 2013). Six TASK-1 loss of function mutations were characterized from two different patient cohorts and four mutations showed the phenotype of pulmonary hypertension (Ma et al., 2013). In addition, three of the TASK-1 mutation carriers showed arrhythmias (Ma et al., 2013). In another study, a large population of Danish patients with AF and an Australian cohort with AF within the family were analysed for mutations in TASK-1 (Liang et al., 2014). Two patients with genetic defects in the TASK-1 channel were identified form the two different patient cohorts. One patient showed a V123L mutation and the other one had two 5'UTR variants in the Kozak sequence of the TASK-1 gene (Liang et al., 2014). Both patients showed reduced cardiac TASK-1 currents in patch clamp analysis (Liang et al., 2014). The findings from TASK-1 mutations in patients are in contrast to the pharmacological analysis of TASK-1 channels with inhibitors which resulted in a prolonged action potential duration preventing AF (Limberg et al., 2011; Schmidt et al., 2014). However, the analysed patients also had additional mutations and were heterozygous for a single-nucleotide polymorphism already correlated with the

development of AF (Liang et al., 2014). The data obtained about the involvement of TASK-1 mutations in the development of AF so far, show indication that TASK-1 mutations contribute to arrhythmogenesis instead of being the exclusive cause for development of AF (Decher et al., 2014).

1.5 Aim of this thesis

The aim of this thesis was to analyse proteins and regulators which are involved in main processes of cardiac excitation and Ca^{2+} handling. Novel interaction partners for two important regulators involved in these processes, namely PLN and TASK channels, were identified.

PLN is a main regulator of the Ca^{2+} pump SERCA responsible for correct Ca^{2+} handling in the heart (MacLennan & Kranias 2003). The SERCA/PLN interaction is regulated by phosphorylation of two different kinases (Coyler, 1998). A putative 14-3-3 interaction motif was identified in the cytosolic domain of PLN, including the phosphorylation residues (Arakel et al., 2014). 14-3-3 binding contain often phospho-residues and stabilize client proteins in a specific conformation or block alternative interaction partners (Fu et al., 2000). A potential 14-3-3/PLN interaction may stabilize PLN and influence the inhibitory effect on SERCA. Consequently, one main aim of this thesis was the analysis of a potential 14-3-3 interaction with PLN. This aim was addressed with complementary experimental approaches: binding assays with recombinant 14-3-3 and cardiac lysate, proteomic mass spectrometry and immunoprecipitation experiments. After a novel interaction between 14-3-3 and PLN was confirmed, the binding site was dissected with recombinant binding assays, surface plasmon resonance measurements and molecular dynamic simulation experiments. The physiological function of the 14-3-3/PLN interaction was analysed by following the hypothesis that 14-3-3 binding to PLN may protect PLN from fast dephosphorylation by phosphatases. Recombinant dephosphorylation assays were performed along with patch clamp experiments in cardiomyocytes. Finally, the 14-3-3/PLN interaction was investigated in a PLN R14del mutation (Haghighi et al., 2006) using recombinant binding assays and homo- and heterozygous disease mouse models.

The class of pH sensitive TASK channels belong to the K_2P ion channel family and contribute with K^+ leak currents to the repolarization of the action potential (Duprat et al., 1997). TASK channels were first identified and characterized in the brain (Duprat et al., 1997; Enyedi & Czirják, 2010; Medhurst et al., 2001). Later, especially TASK-1, but also TASK-3 were identified in the heart (Gurney & Manoury 2009; Rinné et al., 2015). It is known that both channels are regulated by phosphorylation dependent interaction of 14-3-3 and COPI (Kilisch et al., 2016). However, further regulation via A-kinase-anchoring protein or chaperones such as MAGUK or PDZ proteins, as already identified for other potassium channels, is unidentified so far (Mathie et al., 2010). In addition, little is known about TASK channel insertion in the plasma membrane (Mathie et al., 2010). Therefore, the second main goal of this thesis was the analysis of the cardiac proteome of TASK-1

and TASK-3. Binding experiments with recombinant TASK C-termini, considering different phosphorylation states, with cardiac lysate were performed followed by mass spectrometry analysis. Novel potential interaction partners were further investigated with different biochemical approaches.

2 Chapter II: Manuscript

Major parts of my work contributed to a first author manuscript (aaz1436), which is currently edited and prepared for publication in Science Signaling (status June 2020). The protein-protein interaction discovered in this publication have been submitted to the IMEx consortium (http://www.imexconsortium.org) through IntAct and assigned the identifier IM-27195. The manuscript is part of my thesis in the following chapter 2, including a detailed table of my contribution. All data needed to evaluate the conclusions presented in the manuscript are present in the main or in the supplementary materials of the manuscript. Further experiments and projects, I investigated during my PhD studies, are presented in chapter 3 (Further analysis of the PLN/14-3-3 interaction) and chapter 4 (Identification of novel interaction partners for TASK channels in the heart).

Figure contribution in the manuscript “14-3-3 binding creates a memory of kinase action by stabilizing the modified state of PLN”:

Figure 1:	14-3-3 affinity purification experiment analysed by silver staining (JM) and immunoblotting (JM), data analysis (JM)
Figure 2:	PLN proximity proteomics (DKD), MS analysis (CL, HU), data analysis (CL, DKD)
Figure 3:	14-3-3 affinity purification with heated cardiac membranes and immunoblotting (JM), recombinant binding assay upon PKA or CaMKII phosphorylation (JM), data analysis (JM)
Figure 4:	MD simulations for PLN pS16 or PLN pT17 with 14-3-3σ (AB, MM); recombinant binding assay of PLN-GST variants mimicking DCM-causing mutants (JM)
Figure 5:	recombinant de-phosphorylation assay of pT17-PLN-GST in the presence of 14-3-3 (JM), data analysis (JM)
Figure 6:	cardiomyocyte isolation (JM, KUF), immunoprecipitation from cardiac membranes (JM) and corresponding inputs were analysed by immunoblotting (JM), data analysis (JM)

Figure 7:	recombinant purification of 14-3-3γ (JM), measurement of τ of CaT decay after ISO application in cardiomyocytes for 14-3-3γ and control solution (JM, ST), measurement of τ of CaT decay after ISO application in cardiomyocytes for R18, 14-3-3+R18, PLN pS16 and pT17 antibodies (ST), data analysis (ST), graphical representation shown in D (JM)
Supplement Figure 1:	14-3-3 affinity purification experiment analysed by immunoblotting (JM), PLN pS16 and pT17 antibody specificity test (JM)
Supplement Figure 2:	confocal imaging (DKD); PLN proximity proteomics (DKD), data analysis (DKD)
Supplement Figure 3:	recombinant binding assay upon CaMKII phosphorylation for all seven 14-3-3 isoforms (JM)
Supplement Figure 4:	recombinantly purification 14-3-3γ and PLN (JM); SPR experiments (JM), data analysis (JM, MK)
Supplement Figure 5:	MD simulations for PLN pS16 or PLN pT17 with 14-3-3σ (AB, MM), data analysis (AB, MM)
Supplement Figure 6:	recombinant PKA phosphorylation of PLN-GST variants mimicking DCM-causing mutants (JM)
Supplement Figure 7:	recombinant de-phosphorylation assay of pS16-PLN-GST T17A in the presence of 14-3-3 (JM), data analysis (JM)
Supplement Figure 8:	stimulation of cardiomyocytes and Ca transient recording with or without 14-3-3 (JM, ST), relaxation of Ca transients under rapid removal of extracellular Na (ST), data analysis (ST)
Non-experimental contribution:	manuscript conceptualization (JM, MJS; SEL, BS), writing original draft (JM, SEL, BS), writing review and editing (JM, DKD, AB, CL, MM, CO; MJS, SEL, BS)

14-3-3 binding creates a memory of kinase action by stabilizing the modified state of phospholamban

Julia Menzel[1], Daniel Kownatzki-Danger[2†], Sergiy Tokar[3†], Alice Ballone[4,5], Kirsten Unthan-Fechner[1], Markus Kilisch[1], Christof Lenz[6,8], Henning Urlaub[6,8], Mattia Mori[4], Christian Ottmann[5], Michael J. Shattock[3], Stephan E. Lehnart[2,7], and Blanche Schwappach[1,7,8,*]

[1]Department of Molecular Biology, Universitätsmedizin Göttingen, Humboldtallee 23, 37073 Göttingen, Germany.

[2]Heart Research Center Göttingen, Department of Cardiology & Pneumology, Universitätsmedizin Göttingen, Robert-Koch-Straße 42a, 37075 Göttingen, Germany.

[3]School of Cardiovascular Medicine and Sciences, King's College London, Westminster Bridge Road, London, SE17H, UK.

[4]Department of Biotechnology, Chemistry and Pharmacy, Department of Excellence 2018-2022, University of Siena, Via Aldo Moro 2, 53100, Siena, Italy.

[5]Laboratory of Chemical Biology, Department of Biomedical Engineering and Institute for Complex Molecular Systems, Eindhoven University of Technology, P. O. Box 513, 5600MB, Eindhoven, The Netherlands.

[6]Bioanalytics Group, Institute of Clinical Chemistry, University Medical Center Göttingen, Robert-Koch-Straße 40, 37075 Göttingen, Germany

[7]Cluster of Excellence "Multiscale Bioimaging: from Molecular Machines to Networks of Excitable Cells" (MBExC), University of Goettingen, Robert-Koch-Straße 40, 37075 Göttingen, Germany, Germany

[8]Max-Planck Institute for Biophysical Chemistry, Am Faßberg 11, 37077 Göttingen, Germany.

*To whom correspondence should be addressed: blanche.schwappach@med.uni-goettingen.de

† these authors contributed equally.

Abstract

The cardiac membrane protein phospholamban (PLN) is a target of protein kinase A (PKA), at Ser^{16}, and Ca^{2+}/calmodulin-dependent protein kinase II (CaMKII), at Thr^{17}. β-adrenergic stimulation and PKA-dependent phosphorylation of Ser^{16} acutely stimulates the sarcoplasmic reticulum calcium pump (SERCA) by relieving an inhibitory effect of PLN on SERCA. CaMKII-dependent phosphorylation may lead to longer lasting SERCA stimulation and sustain (mal)adaptation of calcium handling. Here, we demonstrated that phosphorylation at either Ser^{16} or Thr^{17} converted PLN into a target for the phosphoadaptor protein 14-3-3 with different affinities. Proximity labelling in live cardiomyocytes identified 14-3-3 proteins within nanometers of PLN and endogenous 14-3-3 coimmunoprecipitated with pentameric PLN from cardiac membranes. There were differences in the molecular contacts of the phosphopeptides phosphorylated at Ser^{16} or Thr^{17} within the binding groove of 14-3-3, as predicted by molecular dynamics simulations, resulting in varied binding affinities. We showed that 14-3-3 binding protected either PLN phosphosite from dephosphorylation. During β-adrenergic stimulation of isolated adult cardiomyocytes, endogenous 14-3-3 proteins were recruited to the membrane fraction. Functionally, the binding of exogenously added 14-3-3 to PLN phosphorylated at Ser^{16} produced by β-adrenergic stimulation prolonged SERCA activation, presumably by protecting $pSer^{16}$-containing PLN pentamers from dephosphorylation. Phosphorylation of Ser^{16} was disrupted by the cardiomyopathy-associated ΔArg^{14} mutation, implying that Thr^{17} phosphorylation by CaMKII may become crucial for 14-3-3 recruitment to ΔArg^{14} PLN. In line with PLN as a dynamic hub in the control of Ca^{2+} handling, our results identify 14-3-3 binding to PLN as a contractility-augmenting mechanism.

Introduction

The cardiac excitation-contraction cycle relies critically on the spatio-temporal control of intracellular Ca^{2+} release and sequestration in the sarcoplasmic reticulum (SR) (*1*). In cardiomyocytes, the RyR Ca^{2+} release channel and the Ca^{2+} pump SERCA cooperate in large protein assemblies to ensure the physiological plasticity of Ca^{2+} handling (*2*). The small membrane protein phospholamban (PLN) negatively regulates SERCA pumps and thereby affects the reuptake kinetics of Ca^{2+} into the SR. The protein is dispensable in mice perhaps because it regulates only 40% of the SERCA pumps (*3, 4*). Yet, mutations found heterozygously in patients with inherited dilated cardiomyopathy suggest that humans require the full complement of PLN (*5-7*). Protein kinase A (PKA)-dependent phosphorylation targets PLN on Ser^{16}, relieves the inhibitory effect of PLN on SERCA, and hence stimulates SERCA (*8, 9*). During β-adrenergic stimulation, this mechanism results in increased force generation and an accelerated relaxation of cardiac muscle. The adjacent Thr^{17} is targeted by Ca^{2+}-calmodulin-dependent kinase (CaMKII) under a variety of stimuli (*10, 11*) although phosphorylation of Ser^{16} is sufficient to mediate the effects of β-adrenergic signal transduction (*12*). Aside from its regulation by phosphorylation, PLN exists in an equilibrium between two assembly states, a monomeric and a pentameric form, which can be observed as an SDS-resistant pentamer (*9*, *13-14*) consistent with the high stability of the oligomer observed by FRET in living cells (15). This equilibrium and a spectrum of conformations assumed by the cytoplasmic domain of PLN are central to the regulatory effect of Ser^{16} or Thr^{17} phosphorylation on PLN (*13, 15*) and may hence be targeted by other modulatory mechanisms including protein-protein interactions (*16*). Indeed, the regulatory subunit of protein phosphatase 1c (PP1c), the membrane protein PPP1R3A (*2, 17*), recruits not only the phosphatase but two additional proteins that inhibit PP1c, inhibitor-1 (I-1) and the small heat shock protein Hsp20.

In previous work on cardiac ATP-sensitive potassium channels (K_{ATP}), we dissected arginine (Arg)-based trafficking motifs in K_{ATP} subunits (*18*). Arg-based motifs bind the vesicle coat complex COPI and in many cases also 14-3-3 phosphoadaptor proteins. 14-3-3 proteins are encoded by a family of seven related genes, which historically have been called isoforms (*19-21*). They bind to various client proteins by engaging with target sequences that often but do not always contain phosphoresidues. Binding may stabilize specific conformations of a client protein or sterically block alternative protein-protein interactions. As a result, the subcellular localization, stability, or posttranslational modification state of the client protein may be affected by 14-3-3 binding. Client binding involves a highly conserved ligand binding groove of 14-3-3 proteins. The relative

abundance and biological relevance of the isoforms, which differ most in their N- and C-terminal regions, remains poorly understood.

The molecular interactions of Arg-based motifs with COPI and 14-3-3 are crucial to the proper assembly, subcellular localization, and regulation of membrane proteins that present Arg-based signals (*22, 23*). For K_{ATP} and the two-pore domain potassium channel TASK-1 (*24*), interactions with COPI and 14-3-3 are regulated by PKA-dependent phosphorylation. Based on its N-terminal sequence (Fig. 1A), we predicted that PLN is a membrane protein with an Arg-based signal that may be regulated in a similar manner (*18*) and set out to test whether PKA-phosphorylated PLN could bind to 14-3-3 proteins. We discovered that two distinct phosphosites, phosphorylated (p) Ser^{16} and $pThr^{17}$, engaged 14-3-3 with different affinities. We propose that this differential binding adapts the lifetimes of the respective phosphostate to its specific biological purpose.

Results

14-3-3 binds to SDS-resistant PLN pentamers

PLN is a major target of PKA in cardiomyocytes (*25*) and its PKA consensus sequence and a putative 14-3-3 binding site (*18*) are highly conserved (Fig. 1A). To test whether PKA-phosphorylated pSer^{16}-PLN interacted with 14-3-3, we incubated recombinantly expressed 14-3-3γ immobilized on a matrix with solubilized cardiac membranes or cytosolic fractions prepared from mouse ventricular tissue (Fig. 1B). The R18 peptide is a high-affinity 14-3-3 ligand (*26, 27*) that is routinely used to verify the specific interaction of a protein with 14-3-3. Structural models of R18 bound to 14-3-3 obtained by X-ray crystallography demonstrate that R18 occupies the canonical peptide-binding groove of 14-3-3 and hence blocks other ligands from binding. Silver staining (Fig. 1C) of the eluate revealed the presence of bound proteins from the membrane fraction, which we probed by Western blotting using an antibody recognizing generic PKA-dependent phosphosites (Fig. 1D, fig. S1A). The strongest band detected was consistent with the presence of a PKA-phosphorylated PLN pentamer in the 14-3-3 eluate, which can be observed by SDS-PAGE under denaturing conditions (*14*), possibility due to its high stability (*15*). To test whether this band corresponded to PLN, we probed the eluates using specific antibodies against PLN (Fig. 1E,F, fig. S1B) and pSer^{16}-PLN (Fig. 1G,H, fig. S1C,D). Because preincubation with R18 reduced PLN binding to background levels (Fig. 1F and H) this experiment identified SDS-resistant PLN pentamers as 14-3-3 ligands that use the canonical ligand-binding groove. PLN monomers, which were present in the solubilized membranes, were not found in the 14-3-3 eluates (Fig. 1D,E,G).

In situ biotinylation reveals that PLN is situated in close proximity to 14-3-3 in cardiomyocytes

To complement this analysis with a method that enables the detection of 14-3-3 in proximity to PLN in situ, we fused an engineered ascorbate peroxidase (V5-APEX2) to the PLN N-terminus and expressed the fusion protein in neonatal rat cardiomyocytes (NRCMs; Fig. 2A, fig. S2A) using cytosolic GFP (fig. S2B) or PLN lacking the cytosolic N-terminus (fig. S2B,C) as negative controls for background binding to the avidin matrix and nonspecific APEX2-mediated labelling, respectively. V5-APEX2-PLN localized to SR membranes as expected (fig. S2A). Six of seven 14-3-3 proteins in the family were specifically labelled when APEX2 fused to full-length PLN was exposed to biotinphenol and H_2O_2 (Fig. 2B, Data File S1), including 14-3-3γ, which was the bait in our 14-3-3 affinity purification (Fig. 1B). PLN itself was strongly enriched in both controls as expected based on auto-labelling within V5-APEX2-PLN and on the oligomeric states of PLN. On the other hand, the functionally best characterized interaction of PLN with SERCA pumps (*8*) could

not be detected, presumably because SERCA2a is a highly abundant cardiac protein leading to substantial background in the biotin-affinity step of the protocol (fig. S2B,C) and because the transmembrane segment of PLN may remain in close proximity to SERCA2a in SR membranes (fig. S2C). Similarly, another membrane protein that associates with PLN, the PP1c regulating protein PPP1R3A (*2, 17*), could not be detected although soluble proteins that interact with PPP1R3A, PP1c itself and Hsp20, were biotin-labelled (Fig. 2B, Data File S1). These two proteins acted as positive controls for the proximity proteomics approach and their detection underscored that proximity labelling could be due to indirect interactions within larger protein complexes. Hence, the enrichment of six out of seven 14-3-3 isoforms could not be interpreted beyond proximity because 14-3-3 proteins exist as different heterodimers. Binding to PLN could occur through one specific isoform that engages in different heterodimers. However, the peptide-binding groove of 14-3-3 proteins is highly conserved and PLN may directly engage with different 14-3-3 proteins, as occurs with many other 14-3-3 ligands (*28*). We conclude that PLN and several endogenous 14-3-3 proteins are present within nanometers of each other in cardiomyocytes and that direct or indirect interactions may explain this proximity.

14-3-3 enriches PLN pentamers more efficiently than PLN monomers

Our specific enrichment of SDS-resistant PLN pentamers that contain PKA-phosphorylated PLN by 14-3-3γ (Fig. 1G) implies an avidity effect in which the two ligand-binding grooves present in the 14-3-3 dimer support binding of 14-3-3 to PLN with a higher apparent affinity than the binding parameters of one peptide ligand binding to a single binding site would allow (*29, 30*). To further test this idea, we converted the majority of PLN present in solubilized mouse cardiac membrane into the monomeric form by gentle heating (*14*). In the heated membrane input, the monomer was the predominant species. However, only 10% of this monomeric PLN was enriched by 14-3-3γ whereas 30% of the pentamer present in the solubilized membranes before heating was bound (Fig. 3A,B). This result supports the concept that an avidity effect is relevant to the interaction between PLN and 14-3-3.

Next, we tested direct binding of 14-3-3 to PLN in an in vitro system. A recombinant protein consisting of the first 31 N-terminal residues of PLN fused to GST did not bind to 14-3-3γ despite efficient phosphorylation of Ser^{16} by purified PKA catalytic subunit in vitro (Fig. 3C,D). This finding may reflect a low affinity of the interaction between $pSer^{16}$-PLN and one 14-3-3 ligand-binding groove. However, when we exchanged the neighboring residue Thr^{17} with an alanine, the enrichment of $pSer^{16}$-T17A-PLN-GST for 14-3-3 was more efficient (Fig. 3C,D). These data confirm that $pSer^{16}$ contributes to a 14-3-3 binding site that is weakened by the neighboring Thr^{17}. The low affinity of 14-3-3 binding to the

monomeric pSer^{16}-PLN-GST construct is consistent with the presence of pSer^{16}-PLN in the 14-3-3 interacting SDS-resistant pentamers but not the monomers (Fig. 1G,H) and the observed avidity effect (Fig. 3A,B).

14-3-3 binds with higher affinity to pThr^{17}-PLN than to pSer^{16}-PLN

After conversion of PLN into monomers by heating, 10% of PLN monomers and 30% of the SDS-resistant pentamers, which have previously been interpreted as a biochemical correlate of endogenous pentamers (*9*,*14*), were enriched on the 14-3-3 matrix (Fig. 3A,B). The kinase CaMKII targets Thr^{17} (*8, 9*), which is adjacent to Ser^{16} targeted by PKA. Because specific antibodies detecting pThr^{17}-PLN are available (fig. S1C,D), we probed solubilized cardiac membranes that had been heated or not as well as the respective eluates from the 14-3-3 matrix (Fig. 3E,F). This antibody was less efficient at detecting monomers compared to pentamers in the input. However, the pThr^{17} monomer and pentamer were equally enriched by the 14-3-3 matrix leading us to infer that monomeric pThr^{17}-PLN could bind to 14-3-3 with higher affinity than pSer^{16}-PLN. We observed robust binding of PLN-GST phosphorylated *in vitro* with CaMKII to 14-3-3 (Fig. 3G,H). This result indicates that either phosphosite generates a 14-3-3 target motif but with apparently different affinities when monomeric PLN is offered as a target.

We found that all seven 14-3-3 isoforms bound to pThr^{17}-PLN-GST (fig. S3). Although this result does not reflect the interactions between endogenous cardiomyocyte proteins, it does show that direct binding of 14-3-3 to PLN can occur . We also measured 14-3-3 binding to immobilized pSer^{16}- or pThr^{17}-PLN-GST by SPR ((*24*); fig. S4A). We determined an equilibrium dissociation constant (K_D) of 4 µM (fig. S4B,C) for the binding of 14-3-3γ to pThr^{17}-PLN-GST. It was difficult to obtain reliable sensograms for PKA-phosphorylated WT (fig. S4D). Hence, we cannot provide equilibrium dissociation constants for these binding events but conclude that the respective affinities are substantially lower than those observed for pThr^{17}-PLN.

pSer^{16} and pThr^{17} determine the conformation of the PLN/14-3-3 complex

Possible differences in the molecular contacts between the distinct PLN phosphoforms and 14-3-3σ were addressed by molecular dynamics (MD) simulations, exploiting the conserved mechanism of 14-3-3σ and 14-3-3γ for phospho-dependent ligand binding (*31*). This approach was also justified by our observation that 14-3-3σ bound to immobilized pThr^{17}-PLN-GST (fig. S3) and that all 14-3-3 proteins engaged with pThr^{17}-PLN. Unrestrained MD trajectories were generated for 250 ns on each system. For the 14-3-3σ/pSer^{16}-PLN complex, the all-atom root mean square deviations (RMSD) (fig. S5A) suggested that conformational convergence is achieved during MD simulation time whereas the comparison of the root mean square fluctuation (RMSF) between 14-3-3σ

residues from the complex and *apo* 14-3-3σ (fig. S5B) showed that residues with the highest fluctuation belonged to loops 64-88 and 208-219 (fig. S5B,C). Notably, the conformational freedom of residues 118-190 that belonged to the 14-3-3σ amphipathic groove was constrained by the phosphopeptide. Moreover, by cluster analysis of the phosphopeptide and residues within 6 Å (fig. S5C-D), we found that the most abundant population of MD frames had a peptide conformation (Fig. 4A) that was comparable to that observed in X-ray crystallographic structures (*32*). Indeed, pSer^{16} is located in the amphipathic groove and establishes hydrogen bonds to Lys^{49} (2.97 Å), Arg^{129} (1.81 Å), and Tyr^{130} (1.86 Å) consistent with a mode II binding motif (*33*).

Similar results were obtained for the 14-3-3σ/pThr^{17}-PLN complex (Fig. 4B, figs. S5E-G). The first cluster featuring a population of 45.6% of MD frames was taken as the most representative model (fig. S5H) for further investigation and comparison with the 14-3-3σ/pSer^{16}-PLN complex. The structure of both peptides in their respective 14-3-3σ complexes does not completely overlap because the first three helices of 14-3-3σ/pSer^{16}-PLN complex show a more opened conformation compared to those in the 14-3-3σ/pThr^{17}-PLN complex (Fig. 4C). Similar to pSer^{16}-PLN, pThr^{17}-PLN occupies the canonical central position in the amphipathic groove (*32, 33*) and establishes H-bond interactions with Lys^{49} (3.94 Å), Arg^{56} (1.83 Å), Arg^{129} (1.68 Å), and Tyr^{130} (1.64 Å). Notably, the spatially similar placement of pSer^{16} and pThr^{17} within the groove shifts the conformation of the rest of the PLN peptide. As a result, the remaining portion of the pThr^{17} phosphopeptide is elongated within the groove, placing Ile^{18}, Glu^{19}, and Met^{20} of PLN in different molecular environments as revealed by electrostatic rendering of 14-3-3 (Fig. 4A,B).

At least one arginine residue located at the -4, -3 or -2 position relative to the phosphoresidue is a key feature of the canonical 14-3-3-binding phosphopeptide motif (*34*). This residue stabilizes the phosphopeptide conformation by forming hydrogen bonds and intramolecular salt bridge with the phosphate group (*35*). In pSer^{16}-PLN, this role is taken by Arg^{14} in the -2 position (Fig. 4A) whereas Arg^{13} (-3 position) is pointing away from the phosphate group. In contrast, there is no arginine close to the phosphoresidue for pThr^{17}-PLN in complex with 14-3-3 (Fig. 4B). Instead, Arg^{14} is pointing away from the phosphoresidue consistent with some previously characterized 14-3-3σ/phosphopeptide complexes (*36*) and Arg^{13} contacts the solvent. Hence, its position is not reliable in the current model. Calculation of the peptide's delta energy of binding to 14-3-3σ along MD trajectories confirmed the binding assay data, showing that pThr^{17}-PLN has a greater affinity for the protein than the pSer^{16}-PLN peptide (-9.17 ± 2.17 kcal/mol and -4.43 ± 1.22 kcal/mol, respectively). Although the precise atomic determinants of the different stabilities await further characterization, modification of PLN by either PKA or CaMKII determines

the conformation in which 14-3-3 binds to the resulting phosphoform and therefore the stability of the complex.

Disease-causing ΔArg^{14} PLN recruits 14-3-3 exclusively through pThr^{17}

Arg^{13} and Arg^{14} are multifunctional residues in the PLN N-terminus because they are also essential elements of an Arg-based COPI-interacting motif (*18*). Indeed, ΔArg^{14} PLN leaves the endoplasmic reticulum (ER) whereas WT PLN is retained (*37*). In addition, Arg^{14} is crucial for the PKA consensus motif resulting in the phosphorylation of Ser^{16}. However, Arg^{14} is lost as a consequence of a tri-nucleotide deletion in an inherited form of dilated cardiomyopathy (DCM; (*5*)). We concluded that this disease-associated variant of PLN lacks the low-affinity 14-3-3 binding site provided by pSer^{16}-PLN (Fig. 3C, fig. S6). However, we found that the CaMKII-dependent binding site provided by pThr^{17} was not altered in this disease-causing variant because we observed robust phosphorylation and 14-3-3 binding to pThr^{17}-ΔArg^{14}-PLN (Fig. 4D). A second disease variant associated with familial forms of DCM is R9C (*7*), which is not predicted to participate directly in the 14-3-3-binding phosphopeptide motif. Accordingly, mutating Arg^{9} to cysteine or alanine did not affect the binding of pThr^{17}-PLN to 14-3-3 (Fig. 4D). These results imply that CaMKII-mediated phosphorylation of Thr^{17} is the only way by which PLN can recruit 14-3-3 in ΔArg^{14}-carrying patients.

14-3-3 slows the kinetics of PLN dephosphorylation

14-3-3 binding has been suggested to protect against dephosphorylation by steric masking (*23, 38*). We measured the effect of 14-3-3γ binding on the kinetics of the dephosphorylation. of immobilized pThr^{17}-PLN-GST or pSer^{16}-T17A-PLN-GST by alkaline phosphatase (Fig. 5A, fig. S7A). We observed a substantial increase in the lifetime of pThr^{17} or pSer^{16} when 14-3-3 was present (Fig. 5B, fig. S7B). Concomitantly with dephosphorylation, binding of 14-3-3 slowly decreased from either PLN phosphoform as expected (Fig. 5C,D, fig. S7A). We conclude that occupancy by 14-3-3 controls phosphatase access and thereby the lifetime of the posttranslational modification on either Ser^{16} or Thr^{17} of PLN.

Signal-transduction recruits 14-3-3 to PLN-containing membranes in cardiomyocytes

PLN is an abundant cardiac membrane protein and a major target of PKA-mediated regulation during β-adrenergic stimulation (*25*). To determine the cellular consequences of PLN phosphorylation and 14-3-3 binding, we stimulated β-adrenergic signal transduction in isolated adult rat cardiomyocytes using the agonist isoprenaline and assessed whether the predicted increase in pSer^{16}-PLN led to the recruitment of 14-3-3. The N-terminus of PLN is short and 14-3-3 may occlude the antibody epitope. Nevertheless, we generated a rabbit antibody that immunoprecipitated SDS-resistant PLN pentamers (Fig. 6A). Detection

of precipitated PLN used commercially available antibodies against PLN raised in mouse and against 14-3-3 raised in rabbit. In HeLa cell and total ventricular lysate, this antibody detected two bands most likely reflecting 14-3-3ε (its primary sequence is ~ten residues longer than that of all other isoforms (*39*)) (Fig. 6B). Untreated and isoprenaline-treated ventricular cardiomyocytes (Fig. 6C, panels labelled "total") showed comparable levels of PLN in the membrane fraction (Fig. 6D). Membranes from isoprenaline-treated cardiomyocytes showed a substantial increase in pSer^{16}-PLN (Fig. 6E) and modestly increased levels of 14-3-3 (Fig. 6F). We performed coimmunprecipitation experiments which suggested that endogenous PLN was associated with endogenous 14-3-3 proteins (Fig. 6C, panels labelled "IP: PLN"). Whether this association is direct cannot be definitively concluded from these experiments, although this interpretation is supported by the direct binding shown in vitro (Fig. 3C,D) and by the preferred binding of 14-3-3 dimers to SDS-resistant PLN pentamers, suggesting an avidity effect (Fig. 3A,B).

We sought to further corroborate the idea that isoprenaline stimulation resulting in an increase in pSer^{16}-PLN might elicit biological effects by 14-3-3 binding and ensuing stabilization of the phosphoform of PLN as observed in vitro (Fig. 5A). Adult cardiomyocytes were patch-clamped and Ca^{2+} transients evoked at 0.5 Hz (fig. S8A). As expected, acute (10 s) stimulation with the adrenergic agonist isoprenaline elicited an apparent accelerated recovery of Ca^{2+} transients as quantified by the time-constant tau of Ca^{2+} transient decay (fig. S8B) due to PKA-dependent PLN phosphorylation and SERCA stimulation. We dialyzed cells with an intracellular pipette solution containing recombinant 14-3-3γ, which slowed the recovery of the time-constant decay of the Ca^{2+} transients back to the baseline as observed before isoprenaline stimulation (Fig. 7A, fig. S8C,D). This effect was blocked by R18 (Fig. 7B) suggesting that it depended on the interaction of 14-3-3 with a target protein through its ligand-binding groove. To support the notion that this effect of 14-3-3 occurred through PLN and SERCA, we showed that in mouse myocytes at 35°C the contribution of the Na^{+}/Ca^{2+} exchanger is negligible and SERCA dominates the Ca^{2+} transient recovery (fig S8E-G).

To test whether the effect of 14-3-3γ on the recovery of the time-constant could be explained by binding to pSer^{16}-PLN, we compared the effect of two phospho-specific antibodies directed against pSer^{16}-PLN or pThr^{17}-PLN (Fig. 7C, fig. S1C,D). Although the latter did not affect recovery, the pSer^{16} antibody led to a prolonged slowing of the recovery of the time-constant, similar to that caused by 14-3-3γ. During isoprenaline stimulation, pSer^{16} PLN is expected to be the dominant phosphoform of PLN. Furthermore, pThr^{17}-PLN may already be saturated with endogenous 14-3-3 due to the higher binding affinity (Fig. 3E-H). We would predict that the pThr^{17} antibody or 14-3-3 would prolong the lifetime of

pThr^{17}-PLN and hence SERCA stimulation under conditions in which PLN becomes acutely and abundantly phosphorylated at this site. The comparison of the effect of the two antibodies during β-adrenergic stimulation and concomitant PKA activation suggests that pSer^{16}-dependent, acute recruitment of a large antibody protein or 14-3-3 to PLN can affect the biological outcome of β-adrenergic stimulation by prolonging the isoprenaline-stimulated state of SERCA in cardiomyocytes. Taken together, we predict that affinity and avidity effects combine to finetune the stability of PLN-14-3-3 complexes (Fig. 7D), resulting in different degrees of protection from phosphatase action.

Discussion

PLN is a key regulator of SERCA. Inherited disorders that result in PLN dysfunction demonstrate a critical role of this regulation in humans. Despite its short sequence, the N-terminus of PLN is emerging as a hub where interactions with proteins distinct from the kinases and phosphatases that modify PLN in response to cardiac signal transduction may enhance or attenuate PLN's potential to inhibit SERCA (*16*). We identified 14-3-3 phosphoadaptor proteins as PLN interactors through several independent lines of evidence. First, 14-3-3 affinity purification enriched SDS-resistant PLN pentamers from solubilized cardiac membranes (Fig. 1E, 3A). APEX2-peroxidase based proximity labelling demonstrated that 14-3-3 proteins are localized within nanometers of PLN in living cardiomyocytes (Fig. 2B). We coimmunoprecipitated PLN with 14-3-3 (Fig. 6C) from isolated cardiomyocytes. Although these complementary approaches do not demonstrate a direct interaction between PLN and 14-3-3, we argue that a direct interaction is plausible because Ser^{16} and Thr^{17} are located in putative 14-3-3 binding sites (*18, 34*), because we showed a direct interaction in a phosphorylation dependent manner (Fig. 3C,G), and because MD simulations yielded plausible structural models for the respective PLN-derived phosphopeptide in the ligand-binding groove of 14-3-3 (Fig. 4A-C).

14-3-3 proteins are dimeric and, hence, susceptible to avidity effects when binding to multimeric targets. Indeed, we found that SDS-resistant pentameric but not monomeric PLN bound 14-3-3 when phosphorylated by PKA (Fig. 1E, 3A). The SDS-resistant PLN pentamers were previously interpreted to be proxies of physiological pentamers (*9*,*14*). Even if our binding experiment performed in a mild detergent (ComplexioLyte48) and subsequent analysis by SDS-PAGE captured only a fraction of all PLN pentamers, the experiment showed unequivocally that PLN pentamers can recruit 14-3-3. However, we reconstituted the interaction between CaMKII-phosphorylated PLN and 14-3-3 using a recombinant non-oligomeric protein (Fig. 3G,H). Hence, we propose a model (Fig. 7D) in which the relative abundance of $pSer^{16}$ and $pThr^{17}$ phosphosites determines the occupancy of PLN pentamers by 14-3-3. Acute PKA-mediated phosphorylation of PLN during β-adrenergic stimulation is expected to raise the apparent affinity for 14-3-3. Indeed, we observed prolonged SERCA activity due to 14-3-3 binding after β-adrenergic stimulation in cardiomyocytes (Fig. 7A). Because 14-3-3 binding slowed the dephosphorylation of PLN phosphosites *in vitro* (Fig. 5A,B, fig. S8C,D), we propose that the biological effects of 14-3-3 binding are due to blocking the access of PP1c to the phosphosite thereby maintaining PLN in the inactive, phosphorylated and SERCA in the active state. Consistently, we mimicked the effect of 14-3-3 after acute β-adrenergic

stimulation in cardiomyocytes by the addition of a specific anti-pSer^{16}-PLN antibody (Fig. 7C). Binding of 14-3-3 dimers to the pSer^{16}-PLN pentamers may also stabilize the pentameric form of PLN and hence reduce the pool of monomeric form that is thought to be the major species that inhibits SERCA (*15*).

The affinity of the respective protein-protein interaction between 14-3-3 and pSer^{16}- or pThr^{17}-PLN translates into a molecular "memory" of which kinase created the 14-3-3 binding site on PLN. At the molecular and atomic level, this memory is because the respective phosphoresidues, which are specific products of either PKA or CaMKII, fit into the same position of the 14-3-3 ligand-binding groove (Fig. 4A,B). Consequently, the surrounding side chains of the PLN N-terminus slot into different, energetically more or less favorable positions of the binding groove. For example, comparison of pSer^{16}-PLN with pSer^{16}-T17A-PLN (Fig. S5) indicated that the side chain of Thr^{17} reduced the energy of binding when Ser^{16} was phosphorylated. When Thr^{17} was phosphorylated, Ile^{18} occupied the corresponding position, which avoided placing the polar side chain of Thr^{17} in this environment and hence resulted in an energetically more favorable fit.

Biologically, a shorter memory for PKA-mediated phosphorylation is consistent with the role of this modification in the acute and reversible adaptation of intracellular Ca^{2+} handling to the cAMP signal elicited by β-adrenergic agonists. CaMKII activation in cardiomyocytes integrates changes in intracellular Ca^{2+} concentrations and other parameters such as redox potential (*40*). In fact, CaMKII activity can become independent of acute changes in intracellular Ca^{2+}. The kinase has many targets in addition to intracellular Ca^{2+} handling proteins, such as ion channels that control cardiomyocyte excitation and proteins that mediate the transcriptional activation of a hypertrophic gene program. The slower effects of CaMKII on gene expression could represent a biological rationale for the longer-lasting memory associated with PLN modification by CaMKII kinase, which translates to a higher affinity of 14-3-3 binding to pThr^{17}-PLN. This mechanism may ensure the adaptation of intracellular Ca^{2+} handling to the hypertrophic state. Expression of CaMKII itself is elevated in heart failure (*41*) and the kinase has attracted attention as a potential therapeutic target (*42*). Our insight into CaMKII-dependent 14-3-3 recruitment to PLN may help to understand the effects of CaMKII inhibitors that are currently under development.

Two forms of genetic PLN-dependent DCM alter the N-terminus of PLN with different effects on phosphorylation and 14-3-3 binding. Our data can therefore help to extend current models (*7, 43, 44*) of the molecular basis of ΔArg^{14}- and R9C-PLN. On the one hand, ΔArg^{14}-PLN cannot be modified by PKA (fig. S6) and hence lacks the low-affinity 14-3-3 binding mode. This may make CaMKII activation upon sustained β-adrenergic

stimulation and 14-3-3 binding to PLN through pThr^{17} more crucial. On the other hand, the introduction of a reactive cysteine side chain instead of Arg^{9} leads to disulfide bridges that stabilize the PLN pentamer and render it less accessible to PKA (*44*). Access of 14-3-3 to the pertinent phosphopeptide in such disulfide-stabilized PLN pentamers would also be impaired resulting in an inability to differentially stabilize the pentamer according to kinase action. The precise consequences of either DCM mutation on 14-3-3 recruitment to PLN will have to be biochemically investigated in the corresponding heterozygous disease models.

In conclusion, PLN represents yet another fascinating example in which the action of 14-3-3 proteins modulates the outcome of signal transduction events by recognizing the phosphorylation and oligomerization state of a target protein. Steric masking of the phosphosite and potentially stabilization of the pentamer through 14-3-3 binding may influence not only the access of other proteins such as phosphatases, but also the dynamics of PLN itself. In line with the different delta energies of binding in the two molecular registers of 14-3-3 binding, these effects and their duration seem to be finetuned according to the kinase that modified PLN.

Materials and Methods

Purification of proteins

Recombinant Gluthathione-S-transferase (GST)- or Maltose binding protein (MBP)-tagged proteins (expressed from the plasmids listed in supplementary table S1) were expressed and purified from *E. coli* strain BL21 Rosetta. Protein expression was induced in 2YT media (2YT mix, AppliChem) using 1 mM isopropyl-beta-D-thiogalactopyranosid (IPTG) for 3 h at 30°C. Cells were harvested and lysed in GST buffer (20 mM HEPES pH 6.8, 150 mM KOAc, 5 mM $Mg(OAc)_2$, 1 mM ethylenediaminetetraacetic acid (EDTA), 1 mM dithiothreitol (DTT), 1 mM phenylmethylsulfonyl fluoride (PMSF), pH 6.8). Crude cell lysate was centrifuged at 100.000 g for 30 min at 4°C. The supernatant was incubated with 1 ml washed glutathione sepharose beads (GE Healthcare) for GST-tagged proteins or 1 ml amylose resin (New England Biolabs) for MBP-tagged proteins for 1h at 4°C under gentle rotation. The bead slurry was transferred to gravity columns and washed with 3 column volumes GST buffer pH 7.4, followed by one column volume of 1 mM adenosine triphosphate (ATP) in GST buffer pH 7.4 and a final wash step in GST buffer pH 7.4. Bound GST-tagged proteins were eluted with GST elution buffer (20 mM HEPES pH 6.8, 150 mM KOAc, 5 mM $Mg(OAc)_2$, 1 mM EDTA, 1 mM DTT, 15 mM L-Glutathione, pH 8.5), meanwhile bound MBP-tagged proteins were eluted with MBP elution buffer (20 mM HEPES pH 6.8, 150 mM KOAc, 5 mM $Mg(OAc)_2$, 1 mM EDTA, 1 mM DTT, 20 mM D-Maltose, pH 7.5). The MBP-tag was cleaved with FactorXa enzyme for 16 h at 25°C according to the supplier's recommendation (Merck MilliPore). After cleavage, proteins were separated by size exclusion chromatography on an Äkta purifier (GE Healthcare) and a Superdex75 size exclusion column in GST buffer pH 7.5.

Heart membrane preparation

Mice hearts were defrosted on ice, fat tissue was removed, and mice hearts were washed in tissue homogenization buffer (50 mM NaCl, 320 mM Sucrose, 2 mM EDTA, 20 mM HEPES, pH 7.4) supplied with protease and phosphatase inhibitors (Roche). Hearts were cut into small pieces and lysed with a MiccraD-1 homogenizer for 30 sec followed by douncing for 30 strokes. Cytosol and membranes were separated by centrifugation at 100.000 g for 30 min at 4°C. The supernatant was the cytosolic fraction. The purified membrane fraction was resuspended once, washed in homogenization buffer, and collected by centrifugation at 100.000 g for 30 min.

Heart membrane solubilization

Purified heart membranes were solubilized in ComplexioLyte 48 (Logopharm) buffer for 30 min on ice. 1 ml ComplexioLyte 48 was used to solubilize membranes with a protein content of 1 mg. Solubilized membranes were centrifuged for 30 min at 55.000 g, 4°C. The supernatant contained solubilized proteins which were used for pull-down experiments or trichloroacetic acid (TCA) precipitated for Western blot analysis.

Separation of PLN pentamer into monomer in cardiac membranes by heating

Mouse heart membranes were purified as described above. Solubilized mouse heart membranes were diluted 1:5 in GST buffer (20 mM HEPES pH 6.8, 150 mM KOAc, 5 mM $Mg(OAc)_2$, 1 mM EDTA, 1 mM DTT, pH 7.4) supplemented with protease and phosphatase inhibitors and divided into two Eppendorf tubes. One tube was stored on ice meanwhile the other one was heated at 75°C for 20 min. After heating, the membranes were

centrifuged at 20.000 g for 10 min at 4°C. Both solubilizes membrane preparations were used as inputs for pull-down experiments (Fig. 3 A,B).

Phos-tag polyacrylamide gel electrophoresis (PAGE)

Phos-tag acrylamide (NARD institute) was used at a concentration of 5 µM according to the supplier's information.

Western Blot detection

Primary antibodies were diluted 1:1000 in blocking buffer (5% w/v milk powder, 1x TBS, 0,1% Tween) and incubated overnight at 4°C or for 2-3 h at room temperature (RT). Western blots were imaged with an LICOR Odyssey CLx imaging system using IRDye LICOR secondary antibodies. Secondary antibodies were diluted 1:10.000 in blocking buffer and incubated for 1h at room temperature.

14-3-3γ pull-down experiments from mouse cardiac membranes and cytosol

Solubilized cardiac membranes or cytosol and recombinant purified MBP, or MBP-14-3-3γ bait protein was used for pull-down experiments. 50 µg MBP or MBP-14-3-3γ protein was immobilized to 5 µl amylose resin bead slurry (New England Biolabs) in GST buffer (20 mM HEPES pH 6.8, 150 mM KOAc, 5 mM $Mg(OAc)_2$, 1 mM EDTA, 1 mM DTT, pH 7.5) supplied with protease and phosphatase inhibitors for 45 min at 4°C under gentle rotation. Immobilized bait protein was washed 3 times in GST buffer, followed by blocking in 4% bovine serum albumin (BSA) dissolved in GST buffer and supplied with protease and phosphatase inhibitors for 30 min at 4°C under gentle rotation to block unspecific binding sites. For the MBP-14-3-3γ protein, which was blocked with R18 trifluoroacetate inhibitor, 5 µM R18 trifluoroacetate was supplied during immobilization and blocking. After blocking, the resin-bound bait proteins were washed 3 times in GST buffer and added to prepared solubilized cardiac membranes or cytosol, which were previously diluted 1:5 in GST buffer pH 7.5. After 1 h incubation at 4°C under gentle rotation, the resin-bound 14-3-3 was washed 4 times in GST buffer followed by elution with 1x SDS sample buffer (containing 100 mM DTT). The pull-down experiment was analyzed by SDS-PAGE or Phos-tag-PAGE followed by silver staining or Western blot detection using primary antibodies described in supplementary table S2.

APEX2 proximity labeling in neonatal rat cardiomyocytes

Neonatal rat cardiomyocytes (NRCMs) were isolated from 0 to 3 days old Wistar rats and $5x10^5$ cells per well were seeded on 6-well plates. NRCMs were cultivated in heavy, medium and light (Eurisotop) SILAC medium (Thermo Fisher Scientific) under humidified conditions at 37 °C. After 13 days, NRCMs were transduced with adenoviral vectors (V5-APEX2-PLN, V5-APEX2-PLN(Δ1-29), or eGFP) with a MOI of 10 for 48 h. The proximity labeling was conducted as described elsewhere (*45*). Briefly, the cells were incubated for 30 min with 0.5 mM biotinphenol at 37 °C followed by 1 mM H_2O_2 for 1 min at room temperature. Cells were washed with quenching buffer (5 mM Trolox, 10 mM NaN_3, 10 mM Na-ascorbate in PBS) and harvested in RIPA buffer (0.5 % Na-deoxycholate, 50 mM Tris/HCl pH 7.5, 150 mM NaCl, 0.2 % SDS, 1 % Triton, 10 mM NaN_3, 5 mM Trolox, 10 mM Na-ascorbate, 1 mM PMSF, complete mini). Cells were lysed by passing 10 times through a 27 G needle and centrifuged at 13000 x g for 10 min. Protein concentrations were determined with the Pierce 660 nm Protein Assay Kit (Thermo Fisher Scientific). The lysates of heavy, medium and light labelled NRCM were mixed in a ratio of 1:1:1 for a total of 250 µg protein. Biotinylated proteins were enriched by avidin pulldown assay (Thermo

Fisher Scientific). Eluted proteins were analysed by LC-MS/MS and MaxQuant. For quantification, log_2 fold changes of ratios of PLN/eGFP and PLN/PLN(Δ1-29) were calculated and proteins that differed positivly from 0 according to a one sample t-test ($p<0.01$) were plotted. The experiment was conducted in three biological and two technical replicates with label switch.

LC-MS/MS analysis

Proteins were separated on 4-12 % Bis-Tris Minigels, visualized with Coomassie blue stain and sliced into 11 sections of equal size regardless of staining. After reduction with DTT, alkylation with 2-iodoacetamide, and overnight digestion with trypsin, digest peptides mixtures were extracted and dried in a speedvac (*46*). For mass spectrometric (MS) analysis, samples were enriched on a self-packed reversed phase-C18 precolumn (0.15 mm ID x 20 mm, Reprosil-Pur120 C18-AQ 5 µm, Dr. Maisch) and separated on an analytical reversed phase-C18 column (0.075 mm ID x 200 mm, Reprosil-Pur 120 C18-AQ, 3 µm, Dr. Maisch) using a 30 min linear gradient of 5-35 % acetonitrile/0.1% formic acid (v:v) at 300 nl min-1). The eluent was analyzed on a Q Exactive hybrid quadrupole/orbitrap mass spectrometer (ThermoFisher Scientific) in data-dependent acquisition mode. Each experimental cycle contained a full MS scan (350-1600 *m/z*, resolution setting 70,000 FWHM, AGC target 1*10e6, maximum fill time of 60 ms) and up to 12 MS/MS experiments (z=2-5, 2*10e4 trigger threshold, dynamic exclusion window 15 s, 2.0 FWHM isolation width, normalized collision energy 25%, resolution setting 17,500 FWHM, AGC target 2*10e5, maximum fill time 60 ms). Two technical replicates per sample were acquired. Raw data were processed using MaxQuant Software version 1.5.2.8 (Max Planck Institute for Biochemistry). The arginine R10/R6 and lysine K8/K4 labels including the 're-quantify' option were specified for relative protein quantitation.

Immunofluorescence

NRCMs were isolated from 1 to 3 days old Wistar rats and plated on coverslips coated with collagen. After 15 days of cultivation and 48 h post transduction cells were fixed in 4 % PFA for 5 min. Next, cells were incubated in blocking/permeabilization buffer for 4 h (10 % bovine calf serum, 0.2 % Triton in PBS). Primary antibodies were diluted in blocking buffer and incubated over night at 4 °C as follows: V5 1:1000 (R960-25, Invitrogen); SERCA2a 1:500 (A010-20, Badrilla). Subsequently, samples were washed three times in blocking buffer and incubated with secondary antibodies diluted 1:1000 and incubated over night at 4 °C: anti-mouse (Alexa Fluor 568, Thermo Fisher Scientific) and anti-rabbit (Alexa Fluor 633, Thermo Fisher Scientific). After washing, samples were embedded in mounting medium (ProLong Gold antifade reagent, Thermo Fisher Scientific). For imaging we used a Zeiss LSM 880 system with a Plan-Apochromat 63x/1.4 Oil DIC objective. Raw images were processed in ImageJ/Fiji (http://imagej.nih.gov/if/).

Binding assay using purified PLN-GST constructs and 14-3-3γ

10 µg purified PLN-GST variants were phosphorylated with recombinant PKA catalytic subunit (New England) or CaMKII (delta) kinases (Thermo Fisher Scientific) accordingly to the supplier's information at 30 °C for 1 h. Phosphorylated bait proteins were bound to 5 µl glutathione sepharose beads (GE Healthcare) in GST buffer (20 mM HEPES, 150 mM KOAc, 5 mM $Mg(OAc)_2$, 1 mM EDTA, 1 mM DTT, 0.1% TritonX-100, pH 7.5) for 45 min at 4°C under gentle rotation. Resin-bound bait proteins were incubated with equimolar amounts of recombinant purified 14-3-3γ protein in GST buffer for 1 h at 4°C under gentle rotation. The resin-bound bait was washed 4 times in GST buffer and eluted in 1 x SDS sample buffer (supplied with 100 mM DTT). The binding assay was analyzed on SDS-

PAGE which was transferred to nitrocellulose and probed with the indicated primary antibodies (compare Supplementary Table S2). Phosphorylation of bait proteins was analysed on Coomassie stained Phos-tag-PAGE and SDS-PAGE gels.

Surface Plasmon Resonance

Binding affinities of recombinant 14-3-3γ protein to the cytosolic domain of recombinant purified PLN-GST were determined with surface plasmon resonance (SPR). SPR experiments were carried out on a Reichert SR 7500DC biosensor instrument at 20°C and a flow rate of 40 µl/min in SPR buffer (150 nM NaCl, 20 mM HEPES, 0,005% (v/v) Tween 20, pH 7.5). All experiments were done in a buffer containing 20 mM HEPES pH 7.5, 150 mM NaCl, 0.005% Tween-20 (*v*/*v*). A HC-1000 SPR sensor chip was activated with 1-ethyl-3-83-dimethylaminopropyl)-carbodiimide and N-hydroxysuccinimide (EDC-NHS) (Xantec Biotechnologies) according to the supplier's instruction. Followed by covalent binding of a GST antibody (Carl Roth, 3998.1) to the chip surface at a flow rate of 15 µl/min and a concentration of 30 µg/ml to a surface density of 4000-8000 µRIU (refractive index units, depending on the maximal capacity of each chip). After antibody coupling, the chip surface was deactivated by quenching with 1 M ethanolamine pH 8.5 for 180s at a flow rate of 30 µl/min. PLN-GST fusion proteins were phosphorylated with recombinant PKA catalytic subunit (New England Biolabs) or CaMKII (delta) (Thermo Fisher Scientific) kinase according to the manufacturer's instruction for 1 h at 30°C and immobilized to the chip surface at a flow rate of 30 µl/min and to a surface density of 200-400 µRIU. The 14-3-3γ analyte was serially diluted and injected over the sensor chip surface at a flow rate of 40 µl/min. Association was done for 4.5 min and dissociation was subsequently done for 7 min. The dilution series ranged from 0.390 mM to a final concentration of 50 µM. Data analysis was performed with Scrubber 2.0c. Equilibrium binding isotherms were analysed with GraphPad Prism 6.0.

Cardiomyocytes isolation and stimulation with isoprenaline

All animal procedures were reviewed and approved by the Institutional Animal Care and Use Committees of the University Medical Center Göttingen in compliance with the humane care and use of laboratory animals. Hearts were perfused by Langendorff solution (120.4 mM NaCl, 17.7 mM KCl, 0.6 mM KH_2Po_4, 0.6 mM Na_2HPO_4, 1.2 mM $MgSO_4$, 10 mM HEPES, 4.6 mM $NaHCO_3$, 30 mM taurine, 10 mM 2,3-butanedione-monoxime, 5.5 mM glucose, pH 7.4) with a flow of 4 ml/min for a period 4 min at 37°C. To digest the tissue the heart was perfused with perfusion buffer supplemented with collagenase type II (2 mg/ml) and $CaCl_2$ (40 µM) for 8 min. The heart was removed from the Langendorff perfusion apparatus, placed in collagenase solution and the tissue was mechanically disrupted with a scissor and by resuspension with a pipette. The collagenase was stopped with bovine calf serum (10%) and $CaCl_2$ (12.5 µM). Isolated cardiomyocytes were collected by filtration with a 100 µM cell sieve and centrifugation at 22 g for 1.5 min. Isolated cardiomyocytes from one animal were split into two Eppendorf tubes in experimental buffer (10 mM HEPES, 136 mM NaCl, 40 mM KCl, 1 mM $MgCl_2$, 10 mM Glucose, 1 mM $CaCl_2$, pH 7.35) and one tube was treated with 100 nM isoprenaline for 30 sec meanwhile the other was not treated. After isoprenanline stimulation the cells were collected by centrifugation and resuspend in sucrose homogenization buffer ((50 mM NaCl, 320 mM Sucrose, 2 mM EDTA, 20 mM HEPES, pH 7.4) supplied with protease and phosphatase inhibitors (Roche) and stored at -80°C.

Immunoprecipitation

Isoprenanline (100 nM, 30 sec) stimulated cardiomyocytes were thawed and membranes were separated as described above (see heart membrane preparation). Cardiomyocytes were lysed and crude membranes were separated from the cytosolic fraction by centrifugation. Purified membranes were washed and solubilized in 500 µl ComplexioLyte 48 (Logopharm) for 30 min on ice. After solubilization the samples were centrifuged at 55.000 g for 30 min at 4°C. 30% of the solubilized membrane fraction was removed and complemented with 5x SDS sample buffer (250 mM Tris-HCl pH 6.8, 10% SDS, 0.5% bromphenolblue, 50% glycerol) to a final concentration of 1 x and analysed by Western blotting detecting the indicated antigens using primary antibodies listed in supplementary table S2. The remaining solubilized membranes were diluted 1:5 in GST buffer (20 mM HEPES pH 6.8, 150 mM KOAc, 5 mM $Mg(OAc)_2$, 1 mM EDTA, 1 mM DTT, pH 7.5) and 5 µl PLN total antibody (r-IgG) was added. The antibody was incubated for 4 h at 4°C under gentle rotation. Washed Sepharose A (GE Healthcare) was added to the samples and incubated overnight at 4°C under gentle rotation. Finally, the beads were washed 2 times in GST Buffer and eluted in 1 x SDS sample buffer. The SDS sample buffer was not supplemented with DTT to avoid reducing conditions. The samples were separated on SDS-PAGE gels, transferred to nitrocellulose, and analysed using the indicated primary antibodies.

Dephosphorylation of $pThr^{17}$- or $pSer^{16}$-T17A-PLN-GST with or without bound 14-3-3γ

10 µg recombinant purified PLN-GST protein was used per sample and time point. Bait protein was phosphorylated with CaMKII kinase (delta) (Thermo Fisher Scientific) or PKA (New England Bioland) accordingly to the supplier's information at 30°C for 1 h. Phosphorylated recombinant protein was bound to 5 µl glutathione sepharose beads (GE Healthcare) in GST buffer (20 mM HEPES pH 6.8, 150 mM KOAc, 5 mM $Mg(OAc)_2$, 1 mM EDTA, 1 mM DTT, 0.1% TritonX-100, pH 7.5) for 45 min at 4°C under gentle rotation followed by 3 wash steps in GST buffer. The immobilized bait protein was divided in two Eppendorf tubes. To one tube equimolar amounts of recombinant purified 14-3-3γ protein was added in GST buffer and allowed to bind for 1 h at 4°C under gentle rotation. After binding, the bait proteins were washed 4 times in GST buffer. The resin-bound proteins were transferred to alkaline phosphatase buffer (Thermo Fisher Scientific) and treated with 8 units alkaline phosphatase (Fast AP, Thermo Fisher Scientific) according to the supplier's information for 0, 5, 10, 25 min at 30°C. After each incubation time point, the resin-bound bait protein was washed two times in GST buffer and eluted in 1 x SDS sample buffer (supplied with 100 mM DTT). The experiment was analyzed on SDS-PAGE or Phos-tag-PAGE. SDS-PAGE were transferred to nitrocellulose membranes and analysed for $pSer^{16}$ or $pThr^{17}$-PLN as appropriate using the antibodies listed in Supplementary Table S2. Phos-tag gels were stained with Coomassie.

Mouse cardiomyocyte isolation and cell culture for patch-clamp experiments

Cells were isolated from hearts of 9-11 week old male mice (c57bl6) by standard collagenase digestion as previously described (*47*). All animal procedures were reviewed and approved by the Institutional Animal Care and Use Committees of King's College London in compliance with the humane care and use of laboratory animals. Myocytes were pelleted by gravity and washed at room temperature with modified M199 (Earle's Salts) culture medium (Thermo Fisher Scientific) containing (per 500ml bottle): 0.113g creatine; 0.313g taurine; 0.198g carnitine; 5ml penicillin/streptomycin (final concentration 1%). Cells were then pelleted, re-suspended in fresh media and transferred to laminin covered coverslips (15mm diameter No1) in 12-well plates at an approximate final density of 150

myocytes/coverslip. Cells were incubated for 24 hours (37°C, 5% CO_2) prior to use in electrophysiological experiments.

Measurement of intracellular [Ca^{2+}] and patch-clamp Experiments

Membrane currents were measured at 35°C in whole-cell ruptured-patch configuration using voltage-clamp with simultaneous intracellular Ca^{2+} measurement as previously described (*48*). Patch-Clamp experiments were performed using an Axopatch 200B amplifier, Digidata 1322A data acquisition and pClamp9.2 software (Molecular Devices, Sunnyvale, CA). Borosilicate glass microelectrodes had tip resistances of 1-2 MΩ when filled with pipette solution containing (in mmol/L): EGTA 0.024, Fluo-3 0.025, GTP-Tris 0.1, HEPES 10, K-aspartate 92, KCl 48, Mg-ATP 1, Na2-ATP 4; (pH=7.25 at 35°C). During experiments myocytes were superfused at 35°C with a Tyrode's containing (in mmol/L): $CaCl_2$ 1, glucose 10, HEPES 10, KCl 4, $MgCl_2$ 1, NaCl 136, probenecid 2; (pH=7.35 at 35°C). Cells were kept at a holding potential of -80mV and Ca^{2+} transients were stimulated through the pipette at 0.5 Hz as previously described [2]. In addition to including Fluo3 in the pipette solution, myocytes were also pre-incubated with Fluo-3-acetoxymethyl ester (Fluo3 AM; Invitrogen, Thermo Fisher Scientific; 1 mM solution in DMSO). Briefly, the cardiomyocyte staining solution was prepared by adding 5 µl of 1 mmol/l Fluo3 solution (in DMSO) to 1 ml of bath solution and 160 µl deionised water to limit the osmotic effects of DMSO. Cardiomyocytes were incubated in staining solution for 40 minutes followed by washing in bath solution (20 min) before use in voltage-clamp experiments. Optical measurements were performed using an Evolve 512 camera (Photometrix) and PTI EasyRatio Pro software (HORIBA Scientific). To avoid over-loading the computer memory (due to high speed acquisition at ~200 Hz), Ca^{2+} transients were recorded in groups of 5 interspersed by 40 s intervals during which cells were continuously paced but data were not recorded. Purified 14-3-3γ (2 µM) or 14-3-3γ (2 µM blocked with R18 peptide as described for the pull-down assay) in other experiments 2.5 µg/ml of either anti-Ser[16] or anti-Thr[17] antibody was added to the in intracellular pipette solution and dialyzed into the cell interior.

Data analysis and statistics

In mouse myocytes the contribution of Na^+/Ca^{2+} exchange to the recovery of the Ca^{2+} transient is minimal. Li *et al* using mouse myocytes at 23^{o}C estimate that SERCA is responsible for 90% of the Ca^{2+} transient recovery, with Na^+/Ca^{2+} exchange contributing only 9% (*49*). In our studies at 35^{o}C (at which active processes may be even more dominant), we found that the rapid removal of extracellular Na^+ (<50msec exchange time) prior to a Ca^{2+} transient did not affect the recovery of the transient (see Figure S8G). This finding suggested that at 35^{o}C the recovery of the Ca^{2+} transient was dominated by SERCA. This recovery phase could therefore be accurately described by a single exponential fit and the time-constant of this Ca^{2+} transient recovery (t) could be used as an index of SERCA activity. Ca^{2+} transients were automatically fitted using custom software written in Matlab (MathWorks, Inc, USA). Time-constants obtained for each of 5 sequential Ca^{2+} transients in each group were averaged to get a single τ value at each time point. To minimise differences caused by cell variability data obtained in each individual cell were normalized to the maximum response amplitude. Differences between experimental groups were tested with two-way ANOVA mixed model test, followed by a Tukey's multiple comparison test.

Computational modelling

The 3D structure of 14-3-3σ in complex with pSer[16]-PLN peptide (RRApSTIEMP – Uniprot identifier P26678) was generated by homology modelling using the PrimeX software, version v5.5 (Schrodinger (*50*)). Input coordinates of the template systems were retrieved

from PDB codes 3MHR and 4DAT that contain the phosphopeptides complexed to 14-3-3σ. With the purpose of modelling the longest peptide sequence, amino acids from the C-terminus to the phosphosite and from the phosphosite to the N-terminus were taken from 4DAT and 3MHR respectively. The homology model was relaxed through molecular dynamics (MD) simulations carried out by Amber18 program. The force field ff14SB (*51*) was used to parametrize protein and peptide while the general amber force field (GAFF) was used for non-standard residues. Parameters for the phosphoserine residue were retrieved from the AMBER Parameter Database (*52*). For MD simulation purposes the system was solvated in a cubic box of TIP3P water molecules buffering 10 Å from the surface. Periodic boundary conditions were applied. In order to keep the system electrically neutral, the total charge was neutralized by the addition of Na^+ counter-ions. Following previous work (*53, 54*), the solvent and Na^+ ions were energy-minimized for 1500 steps using the steepest descent (SD) algorithm and a further 3500 steps using the conjugate gradient (CG) algorithm while keeping the solute as fixed. The solvated solute was then energy-minimized for 1500 steps using the SD and 3500 steps using the CG before being heated at constant volume using the Langevin thermostat from 0 to 300 K over 150 ps. A density equilibration was carried out at constant pressure (NPT ensemble) for 150 ps, before running the production of unbiased MD trajectories for 250 ns (timestep was 2 fs). MD trajectories were processed by the cpptraj software (*55*) and analysed in terms of root mean square deviation (RMSD) or residue fluctuation (RMSF) and cluster analysis. The same parameters were used to relax the *apo* 14-3-3σ by MD simulations. The same procedure as described above was used to generate the 3D structure of 14-3-3σ in complex with $pThr^{17}$-PLN peptide (RASpTIEMP). Electrostatic surface potential was computed with APBS version 27 (*56*) and visualized in VMD molecular graphic software (*57*). The delta energy of binding was computed by the Molecular Mechanics Poisson-Boltzmann Surface Area (MM-PBSA) approach using the MMPBSA.py script in AMBER18 (*58*). Theoretical affinity results are presented as the delta energy of binding +/- standard error of the mean (SEM) (*59*).

Supplementary Materials

fig. S1. Cardiac cytosolic fractions do not show a signal for 14-3-3-bound PLN.

fig. S2. Confocal imaging showing the colocalization of APEX2-PLN or APEX2-PLN (Δ1-29) and SERCA2a in NRCMs.

fig. S3. All seven 14-3-3 isoforms bind pThr^{17}-PLN-GST.

fig. S4. Determination of the equilibrium dissociation constant for 14-3-3 binding to pThr^{17}-PLN.

fig. S5. MD simulation of the 14-3-3σ-pSer^{16}-PLN complex and the 14-3-3σ-pThr^{17}-PLN complex.

fig. S6. PKA does not phosphorylate ΔArg^{14}-PLN monomers.

fig. S7. 14-3-3 binding protects pSer^{16}-T17A-PLN protects from fast dephosphorylation.

fig. S8. Effect of 14-3-3 and Na^+-free superfusion on the kinetics of isoprenaline-induced Ca2+ transients in isolated cardiomyocytes.

table S1. Plasmids used in this study.

Table S2. Antibodies used in this study.

Data File S1. Biotinylated proteins detected by *in-vivo* proximity labelling using V5-APEX2-PLN.

References and Notes

1. D. M. Bers, Cardiac excitation-contraction coupling. *Nature* **415**, 198-205 (2002).
2. K. M. Alsina *et al.*, Loss of Protein Phosphatase 1 Regulatory Subunit PPP1R3A Promotes Atrial Fibrillation. *Circulation*, (2019).
3. A. G. Brittsan, A. N. Carr, A. G. Schmidt, E. G. Kranias, Maximal inhibition of SERCA2 Ca(2+) affinity by phospholamban in transgenic hearts overexpressing a non-phosphorylatable form of phospholamban. *J Biol Chem* **275**, 12129-12135 (2000).
4. W. Luo *et al.*, Targeted ablation of the phospholamban gene is associated with markedly enhanced myocardial contractility and loss of beta-agonist stimulation. *Circ Res* **75**, 401-409 (1994).
5. K. Haghighi *et al.*, A mutation in the human phospholamban gene, deleting arginine 14, results in lethal, hereditary cardiomyopathy. *Proc Natl Acad Sci U S A* **103**, 1388-1393 (2006).
6. K. Haghighi *et al.*, Human phospholamban null results in lethal dilated cardiomyopathy revealing a critical difference between mouse and human. *J Clin Invest* **111**, 869-876 (2003).
7. J. P. Schmitt *et al.*, Dilated cardiomyopathy and heart failure caused by a mutation in phospholamban. *Science* **299**, 1410-1413 (2003).
8. E. G. Kranias, R. J. Solaro, Phosphorylation of troponin I and phospholamban during catecholamine stimulation of rabbit heart. *Nature* **298**, 182-184 (1982).
9. A. D. Wegener, H. K. Simmerman, J. P. Lindemann, L. R. Jones, Phospholamban phosphorylation in intact ventricles. Phosphorylation of serine 16 and threonine 17 in response to beta-adrenergic stimulation. *J Biol Chem* **264**, 11468-11474 (1989).
10. W. Luo *et al.*, Transgenic approaches to define the functional role of dual site phospholamban phosphorylation. *J Biol Chem* **273**, 4734-4739 (1998).
11. D. H. MacLennan, E. G. Kranias, Phospholamban: a crucial regulator of cardiac contractility. *Nat Rev Mol Cell Biol* **4**, 566-577 (2003).
12. G. Chu *et al.*, A single site (Ser16) phosphorylation in phospholamban is sufficient in mediating its maximal cardiac responses to beta -agonists. *J Biol Chem* **275**, 38938-38943 (2000).
13. M. Gustavsson *et al.*, Allosteric regulation of SERCA by phosphorylation-mediated conformational shift of phospholamban. *Proc Natl Acad Sci U S A* **110**, 17338-17343 (2013).
14. C. F. Louis, M. Maffitt, B. Jarvis, Factors that modify the molecular size of phospholamban, the 23,000-dalton cardiac sarcoplasmic reticulum phosphoprotein. *J Biol Chem* **257**, 15182-15186 (1982).
15. D. R. Singh *et al.*, Newly Discovered Micropeptide Regulators of SERCA Form Oligomers but Bind to the Pump as Monomers. *J Mol Biol* **431**, 4429-4443 (2019).
16. K. Haghighi, P. Bidwell, E. G. Kranias, Phospholamban interactome in cardiac contractility and survival: A new vision of an old friend. *J Mol Cell Cardiol* **77**, 160-167 (2014).
17. E. Vafiadaki, D. A. Arvanitis, D. Sanoudou, E. G. Kranias, Identification of a protein phosphatase-1/phospholamban complex that is regulated by cAMP-dependent phosphorylation. *PLoS One* **8**, e80867 (2013).
18. E. C. Arakel *et al.*, Tuning the electrical properties of the heart by differential trafficking of KATP ion channel complexes. *J Cell Sci* **127**, 2106-2119 (2014).
19. A. Aitken, 14-3-3 proteins: a historic overview. *Semin Cancer Biol* **16**, 162-172 (2006).
20. M. K. Dougherty, D. K. Morrison, Unlocking the code of 14-3-3. *J Cell Sci* **117**, 1875-1884 (2004).

21. C. Mackintosh, Dynamic interactions between 14-3-3 proteins and phosphoproteins regulate diverse cellular processes. *Biochem J* **381**, 329-342 (2004).
22. K. Michelsen, H. Yuan, B. Schwappach, Hide and run. Arginine-based endoplasmic-reticulum-sorting motifs in the assembly of heteromultimeric membrane proteins. *EMBO Rep* **6**, 717-722 (2005).
23. A. J. Smith, J. Daut, B. Schwappach, Membrane proteins as 14-3-3 clients in functional regulation and intracellular transport. *Physiology (Bethesda)* **26**, 181-191 (2011).
24. M. Kilisch, O. Lytovchenko, E. C. Arakel, D. Bertinetti, B. Schwappach, A dual phosphorylation switch controls 14-3-3-dependent cell surface expression of TASK-1. *J Cell Sci* **129**, 831-842 (2016).
25. A. Lundby *et al.*, In vivo phosphoproteomics analysis reveals the cardiac targets of beta-adrenergic receptor signaling. *Sci Signal* **6**, rs11 (2013).
26. C. Petosa *et al.*, 14-3-3zeta binds a phosphorylated Raf peptide and an unphosphorylated peptide via its conserved amphipathic groove. *J Biol Chem* **273**, 16305-16310 (1998).
27. B. Wang *et al.*, Isolation of high-affinity peptide antagonists of 14-3-3 proteins by phage display. *Biochemistry* **38**, 12499-12504 (1999).
28. S. Ghorbani *et al.*, Regulation of tyrosine hydroxylase is preserved across different homo- and heterodimeric 14-3-3 proteins. *Amino Acids* **48**, 1221-1229 (2016).
29. L. M. Stevers, P. J. de Vink, C. Ottmann, J. Huskens, L. Brunsveld, A Thermodynamic Model for Multivalency in 14-3-3 Protein-Protein Interactions. *J Am Chem Soc* **140**, 14498-14510 (2018).
30. H. Yuan, K. Michelsen, B. Schwappach, 14-3-3 dimers probe the assembly status of multimeric membrane proteins. *Curr Biol* **13**, 638-646 (2003).
31. E. W. Wilker, R. A. Grant, S. C. Artim, M. B. Yaffe, A structural basis for 14-3-3sigma functional specificity. *J Biol Chem* **280**, 18891-18898 (2005).
32. A. Ballone, F. Centorrino, M. Wolter, C. Ottmann, Protein X-ray crystallography of the 14-3-3zeta/SOS1 complex. *Data Brief* **19**, 1683-1687 (2018).
33. H. Fu, R. R. Subramanian, S. C. Masters, 14-3-3 proteins: structure, function, and regulation. *Annu Rev Pharmacol Toxicol* **40**, 617-647 (2000).
34. M. Gouw *et al.*, The eukaryotic linear motif resource - 2018 update. *Nucleic Acids Res* **46**, D428-D434 (2018).
35. K. Rittinger *et al.*, Structural analysis of 14-3-3 phosphopeptide complexes identifies a dual role for the nuclear export signal of 14-3-3 in ligand binding. *Mol Cell* **4**, 153-166 (1999).
36. F. Centorrino, A. Ballone, M. Wolter, C. Ottmann, Biophysical and structural insight into the USP8/14-3-3 interaction. *FEBS Lett* **592**, 1211-1220 (2018).
37. P. Sharma *et al.*, Endoplasmic reticulum protein targeting of phospholamban: a common role for an N-terminal di-arginine motif in ER retention? *PLoS One* **5**, e11496 (2010).
38. A. Kagan, Y. F. Melman, A. Krumerman, T. V. McDonald, 14-3-3 amplifies and prolongs adrenergic stimulation of HERG K+ channel activity. *EMBO J* **21**, 1889-1898 (2002).
39. C. UniProt, UniProt: a worldwide hub of protein knowledge. *Nucleic Acids Res* **47**, D506-D515 (2019).
40. M. E. Anderson, J. H. Brown, D. M. Bers, CaMKII in myocardial hypertrophy and heart failure. *J Mol Cell Cardiol* **51**, 468-473 (2011).
41. S. Sossalla *et al.*, Inhibition of elevated Ca2+/calmodulin-dependent protein kinase II improves contractility in human failing myocardium. *Circ Res* **107**, 1150-1161 (2010).
42. P. Beauverger *et al.*, Reversion of cardiac dysfunction by a novel orally available calcium/calmodulin-dependent protein kinase II inhibitor, RA306, in a genetic model of dilated cardiomyopathy. *Cardiovasc Res*, (2019).

43. D. K. Ceholski, C. A. Trieber, C. F. Holmes, H. S. Young, Lethal, hereditary mutants of phospholamban elude phosphorylation by protein kinase A. *J Biol Chem* **287**, 26596-26605 (2012).
44. K. N. Ha *et al.*, Lethal Arg9Cys phospholamban mutation hinders Ca2+-ATPase regulation and phosphorylation by protein kinase A. *Proc Natl Acad Sci U S A* **108**, 2735-2740 (2011).
45. V. Hung *et al.*, Spatially resolved proteomic mapping in living cells with the engineered peroxidase APEX2. *Nat Protoc* **11**, 456-475 (2016).
46. I. Atanassov, H. Urlaub, Increased proteome coverage by combining PAGE and peptide isoelectric focusing: comparative study of gel-based separation approaches. *Proteomics* **13**, 2947-2955 (2013).
47. A. K. Snabaitis, A. Muntendorf, T. Wieland, M. Avkiran, Regulation of the extracellular signal-regulated kinase pathway in adult myocardium: differential roles of G(q/11), Gi and G(12/13) proteins in signalling by alpha1-adrenergic, endothelin-1 and thrombin-sensitive protease-activated receptors. *Cell Signal* **17**, 655-664 (2005).
48. N. Voigt *et al.*, Enhanced sarcoplasmic reticulum Ca2+ leak and increased Na+-Ca2+ exchanger function underlie delayed afterdepolarizations in patients with chronic atrial fibrillation. *Circulation* **125**, 2059-2070 (2012).
49. L. Li, G. Chu, E. G. Kranias, D. M. Bers, Cardiac myocyte calcium transport in phospholamban knockout mouse: relaxation and endogenous CaMKII effects. *Am J Physiol* **274**, H1335-1347 (1998).
50. J. A. Bell, Cao, Y., Gunn, J.R., Day, T., Gallicchio, E., Zhou, Z., Levy, R., Farid, R., PrimeX and the Schrödinger computational chemistry suite of programs. *Int. Tables Crystallogr., Major Reference Works*, 534–538 (2012).
51. J. A. Maier *et al.*, ff14SB: Improving the Accuracy of Protein Side Chain and Backbone Parameters from ff99SB. *J Chem Theory Comput* **11**, 3696-3713 (2015).
52. N. Homeyer, A. H. Horn, H. Lanig, H. Sticht, AMBER force-field parameters for phosphorylated amino acids in different protonation states: phosphoserine, phosphothreonine, phosphotyrosine, and phosphohistidine. *J Mol Model* **12**, 281-289 (2006).
53. Y. Cau *et al.*, Molecular Dynamics Simulations and Structural Analysis of Giardia duodenalis 14-3-3 Protein-Protein Interactions. *J Chem Inf Model* **55**, 2611-2622 (2015).
54. M. Mori *et al.*, Functional and structural characterization of 2-amino-4-phenylthiazole inhibitors of the HIV-1 nucleocapsid protein with antiviral activity. *ACS Chem Biol* **9**, 1950-1955 (2014).
55. D. R. Roe, T. E. Cheatham, 3rd, PTRAJ and CPPTRAJ: Software for Processing and Analysis of Molecular Dynamics Trajectory Data. *J Chem Theory Comput* **9**, 3084-3095 (2013).
56. N. A. Baker, D. Sept, S. Joseph, M. J. Holst, J. A. McCammon, Electrostatics of nanosystems: application to microtubules and the ribosome. *Proc Natl Acad Sci U S A* **98**, 10037-10041 (2001).
57. W. Humphrey, A. Dalke, K. Schulten, VMD: visual molecular dynamics. *J Mol Graph* **14**, 33-38, 27-38 (1996).
58. B. R. Miller, 3rd *et al.*, MMPBSA.py: An Efficient Program for End-State Free Energy Calculations. *J Chem Theory Comput* **8**, 3314-3321 (2012).
59. S. Orchard *et al.*, The MIntAct project--IntAct as a common curation platform for 11 molecular interaction databases. *Nucleic Acids Res* **42**, D358-363 (2014).

Acknowledgments: We thank Schwappach and Lehnart lab members for comments on the manuscript. Modelling used a Titan Xp GPU donated by NVIDIA Corporation. **Funding**: JM was funded by the DFG (Deutsche Forschungsgemeinschaft)-funded International Research training Group (IRTG1816). Work on PLN in the Schwappach lab is supported by the DFG (SFB1002; A07 and under Germany's Excellence Strategy - EXC 2067/1-390729940). DKD and SEL were funded by the DFG (SFB1190; P03) and the Leducq Foundation transatlantic network CURE-PLaN. Mass spectrometric analyses were performed by the Core Facility Proteomics at the University Medical Center Göttingen and supported by the DFG (SFB1190; Z02). AB, MM, and CO were supported by the H2020 Marie Curie Action of the European Commission (grant number 675179). The physiological measurements in the Shattock lab were funded by the British Heart Foundation (RG/17/15/33106) and the technical assistance of Shiney Reji is gratefully acknowledged. **Author contributions**: Conceptualization: JM, MJS, SEL, BS; Methodology: JM, DKD, ST, AB, KUF, MK, MM, CO, MJS, SEL, BS; Validation: JM, DKD, ST, AB, MM, CO, MJS, SEL, BS; Formal analysis: JM, DKD, ST, AB, MK, CL, MM, MJS, SEL, BS; Investigation: JM, DKD, ST, AB, KUF, MM, MJS, SEL, BS; Resources: HU, MM, CO, MJS, SEL, BS; Data curation: JM, DKD, ST, AB, CL, MM, MJS, SEL, BS; Writing original draft: JM, SEL, BS; Writing review and editing: JM, DKD, AB, CL, MM, CO, MJS, SEL, BS; Visualization: JM, DKD, ST, AB, MM; Project administration: BS; Funding acquisition: CL, HU, MM; CO; MJS; SEL, BS. **Competing interests**: The authors declare no competing interests. **Data and materials availability**: The protein-protein interactions from this publication have been submitted to the IMEx (http://www.imexconsortium.org) consortium through IntAct (*43*) and assigned the identifier IM-27195. All other data needed to evaluate the conclusions in the paper are present in the paper or the Supplementary Materials.

Figure Legends

Fig. 1. 14-3-3 binds PLN pentamers from cardiac membranes. **(A**) Schematic representation of PLN indicating the PKA consensus site and a putative 14-3-3 binding site (*18*). (**B**) Scheme for the 14-3-3 affinity purification protocol. (**C**) Representative silver-stained gel revealing proteins from the membrane fraction co-purifying with 14-3-3 and background according to workflow shown in (B) (n = 3 mice/group). (**D**) Presence of PKA-phosphorylated proteins in the 14-3-3-bound membrane fraction (n = 3 mice/group). See fig. S1A for the full blot including the cytosol fraction. (**E**) Immunoblotting of the 14-3-3-bound membrane fraction with a PLN antibody (n = 6 mice/group). See fig. S1B for the full blot including the cytosol fraction. (**F**) Quantification of experiments shown in (E). (**G**) Detection with phospho-specific anti-pSer^{16} reveals the presence of pSer^{16}-PLN in the 14-3-3-bound proteins from the membrane fraction (n = 5 mice/group). (**H**) Quantification of experiments shown in (G). In (F) and (H) data are presented as box and whisker plots with mean and median. A one-way ANOVA analysis showed significant differences between the MBP, 14-3-3+R18 and 14-3-3 group in (F) (p=<0.0001) and in H (p=<0.0002). A Tukey test revealed significant differences in (F) between 14-3-3+R18 compared to 14-3-3 (*** p=0.0002) and between MBP compared to 14-3-3 (*** p=0.0003) as well as in (H) between 14-3-3+R18 compared to 14-3-3 (*** p=0.0009) and MBP compared to 14-3-3 (*** p=0.0003). *H.s.*, *Homo sapiens*; *M.m.*, *Mus musculus*; R18, R18 trifluoroacetate; WB, Western blot; M, monomer; P, SDS-resistant pentamer; a.u., arbitrary units.

Fig. 2. PLN proximity proteomics enriches six out of seven 14-3-3 isoforms. (**A**) Scheme of proximity proteomic strategy: N-terminal fusion of the V5-APEX2 peroxidase to full-length PLN was compared to PLN lacking 29 residues of the N-terminus. (**B**) Enrichment of 14-3-3 isoforms (orange circles), PP1c, and Hsp20 with full-length PLN was identified by proximity proteomics in living NRCMs (see Data File S1 for enriched proteins). Enrichment compared to two different negative controls is shown – cytosolic GFP to assess background binding to the biotin affinity matrix and N-terminally truncated PLN (Δ1-29) to assess specific binding to the exposed region of the membrane protein (n = 5 independent experiments from 3 NRCM preparations). In (B), only proteins that positively differed from 0 according to a one sample t-test ($p < 0.05$) in the ratios for both full-length PLN/eGFP and full-length PLN/PLN Δ1-29 mutant are shown. 14-3-3σ was only significantly enriched over eGFP ($p < 0.05$) but not over PLN Δ1-29 mutant (p=0.07). See fig. S2B and S2C for the intensity of detected proteins. APEX, ascorbate peroxidase; SILAC, stable isotope labeling by amino acids in cell culture; δ, 14-3-3 delta; η, 14-3-3 eta; ε, 14-3-3 epsilon; γ, 14-3-3 gamma; σ, 14-3-3 sigma; τ, 14-3-3 tau; ζ, 14-3-3 zeta.

Fig. 3. 14-3-3 preferentially binds PLN pentamer and pThr^{17}-PLN has a higher 14-3-3 binding affinity than pSer^{16}-PLN. (**A**) Effect of heating cardiac membranes to convert PLN pentamers to monomers on binding of PLN to 14-3-3 (n = 7 mice/group). (**B**) Quantification of experiments shown in (A). The proportion of the respective form in the eluate was determined in relation to the pentamer or monomer signal from the input. (**C**) Binding assay using recombinant, monomeric PLN-GST and the indicated variants to assess 14-3-3 binding after PKA-dependent phosphorylation in vitro (n = 3 independent experiments). (**D**) Quantification of experiments shown in (C) using normalized values of 14-3-3 intensity and of the slower migrating band in Phos-tag gels. (**E**) The experiments shown in (A) were probed for pThr^{17}-PLN on independent Western blots (n = 5 mice/group). (**F**) Quantification of experiments shown in (E). The proportion of the respective form in the eluate was determined in relation to the pentamer or monomer signal from the input. (**G**) Binding assay using recombinant, monomeric PLN-GST and the indicated variants to assess 14-3-3 binding after CaMKII-dependent phosphorylation of PLN-GST (n= 3 independent experiments). (**H**) Quantification of experiments shown in (G) using normalized values of the 14-3-3 intensity and of the slower migrating band in the Phos-tag gel. Data in (B), (D), (F), and (H) are presented as box and whisker plots with mean and median. A one-way ANOVA analysis showed significant differences between groups in (B) (p=<0.0001) and in (F) (p=<0.0001), and a Tukey test showed significant differences in (B) between pentamer -75°C and monomer +75°C (* p=0.0143). The multiple comparison test showed no significant difference in (F) between pentamer -75°C and monomer +75°C (p=0.5587). M, monomer; P, SDS-resistant pentamer; pPLN, phosphorylated PLN; WB, Western blot.

Fig. 4. 14-3-3 contacts PLN in two distinct conformations. (**A**) Overview of a 14-3-3σ monomer bound to pSer^{16}-PLN based on the model obtained by MD simulations. 14-3-3σ is shown as a colored surface according to the electrostatic potential computed by APBS (negative potential in red, positive in blue), and peptides are depicted as cyan sticks (n = 2 independent experiments with conformational sampling of 250 ns). (**B**) Overview of a 14-3-3σ monomer bound to pThr^{17}-PLN as obtained by MD simulations. Visualization as in (A) (n = 2 independent experiments with conformational sampling of 250 ns). (**C**) Superimposition of 14-3-3σ/ pSer^{16}-PLN complex (white cartoon/cyan sticks) and 14-3-3σ/ pThr^{17}-PLN (pink cartoon/purple sticks) shown in (A) and (B). (**D**) In vitro phosphorylation of the indicated PLN-GST variants mimicking DCM-causing mutants using CaMKII (n = 5 independent experiments). pPLN, phosphorylated PLN; WB, Western blot.

Fig. 5. 14-3-3 protects PLN from dephosphorylation. (**A**) De-phosphorylation of pThr^{17}-PLN-GST in the presence of 14-3-3 as monitored by anti-pThr^{17}-PLN Western blot (n= 6 independent experiments). (**B**) Quantification of experiments shown in (A) using values of the PLN pThr^{17} intensity at different time points normalized to the PLN pThr^{17} intensity at time point 0 (no 14-3-3). (**C**) Experiments as shown in (A) illustrating the phosphorylation state of PLN-GST (Phos-tag gel), total PLN-GST (SDS PAGE), and bound 14-3-3 (Western blot). (**D**) Quantification of bound 14-3-3 from experiments shown in (A) and (C) using values of the 14-3-3 intensity at different points normalized to the 14-3-3 intensity at time point 0. Data in (B) and (D) are presented as box and whisker plots with mean and median. A paired t-test showed no significant difference between the samples with or without 14-3-3 at 0 min (p=0.2141). A significant difference was shown between the samples with or without 14-3-3 at 5 min (* p=0.0181), at 10 min (* p=0.0136) and at 25 min (* p=0.0370). FastAP, alkaline phosphatase; min, minutes, Norm, normalized.

Fig. 6. 14-3-3 is enriched in mouse cardiac membranes after isoprenaline stimulation. (**A**) Immunoprecipitation from cardiac membranes using PLN (rabbit-IgG) antibody. Detection with PLN (mouse-IgG) antibody (n = 2 mice/group). (**B**) 14-3-3 pan 14122 antibody characterization using HeLa cell and heart lysate. Upper band indicates a slower migrating 14-3-3-positive band, presumably 14-3-3 epsilon based on predicted molecular weights. Asterisk indicates cross-reacting protein. (n = 2 mice or independently transfected cell populations/group). (**C**) Detection of PLN associated 14-3-3 after isoprenaline stimulation in cardiomyocytes. IP = Immunoprecipitation of PLN with PLN (rabbit-IgG) antibody from isoprenaline stimulated cardiomyocytes; total = 15% input membranes. Top two panels: anti-14-3-3 detection of PLN IP (run without DTT) and cardiac inputs (run with DTT); middle three panels: anti-PLN (mouse IgG) or anti-Na/K detection of PLN IP (run without DTT) or cardiac inputs (run with DTT); lower two panels: anti-pSer^{16}-PLN or anti-Na/K detection of cardiac inputs (n = 4 mice/group). Asterisk indicates cross-reacting protein. (**D**-**F**) Quantification of experiments shown in (C). Data are presented as box and whisker plots with mean and median. A paired t-test showed no significant difference in (D) (p=0.8771) but a significant difference was found in (E) (* p=0.0338) and in (F) (* p=0.0222). 14-3-3 detected in membranes from *Pln*$^{-/-}$ mice (negative control for IP) is shown in purple in (F). IP, immunoprecipitation; IgG, immunoglobulin G; m-IgG, mouse immunoglobulin; r-IgG, rabbit immunoglobulin; M, monomer; P, pentamer; WB, Western blot; total, total amount of protein used as input; NaK, Na/K ATPase; ISO, isoprenaline.

Fig. 7. 14-3-3 prolongs SERCA stimulation after β-adrenergic activation in mouse cardiomyocytes. The data in (**A** – **D**) were obtained under control conditions or in the

presence of the tested peptides or antibodies in the patch pipette solution. Ca^{2+} transients were recorded at 0.5 Hz stimulation rate, as it is shown in fig. S8A,C. The time constant (τ) of Ca^{2+} transient decay was measured every 55s. To obtain an individual reading, we averaged τ values calculated by single exponential fitting of decay phase for 3 Ca^{2+} transients, recorded at each time point. The changes in the SERCA function followed the application of 10 nM isoprenaline for 10 sec. To compensate for the cell-to-cell variability in the absolute magnitude of isoprenaline peak response, the relative response from baseline was normalized to the peak response in each cell. (**A**) Ca^{2+} transient decay in cardiomyocytes patched with control pipette solution (7 cells from 4 isolations) or with pipette solution containing 14-3-3γ (2μM) (n=7 cells from 5 isolations). A two-way ANOVA mixed-model analysis revealed significant differences between curves (p=0.0024). A multiple comparison test showed significant differences only at the last time point (* p=0.033). (**B**) Ca^{2+} transient decay in cardiomyocytes patched with control pipette solution (7 cells from 4 isolations) or pipette solution containing R18 (2μM) (n=8 cells from 4 isolations) or a mixture of 14-3-3γ (2μM) and R18 (2μM) (n=6 cells from 4 isolations). Two-way ANOVA indicated no significant differences between the three tested conditions (control, R18 inhibitor and 14-3-3γ blocked with R18) either using mixed-model analysis (p=0.6365). (**C**) Ca^{2+} transient decay in cardiomyocytes patched with control pipette solution (n = 7 cells from 4 isolations) or with pipette solution containing 2.5 μg/ml of either anti-$pSer^{16}$ (n = 6 cells from 5 isolations) or anti-$pThr^{17}$ antibody (n = 6 cells from 4 isolations). A two-way ANOVA mixed-model analysis revealed significant differences between the curves of the three tested conditions (p=0.0131). Multiple comparison tests showed significant differences between anti-$pSer^{16}$ and anti-$pThr^{17}$ antibodies at 380s (* p=0.0143) and further 440s (* p=0.0053). Between control and anti-Ser^{16} group, significant differences were observed at 380s (* p=0.0495) and at 440s (* p=0.0268). All other changes were not significant. (**D**) Scheme illustrating the dependence of the apparent binding affinity of dimeric 14-3-3 protein on the number and kind of different phospho-residues present in the PLN pentamer. Affinity and avidity effects combine with each other resulting in increased 14-3-3 binding to PLN and protection from the phosphatase PP1. ISO, isoprenaline; s, seconds; R18, R18 trifluoroacetate; Ab, antibody, PP1, protein phosphatase 1.

Figure 1

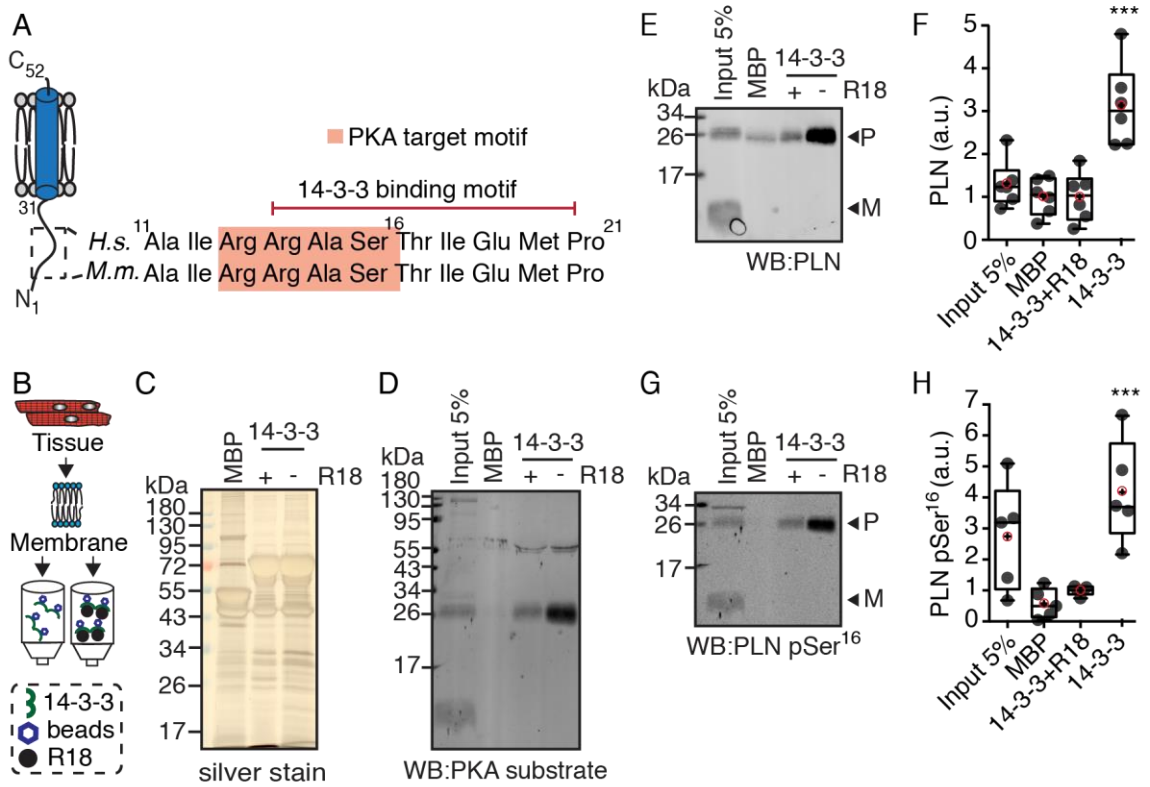
A
C52
31
N1
PKA target motif
14-3-3 binding motif
H.s. 11 Ala Ile Arg Arg Ala Ser Thr Ile Glu Met Pro 21
M.m. Ala Ile Arg Arg Ala Ser Thr Ile Glu Met Pro
B
Tissue
Membrane
14-3-3
beads
R18
C
MBP
14-3-3
+ - R18
kDa
180
130
95
72
55
43
34
26
17
silver stain
D
Input 5%
MBP
14-3-3
+ - R18
kDa
180
130
95
55
43
34
26
17
WB:PKA substrate
E
Input 5%
MBP
14-3-3
+ - R18
kDa
34
26
17
P
M
WB:PLN
F
PLN (a.u.)
***
Input 5%
MBP
14-3-3+R18
14-3-3
G
Input 5%
MBP
14-3-3
+ - R18
kDa
34
26
17
P
M
WB:PLN pSer16
H
PLN pSer16 (a.u.)
***
Input 5%
MBP
14-3-3+R18
14-3-3

Figure 2

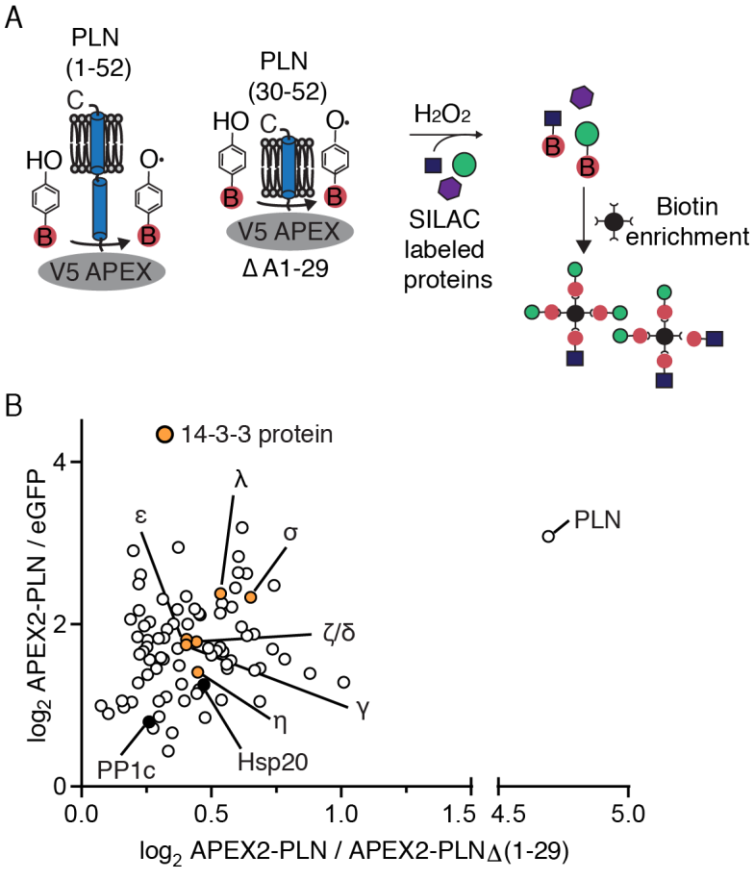
A
PLN
(1-52)
C
HO
O·
B
B
V5 APEX
PLN
(30-52)
HO C
O·
B
B
V5 APEX
Δ A1-29
H2O2
SILAC
labeled
proteins
B
B
Biotin
enrichment
B
14-3-3 protein
PLN
λ
ε
σ
ζ/δ
γ
η
Hsp20
PP1c
4
2
0
log2 APEX2-PLN / eGFP
0.0
0.5
1.0
1.5
4.5
5.0
log2 APEX2-PLN / APEX2-PLNΔ(1-29)

Figure 3

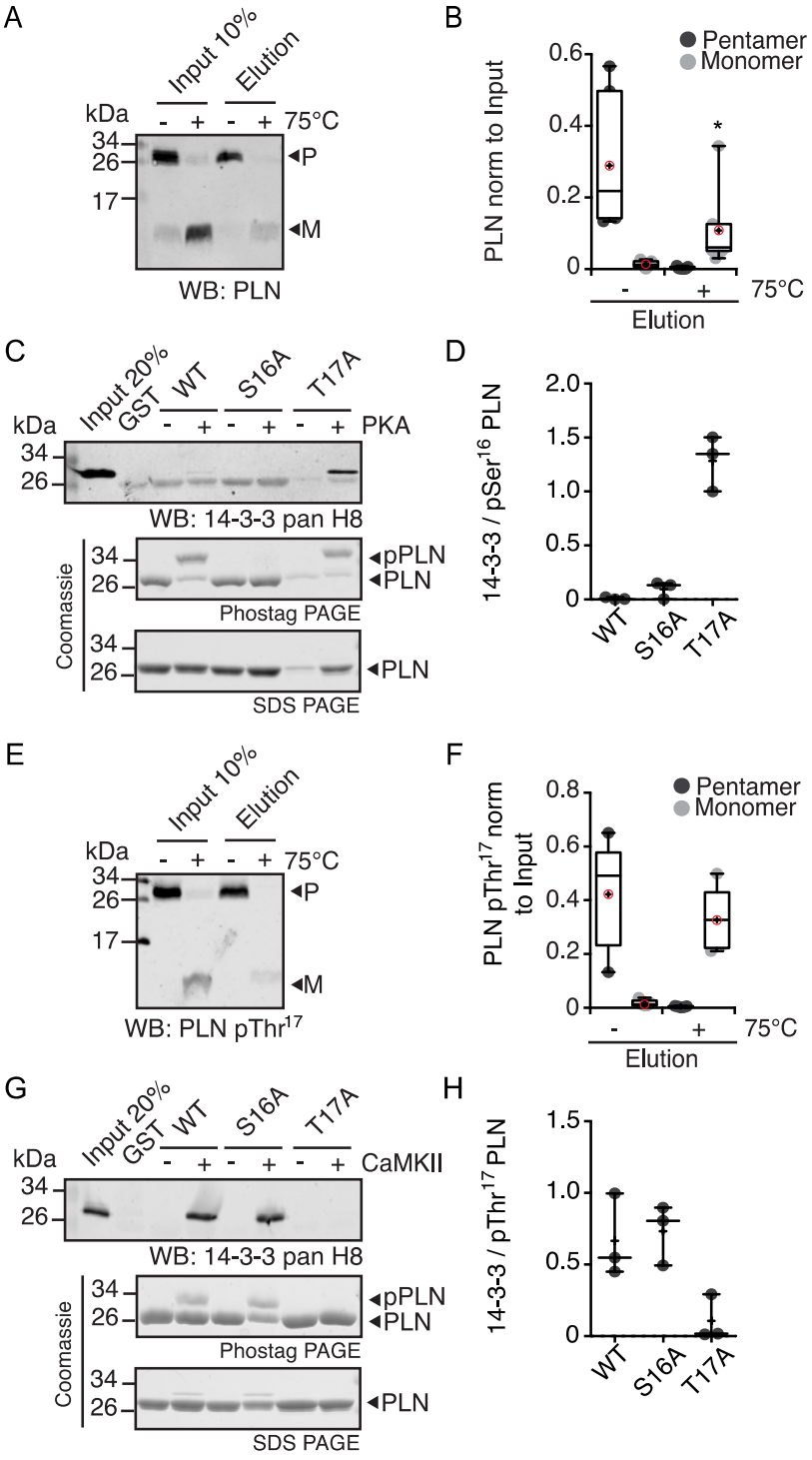
A
Input 10%
Elution
kDa
- + - + 75°C
34
26
17
P
M
WB: PLN
B
Pentamer
Monomer
PLN norm to Input
0.6
0.4
0.2
0
*
- + 75°C
Elution
C
Input 20%
GST
WT
S16A
T17A
kDa
- + - + - + PKA
34
26
WB: 14-3-3 pan H8
Coomassie
34
26
pPLN
PLN
Phostag PAGE
34
26
PLN
SDS PAGE
D
14-3-3 / pSer16 PLN
2.0
1.5
1.0
0.5
0
WT
S16A
T17A
E
Input 10%
Elution
kDa
- + - + 75°C
34
26
17
P
M
WB: PLN pThr17
F
Pentamer
Monomer
PLN pThr17 norm to Input
0.8
0.6
0.4
0.2
0
- + 75°C
Elution
G
Input 20%
GST
WT
S16A
T17A
kDa
- + - + - + CaMKII
34
26
WB: 14-3-3 pan H8
Coomassie
34
26
pPLN
PLN
Phostag PAGE
34
26
PLN
SDS PAGE
H
14-3-3 / pThr17 PLN
1.5
1.0
0.5
0
WT
S16A
T17A

Figure 4

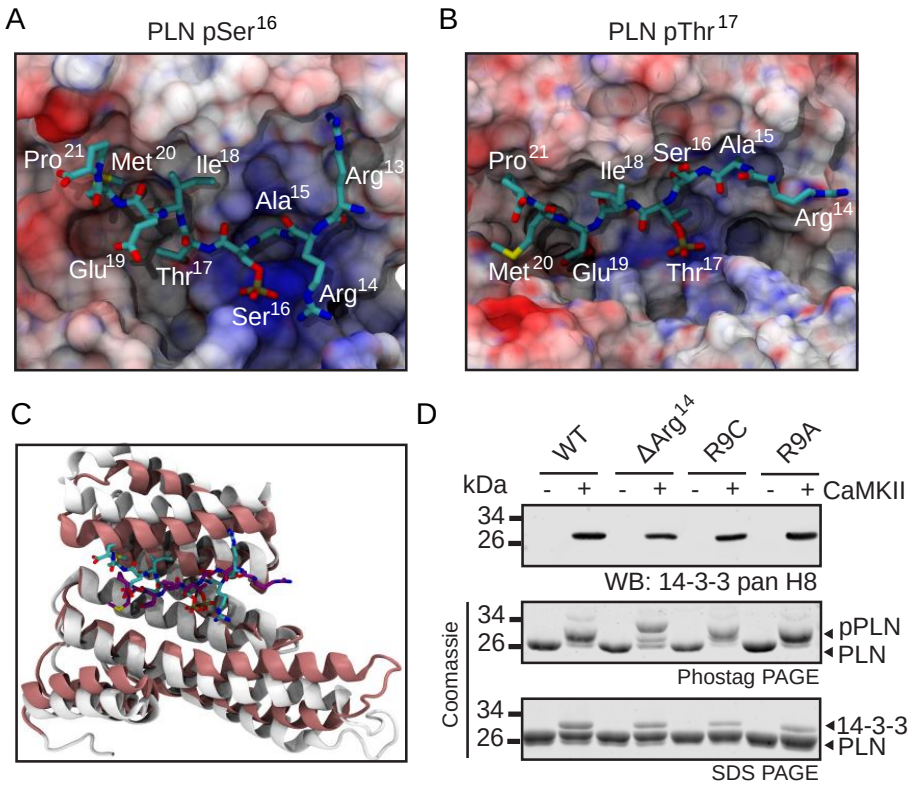
A
PLN pSer16
Pro21
Met20
Ile18
Arg13
Ala15
Glu19
Thr17
Arg14
Ser16
B
PLN pThr17
Pro21
Ile18
Ser16
Ala15
Arg14
Met20
Glu19
Thr17
C
D
WT
ΔArg14
R9C
R9A
kDa
- + - + - + - + CaMKII
34
26
WB: 14-3-3 pan H8
Coomassie
34
26
pPLN
PLN
Phostag PAGE
34
26
14-3-3
PLN
SDS PAGE

Figure 5

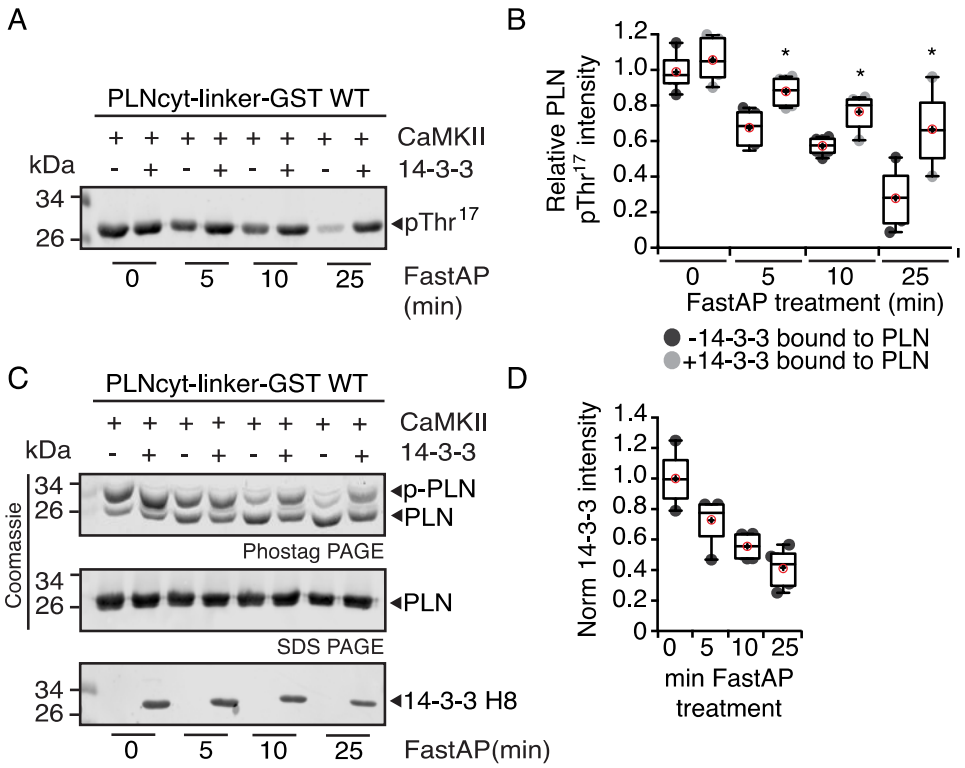
A
PLNcyt-linker-GST WT
CaMKII
kDa
14-3-3
34
26
pThr17
0
5
10
25
FastAP
(min)
B
Relative PLN
pThr17 intensity
1.2
1.0
0.8
0.6
0.4
0.2
0
FastAP treatment (min)
-14-3-3 bound to PLN
+14-3-3 bound to PLN
C
PLNcyt-linker-GST WT
CaMKII
kDa
14-3-3
Coomassie
p-PLN
PLN
Phostag PAGE
PLN
SDS PAGE
14-3-3 H8
FastAP(min)
D
Norm 14-3-3 intensity
1.4
1.2
1.0
0.8
0.6
0.4
0.2
0
min FastAP
treatment

Figure 6

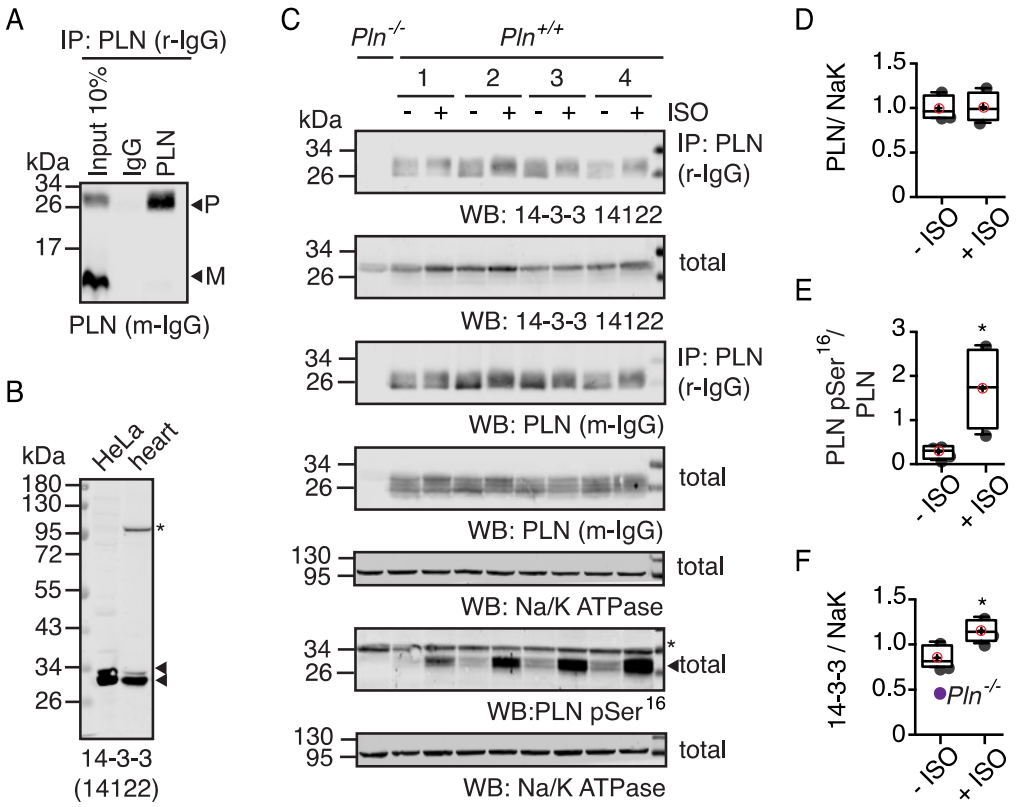
A
IP: PLN (r-IgG)
Input 10%
IgG
PLN
kDa
34
26
17
P
M
PLN (m-IgG)
B
kDa
HeLa
heart
180
130
95
72
55
43
34
26
*
14-3-3
(14122)
C
Pln-/-
Pln+/+
1
2
3
4
- + - + - + - +
ISO
kDa
34
26
IP: PLN
(r-IgG)
WB: 14-3-3 14122
total
WB: 14-3-3 14122
IP: PLN
(r-IgG)
WB: PLN (m-IgG)
total
WB: PLN (m-IgG)
130
95
total
WB: Na/K ATPase
*
total
WB:PLN pSer16
total
WB: Na/K ATPase
D
PLN/ NaK
1.5
1.0
0.5
0
- ISO
+ ISO
E
PLN pSer16/
PLN
3
2
1
0
*
- ISO
+ ISO
F
14-3-3 / NaK
1.5
1.0
0.5
0
*
Pln-/-
- ISO
+ ISO

Figure 7

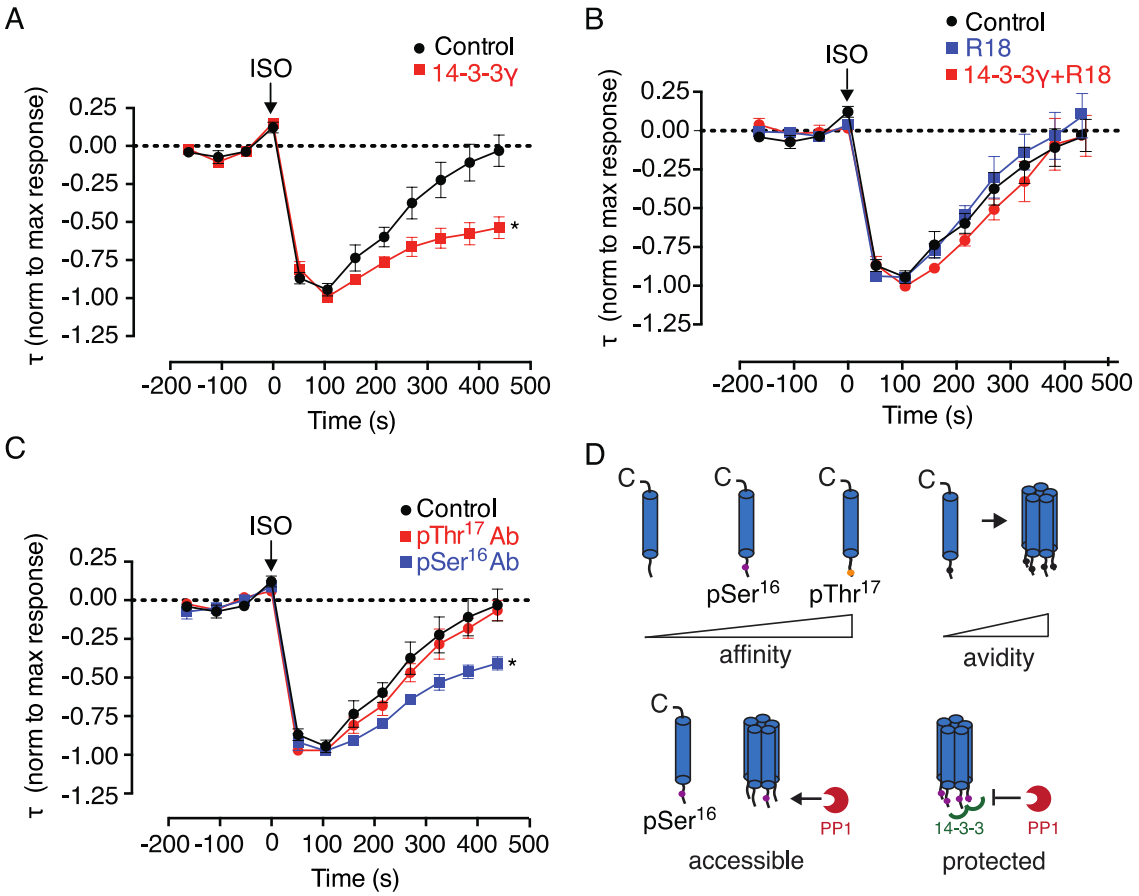
A
Control
14-3-3γ
ISO
τ (norm to max response)
0.25
0.00
-0.25
-0.50
-0.75
-1.00
-1.25
-200 -100 0 100 200 300 400 500
Time (s)
*
B
Control
R18
14-3-3γ+R18
ISO
τ (norm to max response)
Time (s)
C
Control
pThr17 Ab
pSer16 Ab
ISO
τ (norm to max response)
Time (s)
*
D
C
pSer16
pThr17
affinity
avidity
pSer16
PP1
accessible
14-3-3
PP1
protected

Figure - S1

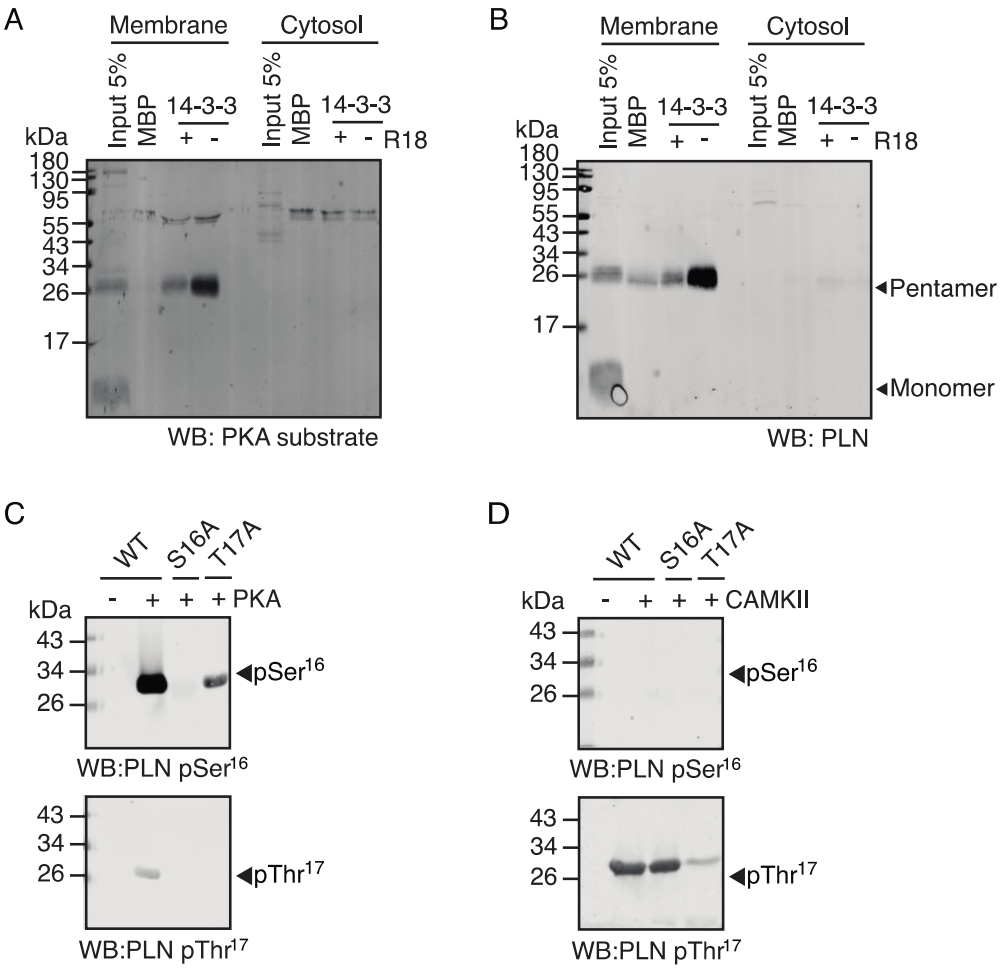

fig. S1. Cardiac cytosolic fractions do not show a signal for 14-3-3-bound PLN. (**A**) Presence of PKA-phosphorylated proteins in the 14-3-3-bound membrane fraction but not in the cytosolic fraction (n = 3 mice/group). (**B**) Detection of 14-3-3-bound proteins from membrane or cytosolic fractions from cardiomyocytes with a PLN antibody (n = 6 mice/group). (**C,D**) Recombinant PLN WT, S16A, or T17A proteins were phosphorylated with either PKA (C) or CaMKII (D). The phosphorylated samples were resolved by SDS-PAGE and probed with $pSer^{16}$-PLN or $pThr^{17}$-PLN antibodies (n = 2 independent experiments). R18, R18 trifluoroacetate; WB, Western blot.

Figure - S2

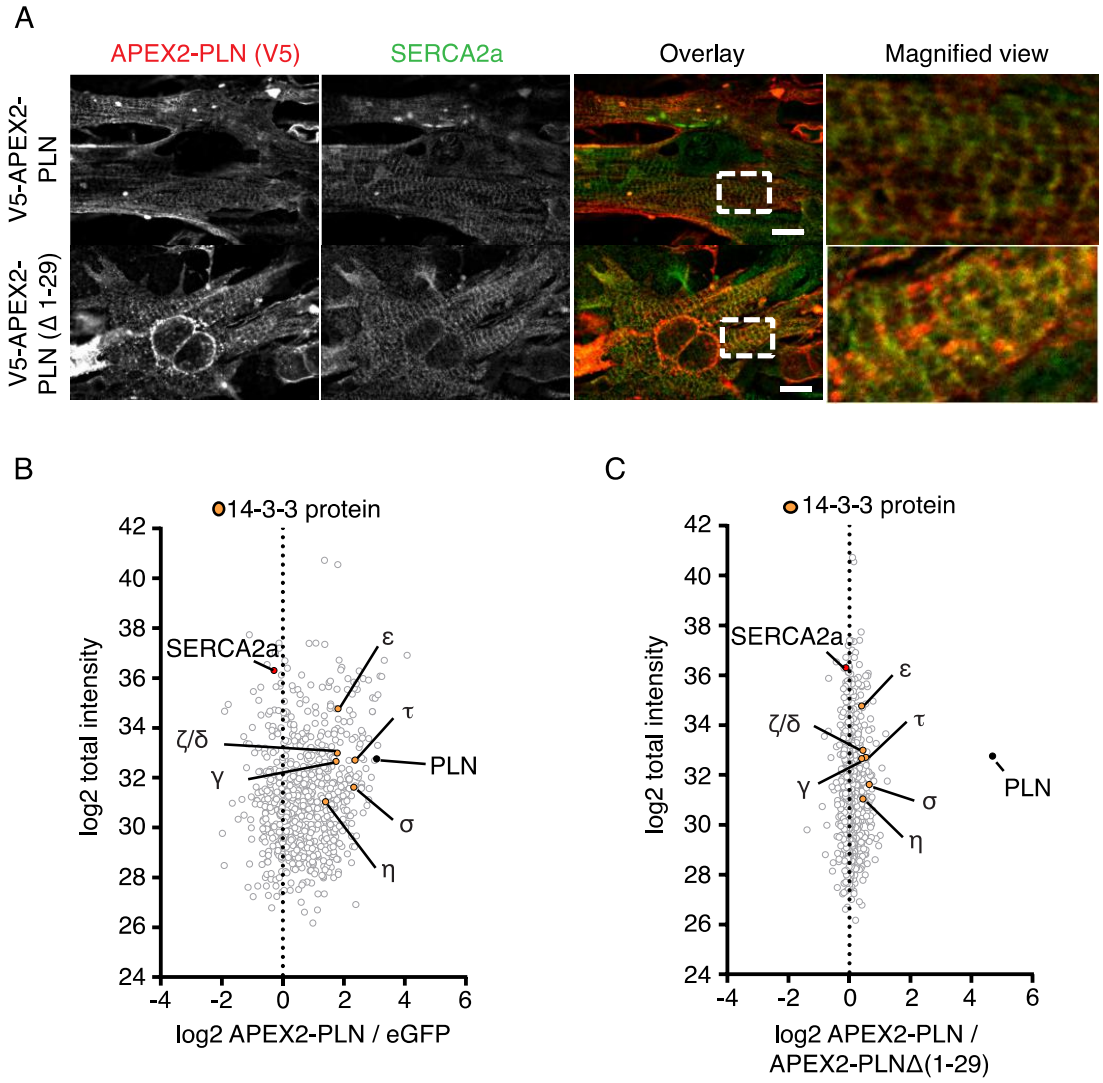

fig. S2. Confocal imaging showing the colocalization of APEX2-PLN or APEX2-PLN (Δ1-29) and SERCA2a in NRCMs. (**A**) NRCMs cultured for 15 days were transduced with adenoviruses (Ad5) expressing either APEX2-PLN or APEX2-PLN(Δ1-29). NRCMs were fixed with 4% paraformaldehyde, immunostained for V5 (red) and SERCA2a (green), and imaged by confocal microscopy (Zeiss LSM 880, 63x/1.4 Oil DIC objective). Dashed boxes indicate areas of magnified views (representative of 2 independent experiments). Scale bars 10 µm. (**B, C**) Log(2) dot plots showing all detected proteins for the ratio V5-APEX2-PLN/eGFP (B) or V5-APEX2-PLNΔ(1-29)/eGFP (C) (n=5 independent experiments from 3 NRCM preparations). δ, 14-3-3 delta; η, 14-3-3 eta; ε, 14-3-3 epsilon; γ, 14-3-3 gamma; σ, 14-3-3 sigma; τ, 14-3-3 tau; ζ, 14-3-3 zeta.

Figure - S3

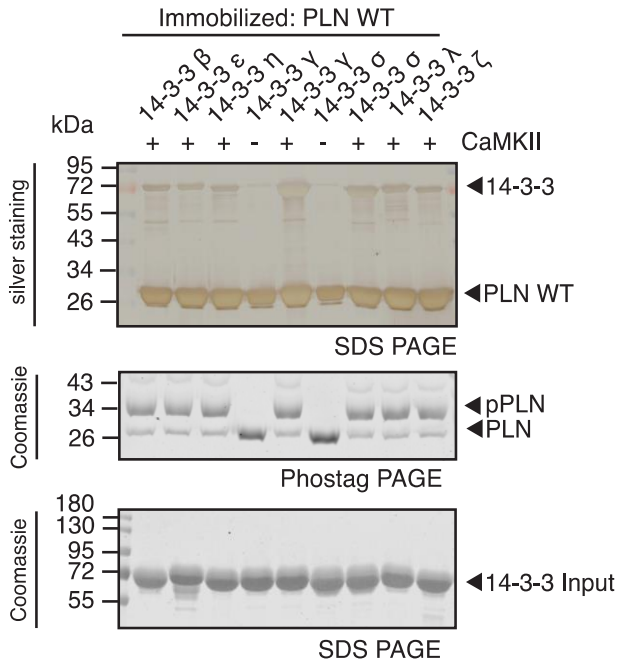

fig. S3. All seven 14-3-3 isoforms bind pThr[17]-PLN-GST. Detection of PLN bound 14-3-3 isoforms with silver-stained SDS-PAGE. Unphosphorylated PLN-GST was used as negative control for the binding of 14-3-3γ and 14-3-3σ. Equal 14-3-3 inputs were confirmed on SDS-PAGE and PLN pThr[17] phosphorylation using activated CaMKII kinase was confirmed on a Phos-tag gel (n = 3 independent experiments). β, 14-3-3 beta; η, 14-3-3 eta; ε, 14-3-3 epsilon; γ, 14-3-3 gamma; σ, 14-3-3 sigma; τ, 14-3-3 tau; ζ, 14-3-3 zeta.

Figure S4

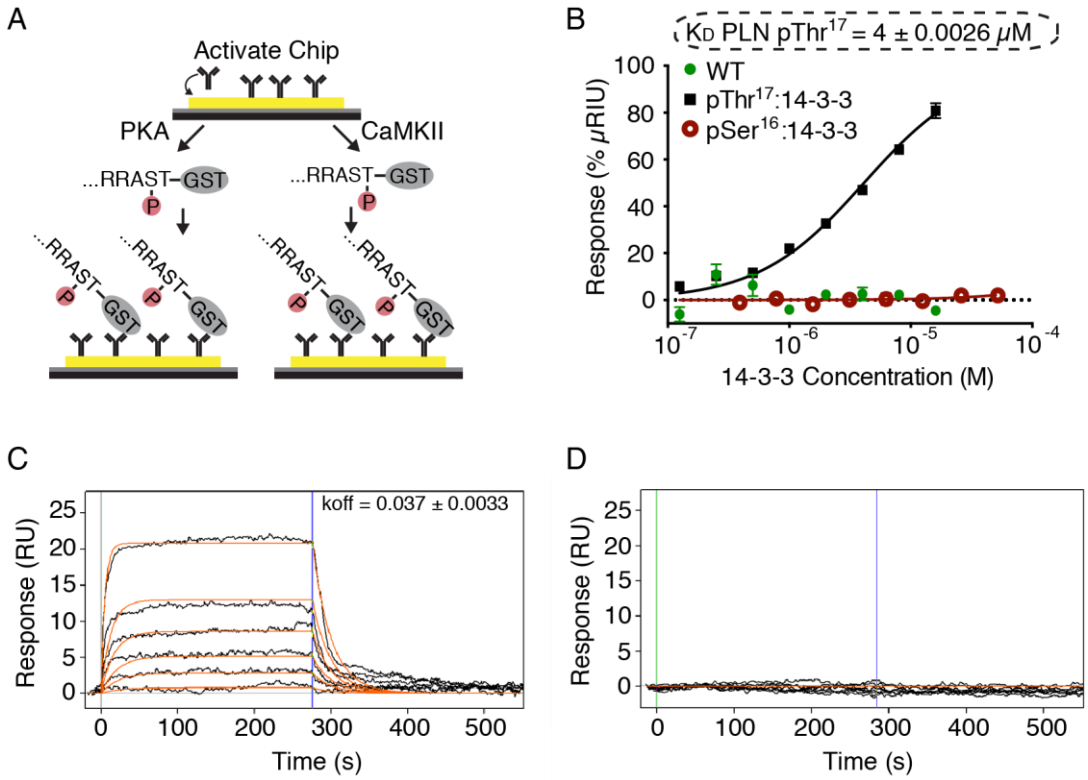

fig. S4. Determination of the equilibrium dissociation constant for 14-3-3 binding to pThr^{17}-PLN. (**A**) Scheme of surface plasmon resonance experiment using pSer^{16}- or pThr^{17}-PLN-GST. (**B**) Binding isotherm obtained from the experiment schematized in (A) and dissociation constant for 14-3-3γ (without MBP-tag) binding pThr^{17}-PLN determined by a sigmoidal dose-response curve fit (n = 3 independent experiments). Error bars depict +/- SEM. (**C, D**) Sensograms underlying (B) for pThr^{17}-PLN (C) and unphosphorylated PLN exposed to the same concentrations of 14-3-3γ (D). K_D, equilibrium dissociation constant; pSer^{16}, PLN phosphorylated at Ser^{16}; pThr^{17}, PLN phosphorylated at Thr^{17}; koff, dissociation rate constant.

Figure - S5

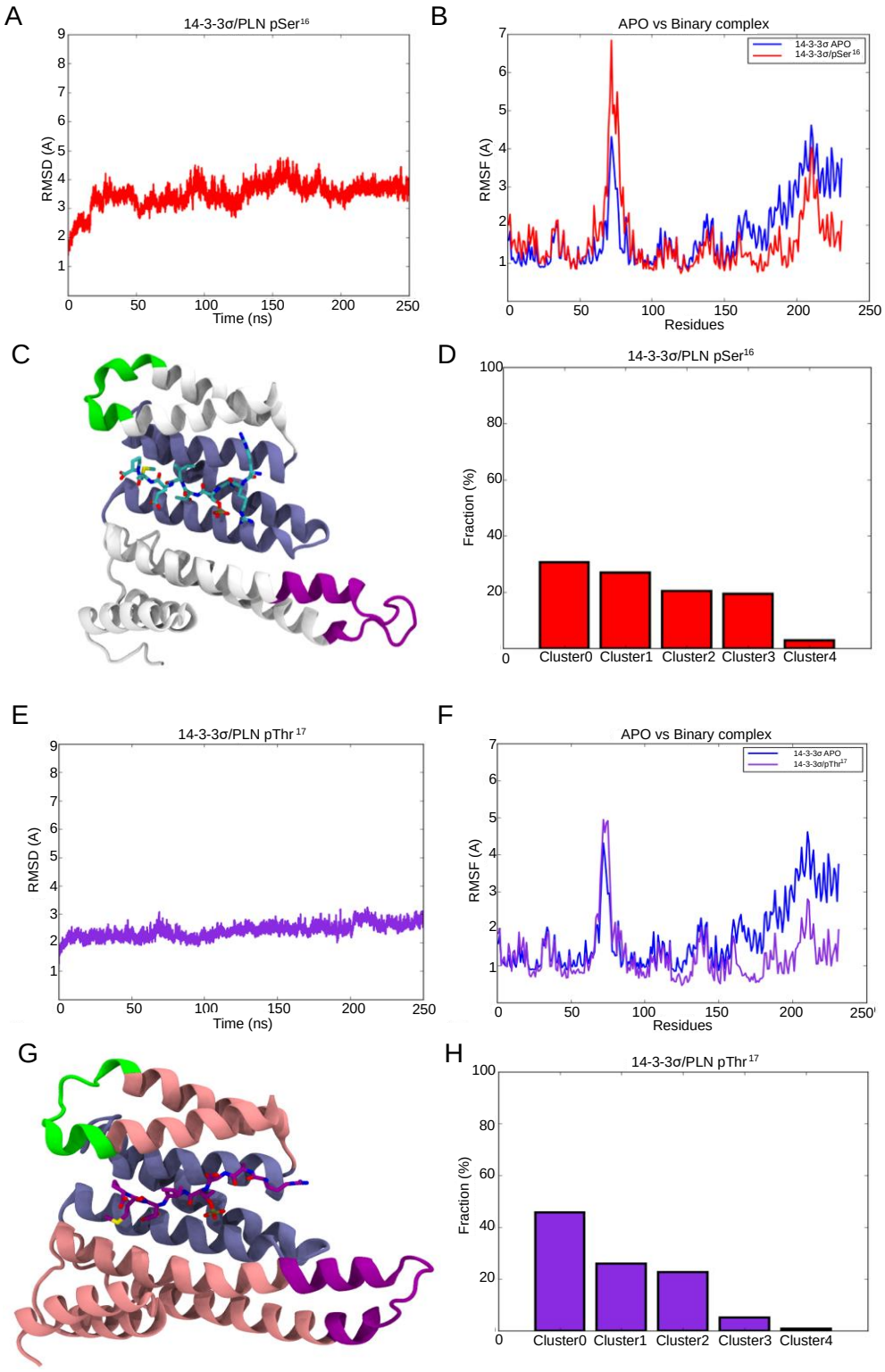

fig S5. MD simulation of the 14-3-3σ-pSer^{16}-PLN complex and the 14-3-3σ-pThr^{17}-PLN complex. (**A**) RMSD of all-atom of 14-3-3σ protein and the peptide as a function of the MD simulation time. (**B**) RMSF of the protein residues of 14-3-3σ/pSer^{16}-PLN complex (red

curve) in comparison with 14-3-3σ apo (blue curve) obtained during the 250 ns simulation (n= 2 independent experiments). (**C**) Overview of 14-3-3σ monomer bound to pSer^{16}-PLN (cyan sticks). Residues showing high conformational freedom in MD simulation are depicted in purple and green (loops 64-88 and 208-219, respectively). Residues 118-190 of the amphipathic groove are highlighted in ice blue. (**D**) Distribution of clusters over 5 population groups. Conformations of the 14-3-3σ-pSer^{16}-PLN complex were clustered along MD trajectory frames. (**E**) RMSD of all-atom of 14-3-3σ protein and the peptide as a function of the MD simulation time. (**F**) RMSF of the protein residues of 14-3-3σ***/***pThr^{17}-PLN complex (blueviolet curve) in comparison with 14-3-3σ apo (blue curve) obtained during the 250 ns simulation (n = 2 independent experiments). (**G**) Overview of 14-3-3σ monomer bound to pThr^{17}-PLN (purple sticks). Residues unfavourable for stability during the simulation are depicted in purple and green. The amphipathic groove is highlighted in ice blue. (**H**) Distribution of average cluster over 5 population groups. Conformations of the 14-3-3σ-pThr^{17}-PLN complex were clustered along MD trajectory frames. 14-3-3σ, 14-3-3 sigma; RMSD, all-atom root mean square deviations; RMSF, root mean square fluctuation.

Figure - S6

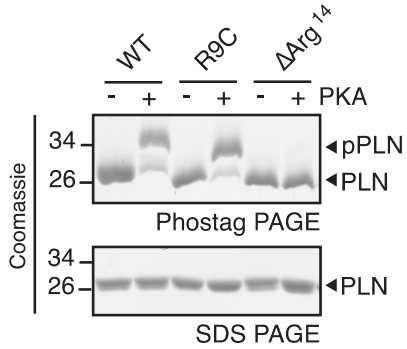

fig S6. PKA does not phosphorylate ΔArg^{14}-PLN monomers. In vitro phosphorylation of the indicated PLN variants using PKA (n = 3 independent experiments), visualized on Phos-tag gel or SDS-PAGE gel. pPLN, phosphorylated PLN.

Figure - S7

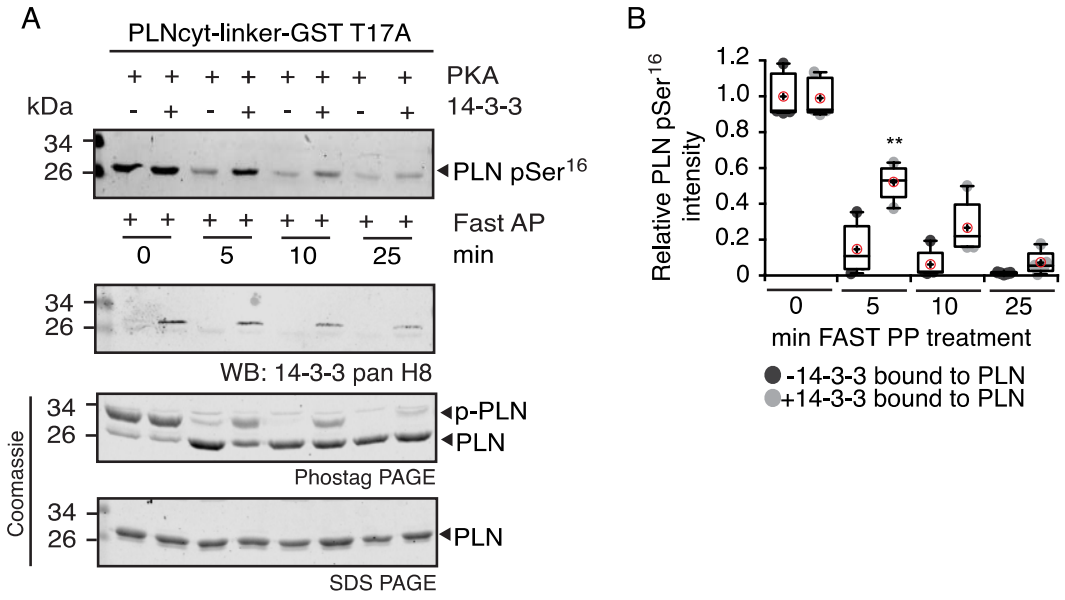

fig S7. 14-3-3 binding protects pSer^{16}-PLN protects from fast dephosphorylation. (**A**) Dephosphorylation of pSer^{16}-PLN T17A-GST in the presence of 14-3-3 was analysed by Western blot with anti-pSer^{16}-PLN and 14-3-3 pan H8 antibodies (n = 5 independent experiments). In addition, pSer^{16}-PLN was also monitored on Phos-tag gel and SDS-PAGE gel. (**B**) Quantification of slower-migrating band observed in Phos-tag-PAGE normalized to slower-migrating band at time point 0 (no 14-3-3) shown in (A). Data is presented as box and whisker plot with mean and median. A paired t-test showed no significant difference between the samples with or without 14-3-3 at 0 min (p=0.4279), at 10 min (p=0.0540) or at 25 min (p=0.0947). A significant difference was observed at 5 min (** p=0.0061). FastAP, alkaline phosphatase; min, minutes; pPLN, phosphorylated PLN.

Figure - S8

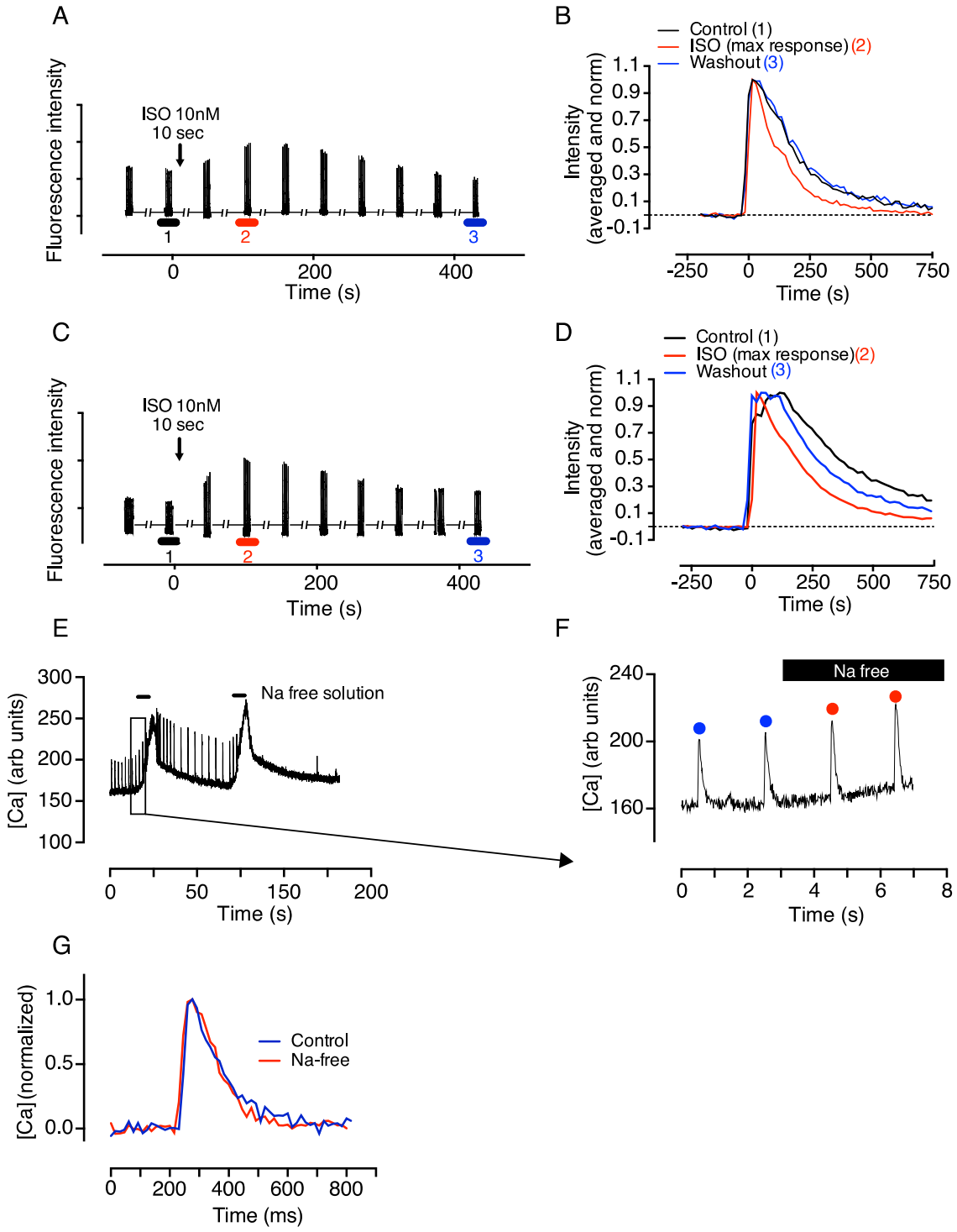

Fig S8. Effect of 14-3-3 and Na^+-free superfusion on the kinetics of isoprenaline-induced Ca^{2+} transients in isolated cardiomyocytes. (**A**) Ca^{2+} transients were stimulated at 0.5 Hz by patch pipette and Ca^{2+} transients recorded discontinuously (due to memory buffering limitations of the video capture system). A 10 sec pulse of isoprenaline (ISO, 10 nM) was

applied at the time point indicated. Representative traces from 7 myocytes isolated from 4 mice recorded with control pipette solution. (**B**) Ca^{2+} transient profiles averaged from 3 consecutive Ca^{2+} transients recorded at the points marked 1, 2 and 3 in (A). Data were normalized to maximum amplitude before plotting. (**C**) Ca^{2+} transients recorded as in (A) with a pipette solution containing 2µM of 14-3-3 in the whole-cell configuration. Representative of 7 myocytes isolated from 5 mice. (**D**) Ca^{2+} transient profiles averaged from 3 consecutive Ca^{2+} transients recorded with 14-3-3 in the pipette at the points marked 1, 2 and 3 in (C). Data were normalized to maximum amplitude before plotting. (**E**) Recovery of the Ca^{2+} transient in mouse myocytes at 35^{o}C was unaffected by the rapid removal of extracellular Na^{+}. Myocytes were stimulated throughout at 0.5 Hz by patch pipette and Ca^{2+} transients recorded. At the time points indicated, extracellular Na^{+} was rapidly and transiently replaced with an equimolar amount of mannitol. Representative of 5 myocytes isolated from 2 mice. (**F**) Magnified section of pane (E) showing Ca^{2+} transient profiles immediately before and during perfusion with the Na^{+}-free solution. Representative of 5 myocytes isolated from 2 mice. (**G**) The final two Ca^{2+} transients in normal Tyrode (blue) and the first two transients in Na^{+}-free (red) were baseline corrected, normalized and averaged. Because Na^{+}-free perfusion inevitably loads the cell with Ca^{2+} and causes an inotropy and diastolic shortening from which the cell ultimately does not recover. For this reason, only the first two Na^{+}-free transients were analyzed. Similar results were observed in 4 other cells. Isoprenaline, ISO.

table S1. Plasmids used in this study.

Plasmid name	Description	Restriction sites	Source
pMal2CX	Bacterial expression vector for N-terminal MBP-tagged proteins	EcoRI - HindIII	New England BioLabs
pMal2CX 14-3-3β	Bacterial expression vector for MBP-14-3-3β	EcoRI - HindIII	M. Kilisch
pMal2CX 14-3-3ε	Bacterial expression vector for MBP-14-3-3ε	EcoRI - HindIII	M. Kilisch
pMal2CX 14-3-3η	Bacterial expression vector for MBP-14-3-3η	EcoRI - HindIII	M. Kilisch
pMal2CX 14-3-3γ	Bacterial expression vector for MBP-14-3-3γ	EcoRI - HindIII	J.Menzel
pMal2CX 14-3-3σ	Bacterial expression vector for MBP-14-3-3σ	EcoRI - HindIII	M. Kilisch
pMal2CX 14-3-3τ	Bacterial expression vector for MBP-14-3-3τ	EcoRI - HindIII	M. Kilisch
pMal2CX 14-3-3ζ	Bacterial expression vector for MBP-14-3-3ζ	EcoRI - HindIII	M. Kilisch
pMal2CX - GST modified	Bacterial expression for C-terminal tagged GST proteins (MBP-tag removed)	NdeI - BamHI	J. Menzel
pMal2CX modified PLN N31 WT	Bacterial expression vector for PLNcyt-linker-GST N31 WT	NdeI-XhoI	J. Menzel
pMal2CX modified PLN N31 S16A	Bacterial expression vector for PLNcyt-linker-GST N31 S16A	NdeI-XhoI	J. Menzel
pMal2CX modified PLN N31 T17A	Bacterial expression vector for PLNcyt-linker-GST N31 T17A	NdeI-XhoI	J. Menzel
pMal2CX modified PLN N31 S10A	Bacterial expression vector for PLNcyt-linker-GST N31 S10A	NdeI-XhoI	J. Menzel

pMal2CX modified PLN N31 R9C	Bacterial expression vector for PLNcyt-linker-GST N31 R9C	NdeI-XhoI	J. Menzel
pMal2CX modified PLN N31 R9A	Bacterial expression vector for PLNcyt-linker-GST N31 R9A	NdeI-XhoI	J. Menzel
pMal2CX modified PLN N31 ΔArg14	Bacterial expression vector for PLNcyt-linker-GST N31 R14del	NdeI-XhoI	J. Menzel

table S2. Antibodies used in this study.

Name	Raised in	Supplier	Cat. No.	Dilution	Technique	PID*
14-3-3 pan (H8)	mouse	Santa Cruz	sc-1657	1:1000	Western	16
14-3-3 pan	rabbit	Abcam	ab14112	1:1000	Western	974
GST	rabbit	Carl Roth	3998.1	200 nM	SPR	66
Na/K ATPase α	mouse	Santa Cruz	sc-21712	1:1000	Western	20
p-PKA substrate	rabbit	Cell Signaling	9624	1:500	Western	522
PLN	mouse	Abcam	ab2865	1:1000	Western	520
PLN	rabbit	Lehnart lab	-	5 µl	IP	-
PLN pSer[16]	rabbit	Badrilla	A010-12	1:1000	Western	519
PLN pThr[17]	rabbit	Badrilla	A010-13	1:1000	Western	975
SERCA2a	rabbit	Badrilla	A010-20	1:200	IF	976
V5	mouse	Invitrogen	R960-25	1:200	IF	977

*persistent identifier generated by ePIC (https://www.pidconsortium.net)

https://hdl.handle.net/11022/umg-sfb1002-antibody-primary-XXX

Data File S1. *In vivo* proximity labeling. List of biotinylated proteins detected with a significance of p<0.01 by in vivo proximity labeling using V5-APEX2-PLN.

The file can be found under this link:
https://owncloud.gwdg.de/index.php/s/v18RVghJqu0uE5w

3 Chapter III: Further analysis of the PLN/14-3-3 interaction

3.1 Introduction

Every heartbeat is an interplay between contraction and relaxation. This is regulated by complex cardiac signaling pathways and the flux of ions as well as other intracellular secondary messengers, like cAMP and Ca^{2+} (MacLennan & Kranias 2003). Cardiac contraction is induced by an electrical stimulus that travels from the atria to the ventricle and from cardiomyocyte to cardiomyocyte due to voltage-sensitive ion channels (Bartos et al., 2015). Cardiomyocyte membrane depolarization activates, amongst other ion channels, voltage gated Ca^{2+} channels which lead to an influx of Ca^{2+} ions into the cytoplasm (Fearnley et al., 2011). The increased cytoplasmic Ca^{2+} levels activates the Ca^{2+}-release channel RyR which releases large amounts of Ca^{2+} from the SR into the cytoplasm (Laver, 2007). The large intracellular Ca^{2+} concentration leads to muscle contraction (Potter & Gergely, 1974). After contraction, Ca^{2+} is released by PMCAs and NCX located at the plasma membrane or by SERCA located at the SR (Calderón et al., 2014). More than 70% of the intracellular Ca^{2+} is transported by SERCA back into the SR in humans (MacLennan & Kranias 2003). As Ca^{2+} is an important regulator of the excitation-contraction coupling in the heart, all factors which regulate Ca^{2+} handling in cardiomyocytes have a great impact on heart function.

SERCA is mainly responsible for the transport of Ca^{2+} ions into the SR and for the relaxation of the heart after each contraction. SERCA is a single polypeptide with a molecular mass of 110 kDa and belongs to the P-type ATPase family such as PMCA and sodium/potassium ATPase (Na/K ATPase) (Sweadner & Donnet, 2001). As an ATPase pump SERCA transports two Ca^{2+} ions against a calcium gradient into the SR upon the hydrolysis of one ATP molecule (Periasamy & Kalyanasundaram, 2007). Hydrolysis of an ATP molecule transfers the phosphate to an aspartate residue located in the catalytic domain of SERCA, resulting in a reversible conformational change (Sweadner & Donnet, 2001). SERCA is encoded by three genes, SERCA 1, 2 and 3 that are highly conserved and localized on different chromosomes. The SERCA isoform variability is enhanced by alternative splicing resulting in ten different isoforms expressed in humans. Two of these are expressed in muscle cells and only SERCA2a is expressed in cardiac muscle (Periasamy & Kalyanasundaram, 2007).

SERCA2a activity itself is modulated via a small tail-anchor protein PLN, which is able to directly bind to SERCA's transmembrane domain. The interaction between PLN and SERCA is regulated by the phosphorylation of PLN (Gustavsson et al., 2013). Unphosphorylated PLN binds SERCA and reduces SERCA's affinity to Ca^{2+} causing the inhibitory effect. Upon phosphorylation of PLN the interaction between PLN and SERCA

is disturbed and as a consequence SERCA transports Ca^{2+} ions back into the SR (MacLennan & Kranias 2003). Therefore, PLN is a reversible inhibitor of SERCA and has influence on the heart relaxation rate.

PLN itself is a small protein of 52 amino acids and very abundant in the heart (Traaseth et al., 2008). The cytosolic region of PLN has two potential phosphorylation sites, S16 and T17 residues, which can be phosphorylated by PKA or by CaMKII respectively (Mattiazzi & Kranias, 2014). CaMKII kinase needs to be auto-phosphorylated in order to be active, which is achieved by high intracellular Ca^{2+} levels or by high cAMP levels after beta-adrenergic stimulation (Mattiazzi et al., 2005). Upon beta-adrenergic stimulation, both phospho-residues in PLN become phosphorylated and contribute equally to total PLN phosphorylation (Mundiña-Weilenmann et al., 1996). It was reported that both residues can be phosphorylated individually and independent from each other *in vitro* (Mundiña-Weilenmann et al., 1996). For the S16 phospho-site a predominant role in PLN regulation was suggested based on experiments showing that S16 phosphorylation is sufficient for maximal cardiac response upon highest beta adrenergic stimulation (Mattiazzi & Kranias, 2014). For the T17 phospho-residue it was shown, that upon phosphatase inhibition and increased Ca^{2+} levels, T17 was phosphorylated by CaMKII *in-vivo* independently, without S16 phosphorylation (Mattiazzi et al., 2005; Mattiazzi & Kranias, 2014). In addition, there is another phosphorylatable residue in PLN (S10) which is targeted by PKC. However, phosphorylation of S10 in PLN has not been associated with a physiological effect or SERCA inhibition (Coyler, 1998).

Two physiological forms of PLN are present in the heart, a monomeric or pentameric conformation which are in an intracellular equilibrium (Smeazzetto et al., 2013; Wittmann et al., 2015). The oligomerization state of PLN plays, along with PLN phosphorylation, an important role in SERCA regulation. Initially, it was reported that only monomeric PLN directly interacts with SERCA and thus has an inhibitory effect on it (Kimura et al., 1997). In 2015 Wittmann et al showed that PKA has a higher affinity for PLN pentamers than for PLN monomers, resulting in a delayed phosphorylation of monomers and a prolonged interaction between monomeric PLN and SERCA. These findings indicate indirect effects of the PLN pentamer on the SERCA/PLN interaction (Wittmann et al., 2015). While PKA and CaMKII are responsible for the phosphorylation of PLN, the phosphatase PP1 is responsible for its dephosphorylation which makes PP1 an important regulator of the PLN/SERCA interaction as well (Kranias & Hajjar, 2012).

The human PLN gene is highly conserved among mammals (Han et al., 2018; McTiernan et al., 1999). Yet, gene knockout of PLN has various effects in mammals. In mice it leads to hyperdynamic hearts, but has little consequence overall (Haghighi et al., 2003). In contrast, in humans all identified mutations in the PLN gene were identified in

heterozygous patients. For a leucine 39 stop (L39Stop) mutation two homozygous patients were identified, both developed lethal DCM underlying the importance of PLN in human hearts (Haghighi et al., 2003). Several disease-associated mutations were identified in the human PLN gene, causing serious contraction problems with the progression to HF and a high risk of early death (Young et al., 2015). One mutation is the deletion of the R14 residue in PLN, which forms a part of the PKA consensus motif. Therefore, the absence of R14 will impair PKA binding and subsequent phosphorylation of S16 in R14del patients (Ceholski et al., 2012; Haghighi et al., 2006). In a heterozygous disease background, the R14del mutation was identified to be a very strong SERCA inhibitor causing cardiac remodeling over time (Haghighi et al., 2006; Hof et al., 2019). Expressed in mammalian cells, R14del PLN was found to be located at the plasma membrane interacting with the Na/K ATPase (Haghighi et al., 2012). The second disease mutation is a arginine to cysteine mutation at position 9 (R9C) which was identified in several families with dilated cardiomyopathy (Ha et al., 2011). The R9C mutation was initially found to trap PKA and therefore prevents phosphorylation of S16 (Schmitt et al., 2003). Later it was reported, that hydrophobic interactions cluster PLN R9C proteins tightly together into inactive pentamers (Ha et al., 2011). In line with this observation, it was found that PKA phosphorylation was disrupted as well as the SERCA interaction (Ha et al., 2011).

The PLN/SERCA interaction is regulated by several factors such as the PLN monomer to pentamer ratio, different kinases, and several interaction partners. As already described in chapter 2, I identified the phospho-adaptor protein 14-3-3 as a novel interaction partner of PLN. 14-3-3 proteins are a family of universal regulators involved in numerous regulatory functions via a broad number of ligands (Sluchanko, 2018). Seven different 14-3-3 isoforms are expressed in humans (Fu et al., 2000). In many cases 14-3-3 proteins bind the ligands by recognizing phosphorylated residues, but phosphorylation is not always required (Fu et al., 2000). The 14-3-3 interaction can have several functions such as stabilization of phosphorylated proteins, stabilization of protein-protein interactions, conformational alterations, or different subcellular localization of ligands (van Heusden, 2005).
In this chapter, I further characterized the 14-3-3/PLN interaction with the main focus on the role of 14-3-3 in the R14del PLN disease mutation.

3.2 Material and Methods

3.2.1 Chemicals

Chemicals used in this study were purchased from Sigma Aldrich, Carl Roth, Roche, GE HealthCare, AppliChem, Merck, and Serva. Restriction enzymes were purchased from Thermo Fisher Scientific. DNA oligonucleotides and phosphorylated oligonucleotides were synthesized by Sigma-Aldrich. Phusion DNA polymerase was homemade. PKA catalytic subunit was purchased from New England Biolabs. CaMKII delta kinase was purchased from Thermo Fisher Scientific. T4 DNA ligase and corresponding buffer was purchased from Thermo Fisher Scientific. FastAP Thermosensitive Alkaline Phosphatase was purchased from Thermo Fisher Scientific. FactorXa cleavage enzyme was purchased as a Cleavage Capture Kit from Merck Millipore. Phos-tag™ acrylamide was purchased from NARD institute. Protease and phosphatase inhibitors were purchased from Roche. Dulbecco's modified eagle medium (DMEM), reduced serum medium (Opti-MEM, Gibco), Trypsin-EDTA (0.05%) and Lipofectamine 2000 transfection reagent were purchased from Thermo Fisher Scientific.

3.2.2 Mouse models

Wild-type (Black6), *Pln* $^{+/+}$ (Black6J), *Pln*$^{\Delta R14/\Delta R14}$ (C57B16/N), *Pln*$^{+/\Delta R14}$ (C57B16/N) and *Pln*$^{-/-}$ (Black6N) mice were used. The *Pln*$^{-/-}$ mouse was provided by the lab of Prof. Dr. Stephan Lehnart and previously described (Kiriazis et al., 2002). The *Pln*$^{\Delta R14/\Delta R14}$ and *Pln*$^{+/\Delta R14}$ mice were generated by the laboratory of Prof. Dr. Herman Silljé and already characterized (Eijgenraam et al., 2020). All mice were male and aged between 8-12 weeks. The only exception was the *Pln*$^{\Delta R14/\Delta R14}$ mouse, where the animals were females and 3 weeks old. Animals were anesthetized with isoflurane and killed by cervical dislocation. Cardiomyocytes were isolated or organs were dissected and stored by -80°C. All animal procedures were performed under revision of the Animal Care and Use Committees of the University Medical Center Göttingen or University Medical Center Groningen.

3.2.3 Human atrial tissue samples

Right atrial appendages were obtained from 4 normal sinus rhythm patients undergoing cardiac surgery and kindly provided by the laboratory of Prof. Dr. Niels Voigt. Experimental protocols were approved by the ethics committee of the Göttingen University (No. 4/11/18).

3.2.4 Methods

3.2.4.1 Molecular cloning

Several protein expression plasmids for expression in bacteria and mammalian cells were generated with the use of well-established molecular cloning techniques based on the 1987 first established polymerase chain reaction (PCR) technique by K.B. Mullis. This technique was further development to insert point mutations, deletions and affinity sequences with the help of oligonucleotide-driven mutagenesis. Molecular cloning techniques such as PCR, restriction enzyme digest, purification of DNA and transformation in *Escherichia coli* (*E.coli)* were performed according to standard methods. Generated expression plasmids, oligonucleotides and restriction enzymes used in this study can be found in table 4-5.

3.2.4.2 Polymerase chain reaction

For the enzymatic amplification of DNA and the generation of expression vectors different PCR reactions were used together with specific designed oligonucleotides. Two different types of oligonucleotides were designed: oligonucleotides including enzymatic restriction sites and oligonucleotides which carry a specific point mutation (see table 4-5). PCR reactions were performed according to standard protocols and for each reaction optimized.

Table 1. Standard PCR reaction mix and amplification cycles.

*where TM (°C)=4x(G+C) + 2x(A+T).

Component	Concentration
10x *Phusion* Poly. buffer mix	1x
0.2 mM dNTP's	16 µM
Forward (Fw) Oligonucleotide	0.2 µM
Revers (Rw) Oligonucleotide	0.2 µM
DMSO	5%
DNA template	50 ng
Phusion DNA Polymerase	2 units
Sterile dH_2O	to 50 µl

Temperature	Time	Cycles
95 °C	2 min	X 1
95 °C	30 sec	X 35
55-65°C	30 sec	
72°C	1 min/kb	
72°C	10 min	X 1
4°C	-	-

All PCR reactions were prepared on ice accordingly to the pipette scheme described in table 1. After amplification PCR products were analysed on 1-2% agarose gels depending on the size of the fragment. The agarose solution was supplemented with SafeView (abm), a fluorescence dye with an emission wavelength of approximate 490 nm, to visualize DNA-bands upon irradiation with UV-light. Prior to electrophoreses, samples were diluted with 6x sample buffer (0.2% bromophenol blue, 0.2% xylene cyanol, 60% glycerol, 60 mM EDTA) and loaded on the gel together with a 100 bp or 1 kb marker, followed by electrophoresis at 200 V in 1x TAE buffer (40 mM Tris/HCl pH 8.0, 20 mM actetic acid, 1 mM EDTA). Subsequently, gel bands according to the correct size of the PCR product were excised from the gel and purified using a PCR clean up kit (High Pure Kit, Roche) following the manufactures instructions.

3.2.4.3 Restriction enzyme digest

PCR products and recipient plasmid DNA vectors were digested with one or multiple restriction enzymes. In general, all digests were pipetted on ice and carried out in a total reaction volume of 30 µl. Purified DNA products obtained by PCR were digested with 10 units of restriction enzyme(s) in the respective buffer according to the manufacture's instruction for 1 h at 37°C.

The digestion of 1-2 µg plasmid DNA was performed as already described for the insert, followed by a dephosphorylation reaction. To avoid that the linearized vector re-anneals in the ligation reaction, the phosphate groups were removed with 1 unit of Fast Alkaline Phosphatase for 10 min at 37°C. Whenever possible, restriction enzyme digests were carried out with multiple restriction enzymes in one reaction. Digested DNA inserts, as well as vectors, were analysed by gel electrophoresis, visualized and extracted from the agarose gel as described in section 3.2.4.2. Digested and purified DNA fragments of the expected size were used for ligation.

3.2.4.4 Ligation

Ligation reactions were done with 100 ng linearized vector and 5-fold molar excess of linearized and purified insert. These products were mixed in 3 µl 10x T4 DNA ligase buffer, 2 units T4 DNA ligase and diluted to a final reaction volume of 30 µL with sterile dH_2O. Ligation reactions were performed at 18°C for 16 h or at RT for 1-2 h. In both cases the ligase was heat inactivated at 65 °C for 10 min. Ligated products were stored at 4°C until further use.

3.2.4.5 Transformation of bacterial cells by electroporation

DNA was transformed into bacteria via electroporation. Therefore, 0.5 ng of plasmid DNA was transformed in either electro-competent Electro Ten Blue cells (Agilent Technologies) for amplification of plasmid DNA or in BL21 pRosetta for protein expression. In preparation, cuvettes (Gene Pulser Cuvettes, BioRad) were cooled on ice, the competent cells were thawed on ice, SOC medium (20 g/L tryptone, 5g/L yeast extract, 0.5 g/L yeast extract, 0.5 g/L NaCl, 2.5 mM KCL, 10mM $MgCl_2$, 20 mM glucose) for the reconstitution was pre-warmed to 37°C and the electroporator was set at 25 µF and 2.25 V. Plasmid DNA was added into the electro-competent cell aliquot (50 µl), mixed and filled into the cuvette. The cuvette was placed in the electroporator and a pulse at 2.25 V was initiated. After the pulse, the cells were resuspended in 1 ml pre-warmed SOC medium, transferred to a tube and incubated at 37°C for 30 min under gentle shaking. Finally, the cells were centrifuged in a table centrifuge at full-speed for 1 min, the supernatant was removed, the cell pellet was dissolved in sterile dH_2O and streaked out on a LB-Agar plate with corresponding antibiotic selector. Plates were incubated at 37°C overnight.

3.2.4.6 Amplification of plasmid DNA

Single colonies obtained on agar plates after transformation of amplified plasmid DNA in ElectroTen blue cells were inoculated under sterile conditions in 5 ml LB media under the respective antibiotic selection. Cultures were incubated overnight at 37°C under agitation. Bacteria cells were harvested by centrifugation in a table centrifuge at full speed for 2 min. The supernatant was removed and plasmid DNA was amplified with a NucleoSpin DNA amplifier kit (Machery Nagel) according to the manufacture instructions. Extracted DNA was dissolved in 50 µl dH_2O and stored at 4°C. When larger DNA yields were required, the same protocol was performed with a 100 ml bacteria culture and NucleoBond Xtra Midi kit (Machery-Nagel).

3.2.4.7 PCR site-directed mutagenesis

Single point mutations or deletions were introduced in oligonucleotides which were able to anneal with the target region of the gene of interest. In general, the site-directed mutagenesis PCR was pipetted on ice and carried out in a total reaction volume of 50 µl according to the pipetting scheme in table 2. After the PCR reaction, the entire samples were mixed with 6x sample buffer and analysed by gel electrophoresis as described in section 3.2.4.2. The purified DNA was digested with 1 µl *Dpn*I enzyme in the corresponding buffer at 37°C for 2-4 h. After the digest, 3 µl of the plasmid DNA was transferred in

ElectroTen blue cells by electroporation and positive clones were confirmed by sequencing.

Table 2. Pipetting scheme for site directed mutagenesis via PCR.

Component	Concentration
10x *Phusion* Poly. buffer mix	1x
2 mM dNTP's	16 µM
Forwards (Fw) Oligonucleotide	0.25 µM
Revers (Rw) Oligonucleotide	0.25 µM
DMSO	5%
DNA template	50 ng
Phusion DNA Polymerase	2 units
Sterile dH_2O	to 50 µl

Temperature	Time	Cycles
95 °C	2 min	x 1
95 °C	30 sec	x 18
52-56°C	30 sec	
72°C	1 min/kb	
72°C	12 min	x 1
4°C	-	-

3.2.4.8 Expression and affinity-purification of GST-tag proteins

Recombinant glutathione-S-transferase (GST)- tagged proteins were expressed and purified from *E.coli* strain BL21 Rosetta. Protein expression was done in 2 YT media (2YT mix, AppliChem) and induced with 1 mM IPTG for 3 h at 30°C. Cells were harvested and lysed in GST Lysis buffer (20 mM HEPES pH 6.8, 150 mM KOAc, 5 mM $Mg(OAc)_2$, 1 mM EDTA, 1 mM DTT, 1 mM PMSF). Crude cell lysate was centrifuged at 100.000 g for 30 min at 4°C. The supernatant was incubated with 1 ml washed glutathione sepharose beads (GE Healthcare) for GST-tagged proteins for 1 h at 4°C under gentle rotation. The bead slurry was transferred to gravity columns and first washed with 3 column volumes GST buffer pH 7.4, followed by one column volume 1mM ATP dissolved in GST buffer pH 7.4 and a final wash step in GST buffer pH 7.4. Bound GST-tagged proteins were eluted with GST elution buffer (20 mM HEPES pH 8.5, 150 mM KOAc, 5 mM $Mg(OAc)_2$, 1 mM EDTA, 1 mM DTT, 15 mM L-Glutathione). Eluted proteins were dialyzed overnight in GST buffer pH 7.4. After dialysis proteins were centrifuged in a table-top centrifuge at full speed for 10 min at 4°C to remove precipitated proteins. Protein concentrations were measured with

Bradford and the purified proteins were aliquoted and stored by -80°C. Every aliquot was thawed once.

3.2.4.9 Expression and affinity-purification of MBP-tag proteins

Recombinant MBP-tagged proteins were expressed and amplified from *E.coli* strain BL21 Rosetta. Proteins expression, lysis and purification was done as already described (section 3.2.4.8) with the following modifications: Lysis was performed in GST buffer pH 7.4 and the supernatant was incubated with Amlyose affinity resin (New England Biolabs). After washing, the purified proteins were eluted from the resin with 20 mM Maltose Elution buffer (20 mM HEPES pH 7.4, 150 mM KOAc, 5 mM $Mg(OAc)_2$, 1 mM EDTA, 1 mM DTT, 20 mM D-Maltose).

3.2.4.10 SDS PAGE electrophoresis

SDS PAGE gel electrophoresis was performed accordingly to the 1970 developed method from Laemmli where proteins are separated respective to size and charge. Glas plates and spacer were cleaned, assembled and placed in a gel casting station (Hoeffer). 3.5 ml resolving gel was casted into the assembled glass plates per gel and covered with 0.5 ml isopropanol to get an even surface. The gel was allowed to polymerize for 30 min, the isopropanol was removed and the surface was washed with H_2O a couple of times before the stacking gel (4%) was casted. The combs were added to the stacking gel and the gel was allowed to polymerize. The height of the stacking gel was always 1.5 cm. The gels were electrophoresed in SDS running buffer (5 mM Tris, 50 mM Glycine pH 8.3, 0,02 % SDS) at 15 mA (constant amperage) for 120 min.

3.2.4.11 Phos-tag-PAGE electrophoresis

Phos-tag SDS-PAGE was used to visualize phosphorylated residues in proteins of interest, by retarding the migration of phosphorylated proteins on a SDS-PAGE gel (leads to a shift). Therefore, standard SDS-PAGE gels (section 3.2.4.10) were supplemented with 50 µM Phos-tag acrylamide and 50 µl $MnCl_2$. Phos-tag-PAGE gels were electrophoresed at 15 mA (constant amperage) for 120 min. After electrophoresis, the gels were either Coomassie (section 3.2.4.12) stained or transferred to a nitrocellulose membrane by electroblotting (section 3.2.4.13).

3.2.4.12 Coomassie staining of SDS-PAGE

SDS PAGE or Phos-tag-PAGE gels were visualized after the run with Coomassie brilliant blue G-250. After the gel run, the gels were carefully removed and soaked for 10 min in

destainer solution (30% ethanol, 10% acidic acid, diluted with MilliQ-H_2O). This step can improve the intensity of the bands. Afterwards the gels were placed in Coomassie solution (45% Coomassie brilliant blue G-250, 20% CH_2COOH, diluted in MilliQ-H_2O), boiled in the microwave for around 30 seconds and incubated on a shaker for 30 min. After staining, the gel was rinsed with H_2O and destained in destainer solution for 30 min. The gels were stored in H_2O.

3.2.4.13 Western blot transfer with electro blotting

After electrophoresis of SDS-PAGE gels, the gels were carefully removed and briefly rinsed in Transfer buffer (25 mM Tris pH 8.3, 192 mM Glycine). In general, transfer was done with the wet blot technique and nitrocellulose membrane (Amersham, Hybond-ECL, GE Healthcare). The blotting chamber, cassettes and sponges were washed and incubated in cold transfer buffer for 5 min. The sandwich was assembled in the following way: a sponge was placed in a blotting cassette, followed by blotting paper (Whatman), the nitrocellulose membrane, the SDS-PAGE gel, another layer of blotting paper and another sponge. The cassette was placed in the transfer chamber so that the membrane was directed towards the anode. The transfer was done in cold transfer buffer at 60V, 0.5 mA for 70 min at RT. After the run, the membrane was removed and blocked in milk blocking solution (5% milk powder dissolved in 1x TBS supplemented with either 0.1% Tween-20 or 0.02% NP-40, depending on the antibody) for 1h at RT. Finally, the primary antibody was diluted in blocking buffer and added to the membrane overnight at 4°C or for at least 3h at RT.

3.2.4.14 Western blot transfer with electro blotting for Phos-tag-PAGE

After electrophoresis the Phos-tag-PAGE was washed twice in transfer buffer with 1 mM EDTA for 5 min and washed twice more in transfer buffer without EDTA. The Phos-tag-PAGE was transferred to a nitrocellulose membrane in a blotting tank at 15 V, 75 mA for 18 h at 4°C.The nitrocellulose membrane was then blocked in a suitable blocking solution and incubated in primary antibody.

3.2.4.15 Western Blot detection

After primary antibody incubation, the membrane was washed 3 times in washing buffer (1x TBS supplemented with either 0.1% Tween-20 or 0.02% NP-40) for 10 min each at RT. Then the fluorescent labeled secondary antibody (LiCOR) was diluted 1:10.000 in blocking solution and incubated on the membrane for 1-1.5 h at RT under light exclusion. After secondary antibody incubation, the membrane was washed again 3 times in washing

buffer for 10 min each at RT. Western blots were developed with the Odyssey CLx LiCOR imaging system.

3.2.4.16 Cell culture – passaging of mammalian cells

HeLa and HEK293T cells were cultured in DMEM (Dulbecco's modified eagel medium Gibco) at 37°C. Cells were cultured until 70-80% confluency was reached. Briefly, all work was done under a sterile hood and all equipment used for passaging cells was sterilized with 70% ethanol directly before use. All media were pre-warmed to 37°C before use. The medium was carefully aspirated from the plate and the cells attached to the bottom of the petri dish were washed in 10 ml 1x PBS. After washing, 2 ml trypsin (for 10 cm dish) was added and the plate was turned to cover the surface with trypsin. The plate was incubated at 37°C for 5 min. Followed by resuspension of the cells in 10 ml DMEM medium was added and the cell suspension was pipetted up and down in a 10 ml pipette to avoid cell clumps. Finally, the cell suspension was plated on a new plate. To maintain cells in culture, they were plated on a 10 cm dish or a 20 cm dish. For transfection cells were plated in 6-well plates.

3.2.4.17 DNA transfection of mammalian cells

Cells were always seeded one day before transfection to be 80% confluent at the time point of transfection. On the day of transfection, media was removed and pre-warmed Opti-MEM was added. Lipofectamine 2000 and the plasmid were prepared in Opti-MEM medium as described in table 3.

Table 3. Pipetting scheme to transfect mammalian cells.

		Tube 1		Tube 2	
Plate	**Plate volume (ml)**	**OptiMEM volume (µl)**	**Liptofectamine 2000 volume (µl)**	**OptiMEM volume (µl)**	**Amount of plasmid (µg)**
10 cm	10	1000	30	1000	14
6-well	2	200	6	200	2.8
12-well	0.85	85	2.55	85	1.2
24-well	0.5	50	1.5	50	0.7

The prepared lipofectamine solution in tube 1 and the plasmid solution in tube 2 were incubated at RT for 5 min. Tube 1 and 2 were mixed and incubated for 15 min at RT and

finally added to the cells. Cells were incubated for 6h, then trypsinized and diluted 1:5 in DMEM medium. Cells were harvested 48 hours after transfection.

3.2.4.18 Immunofluorescence

Cells were seeded before all IF experiments in a 6-well or 12-well plate in DMEM. Medium was aspirated and each well was washed at least twice in 1x PBS (use 1ml per well for a 12 well dish). Cells were fixed for 20 min with 4% paraformaldehyde in 1x PBS (pH 7.4) and afterwards washed twice with PBS. Cells were permeabilized for 10 min with 0.3% TritonX-100, 0,05% SDS in 1x PBS at RT. After permeabilization, the cells were washed twice in PBS followed by blocking against unspecific antibody binding with 10% fetal bovine serum (FCS) diluted in 1x PBS. Blocking was done for 30 min at RT or overnight at 4°C. The primary antibody was diluted in 5% FCS and incubated overnight at 4°C. After primary antibody incubation, each well was washed 3 times in 1x PBS followed by secondary antibody incubation. The secondary antibody was diluted in 5% FCS 1:10.000 and incubated for 1h at RT under light exclusion. After secondary incubation, each well was washed 3 times in 1x PBS. For mounting the coverslips, each coverslip was briefly washed in dH_2O to remove salts from the PBS and directly mounted on the coverslip in a Mowiol/DAPI drop. The mounted coverslips were dried at 37°C for at least 1 h or overnight at RT. The cells were imaged with a LSM-510 microscope (Zeiss).

3.2.4.19 TCA precipitation of proteins

Prepared solubilized heart membranes or cytosol or complete lysate was precipitated by adding TCA up to a final concentration of 12.5% and incubated on ice for 30 min, followed by centrifugation at 11.000 g for 7 min at 4°C. The supernatant was discarded and the pellet was washed two times with ice-cold acetone. After the last washing step, the supernatant was removed and the pellet was dried at 37°C for 10 min. Finally, SDS sample buffer (2% SDS, 0.1% bromophenol blue, 10% glycerol, 50 mM Tris-HCl pH 6.8) supplemented with 100 mM DTT was added and the pellet was dissolved at 30°C for at least 10 min.

3.2.4.20 PKA or CaMKII phosphorylation of recombinant protein

10 µg recombinant purified PLN-GST mutants were phosphorylated with recombinant PKA (NEB) or CaMKII kinases (Thermo Scientific) according to the suppliers information at 30°C for 1 h. CaMKII kinase was auto-phosphorylated before use according to suppliers information at 30°C for 10 min. Phosphorylated protein was either used for further

experiments or solved in 1 x SDS sample buffer and analysed by SDS-PAGE and Phos-tag-PAGE.

3.2.4.21 Phosphorylation with cardiac cytosol

10 µg recombinant purified PLN-GST mutants were immobilized to 5 µl glutathione sepharose beads (GE Healthcare) in GST buffer (20 mM HEPES pH 7.5, 150 mM KOAc, 5 mM $Mg(OAc)_2$, 1 mM EDTA, 1 mM DTT) for 45 min at 4°C under gentle rotation.
For the preparation of cardiac cytosol, a mice heart disrupted with a MiccraD-1 tissue homogenizer in homogenization buffer (50 mM NaCl, 320 mM Sucrose, 2 mM EDTA, 20 mM HEPES pH 7.4, 1x protease inhibitor, 1 x phosphatase inhibitor). The lysate was centrifuged at 100.000 g for 30 min. The supernatant after centrifugation is the cytosol, which was diluted 1:5 in GST buffer supplemented with 1x protease inhibitor, 1 x phosphatase inhibitor and 1 x EM (EM, an ATP regeneration system (10 mM phosphocreatine, 0.5 mM ATP, 0.5 mM GTP, 50 µg/ml creatine phosphokinase). The resin bound PLN-GST mutant proteins were incubated for 1 h in cardiac cytosol at 4°C under gentle rotation. The resin bound proteins were collected and washed 4 times in GST buffer, followed by elution with 1x SDS sample buffer supplied with 100 mM DTT. The phosphorylation assay was analysed on Coomassie stained SDS-PAGE and Phos-tag-PAGE.

3.2.4.22 Binding assay with recombinant PLN-GST constructs and 14-3-3 gamma

10 µg recombinant purified PLN-GST mutants were phosphorylated with recombinant PKA (NEB) or CaMKII kinases (Thermo Scientific) according to the suppliers information at 30°C for 1 h. Phosphorylated bait proteins were bound to 5 µl glutathione sepharose beads (GE Healthcare) in GST buffer (20 mM HEPES pH 7.5, 150 mM KOAc, 5 mM $Mg(OAc)_2$, 1 mM EDTA, 1 mM DTT, 0.1% TritonX-100) for 45 min at 4°C under gentle rotation. Resin-bound bait proteins were incubated with equimolar amounts of recombinant purified 14-3-3 protein in GST buffer for 1 h at 4°C under gentle rotation. The resin-bound bait was washed 4 times in GST buffer and eluted in 1 x SDS sample buffer (supplied with 100 mM DTT). The binding assay was analysed on SDS-PAGE, which was transferred to nitrocellulose and probed with the 14-3-3 pan antibody (Santa Cruz) and on a Coomassie stained Phos-tag-PAGE.

3.2.4.23 Separation of heart membranes and cytosol

Binding experiments with recombinant 14-3-3 proteins were done with mice or human heart membranes and cytosol. Hearts or tissue samples were thawed on ice, fat tissue was removed and the heart was cut in small pieces. The tissue was mechanically disrupted with a MiccraD-1 homogenizer for 30 sec in tissue homogenization buffer (50 mM NaCl, 320 mM Sucrose, 2 mM EDTA, 20 mM HEPES, pH 7.4, 1x protease inhibitor, 1 x phosphatase inhibitor). Lysed tissue was dounced for 30 strokes on ice. The lysate was centrifuged at 100.000 g for 30 min at 4°C to separate membrane and cytosol. The supernatant is the cytosolic fraction and the pellet is the membrane fraction. The membranes were either stored at -80°C in tissue homogenization buffer with protease and phosphatase inhibitors or directly solubilized (section 3.2.4.24). The cytosol was cleared with another centrifugation step at 100.000 g for 30 min and either stored at -80°C or on ice until further use.

3.2.4.24 Heart membrane solubilization

Separated heart membranes were washed once in tissue homogenization buffer (50 mM NaCl, 320 mM Sucrose, 2 mM EDTA, 20 mM HEPES, pH 7.4, 1x protease inhibitor, 1 x phosphatase inhibitor). 1 mg of washed crude membrane was solubilized in 1 ml ComplexioLyte48 (Logopharm) solubilization buffer on ice for 30 min, followed by centrifugation at 55.000 g for 30 min at 4°C. The supernatant contains solubilized heart membrane proteins, the detergent was diluted 1:5 with GST buffer pH 7.4 (20 mM HEPES pH 7.4, 150 mM KOAc, 5 mM $Mg(OAc)_2$, 1 mM EDTA, 1 mM DTT, 1x protease inhibitor, 1x phosphatase inhibitor). Solubilized heart membranes were used for pull-down experiments or for Western blot analysis.

3.2.4.25 14-3-3 pull-down experiment with heart membranes

The pull-down experiments were done with solubilized heart membranes or cytosol and recombinant purified MBP-14-3-3 bait protein. 50 µg of bait protein was recombinantly phosphorylated with either PKA (NEB) or CaMKII kinase (Thermo Fisher) as described in section 3.2.4.20. Phosphorylated proteins were immobilized to 5 µl amylose resin bead slurry (NEB) in GST buffer (20 mM HEPES pH 7.5, 150 mM KOAc, 5 mM $Mg(OAc)_2$, 1 mM EDTA, 1 mM DTT) supplied with protease and phosphatase inhibitors for 45 min at 4°C under gentle rotation. Immobilized bait protein was washed 3 times in GST buffer, followed by blocking in 4% BSA dissolved in GST buffer and supplemented with protease and phosphatase inhibitors for 30 min at 4°C under gentle rotation to block unspecific binding sites. After blocking, the resin-bound bait proteins were washed 3 times in GST buffer and

added to prepared solubilized heart membranes or cytosol. After 1 h incubation at 4°C under gentle rotation the resin-bound bait was washed 4 times in GST buffer followed by elution with SDS-sample buffer (containing 100 mM DTT). The pull-down experiment was analysed on SDS-PAGE transferred to nitrocellulose and detected with anti-PLN total, PLN pS16 and PLN pT17 antibodies.

Table 4. Plasmids generated and used in chapter III.

Plasmid name	Description	Restriction enzymes	Source
pMal2CX	Bacterial expression vector for N-terminal MBP-tagged proteins	Insert at EcoRI - HindIII	New England BioLabs
pMal2CX 14-3-3 gamma	Bacterial expression vector for MBP-14-3-3 gamma	Insert at EcoRI - HindIII	J. Menzel
pMal2CX - GST modified	Bacterial expression for C-terminal tagged GST proteins (MBP-tag removed)	NdeI - BamHI	J. Menzel
pMal2CX modified PLN N31 WT	Bacterial expression vector for PLNcyt-linker-GST N31 WT	Insert at NdeI-XhoI	J. Menzel
pMal2CX modified PLN N31 S16A	Bacterial expression vector for PLNcyt-linker-GST N31 S16A	Insert at NdeI-XhoI	J. Menzel
pMal2CX modified PLN N31 T17A	Bacterial expression vector for PLNcyt-linker-GST N31 T17A	Insert at NdeI-XhoI	J. Menzel
pMal2CX modified PLN N31 S10A	Bacterial expression vector for PLNcyt-linker-GST N31 S10A	Insert at NdeI-XhoI	J. Menzel
pMal2CX modified PLN N31 R9C	Bacterial expression vector for PLNcyt-linker-GST N31 R9C	Insert at NdeI-XhoI	J. Menzel
pMal2CX modified PLN N31 R14del	Bacterial expression vector for PLNcyt-linker-GST N31 R14del	Insert at NdeI-XhoI	J. Menzel
pCDNA3.1(zeo+)	Mammalian expression vector	BamHI - XhoI	Invitrogen
pCDNA3.1 PLN N31 WT opsin	Mammalian expression vector for PLNcyt-WT-opsin	Insert at BamHI - XhoI	J.E. Rivera-Monroy
pCDNA3.1 PLN N31 S10A opsin	Mammalian expression vector for PLNcyt-S10A opsin	Insert at BamHI - XhoI	J. Menzel
pCDNA3.1 PLN N31 S16A opsin	Mammalian expression vector for PLNcyt-S16A opsin	Insert at BamHI - XhoI	J. Menzel

pCDNA3.1 PLN N31 R9C opsin	Mammalian expression vector for PLNcyt-R9C opsin	Insert at BamHI - XhoI	J.E. Rivera-Monroy
pCDNA3.1 PLN N31 R14del opsin	Mammalian expression vector for PLNcyt-R14del opsin	Insert at BamHI - XhoI	J.E. Rivera-Monroy

Table 5. Oligonucleotides used for PCR's.

Name	Description	Sequence (5'-3')
14-3-3 gamma-FP	Used to generate 14-3-3 gamma, forward primer	GGA TTT CAG AAT TCA TGG TGG ACC GCG AGC AAC TGG TGC AGA AAG CCC
14-3-3 gamma-RP	Used to generate 14-3-3 gamma, reserve primer	GGG CTT TCT GCA CCA GTT GCT CGC GGT CCA CCA TGA ATT CTG AAA TCC
BamHI-PLN For	Used to generate pCDNA3.1 PLN, forward primer	GCG GCG GGA TCC ATG GAA AAA GTG CAA TAC CTC AC
opsin-XhoI-Rev	Used to generate pCDNA3.1 PLN, reverse primer	CGG CGG CTC GAG TCA GCC CGT CTT GTT GGA G
pCDNA.3.1-PLN-S10A For	Used to generate mammalian PLN S10A, forward primer	GGA AAA AGT GCA ATA CCT CAC TCG CGC CGC TAT CAG GAG AGC CTC CAC
pCDNA.3.1-PLN-S10A Rev	Used to generate mammalian PLN S10A, reverse primer	GTG GAG GCT CTC CTG ATA GCG GCG CGA GTG AGG TAT TGC ACT TTT TCC
pCDNA.3.1-PLN-S16A For	Used to generate mammalian PLN S16A, forward primer	CTC GCT CGG CTA TCA GGA GAG CCG CCA CTA TTG AAA TGC CTC AGC AAG C
pCDNA.3.1-PLN-S16A Rev	Used to generate mammalian PLN S16 construct, reverse primer	GCT TGC TGA GGC ATT TCA ATA GTG GCG GCT CTC CTG ATA GCC GAG CGA G
NdeI-PLNcyt-tev-GST For	Used to generate PLNcyt-linker-GST protein, forward primer	ATA CTA CAT ATG ATG GAA AAA GTG CAA TAC CTC
PLNcyt-linker-XhoI-Rev	Used to generate PLNcyt-linker-GST protein, reverse primer	CCG CCG CTC GAG GCT GCC GCC GCC GCC GCT GCC GCC GCC GCC GCT GCC GCC GCC GCC GCT GCC GCC GCC TAG GTT CTG GAG ATT CTG ACG TGC TTG C
Overlapping PLN For	Used to generate PLNcyt-linker-GST protein, reverse primer	GGC GGC GGC GGC AGC GGC GGC GGC GGC AGC GGC GGC GGC GGC AGC ATG TCC CCT ATA CTA GGT TAT TGG AAA ATT AAG GGC C

Overlapping PLN For	Used to generate PLNcyt-linker-GST protein, reverse primer	GCC GCC GCT GCC GCC GCC GCC TAG GTT CTG GAG ATT CTG ACG TGC TTG C
PLNcyt-S10A For	Used to generate PLNcyt-S10A-GST protein, forward primer	GGA AAA AGT GCA ATA CCT CAC TCG CGC CGC TAT CAG GAG AGC CTC CAC
PLNcyt-S10A Rev	Used to generate PLNcyt-S10A-GST protein, reverse primer	GTG GAG GCT CTC CTG ATA GCG GCG CGA GTG AGG TAT TGC ACT TTT TCC
PLNcyt-S16A For	Used to generate PLNcyt-S16A-GST protein, forward primer	CTC GCT CGG CTA TCA GGA GAG CCG CCA CTA TTG AAA TGC CTC AGC AAG C
PLNcyt-S16A Rev	Used to generate PLNcyt-S16A-GST protein, reverse primer	GCT TGC TGA GGC ATT TCA ATA GTG GCG GCT CTC CTG ATA GCC GAG CGA G
PLNcyt-T17A For	Used to generate PLNcyt-T17A-GST protein, forward primer	GCT CGG CTA TCA GGA GAG CCT CCG CCA TTG AAA TGC CTC AGC AAG CAC G
PLNcyt-T17A Rev	Used to generate PLNcyt-T17A-GST protein, reverse primer	CGT GCT TGC TGA GGC ATT TCA ATG GCG GAG GCT CTC CTG ATA GCC GAG C

Table 6. Antibodies used in chapter III.

Name	Supplier	Cat. No.	Dilution	Technique	Clonality
14-3-3 pan (H8)	Santa Cruz	sc-1657	1:1000	WB	polyclonal
p-CAMKII (Thr286)	abcam	ab32678	1:1000	WB	polyclonal
EEA-1	BD Transduction Laboratories	610456	1:200	IF	monoclonal
GAPDH	NeoBiotech	NB-29-00852	1:5000	WB	polyclonal
MBP	New England BioLabs	E8032S	1:10000	WB	monoclonal
Na/K ATPase alpha	Santa Cruz	sc-21712	1:1000	WB	monoclonal
Opsin	from Bernhardt Dobbelstein	-	1:1000	WB	polyclonal
PLN	Abcam	ab2865	1:1000 1:100	WB,IF	monoclonal
PLN pS16	Badrilla	A010-12	1:1000	WB	polyclonal
PLN pT17	Badrilla	A010-13	1:1000	WB	polyclonal
Sec61beta	from Bernhardt Dobbelstein	-	1:200	IF	polyclonal
SERCA	Santa Cruz	sc-8093	1:1000	WB	polyclonal
Rab7	Cell signaling	9367	1:200	IF	polyclonal

3.3 Results

3.3.1 Recombinant PLN is phosphorylated at S16 by PKA and at T17 by CaMKII

I identified a novel interaction between PLN and the phospho-adaptor protein 14-3-3 using binding assays with solubilized mouse heart membranes as input (see chapter 2, figure 1). PLN has two main phosphorylation sites within the N-terminus, the S16 and T17 residues. Phosphorylation of PLN disrupts its interaction with SERCA and leads to an inhibitory effect on SERCA. Therefore, phosphorylation of PLN is important for Ca^{2+} handling in cardiomyocytes. To determine the 14-3-3 binding site, recombinant PLN protein variants relevant for PLN phosphorylation were designed (Table 7). The cytosolic region of PLN (31 aa) was fused to a linker and a GST-tag separated by a flexible linker (Table 7). Phospho-dead mutants for the three phosphorylatable residues were generated as well as two human-disease causing mutations (Table 7).

Table 7. PLN protein variants designed for bacterial expression.

The first 31 N-terminal amino acids were fused with a linker and a GST-tag. Different mutations regarding the different phosphorylation sites in PLN (S10A, S16A, T17A) as well as two disease-causing mutations (R9C, R14del) were generated. The di-arginine ER-retention signal in the PLN sequence is marked in green and the 14-3-3 target site is highlighted in orange. The single amino acid mutations inserted in the constructs are shown in red.

Peptide name	Amino acid sequence
PLN_{cyt}-linker-GST WT	MEKVQYLTRSAIRRASTIEMPQQARQNLQNL-linker-GST
PLN_{cyt}-linker-GST R9C	MEKVQYLTCSAIRRASTIEMPQQARQNLQNL-linker-GST
PLN_{cyt}-linker-GST R14del	MEKVQYLTRSA_IRASTIEMPQQARQNLQNL-linker-GST
PLN_{cyt}-linker-GST S10A	MEKVQYLTRAAIRRASTIEMPQQARQNLQNL-linker-GST
PLN_{cyt}-linker-GST S16A	MEKVQYLTRSAIRRAATIEMPQQARQNLQNL-linker-GST
PLN_{cyt}-linker-GST T17A	MEKVQYLTRSAIRRASAIEMPQQARQNLQNL-linker-GST

The recombinant PLN protein variants were expressed and purified from *E. coli*, analysed on Coomassie stained SDS-PAGE (Figure 14) and confirmed by Western blot using a PLN antibody (Figure 14). The PLN antibody (2D12, abcam) could not detect the R9C variant, probably because the R9 residue is part of the epitope recognized by the antibody. Besides the PLN R9C mutant, all recombinant purified PLN variants were detected by the PLN antibody (Figure 14).

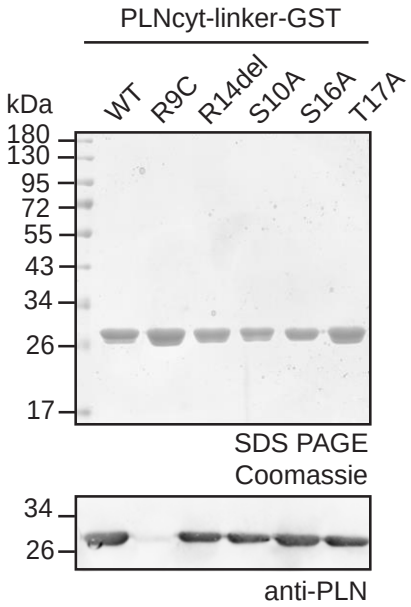

Figure 14. Purification of recombinant PLNcyt-linker-GST proteins.

Purified proteins were analysed on a Coomassie stained SDS-PAGE and verified by Western blotting with an anti-PLN antibody.

Recombinant phosphorylation of the purified PLN constructs was required for detailed analysis of the PLN 14-3-3 interaction *in-vitro*. Therefore, purified PLN WT, S10A, S16A and T17A variants were phosphorylated using the recombinant kinases. The purified PLN mutant proteins were *in-vitro* phosphorylated with either recombinant catalytic subunit of PKA (Figure 15A) or recombinant CaMKII (Figure 15B). Samples were then subjected to Phos-tag-PAGE and SDS-PAGE and stained in Coomassie solution for analysis. Phosphorylated residues form complexes with $MnCl_2$ in a Phos-tag-PAGE and therefore run slower through the gel, which lead to an upward shift (Kumar, 2018). PLN WT was phosphorylated after PKA treatment which was visible by a shift on the Phos-tag-PAGE that is absent in samples lacking PKA treatment (Figure15A). PLN S10A and T17A were phosphorylated after PKA treatment as well but not the PLN S16A protein (Figure 15A). In parallel, the PLN constructs were *in-vitro* phosphorylated with CaMKII and analysed on Coomassie stained Phos-tag-PAGE and SDS-PAGE (Figure 15B). PLN WT, PLN S10A, and PLN S16A constructs were phosphorylated, but not the PLN T17A protein (Figure 15B). Altogether, recombinant phosphorylation of PLN variants confirmed that PKA phosphorylated S16 in PLN, meanwhile CaMKII phosphorylated the T17 residue in PLN.

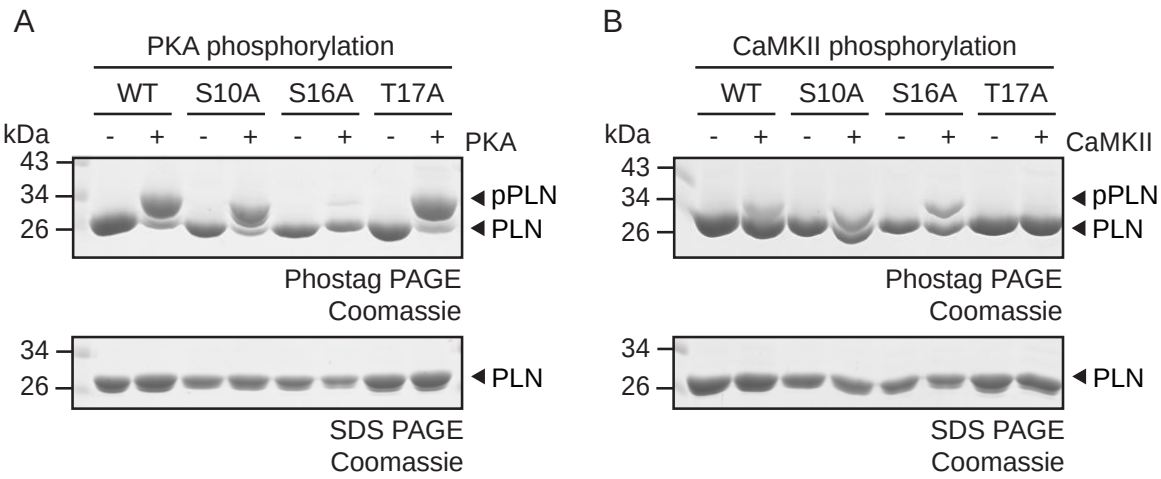

Figure 15. PKA specifically phosphorylates S16 and CaMKII kinase T17 in PLN.

Purified PLN mutant variants were *in-vitro* phosphorylated with either (**A**) PKA or (**B**) CaMKII kinase. Results were analysed on Coomassie stained Phos-tag-PAGE or SDS-PAGE. Phosphorylated PLN (pPLN) is indicated.

Phosphorylation of recombinantly purified PLN proteins as seen with *in-vitro* supplied PKA or CaMKII kinases were corroborated by phosphorylating them with kinases present in mouse heart cytosol. Prepared cytosol contains native catalytic subunits of PKA as well as CaMKII kinase. The cytosol was supplied with an ATP regeneration system (“energy mix”; EM) to keep the kinases functional. The recombinantly purified PLN proteins were incubated in heart cytosol, followed by analysis on Coomassie stained Phos-tag-PAGE and SDS-PAGE (Figure 16). All different PLN variants were phosphorylated as indicated by the shift on the Phos-tag-PAGE (Figure 16). Upon closer inspection, it was noticeable that the PLN WT protein showed two phosphorylation bands in comparison with the other PLN variants. Even though, the upper band was very weak this result indicated that the PLN WT construct was double phosphorylated by PKA and CaMKII kinase after incubation with heart cytosol. Meanwhile the PLN S16A and T17A mutants were single phosphorylated (Figure 16).

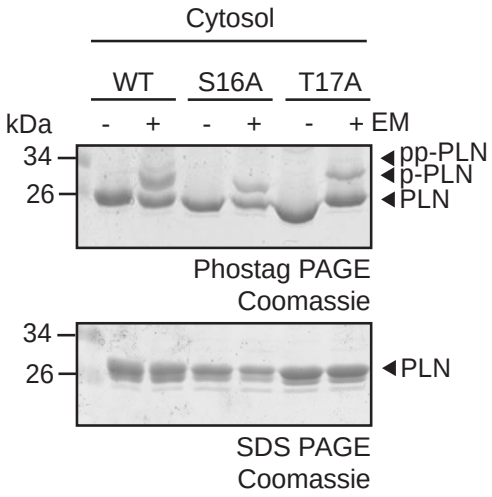

Figure 16. Double phosphorylation of purified PLN WT protein with native kinases from heart cytosol.

The cytosol was supplied with an ATP regeneration system (EM). Cytosol without EM was used as a negative control. Phosphorylated recombinant PLN variants were analysed on Coomassie stained Phos-tag-PAGE and SDS-PAGE. Single phosphorylated PLN (pPLN) and double phosphorylated PLN (pp-PLN) are indicated.

Altogether, recombinant *in-vitro* phosphorylation of PLN variants using recombinant PKA or CaMKII showed that PKA specifically phosphorylated the S16 residue in PLN, meanwhile CaMKII phosphorylated T17 in PLN. Recombinant PLN protein variants were also phosphorylated with native PKA and CaMKII kinase from mouse tissue, confirming that PLN can be double phosphorylated, meanwhile the PLN S16A and T17A variants were both single phosphorylated.

3.3.2 14-3-3 is unable to bind double phosphorylated PLN at S16 and T17

The binding affinities of 14-3-3 to the two different phosphorylation sites in recombinant PLN proteins were already analysed in chapter 2. I was able to show that 14-3-3 binds the two different phosphorylated residues in PLN with different affinities (chapter 2, figure 3). In brief, phosphorylated T17 showed a higher affinity to 14-3-3 than phosphorylated S16 in PLN. Next, I wondered whether 14-3-3 could interact with the double phosphorylated PLN protein, namely phosphorylated at S16 and T17 at the same time. To this end, recombinant PLN-GST protein variants were phosphorylated with both PKA and CaMKII kinases simultaneously followed by 14-3-3 binding. The 14-3-3 interaction was detected by Western blotting with a 14-3-3 antibody and Coomassie stained SDS-PAGE and Phos-tag-PAGE showing the efficiency of *in-vitro* phosphorylation (Figure 17). 14-3-3 binding was observed for phosphorylated PLN S16A and T17A variants but not for the WT PLN

(Figure 17). Phos-tag gels indicate that the S16 as well as the T17 residues were phosphorylated in the respective mutants and the WT was double phosphorylated. However, the phosphorylation efficiency was best for the T17A mutant and both S16A and WT showed lower phosphorylation efficiencies. Taken together, 14-3-3 can bind the single phosphorylated S16 or T17 residues in PLN, but not to the double phosphorylated monomeric PLN.

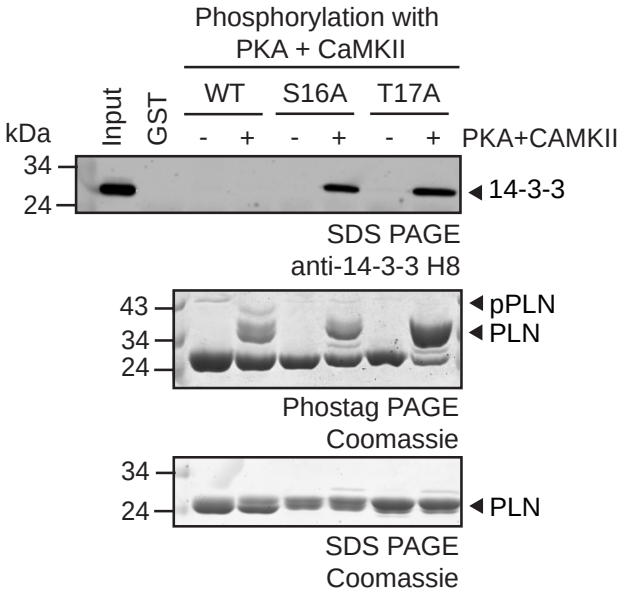

Figure 17. Double phosphorylation of pS16 and pT17 residue in monomeric PLN prevents 14-3-3 binding.

Recombinant PLN-GST protein variants were recombinantly phosphorylated with PKA and CaMKII kinases at the same time, followed by 14-3-3 binding and analysis by Western blot, Coomassie stained Phos-tag-PAGE and SDS-PAGE. Phosphorylated PLN (pPLN) is indicated.

3.3.3 PLN R14del mutation is either mislocated or aggregates in the homozygous mouse model

Two mutations in the PLN sequence, R14del and R9C mutation, lead to severe dilated cardiomyopathy in heterozygous patients. 14-3-3 was already identified to also interact with recombinant PLN R9C and R14del disease-related mutations (chapter 2, figure 4D). Patients who suffer the R14del mutation are missing the arginine 14 residue, which is located in the PKA consensus motif. Therefore, PKA is unable to phosphorylate S16. PLN phosphorylation by CaMKII remains unaffected by this mutation (Haghighi et al., 2006). I could already show that CaMKII kinase phosphorylation is a requirement for 14-3-3 interaction with the R14del PLN mutation (chapter 2, figure 4D). PLN R14del homozygous (*Pln*$^{\Delta R14/\Delta R14}$) and heterozygous (*Pln*$^{+/\Delta R14}$) mouse models have been developed at the lab of Prof. Dr. Herman Silljé (Eijgenraam et al., 2020). Furthermore, the lab of Prof. Dr. Stephan Lehnart breeds a PLN knockout (*Pln*$^{-/-}$) mouse model. The results of the

Pln$^{\Delta R14/\Delta R14}$ mice were always compared to a PLN WT mouse *(Pln*$^{+/+}$*),* corresponding to littermates without the *Pln*$^{\Delta R14/\Delta R14}$ mutation introduced into the genome. I obtained ventricular tissue samples from the aforementioned mouse models to analyze PLN steady-state levels and the phosphorylation state of PLN. Ventricular samples were subjected to subcellular fractionation followed by the analysis of the steady-state levels of PLN and 14-3-3 by Western blot. The rationale behind this experiment was the hypothesis that phospho-PLN is a major 14-3-3-binding protein in cardiac membranes and that less phosphorylated PLN would translate into lower 14-3-3 steady-state levels.

The amount of total PLN protein was strongly reduced in *Pln*$^{\Delta R14/\Delta R14}$ mice membranes in comparison to *Pln*$^{+/+}$ animals as indicated by Western blotting (Figure 18). This loss was also reflected in both phosphorylated forms of PLN, i.e. the pS16 and the pT17. Meanwhile the *Pln*$^{+/+}$ control samples showed phosphorylation at both phospho-sites (Figure 18). In parallel, I was interested in knowing whether the steady-state level of SERCA, as a known interaction partner of PLN, was affected by the absence of PLN. Interestingly, SERCA steady-state levels were also reduced in the *Pln*$^{\Delta R14/\Delta R14}$ mouse in comparison with *Pln*$^{+/+}$ control animals (Figure 18).

Altogether, PLN and SERCA steady-state levels were strongly reduced in the *Pln*$^{\Delta R14/\Delta R14}$ mouse membranes from ventricles.

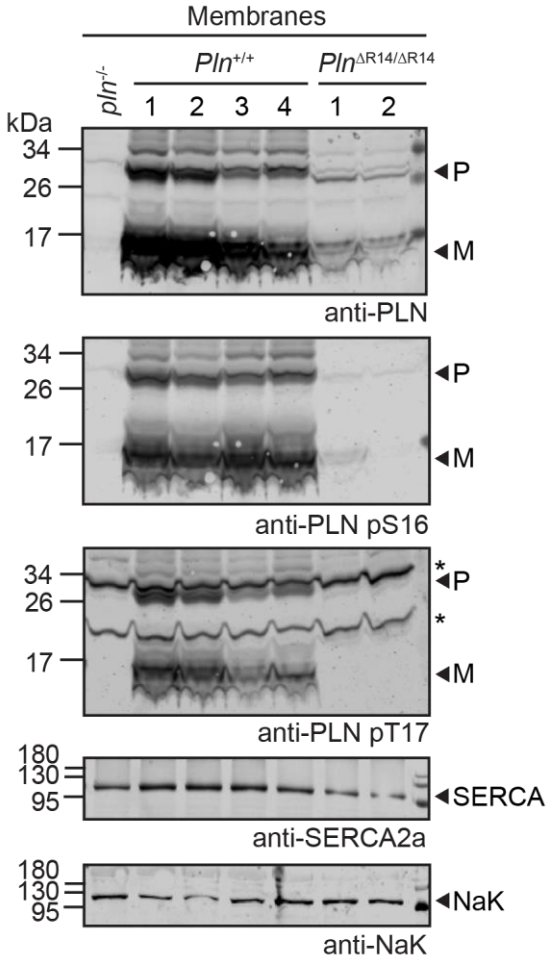

Figure 18. PLN steady-state levels were reduced in *Pln*$^{\Delta R14/\Delta R14}$ mouse heart membranes.
WT (*Pln*$^{+/+}$), PLN K.O. (*Pln* $^{-/-}$), and PLN R14del homozygous (*Pln*$^{\Delta R14/\Delta R14}$) mice membranes were analysed by Western blotting with PLN, phosphorylated S16, phosphorylated T17 or SERCA2a antibodies. Equal loading of membrane samples was confirmed by Western blotting for Na/K ATPase (NaK). PLN monomer (M) and pentamer (P) are indicated.

Having found that the PLN steady-state-levels were strongly reduced in the *Pln*$^{\Delta R14/\Delta R14}$ mouse model, I was interested whether the 14-3-3 steady-state-levels were also influenced in the disease model. In addition, I analysed phosphorylated CaMKII (pCaMKII) steady-state levels in the *Pln*$^{\Delta R14/\Delta R14}$ mouse model since the PKA interaction site is disrupted in the R14del PLN mutation. Again, subcellular fractions were prepared from the ventricular tissue samples of the mouse models and the 14-3-3 and pCaMKII levels at steady-state were analysed by Western blot (Figure 19). 14-3-3 as well as pCaMKII steady-state-levels were not influenced in the *Pln*$^{\Delta R14/\Delta R14}$ mouse neither in membranes (Figure 19A) nor in cytosol (Figure 19B). Equal loading of membrane or cytosol samples were controlled by analysing Na/K ATPase in membranes (Figure 19A) and glycerinaldehyde-3-phosphate-dehydrogenase (GAPDH) in the cytosol (Figure 19B). These results indicated that neither 14-3-3 nor activated pCaMKII steady-state levels are altered due to the PLN R14del mutation.

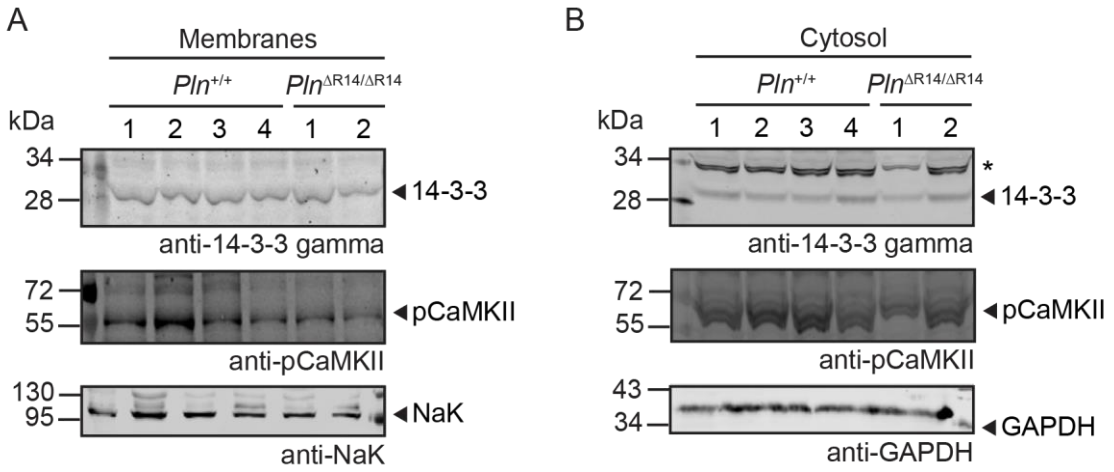

Figure 19. 14-3-3 and pCaMKII steady-state levels were unaltered in *Pln*$^{\Delta R14/\Delta R14}$ mouse heart membranes and cytosol.

Analysis of 14-3-3 and pCaMKII steady-state levels in WT (*Pln*$^{+/+}$) and PLN R14del homozygous (*Pln*$^{\Delta R14/\Delta R14}$) mice membranes (**A**) and cytosol (**B**) analysed by Western blot with 14-3-3 and pCaMKII antibodies. Equal loading of membrane and cytosol samples were confirmed with Western blotting for Na/K ATPase and GAPDH respectively.

Finally, a 14-3-3 binding experiment with the *Pln*$^{\Delta R14/\Delta R14}$ mouse model and corresponding controls was performed, to investigate whether the R14del PLN protein is still able to bind 14-3-3. Strongly reduced levels of PLN R14del protein were detected in the analysis of PLN protein steady-state levels (Figure 18). However, solubilized membranes from the *Pln*$^{\Delta R14/\Delta R14}$ and *Pln*$^{+/+}$ mouse models were used for an affinity purification experiment and incubated with recombinant MBP-14-3-3 gamma protein. Recombinant MBP and MBP-14-3-3 gamma bound to the 14-3-3 blocking peptide R18 served as negative controls of

the experiment. Eluates were analysed by Western blot with PLN antibody and phospho-PLN antibodies (Figure 20). As expected, the PLN pentamer was enriched with recombinant 14-3-3 protein from *Pln*$^{+/+}$ mouse membranes (Figure 20). Very small amounts of the PLN R14del pentamer were enriched from membranes of the *Pln*$^{\Delta R14/\Delta R14}$ disease model (Figure 20). PLN pentamers enriched from *Pln*$^{+/+}$ mouse membranes contained both phosphorylated S16 and T17 residues (Figure 20). However, no phosphorylated residues could be observed in the R14del PLN pentamers enriched from the membranes of the *Pln*$^{\Delta R14/\Delta R14}$ disease mouse. This observation is hard to interpret due the very reduced amounts of enriched PLN R14del pentamers since both antibodies detecting phospho-PLN were less sensitive.

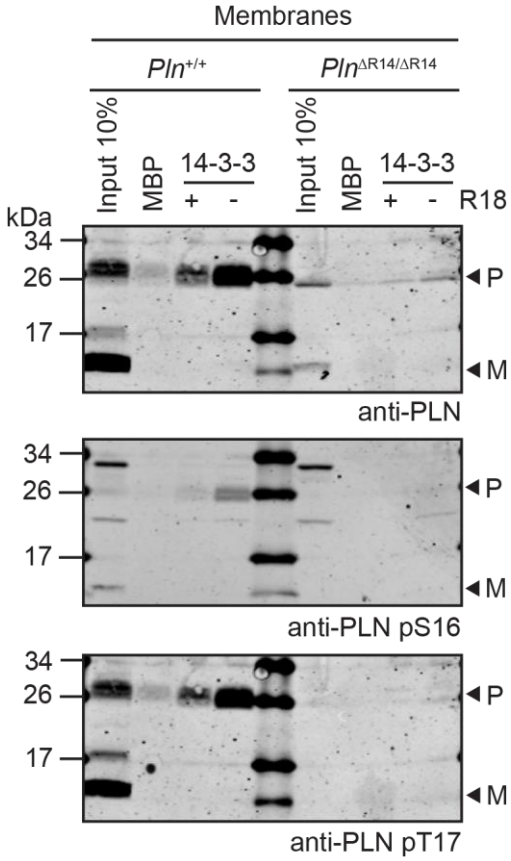

Figure 20. R14del PLN pentamers were enriched with recombinant 14-3-3 gamma from the *Pln*$^{\Delta R14/\Delta R14}$ mouse model.

Binding assay with solubilized WT (*Pln*$^{+/+}$) and PLN R14del homozygous (*Pln*$^{\Delta R14/\Delta R14}$) mice membranes and recombinant MBP-14-3-3. MBP and MBP-14-3-3 blocked with R18 were negative controls. Eluates were probed by Western blot for enriched PLN, PLN pS16 and pT17 proteins with corresponding antibodies. PLN monomer (M) and pentamer (P) are indicated.

In summary, PLN steady-state levels were found to be strongly reduced in the *Pln*$^{\Delta R14/\Delta R14}$ disease mouse which indicates either mislocalization or aggregation of the mutant protein. However, 14-3-3 and pCaMKII steady-state levels were not influenced in the *Pln*$^{\Delta R14/\Delta R14}$ disease mouse. Even though, PLN R14del was severely reduced at steady-state level in the homozygous mouse tissue, I was able to enrich small amounts of R14del PLN pentamers in binding experiments with recombinant MBP-14-3-3 gamma. This suggests that the PLN R14del protein is able to bind 14-3-3 and confirms results from in vitro-binding assays performed in chapter 2 (Figure 4D).

3.3.4 PLN R14del mutation is either mislocated or aggregates in the heterozygous mouse model

I also analysed the interaction between 14-3-3 and PLN in a PLN R14del heterozygous (*Pln*$^{+/\Delta R14}$) mice model. Patients suffering from the PLN R14del mutation are heterozygous carriers. Until today, no homozygous carrier has been identified (Haghighi et al., 2006).
Ventricular tissue from the *Pln*$^{+/\Delta R14}$ mouse model was analysed to assess the steady-state level of PLN as well as the PLN phosphorylation status. A PLN WT mouse (*Pln*$^{+/+}$) was used as a control as well as a PLN K.O. mouse (*Pln*$^{-/-}$). First, membranes and cytosol were separated from all ventricular heart samples and analysed by a Western blot for total PLN and phosphorylated states of PLN (Figure 21). PLN monomers and pentamers were detected for both the *Pln*$^{+/+}$ and the *Pln*$^{+/\Delta R14}$ mice (Figure 21). For two samples from *Pln*$^{+/\Delta R14}$ (2 and 3), the steady-state level of PLN was reduced (Figure 21) in comparison to the controls. The steady-state level of PLN in the *Pln*$^{+/\Delta R14}$ sample 1 showed comparable PLN levels to the *Pln*$^{+/+}$ control animals (Figure 21). The same irregularity was observed for PLN phosphorylated at S16 (Figure 21) and T17 (Figure 21). Mentionable, no difference in PLN protein expression levels of pS16 or pT17 phosphorylation were observed for the *Pln*$^{+/\Delta R14}$ disease model in comparison with control animals.
Overall, slightly reduced PLN steady-state levels were detected in the *Pln*$^{+/\Delta R14}$ disease model but the PLN phosphorylation status was not altered in the *Pln*$^{+/\Delta R14}$ mouse in comparison with control animals.

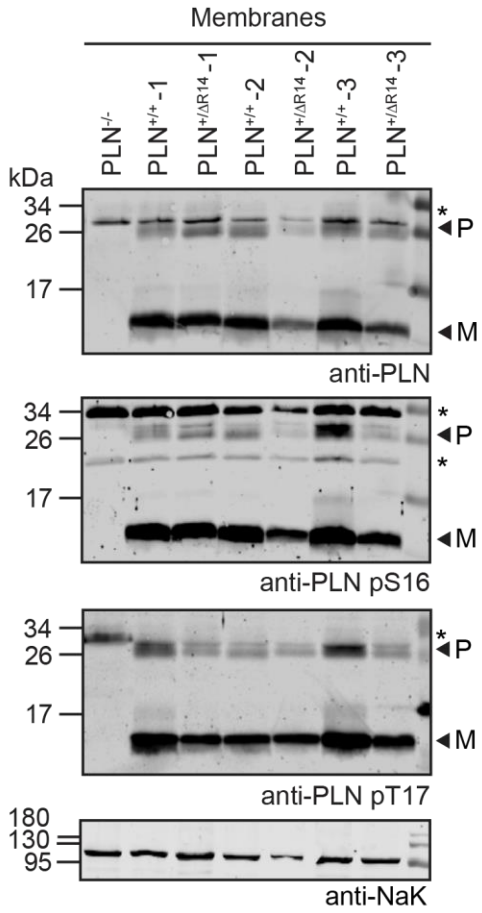

Figure 21. PLN steady-state levels and phosphorylation distribution was not altered in *Pln*$^{+/\Delta R14}$ mouse heart membranes.

WT (*Pln*$^{+/+}$), PLN K.O. (*Pln*$^{-/-}$), and PLN R14del heterozygous (*Pln*$^{+/\Delta R14}$) mice membranes were analysed by Western blot and analysed for PLN, PLN pS16 and PLN pT17 with specific antibodies. Equal loading of membrane samples was confirmed with Western blotting for Na/K. PLN monomer (M) and pentamer (P) are indicated.

In addition to the analysis of PLN steady-state levels in *Pln*$^{+/\Delta R14}$ animals, I was interested whether known PLN interaction partners such as SERCA, 14-3-3, or pCaMKII are influenced due to the heterozygous PLN R14del mutation. Therefore, steady-state levels of 14-3-3, SERCA and pCaMKII kinase, were analysed by Western blotting from separated membranes and cytosol prepared from *Pln*$^{+/\Delta R14}$ and *Pln*$^{+/+}$ control animals (Figure 22). In the membrane fractions from both *Pln*$^{+/\Delta R14}$ and *Pln*$^{+/+}$ mice, very reduced amounts of 14-3-3 protein was detected (Figure 22A). In the corresponding cytosolic fractions, 14-3-3 was detected in both *Pln*$^{+/\Delta R14}$ and *Pln*$^{+/+}$ animals. Yet, the 14-3-3 steady-state levels did not show drastic differences between them that could be attributed to the R14del mutation (Figure 22B). Phosphorylated CAMKII kinase levels were found to be strongly reduced in isolated membrane and cytosolic fractions from both *Pln*$^{+/\Delta R14}$ and *Pln*$^{+/+}$ animals (Figure

22A) indicating that the mutation does not increase steady-state levels of pCaMKII. SERCA steady-state levels were not influenced by the R14del PLN mutation in the *Pln*$^{+/\Delta R14}$ disease animals (Figure 22A). Equal loading of samples was controlled by analysing Na/K ATPase in membranes (Figure 22A) and GAPDH in the cytosol (Figure 22B).

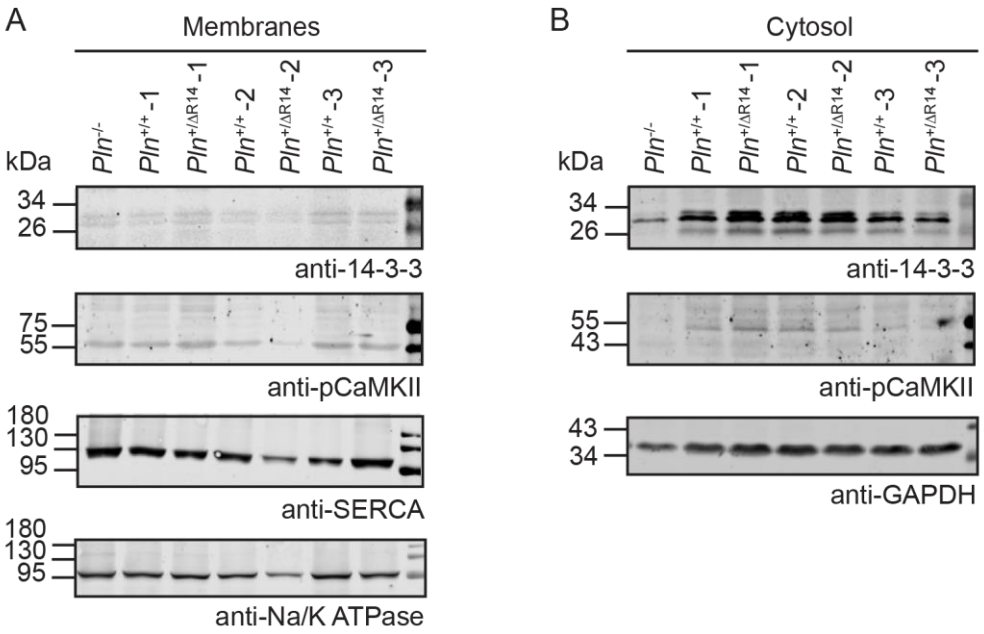

Figure 22. 14-3-3 or pCaMKII steady-state levels were unaltered in *Pln*$^{+/\Delta R14}$ mouse heart membranes and cytosol.

(**A**) Analysis of 14-3-3, pCaMKII, SERCA steady-state levels in WT (*Pln*$^{+/+}$), PLN K.O. (*Pln*$^{-/-}$), and PLN R14del heterozygous (*Pln*$^{+/\Delta R14}$) mice membranes. (**B**) Analysis of 14-3-3 and pCaMKII steady-state levels in WT (*Pln*$^{+/+}$), PLN K.O. (*Pln*$^{-/-}$), and PLN R14del heterozygous (*Pln*$^{+/\Delta R14}$) mice cytosol. Equal loading of membrane and cytosol samples were confirmed with Western blotting for Na/K ATPase and GAPDH respectively. (A) and (B) were analysed by Western blotting with corresponding antibodies.

Further, I aimed to test whether the PLN R14del mutation in a heterozygous mice model influences the ability of PLN to interact with 14-3-3. Therefore, a 14-3-3 binding assay with recombinant MBP-14-3-3 gamma was performed with ventricular membranes from the *Pln*$^{+/\Delta R14}$ or *Pln*$^{+/+}$ mouse. The eluates were analysed by Western blotting and showed that the PLN pentamer was enriched from both, membranes of the *Pln*$^{+/\Delta R14}$ disease model or *Pln*$^{+/+}$ control mouse (Figure 23A,B). MBP and MBP-14-3-3+R18 served as controls and did not show any non-specific PLN binding (Figure 23A,B). Surprisingly, the enriched PLN pentamer from the *Pln*$^{+/\Delta R14}$ mouse was phosphorylated at S16 and T17 (Figure 23B). Given what is already known about the PLN R14del mutation, which disrupts the PKA target motif and therefore should be not able to be phosphorylated at S16 (Ceholski et al., 2012; Haghighi et al., 2006), the detected amount of PLN pS16 was surprisingly high. In

the *Pln*$^{+/\Delta R14}$ mouse model PLN proteins without the PLN R14del mutation are present, although I expected a reduction of PLN phosphorylated at S16 in pentamers enriched from the *Pln*$^{+/\Delta R14}$ mouse. In line with the unexpected observation, also the steady-state-PLN analysis of *Pln*$^{+/\Delta R14}$ membranes, performed before the 14-3-3 pull-down, did not revealed differences regarding the phosphorylation distribution of pS16 and pT17 (Figure 21).

Altogether, the pull-down experiment from *Pln*$^{+/\Delta R14}$ mouse model enriched PLN pentamers equally phosphorylated at S16 and T17 residues as compared to the WT control. Further analysis of the PLN R14del protein in the *Pln*$^{+/\Delta R14}$ mouse model would be required to distinguish between the PLN R14del disease and WT PLN protein.

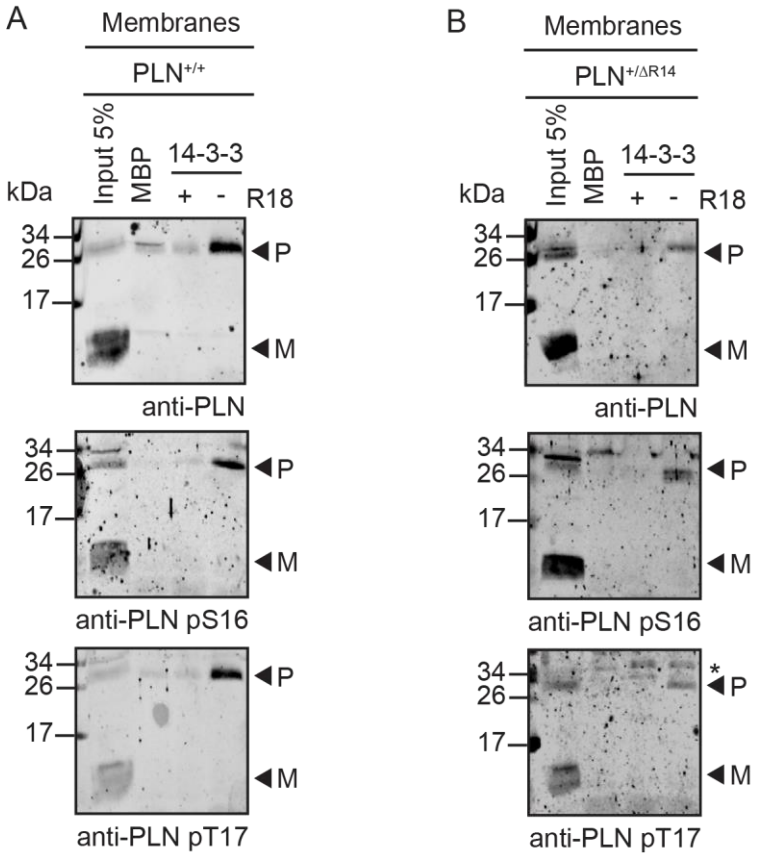

Figure 23. PLN pentamers phosphorylated at pS16 and pT17 were enriched with 14-3-3 pull-down experiments from *Pln*$^{+/\Delta R14}$ mouse heart membranes.

14-3-3 binding assay with membranes from the *Pln*$^{+/+}$ control (**A**) and *Pln*$^{+/\Delta R14}$ disease membranes mouse (**B**) were performed. Eluates were probed by Western blot for enriched PLN proteins and their phosphorylation status with corresponding antibodies.

From the performed pull-down experiment with *Pln*$^{+/\Delta R14}$ disease model membranes I could not conclude if the PLN pentamers that were enriched with 14-3-3, were hetero-pentamers containing both WT and R14del PLN monomers or homo-pentamers of WT PLN. To answer this question, I enriched PLN pentamers with 14-3-3 gamma from *Pln*$^{+/+}$ mice and *Pln*$^{+/\Delta R14}$ disease model membranes and separated the eluates on a Phos-tag-PAGE. The hypothesis was that PLN pentamer enriched from the PLN$^{+/\Delta R14}$ disease mouse should show less phosphorylated bands on a Phos-tag-PAGE because the PLN R14del protein cannot be phosphorylated at S16 by PKA (Haghighi et al., 2006). The Phos-tag-PAGE was transferred to nitrocellulose and analysed with a PLN antibody for the number of phosphorylation bands (Figure 24A). The phosphorylation band pattern did not differ between PLN pentamers enriched from *Pln*$^{+/+}$ animals or *Pln*$^{+/\Delta R14}$ disease model membranes (Figure 24A). However, the intensity of the bands is clearly reduced for all three enriched pentamers from *Pln*$^{+/\Delta R14}$ membranes in comparison with the control (Figure 24A,C). The same effect was visible when the eluates were analysed on a standard SDS-PAGE for total PLN levels (Figure 24A), while the amount of MBP-14-3-3 bait protein used for the affinity enrichment experiments was equal as shown by Western blotting with a MBP antibody (Figure 24A). Solubilized membranes from *Pln*$^{+/\Delta R14}$ and *Pln*$^{+/+}$ which served as input samples, were analysed by Western blot with an PLN antibody, showing equal amounts of PLN pentamer and monomers before they were added to the MBP-14-3-3 bait (Figure 24B). The strongly reduced enrichment of the PLN pentamer with the *Pln*$^{+/\Delta R14}$ disease model was significant over the controls (Figure 24C). This result suggested that exclusively PLN WT was presented in the enriched pentamer from the *Pln*$^{+/\Delta R14}$ disease model. It further indicates the PLN R14del protein was not addressable which may confirms already reported mislocalization or aggregation (Haghighi et al., 2012; te Rijdt et al., 2016).

Altogether, I could show that the PLN protein expression level and the distribution of phosphorylation at S16 or T17 do not differ in the *Pln*$^{+/\Delta R14}$ heterozygous disease model. However, in the 14-3-3 affinity purification experiment PLN pentamer was enriched from the *Pln*$^{+/\Delta R14}$, mice which did not differ regarding the number of phosphorylated residues. Both the phosphorylation distribution and the reduced amount of PLN pentamers from the *Pln*$^{+/\Delta R14}$ mouse membranes indicated, that exclusively homo-pentamers containing PLN WT monomers were enriched. This allows the assumption that the PLN R14del protein did not form 14-3-3-binding competent pentamers in the *Pln*$^{+/\Delta R14}$ disease model.

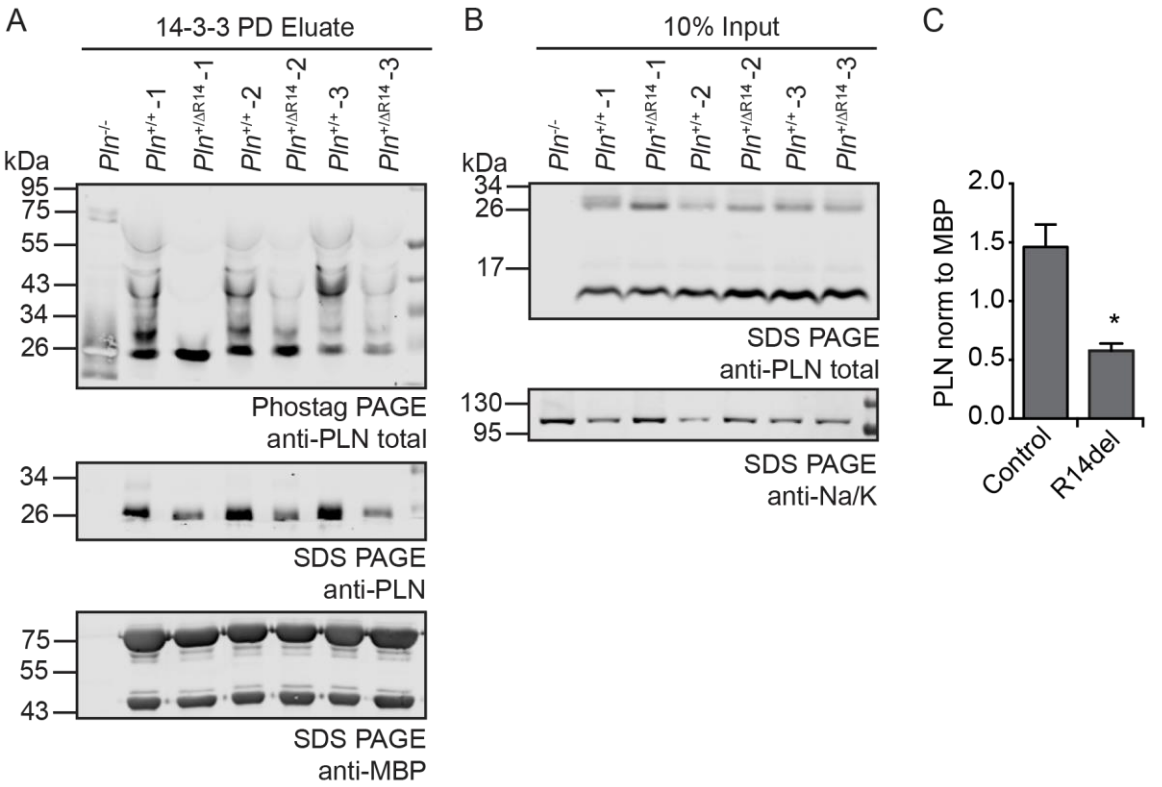

Figure 24. Phosphorylation distribution did not change in R14del PLN pentamers enriched from *Pln*$^{+/\Delta R14}$ disease mice membranes .

(**A)** Elution of 14-3-3 enrichment purification experiments from PLN *Pln*$^{+/\Delta R14}$ and *Pln*$^{+/+}$ mice membranes were loaded on Phos-tag-PAGE and analysed with an PLN antibody (upper panel). Membranes from *Pln*$^{-/-}$ animals were loaded as well to exclude unspecific antibody bands. In parallel elutions were analysed on SDS-PAGE with a PLN and MBP antibody. (**B**) Solubilized membranes from *Pln*$^{+/\Delta R14}$ and *Pln*$^{+/+}$ mice were analysed by Western blot with a PLN antibody to confirm equal input samples which then served for the pull-down experiment shown in (A). Loading of the input samples was monitored with detection for Na/K ATPase. (**C**) Quantification of experiment shown in (A) using values of enriched PLN pentamer intensity normalized to the signal observed for used MBP-14-3-3 gamma bait protein. The experiment was performed with 3 biological replicates. Data are presented as mean ± standard error of the mean (SEM). An unpaired t-test showed significant differences in (C) (*p=0.0117).

3.3.5 Different PLN mutations do not alter the ER localization of PLN in mammalian cells

The analysis of the *Pln*$^{\Delta R14\ /\Delta R14}$ and *Pln*$^{+/\Delta R14}$ mouse disease models indicated for both models reduced amounts of the PLN R14del protein in membrane fractions. I wondered whether the disease-causing mutations would provoke some trafficking defect for which I wanted to analyse the subcellular localization of these mutants. Different PLN constructs were designed for mammalian expression and used in HEK293T and HeLa cells. Besides

the PLN R14del mutation, also PLN R9C was included as well as different phospho-dead constructs (Table 8). The PLN variants were fused with an opsin-tag at the C-terminus. The opsin-tag is a short tag that contains an N-glycosylation site which can be glycosylated when exposed in the ER lumen (Bulbarelli et al., 2002). These tags have been used in the literature to monitor the ER insertion of the tagged-protein by analysis of the glycosylation state (Buentzel & Thoms, 2017). The different PLN mutations were analysed along with different known organelle-marker proteins in order to determine the subcellular localization of the construct.

Table 8. Sequence of PLN-opsin tagged constructs for expression in mammalian cell.
Full-length PLN was fused with an opsin-tag. The di-arginine ER-retention signal in the PLN sequence is marked in green and the 14-3-3 binding site is highlighted in orange. Inserted point mutations are shown in red.

Name	Sequence
PLN WT-opsin	MEKVQYLTRSAIRRASTIEMPQQARQNLQNLFINFCLILICLLLICIIVMLL-linker-opsin
PLN R9C-opsin	MEKVQYLTCSAIRRASTIEMPQQARQNLQNLFINFCLILICLLLICIIVMLL-linker-opsin
PLN ΔR14-opsin	MEKVQYLTRSAIR_ASTIEMPQQARQNLQNLFINFCLILICLLLICIIVMLL-linker-opsin
PLN S10A-opsin	MEKVQYLTRAAIRRASTIEMPQQARQNLQNLFINFCLILICLLLICIIVMLL-linker-opsin
PLN S16A-opsin	MEKVQYLTRSAIRRAATIEMPQQARQNLQNLFINFCLILICLLLICIIVMLL-linker-opsin

The expression of the opsin-tagged PLN mutants in human cells was analysed by Western blotting with an anti-opsin antibody (Figure 25). The WT, S10A and S16A variants had similar steady-state levels whereas the expression of the R9C and R14del disease variants was reduced in both tested cell lines (Figure 25A, B). In both HEK and HeLa cells, only monomeric PLN was detected (Figure 25A,B). Altogether, the expressed PLN mutant proteins behaved similar in HEK293 and HeLa cells. After the expression of the PLN mutant proteins was confirmed I analysed their subcellular localization using indirect IF experiments.

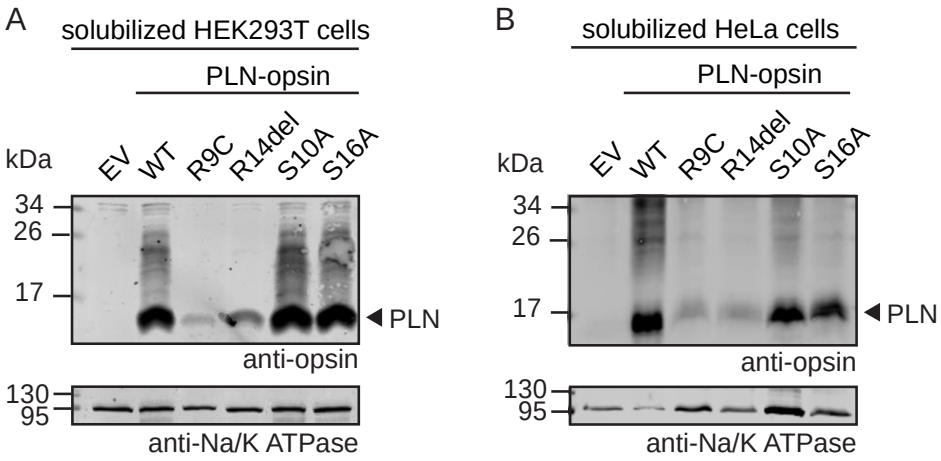

Figure 25. PLN-opsin protein variants expressed in HEK293T or HeLa cells.

Transfected HEK293T cells (**A**) or HeLa cells (**B**) were solubilized and PLN protein levels were analysed by Western blot with anti-opsin and anti-Na/K ATPase antibodies. EV indicates empty vector control.

First, the localization of the opsin-tagged PLN mutants at the ER compartment was analysed by co-staining against the Sec61beta translocon in HEK293 cells. All PLN variants co-localized with Sec61beta indicating localization within the ER (Figure 26). Interestingly, also the two PLN disease-causing mutations, R9C and R14del co-localized with Sec61beta at the ER (Figure 26).

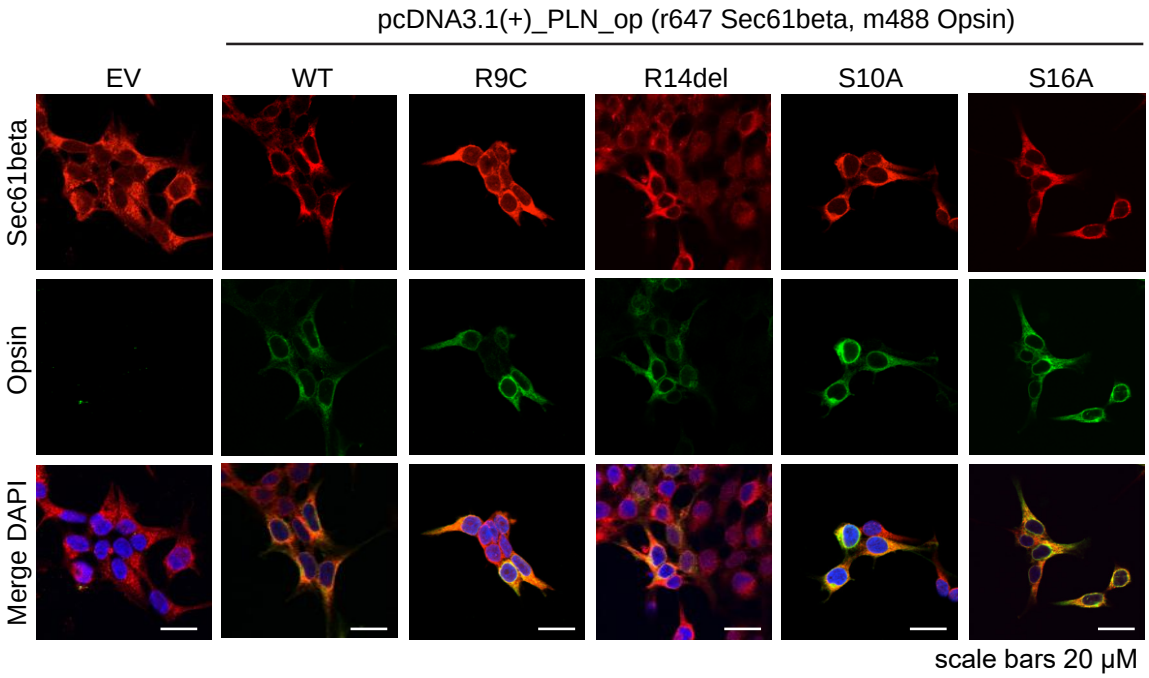

Figure 26. PLN-opsin mutants co-localized with Sec61beta in HEK293T cells.

Co-staining for Sec61beta (red) and opsin (green). Cells were cultured for 48 h after transfection, fixed with PFA and imaged by confocal microscopy. EV indicates empty vector control. All micrographs were obtained at the same exposure settings of the camera. Scale bars 20 µm.

Second, the localization of PLN-opsin mutants and the early endosomal marker protein EEA1 were analysed (Figure 27). The early endosome transports cargo between the plasma membrane and Golgi (Jovic et al., 2010). Cells expressing the PLN R14del or R9C disease mutant showed an increased number of EEA1 positive vesicles in contrast to cells expressing PLN WT or phospho-dead mutants (Figure 27). However, none of the analysed PLN mutants show co-localized with EEA1 positive vesicles in HeLa cells (Figure 27).

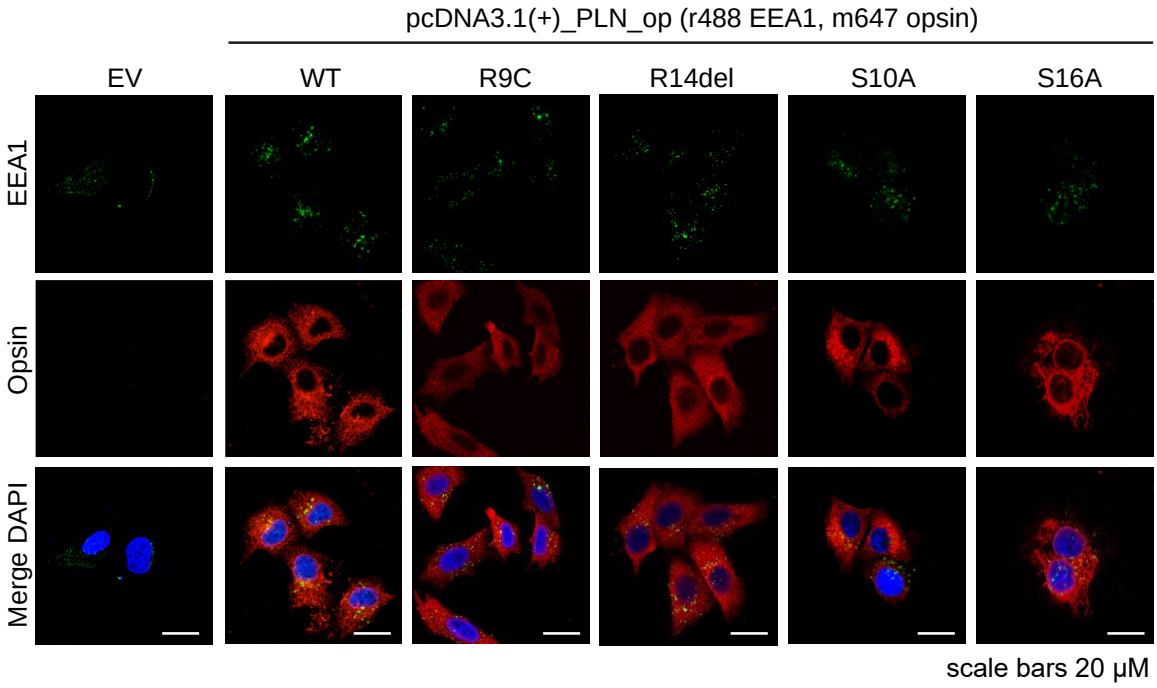

Figure 27. PLN-opsin protein variants showed no co-localization with the early endosomal marker protein EEA1 in HeLa cells.

Co-staining for the early endosomal maker protein EEA1 (green) and opsin (red). Cells were cultured for 48 h after transfection, fixed with PFA and imaged by confocal microscopy. EV indicates empty vector control. All micrographs were obtained at the same exposure settings of the camera. Scale bars 20 µm.

Finally, co-localization between the middle-late endosomal marker protein Rab7 and PLN mutants was investigated (Figure 28). Late endosomes fuse with lysosomes for degradation (Huotari & Helenius, 2011). The PLN mutants showed no co-localization with Rab7 as well. The PLN WT looked close to Rab7 vesicles in the merged view but the Rab7 vesicles shown in green are still separated (Figure 28).

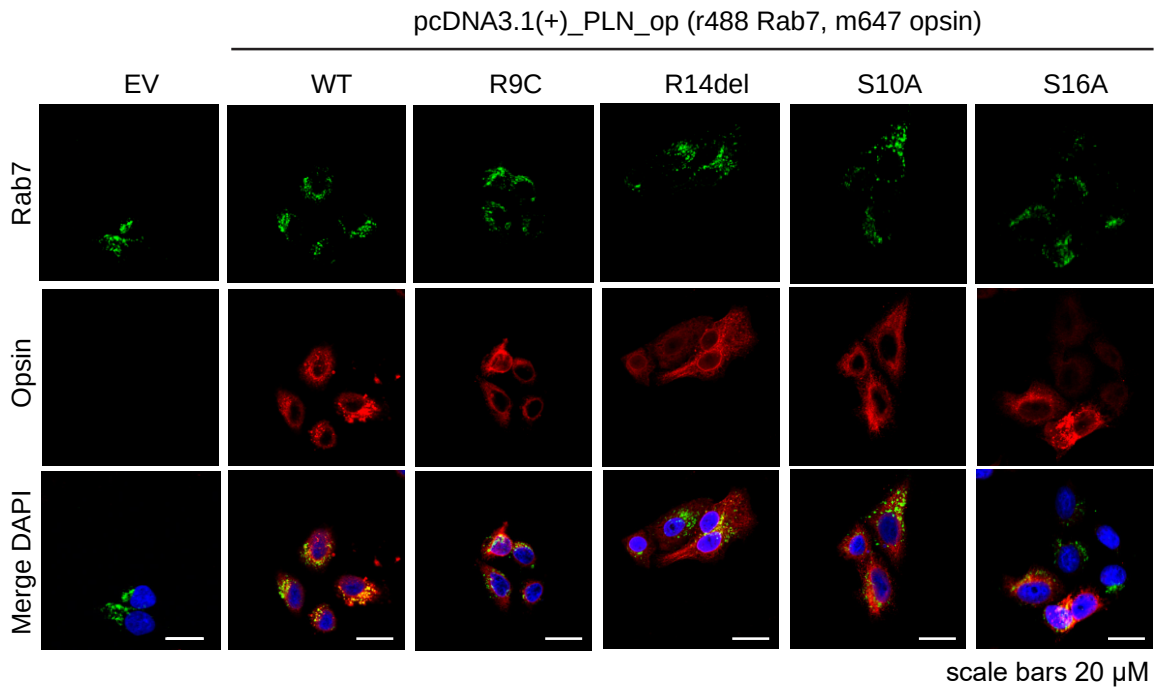

Figure 28. PLN-opsin protein variants showed no co-localization with the late endosomal marker protein Rab7 in HeLa cells.

Co-staining with the middle to late endosomal marker protein Rab7 (green) and opsin (red). Cells were cultured for 48 h after transfection, fixed with PFA and imaged by confocal microscopy. EV indicates empty vector control. All micrographs were obtained at the same exposure settings of the camera. Scale bars 20 µm.

Altogether, subcellular localization of opsin-tagged PLN variants, that cover different PLN disease mutations and phospho-dead mutants, were analysed in mammalian cells. All PLN mutants were found to localize in the ER compartment, as shown by co-staining with the ER marker protein Sec61beta. Interestingly, no different localization could be observed for the PLN disease mutations (R9C and R14del) in the ER in this experimental set up. In addition, localization with endosomal vesicles was analysed to further investigate if the PLN mutations are mistargeted to the plasma membrane as already reported (Haghighi et al., 2012). The PLN WT construct, as well as all mutants were found to be localized in the ER. Contrarily to already published results about mislocalization of the PLN R14del mutation to the plasma membrane (Haghighi et al., 2012), in this study no altered subcellular localization was observed for the mutations tested. Moreover, no co-localization of the PLN mutant proteins with the early endosomal marker protein EEA1 or with the middle to late endosomal marker Rab7 could be determined, indicating that the different mutations in the PLN protein do not alter the protein localization in the cell.

3.3.6 14-3-3 interacts with PLN pentamers in human atria

The interaction I observed between 14-3-3 and PLN was identified in rodent cardiac tissue. The PLN protein itself is highly conserved but there are physiological differences in humans and mice (Haghighi et al., 2003). To analyse whether the interaction between 14-3-3 and PLN is possible in human hearts, enrichment purification experiments with recombinant 14-3-3 and human atrial heart membranes were performed. The experiment was analysed by Western blotting with a PLN and PLN phospho-specific antibodies. Although the PLN pentamer was reduced in comparison with the monomer in the input, pentameric PLN was enriched with 14-3-3 from the human heart membranes (Figure 29A). The MBP and 14-3-3+R18 control excluded any unspecific binding (Figure 29B). The enriched PLN pentamer from human heart membrane contained both phosphorylated pS16 and pT17 residues (Figure 29A). Altogether, the interaction between 14-3-3 and the PLN pentamer could be also verified with human atrial membrane samples.

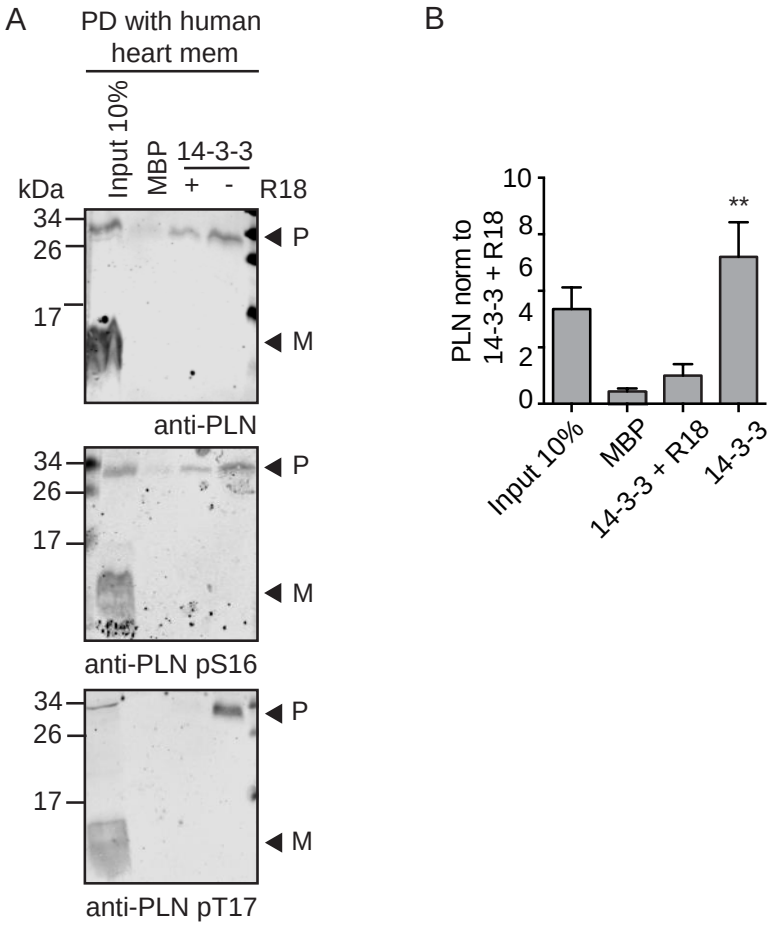

Figure 29. PLN pentamers interact with 14-3-3 in human atrium.

(**A**) 14-3-3 pull-down experiments with recombinant MBP-14-3-3 and membranes from human atriums were analysed by Western blot with antibodies detecting PLN and PLN pS16 or pT17 protein levels. (**B**) Quantification of the experiment shown in (A) using values of enriched PLN pentamer intensity normalized to the MBP-14-3-3+R18 control. The experiment was performed with four biological replicates. Data are presented as mean ± SEM. A one-way ANOVA analysis showed significant difference between the groups presented in (B) ($p=0.0026$), followed by a Tukey test indicating differences in between 14-3-3+R18 versus 14-3-3 (**$p= 0.0089$).

3.4 Discussion

A novel interaction between the cardiac regulator protein PLN and a phospho-adaptor protein 14-3-3 was identified in this study. The binding sites and the function of the novel interaction is shown and discussed in chapter 2. This chapter further characterizes the PLN/14-3-3 interaction and investigates two different R14del PLN disease animal models.

3.4.1 14-3-3 binds adjacent phosphorylated PLNs rather than the two proximal phospho-sites

In chapter 2, I could already show, that 14-3-3 binds to phosphorylated PLN. However the cytosolic region of PLN includes two physiologically relevant phosphorylation sites. The S16 residue, which is a target site of PKA, and the T17 residue, which is phosphorylated by CaMKII kinase (Mattiazzi & Kranias, 2014). Recombinant PKA phosphorylated PLN WT, S10A and T17A mutant proteins very efficiently, but not the PLN S16A protein (Figure 15A). This result confirmed that PKA phosphorylates the S16 residue in PLN. Single phosphorylation bands for the PLN WT and S10A proteins indicated that all constructs were singly phosphorylated and no cross phosphorylation of other potential phosphorylation residues occurred. CaMKII phosphorylated the PLN WT, S10A, S16A protein variants, but not the PLN T17A protein (Figure 15B). This verifies that the T17 residue in PLN is specifically phosphorylated by CaMKII kinase. However, the phosphorylation efficiency was higher with PKA as indicated by the abundance of phosphorylated protein on a Phos-tag-PAGE. I was particularly interested in investigating whether double phosphorylation, which leads to two very proximal phospho-groups, would abolish 14-3-3 binding as observed in the context of another 14-3-3-binding motif with two closely spaced phospho-residues (Kilisch et al., 2015). Double phosphorylation of the PLN WT protein was possible as indicated by two shifts on a Phos-tag-PAGE subsequently 14-3-3 binding indeed revealed that 14-3-3 binding was abolished (Figure 17). It was already shown that PKA has a higher affinity towards beta-adrenergic stimulation as CaMKII and can be phosphorylated individually (Coyler, 1998; Mundiña-Weilenmann et al., 1996) . But under full beta-adrenergic stimulation both kinases are activated leading to a double phosphorylation of PLN monomers (Coyler, 1998). How does 14-3-3 bind to PLN in such a situation? Based on pull-down experiments with recombinant 14-3-3 and cardiac lysate I showed that 14-3-3 binds preferably the PLN pentamer (chapter 2, figure 1,3). This result together, with the findings from the binding assay with double phosphorylated PLN (Figure 17) allow me to hypothesize that 14-3-3 binds to adjacent phosphorylated PLNs rather than the two proximal phospho-sites within the same PLN.

3.4.2 PLN R14del mutation may form aggregates in homozygous and heterozygous disease models

Two PLN disease causing mutations in humans, the R14del and R9C mutation were further investigated regarding the 14-3-3/PLN interaction.

The R14del PLN mutation is of great interest because the PKA binding motif is disrupted and prevents S16 phosphorylation (Haghighi et al., 2006). As a consequence, phosphorylation of T17 via CaMKII kinase is the only opportunity to phosphorylate PLN and partially relieve SERCA inhibition in the R14del disease mutation. I was already able to show that phosphorylated T17 is the high 14-3-3 binding affinity site in PLN (chapter 2, figure 3,4). Furthermore, I showed that 14-3-3 still physically interact with R14del PLN in a recombinant binding assay (chapter 2, figure 4). How the R14del PLN mutation influences the 14-3-3/PLN interaction was analysed in PLN R14del mouse models. In purified heart membranes from the homozygous R14del transgenic mice barely any PLN protein was identified, indicating that the PLN protein expression level was strongly reduced (Figure 18). 14-3-3 and activated CaMKII kinase protein steady-state levels were not affected by the R14del mutation. Interestingly, also SERCA protein levels were reduced in the disease model. Overall, the R14del PLN mutation in a homozygous mouse model negatively influences proteins which are involved in cardiac Ca^{2+} handling. Although the PLN steady-state levels were strongly reduced in the homozygous disease model, small amounts of R14del PLN were enriched with recombinant 14-3-3. The amount of enriched R14del PLN pentamer was too small to detect for phosphorylation with phospho-specific antibodies. Due to the disrupted PKA site in the R14del PLN protein the interaction could be only mediated via T17 phosphorylation. This result confirms findings from recombinant binding assays (chapter 2, figure 4) and showed that R14del PLN is still able to physically interact with 14-3-3. However, the enriched R14del PLN protein was very low and additional approaches to further investigate a possible 14-3-3/PLN R14del interaction are required, like an APEX proximity assay with R14del induced pluripotent stem cells or complexome profiling with cardiac lysate from homozygous or heterozygous mouse models and subsequently MS analysis.

In addition, the 14-3-3/PLN interaction was also investigated in a R14del PLN heterozygous mouse model, which corresponds to the zygosity in patients. In the heterozygous R14del mouse model, the PLN steady-state level were found to be similar to healthy control mice. Furthermore, the PLN phosphorylation distribution of S16 or T17 was not altered either (Figure 21). This was surprising as a different phosphorylation distribution for R14del PLN was expected due to the disrupted PKA interaction site. The heterozygous disease model expresses both PLN WT and R14del proteins, but a reduction of S16 phosphorylation in comparison with WT animals was expected. However, the

steady-state levels of all analysed PLN interaction partners such as SERCA, 14-3-3 or pCaMKII were found to be not altered due to the R14del mutation (Figure 22). To further characterize the *Pln*$^{+/\Delta R14}$ mouse model, PLN pentamers were enriched from the *Pln*$^{+/\Delta R14}$ mouse and analysed for the phosphorylated S16 and T17 distribution. Again, the S16 phosphorylation was not found to be reduced in PLN pentamers enriched from the *Pln*$^{+/\Delta R14}$ mouse with recombinant 14-3-3 (Figure 23). This result indicated that either hetero-pentamers, including both R14del PLN and WT PLN monomers, or PLN WT homo-pentamers were enriched. Clearly, no R14del PLN homo-pentamer was enriched in the pull-down experiment. If in a heterozygous R14del PLN background homo- or hetero-pentamers are formed is not known so far. To further analyse the composition of the PLN pentamers in the R14del mice, pentamers enriched by 14-3-3 were analysed on a Phos-tag-PAGE to separate the various present phosphorylation sites. Pentamers containing several R14del PLN monomers should show less phosphorylation bands on a Phos-tag-PAGE than healthy PLN pentamers, due to the absent S16 phosphorylation. The enriched PLN R14del pentamers showed exactly the same phosphorylation band pattern on a Phos-tag-PAGE as PLN WT pentamers (Figure 24). Only the amounts of enriched pentamers from the R14del disease mice were significantly reduced in comparison to the control mice. This result strongly suggests that only homomeric WT PLN pentamers were enriched by 14-3-3 from the R14del heterozygous mouse model. Overall, in the experiments I performed to investigate the *Pln*$^{+/\Delta R14}$ mouse model, I never obtained any altered phosphorylation distribution of the PLN. These results gave me the impression that the R14del PLN protein was not amenable to the types of extraction or fractionation protocols tested by my experiments. Taken together, barely any R14del PLN protein was identified either in the homozygous or in the heterozygous mouse model. A mis-localization of the R14del PLN was previously described in a heterozygous context (Haghighi et al., 2012). In addition, evidence that PLN forms large protein aggregates in ventricles of R14del patients was identified with immunohistochemistry and electron microscopy experiments (te Rijdt et al., 2016). In this study, 20 hearts from patients suffering under the R14del mutation were analysed and PLN aggregates were identified in all of them (te Rijdt et al., 2016). Aggregation of the PLN R14del protein would explain why I could barely identify R14del PLN protein in either homozygote or heterozygote animal models. I assume that during the membrane separation of the samples the aggregates end up in the insoluble fraction and therefore were not amenable to further biochemical analysis. To test whether the R14del PLN protein aggregated in both R14del disease models immunohistochemical examination of PLN should be performed.

Not much is known about the composition of PLN pentamers in the PLN R14del heterozygous background. The data I obtained, suggest that no hetero-multimeric PLN

pentamers are formed. However, I cannot exclude that possibly a single R14del PLN monomer was integrated in a pentamer with four WT PLN monomers. This would result in a change of a single phosphorylation site within the PLN pentamer which is maybe not visible on a Phos-tag gel. The PLN pentamer formation in a heterozygous disease background of PLN mutations is very interesting. To further investigate the R14del PLN pentamer distribution, an antibody detecting exclusively the R14del mutation in PLN would be helpful. As long as such an antibody is not available another experimental approach could be the analysis of enriched PLN pentamers from different PLN R14del disease models for the number of different S16 or T17 phosphorylation residues by MS analysis.

3.4.3 PLN disease mutations are localized in the ER in mammalian cells

In parallel to the investigation of the PLN R14del mice disease models, expression and localization of PLN mutant proteins in mammalian cell lines were investigated. Protein expression was analysed by Western blotting in HEK293T and HeLa cells. The expression levels of the two human disease mutants were found to be reduced by Western blotting in both cell lines. The PLN-opsin mutant proteins did not form SDS-resistant pentamers in HEK or HeLa cells (Figure 25). Pentamer formation is achieved by the transmembrane domain of PLN (Kimura et al., 1997), which is present in these constructs. Perhaps the opsin-tag prevented pentamer formation. Overall, there was no difference visible in HEK293T or HeLa cells regarding the expression of the PLN constructs (Figure 25). Localization analysis of the PLN mutant variants in mammalian cells demonstrated the correct localization of all PLN mutants to the ER compartment by co-staining with the ER marker Sec61beta (Figure 26). Interestingly, also the PLN R14del mutation was identified in the ER by co-staining with SEC61beta. In the literature the PLN R14del mutation has been reported to be localized at the plasma membrane after expression in HEK cells (Haghighi et al., 2012). I have not been able to confirm this result in my experimental set up.

In addition to ER localization, different cellular compartments were investigated such as early and late endosomes. If the PLN disease mutants would be misrouted to the plasma membrane, they should be also visible at some point in the endosome, since endosomal pathways receive all incoming material from the plasma membrane and serve as an initial sorting route for either recycling or degradation (Scott et al., 2014). I performed IF experiments with early and late endosomal marker proteins and the opsin-tag fused to PLN mutants were performed. No localization of any PLN mutant could be observed in either early nor late endosomal vesicles. The PLN R14del mutation was also not localized in endosomal vesicles (Figure 227,28). Altogether, I could not confirm mislocalization of the R14del PLN mutation expressed in mammalian cells. Taken together with the results from

homozygous and heterozygous PLN R14del mouse models, where barely any R14del PLN protein could be identified, my data support the already suggested hypothesis of PLN R14del aggregate formation (te Rijdt et al., 2016) rather than mislocalization. To further proof this hypothesis, cardiac myocytes should be isolated from the homozygous and heterozygous PLN R14del mouse model and the staining experiments should be repeated. In addition, my IF analysis supports published work from Butler et al who also did not observe any PLN localization in early endosomes (Butler et al., 2007). Interestingly, Butler et al identified PLN in the ERGIC and suggested a model where PLN is maintained in the ER by retrieval trafficking between ERGIC and ER (Butler et al., 2007). To further confirm the PLN localization in the ERGIC a corresponding IF experiment should be performed. In addition, it seems worthy to also repeat the experiment with an alternative tag, such as a myc-tag to exclude that the opsin-tag is influencing the ability of PLN to form pentamers and thereby alter the localization. In addition, it would be interesting if phosphorylation of PLN in mammalian cells influences the localization. Therefore, cells could be stimulated with isoprenaline to activate beta-adrenergic stimulation.

3.4.4 14-3-3 binds PLN pentamers in human atria

Most of the analysis of the 14-3-3/PLN interaction was performed with *in-vitro* approaches or in mouse models. Although PLN is very conserved in human and mouse (McTiernan et al., 1999) differences between both species were observed. PLN deletion in mice shows increased cardiac contractile function without the development of HF (Haghighi et al., 2003). In humans all PLN mutations that lead to protein truncation are lethal due to dilated cardiomyopathy and subsequent HF (Haghighi et al., 2003).

As a consequence, it is important to understand the differences in cardiac physiology and Ca^{2+} handling in mice and humans. The heart rate in mice is 10 times faster than in humans. Moreover, 92% of Ca^{2+} removal is achieved by SERCA in mice, meanwhile just 70% of Ca^{2+} is transported by SERCA in humans. In addition the basic ventricular motor proteins responsible for cardiac contraction differ in mice and human (Haghighi et al., 2003). With a 14-3-3 pull-down experiment and cardiac membranes separated from human atrial biopsy samples I enriched PLN pentamers (Figure 29). This verifies a physical 14-3-3/PLN interaction in human atrium. Atria and ventricle show different characteristics such as myocardial mass or wall thickness (Filgueiras-Rama & Jalife, 2016). In addition, they show functional differences in intracavitary pressures, ion channel composition, and electrophysical characteristics (Filgueiras-Rama & Jalife, 2016). As a consequence, it is important to also investigate the 14-3-3/PLN interaction in human ventricular samples. Alternatively, induced pluripotent stem cells derived from atrial ventricular cardiomyocytes (Cyganek et al., 2018) could be used.

4 Chapter IV: Identification of novel interaction partners for TASK channels in the heart

4.1 Introduction

The family of K_2P channels is one out of three K^+ ion channel families involved in cardiac action potential generation and electrical signal transduction. K_2P channels are background leak channels for potassium currents which are important regulators of the resting membrane potential (Hughes et al., 2017). The K_2P channel family is defined by a structure of four transmembrane domains and two-pore forming domains per monomer (Goldstein et al., 2005). K_2P channels are strongly expressed in the brain and central nervous system (Lesage, 2003). However, several members of K_2P channels also were identified to be expressed in the heart like TASK channels (Gurney & Manoury, 2009).

TASK channels are one group within the K_2P channel family, defined by their high sensitivity to extracellular acidic stress (Duprat et al., 1997; Talley et al., 2000). Three different channels belong to the group of TASK channels: TASK-1, TASK-3 and the silent TASK-5 channel. TASK-1 is expressed on mRNA and protein levels in the heart and mostly in the atrium. Whereas for TASK-3, only mRNA transcripts could be found in the heart and in the aorta but was absent based on protein levels (Gurney & Manoury 2009).

Homo- and heterodimeric TASK channels have been identified within the same channel family but also within different K_2P channel families. For the TASK-1/TASK-3 heterodimeric channel different electrophysical and pharmacological properties were identified in comparison with the corresponding homodimers (Czirják & Enyedi, 2002). In 2007, Putzke et al detected first TASK-1 like currents in rat ventricular myocytes. They reported that the TASK-1 current contributes substantially to the total outward current during the plateau phase of the action potential (Putzke et al., 2007) indicating the physiological importance. In line, TASK homo- and heterodimers have been shown to be physiologically relevant in various tissues (Gurney & Manoury 2009). Interestingly, Rinné et al suggested the presence of a functional heteromeric TASK-1/TASK-3 channel in hearts (Rinné et al., 2015). Altogether, TASK channels have been reported as an important regulator of the action potential duration and for resetting the resting membrane potential in the mammalian cardiovascular system.

Functional TASK channels need to be exposed at the cell surface. Hence, trafficking of TASK channels is tightly regulated. The TASK-1 and TASK-3 proteins are highly conserved except for the cytosolic C-terminal domain which shows only 34% homology (O'Kelley et al., 2015, Rajan et al., 2002). The last 15 AA of the C-terminus of TASK-1 as well as TASK-3 channels contain a so called “trafficking control region” with several overlapping binding motifs, which regulate trafficking of these channels to the cell surface

(Figure 30) (Kilisch et al., 2015). The trafficking control region of TASK-1 and TASK-3 include an ER retrieval sequence (KRR), as well as an overlapping 14-3-3 binding motif containing one phosphorylatable serine residue (Zuzarte et al., 2009). Several binding partners are already known to interact with the TASK C-terminus, like the COPI vesicular coat as well as the phospho-adaptor protein 14-3-3. Binding of COPI or 14-3-3 to the TASK channel is regulated by PKA-dependent phosphorylation of the C-terminal trafficking control region (Mant et al., 2011). The phosphorylated serine residue S393 in TASK-1 and S373 in TASK-3 bind 14-3-3 with high affinities. 14-3-3 binding sterically hinders COPI interaction, promoting forward trafficking of the channels to the cell surface (Kilisch et al., 2016). After 14-3-3 binding the TASK channels leave the early secretory pathway on their way to the cell surface, where they get glycosylated. Glycosylation is an important step for correct surface expression of many ion channels as shown for K_{ATP} or $K_v1.4$ (Steele et al., 2007). COPI binding initiates retrograde trafficking of the channels to the ER and cis-Golgi (together also called “early secretory pathway”) thus allowing for correct assembly prior to cell surface expression of the channel (Mathie, 2007).

Interestingly, the TASK-1 channel has a second serine residue in the trafficking control region adjacent to the 14-3-3 binding S393 (Figure 30), which is absent in the TASK-3 channel. It was shown that the second serine residue (S392) in TASK-1 can also be targeted by PKA *in vitro* and *in vivo* (Kilisch et al., 2016). The S392 residue was found to be an inhibitory residue for 14-3-3 binding upon phosphorylation (Kilisch et al., 2016). Presence of the phosphorylated S392 residue in the TASK-1 C-terminus significantly reduced the affinity for 14-3-3. Consequently, the surface expression of TASK-1 was also strongly reduced upon S392 phosphorylation (Kilisch et al., 2016). Although TASK-1 and TASK-3 channels are very conserved a couple of protein interaction partners were exclusively identified for TASK-1. The cytosolic adaptor protein p11 binds TASK-1 via a 20 aa long stretch in the C-terminus, which is also called p11 binding site and is located upstream over the trafficking control region (Figure 30). The TASK-1 p11 interaction leads to the retrieval of the channel to intracellular compartments of the early secretory pathway (Renigunta et al., 2006). Moreover, it was shown that TASK-1 interacts with the endosomal SNARE protein syntaxin-8. Interestingly, the interaction which syntaxin-8 and TASK- 1 was found to be involved in endocytosis processes (Renigunta et al., 2014).

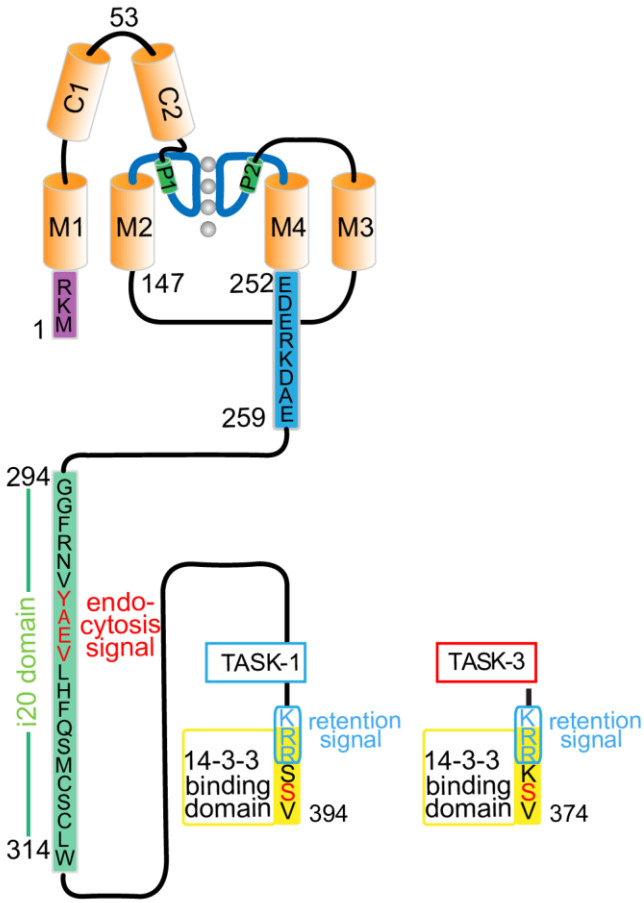

Figure 30. Schematic representation of TASK-1 and TASK-3.

Both channels show high sequence homology except for the C-terminus. The trafficking control region is represented in yellow (14-3-3 binding motif) and blue (ER retention/retrieval motif). The i20 domain is shown in green and a potential internalization motif is displayed in red (aa 294-314). Compared to TASK-1 (two adjacent serine residues, S392, S393), TASK-3 possesses a lysine residue adjacent to the serine residue, which is part of the 14-3-3 binding motif. The 14-3-3 phospho-binding residue in the TASK-1 (S393) and TASK-3 (S373) trafficking control domain is depicted in red. Figure adapted from (Kilisch et al., 2015).

Endocytosis can mediate retrieval from the cell surface, recycling, and degradation of membrane proteins. Therefore, endocytosis is also important to regulate cell surface expression of TASK channels (Mant et al., 2013). Clathrin-dependent endocytosis is one of the best investigated endocytosis pathways and involves adaptor proteins like AP-2, which direct the cargo protein into the vesicle (Lafer, 2002). It was already shown that TASK-1 and TASK-3 co-localize with clathrin. The co-localization was strongly decreased after disruption of the clathrin-mediated pathway (Gabriel et al., 2012; Mant et al., 2013). However, for TASK-3 it was shown that endocytosis is happening more rapidly than for TASK-1 (Mant et al., 2013). Although TASK-1 and TASK-3 both were found to co-localize

with proteins involved in the clathrin-dependent endocytosis, the syntaxin-8 interaction was only identified with TASK-1. This interaction was found to initiate co-endocytosis of both proteins together in a cooperative manner (Renigunta et al., 2014). It was suggested that the C-terminus of TASK-1 and the N-terminus of syntaxin-8 bind AP-2, which initiates clathrin-dependent co-endocytosis. A potential benefit resulting from the co-endocytosis could be that syntaxin-8 may influence the final destination of the vesicle by the interaction with SNARE proteins localized in different compartments (Renigunta et al., 2014). In addition it has been reported that PKC is involved in TASK-1 regulated endocytosis and that another endocytosis motif (SRERKLQYSIP) very close to the p11 binding motif in the TASK-1 C-terminus is involved in this process (Gabriel et al., 2012). The authors showed reduced TASK-1 currents after PKC stimulation in mammalian cells and an increased TASK-1 internalization and intracellular puncta formation by microscopy analysis. Interestingly, Gabriel et al suggested that PKC phosphorylation of the second serine (S324) in the identified endocytosis motif (SRERKLQYSIP) of TASK-1 may allow 14-3-3 binding and subsequent endocytosis.

The function and regulation of TASK channels in the heart is still in its infancy and not much is known about cardiac mediators, which may be involved in this regulation. The fact, that more interaction partners were identified for TASK-1 and the stronger expression in heart, indicate that TASK-1 channels are regulated in a more complex way. In line with this notion, the TASK-1 channel has a second PKA phosphorylatable serine residue (S392) in the trafficking control region which function is not fully understood so far. The goal of this chapter was the analysis of the cardiac interactome for the extreme C-terminus of TASK-1 and TASK-3, including the trafficking control domain. Phosphorylation is an important regulator of TASK channels thereby the analysis was performed differentiated between the phosphorylated or unphosphorylated status of the C-terminus of the channels.

4.2 Material and Methods

4.2.1 Chemicals

Chemicals used in this study were purchased from Sigma Aldrich, Carl Roth, Roche, GE HealthCare, AppliChem, Merck, and Serva. Restriction enzymes were purchased from Thermo Fisher Scientific. DNA oligonucleotides and phosphorylated oligonucleotides were synthesized by Sigma-Aldrich. Phusion DNA polymerase was homemade. PKA catalytic subunit was provided by Dr. Daniela Bertinetti (Kilisch et al., 2016) or purchased from New England Biolab. Phos-tag™ acrylamide was purchased from NARD institute.

4.2.2 Methods

4.2.2.1 Molecular Cloning and Polymerase Chain Reaction (PCR)

Plasmids for recombinant expression of proteins in bacteria and mammalian cells were generated as previously described (chapter 3, section 3.2.4.1). Plasmids for the recombinant expression of proteins and oligonucleotides used in this chapter can be found in table 10 - 12. For the exponential amplification of DNA fragments, encoding the proteins of interest, PCR reactions were employed as already described (chapter 3, section 3.2.4.2) with the following modifications: For the generation of TASK-1 and TASK-3 recombinant expression vectors phosphorylated oligonucleotides and corresponding cloning techniques were used.

4.2.2.2 Cloning with phosphorylated oligonucleotides

The ligation of DNA depends on interactions between the phosphorylated 5’ end of DNA with an unphosphorylated 3’end of the same or another DNA strand. This property was used to ligate short, synthetic and phosphorylated oligonucleotides into dephosphorylated recipient vectors. This allowed for a significant reduction of unspecific ligated plasmids during cloning. In general, every reaction was prepared in a total volume of 20 µl and pipetted on ice. For oligonucleotide hybridization 8 µl of the phosphorylated forward oligonucleotide was mixed with 8 µl of the phosphorylated reverse oligonucleotide in 1x annealing buffer (50 mM Tris HCl, 20 mM MgCl2, 50 mM NaCl, pH 7.5) and incubated for 5 minutes at 90 °C to anneal the oligonucleotides. The samples were allowed to cool down to 37°C at RT and subsequently transferred to ice. The annealed oligonucleotide mixture was diluted 1:100, 1:1000 and 1:10.000 with sterile dH_2O and ligated into the recipient vector.

4.2.2.3 Restriction enzyme digest, ligation and transformation in bacterial cells

PCR products and recipient plasmid DNA vectors were digested with one or multiple restriction enzymes as already described (chapter 3, section 3.2.4.3). Followed by ligation reactions which were performed with 100 ng linearized vector and 5-fold molar excess of purified insert, which was either a PCR product or an annealed phosphorylated oligonucleotide. The ligation reaction was performed as already described (chapter 3, section 3.2.4.4). Finally, the DNA was transformed into bacteria via electroporation as already mentioned (chapter 3, section 3.2.4.5).

4.2.2.4 Expression and affinity-purification of GST- or MBP-tagged proteins

GST- or MBP- tagged proteins were recombinantly expressed and affinity-purified from *E.coli* (strain BL21 Rosetta) as already described (chapter 3, section 3.2.4.8, 3.2.4.9).

4.2.2.5 SDS PAGE and Phos-tag-PAGE electrophoresis

SDS PAGE gel electrophoresis was performed as already described (chapter 3, section 3.2.4.10). Phos-tag-PAGE was used to visualize phosphorylated residues in proteins. Phos-tag-PAGE and electrophoresis were performed as indicated (chapter 3, section 3.2.3.11).

4.2.2.6 Coomassie staining of SDS-PAGE or Western blot transfer

SDS PAGE or Phos-tag-PAGE gels were stained after the electrophoresis with Coomassie brilliant blue G-250 to visualize protein bands or transferred onto a nitrocellulose membrane in a wet blot electro transfer technique as already described in detail (chapter 3, section 3.2.4.12 and 3.2.4.14). Western blot detection was performed with fluorescent labeled secondary antibody (LiCOR) and an Odyssey CLx LiCOR imaging system as indicated (chapter 3, section 3.2.15).

4.2.2.7 TCA precipitation of proteins

Prepared solubilized heart membranes or cytosol or complete lysate were precipitated by adding 12.5% final concentration of TCA as already described in detail (chapter 3, section 3.2.4.19).

4.2.2.8 *In-vitro* phosphorylation of recombinant proteins by PKA

Recombinant affinity-purified TASK-1 and TASK-3 C-terminal fusion proteins were phosphorylated with recombinant catalytic subunit PKA (provided from Dr. Daniela

Bernetti), *in vitro*. In general, 200 µg recombinant GST-fusion protein was immobilized onto 50 µl glutathione sepharose resin (GE Healthcare) in GST buffer pH 7.4 (20 mM HEPES pH 7.4, 150 mM KOAc, 5 mM $Mg(OAc)_2$, 1 mM EDTA, 1 mM DTT) in a total volume of 1 ml for 90 min at 4°C gently rotating. Beads were subsequently washed 3 times in GST Buffer pH 7.4 and resuspended in a total volume of 300 µl phosphorylation buffer (150 mM NaCl, 50 mM Tris-HCl, 10 mM $MgCl_2$, pH 7.5) supplemented with energy mix (EM, an ATP regeneration system (10 mM phosphocreatine, 0.5 mM ATP, 0.5 mM GTP, 50 µg/ml creatine phosphokinase)), as shown in table 9. The phosphorylation reaction was performed overnight at 4°C gently rotating.

Table 9. Scheme for *in-vitro* phosphorylation of recombinant TASK mutant proteins.

PKA phosphorylation of recombinant protein		**Unphosphorylated control**	
200 µg	recombinant protein	200 µg	recombinant protein
284 µl	phosphorylation buffer	299 µl	phosphorylation buffer
15 µl	20x Energy mix		-
1 µl	PKA	1 µl	PKA

4.2.2.9 Preparation of total rat heart lysate

Whole rat hearts were thawed on ice, fatty tissue was removed and the remaining heart was cut into small pieces. The tissue was mechanically disrupted with a MiccraD-1 homogenizer for 30 sec in tissue homogenization buffer (20 mM HEPES pH 7.4, 220 mM Mannitol, 70 mM Sucrose, 1 mM EDTA, 1x protease inhibitor, 1x phosphatase inhibitor). Crudely lysed tissue was subjected to dounce homogenization for 30 strokes on ice. Mitochondria were removed by centrifugation at 10.000 g for 10 min at 4°C. Afterwards, the supernatant was centrifuged at 100.000 g for 30 min at 4°C to separate membrane and cytosol. The supernatant was the cytosolic fraction which was transferred into a Falcon tube and kept on ice until further processing. The pellet contains separated membranes which were washed once in tissue homogenization buffer. After washing, 1 mg of crude membrane was solubilized in 1 ml ComplexioLyte48 (Logopharm) solubilization buffer on ice for 30 min, followed by centrifugation at 55.000 g for 30 min at 4°C to separate solubilized proteins from insolubilized protein. The supernatant contains solubilized heart membrane proteins.

For the preparation of total heart lysate the cytosolic fraction and the solubilized membranes were pooled 1:1. The detergent was removed from the sample by dialysis overnight in GST buffer pH 7.4 (20 mM HEPES pH 7.4, 150 mM KOAc, 5 mM $Mg(OAc)_2$, 1 mM EDTA, 1 mM DTT, 1 mM PMSF).

4.2.2.10 Preparation of 14-3-3 and COPI-depleted rat heart lysate

Rat heart lysate was centrifuged at 100.000 g for 15 min after dialysis to remove precipitated proteins. The lysate was treated with 2 mM R18 peptide inhibitor to block native 14-3-3 from binding to in vitro phosphorylated GST-bait proteins (e.g. GST-MST27-T1WT-CT) and 1 µM H-89 to inhibit PKA, for 1h at 4°C. After inhibitor treatment the lysate was diluted 1:2 in GST buffer pH 7.4 (20 mM HEPES pH 7.4m 150 mM KOAc, 5 mM $Mg(OAc)_2$, 1 mM EDTA, 1 mM DTT, 1x protease inhibitor, 1 x phosphatase inhibitor). Native COPI protein was removed from the cardiac lysate by incubation with recombinant GST-MST27-KKXX protein. 1 mg GST-MST27-KKXX was immobilized onto glutathione sepharose beads (GE Healthcare), washed and subsequently incubated with total rat heart lysate for 45 min at 4°C gently rotating. After incubation the resin-bound GST-MST27-KKXX protein was removed by separation through filter tip columns. The process was repeated twice.

4.2.2.11 TASK-3 pull-down with rat heart lysate for mass spectrometry analysis

Recombinant purified GST-MST27-TASK-3 protein variants were immobilized to glutathione sepharose affinity resin and recombinant phosphorylated with PKA as described in section 4.2.2.8. Briefly, 200 µg TASK-3 protein variants were immobilized to 50 µl glutathione sepharose affinity resin (GE Healthcare), followed by phosphorylation overnight with the catalytic subunit of PKA and EM. For the unphosphorylated control the TASK-3 protein variant was treated in the same way but without EM in the phosphorylation set up. After overnight phosphorylation, the TASK-3 proteins were washed 3 times in GST buffer pH 7.4 (20 mM HEPES pH 7.4, 150 mM KOAc, 5 mM $Mg(OAc)_2$, 1 mM EDTA, 1 mM DTT 1x protease inhibitor, 1 x phosphatase inhibitor) and incubated with prepared total rat heart lysate (section 4.2.2.9) for 2h at 4°C under gentle rotation. After incubation, the resin-bound recombinant TASK-3 proteins were collected, washed 4 times in GST buffer pH 7.4. Finally, proteins were eluted with incubation in L-Gluthathione elution buffer (20 mM HEPES pH 7.4, 150 mM KOAc, 5 mM $Mg(OAc)_2$, 1 mM EDTA, 20mM L-Gluthathione, 1x protease inhibitor, 1 x phosphatase inhibitor), followed by TCA precipitation (section 4.2.2.7). The precipitated pellet was solved in 1x NuPAGE LDS sample buffer (Thermo Fisher Scientific) for 10 min at 30°C. Eluted proteins were analysed by LC-MS/MS (performed in collaboration with Dr. Christoph Lenz (UMG Göttingen)), followed by MaxQuant analysis. The experiment was conducted in three technical replicates.

4.2.2.12 TASK-1 pull-down with separated rat heart membrane or cytosol for mass spectrometry analysis

The pull-down experiment of TASK-1 with separated heart membranes and cytosol was done as already described for TASK-3 in section 4.2.2.11. In contrast to the TASK-3 affinity purification experiment, the TASK-1 affinity experiment was performed with separated rat heart membranes and cytosol and eluted with 1M NaCl.

Rat heart lysate was prepared as described in 4.2.2.9 but separated cytosol and solubilized membranes were used separately for the TASK-1 pull-down. Solubilized membranes were dialysed overnight, as described in section 4.2.2.9. Prepared cytosol was shock frozen and stored at -80°C overnight. After the dialysis of the membranes, the cytosol was thawed on ice and both were centrifuged at 100.000 g for 10 min at 4°C to remove precipitated proteins. Cytosol and membrane fractions were treated with protease-, phosphatase-, 14-3-3- and PKA-inhibitors and native COPI was removed with GST-MST27-KKXX affinity peptides as described in section 4.2.2.9. The elution of the bait proteins was done with 600 µl 1M NaCl solved in GST Buffer pH 8.5. The elution was incubated for 15 min at RT and collected by centrifugation. The eluted samples were TCA precipitated as described in section 4.2.2.7 and finally solved in 1x NuPAGE LDS sample buffer (Thermo Fisher Scientific) for 10 min at 30°C. The TASK-1 pull-down samples were analysed by LC-MS/MS (performed in collaboration with Dr. Christoph Lenz (UMG Göttingen)), followed by MaxQuant analysis. The experiment was conducted in two biological and each three technical replicates.

4.2.2.13 Langendorff perfusion of rat hearts

The Langendorff perfusion protocol was developed based on a combination of the biotin labelling method used by Sierra et al (Sierra et al., 2013) in rat hearts, and the ouabain-induced Na/K internalisation described by Cherniavsky-Lev et al (Cherniavsky-Lev et al., 2014). In general, hearts were perfused with Krebs-Henseleit buffer (118.5 mml/l NaCl, 1.4 mmol/l $CaCl_2$, 11 mmol/l glucose, 1.19 mmol/l $MgSO_4$, 25 mmol/l $NaHCO_3$, 1.18 mmol/l NaH_2PO_4, 4.75 mmol/l KCL) bubbled with 95% O_2, 5% CO_2 at 37°C and pH 7.4. Perfusion with different ouabain concentrations was done at constant pressure of 80 mghh. Perfusions with PBS and biotin as well as perfusions with PBS and glycine were done at 4°C and constant flow. The last flow during ouabain perfusion was used (10-15 ml/min). During the whole perfusion process the heart viability was monitored with an OICG electrode pierced in the ventricle. Only hearts with a heart rate above 200 beats/min were used for this study. For every perfusion all reservoirs were either warmed up to 37°C or chilled until 4°C and filled with buffers, all air bubbles were carefully removed from the perfusion system and the perfusion pressure as well as the flow were checked. The heart

was removed from a euthanatized rat and directly dropped in cold Krebs buffer, fat tissue was removed and the first and second entry of the aorta were opened with a cut for easier cannulisation. After cannulisation the heart was tightened on the canula with a string and perfusion with 38°C warm Krebs buffer at constant pressure of 80 mmgh were started. After 5 min set up time, the heart was perfused for another 20 min with 38°C warm Krebs buffer at constant pressure. Followed by 1h perfusion with 38°C warm Krebs buffer with different concentrations of ouabain (100 nM or 50 µM) at constant pressure. After ouabain perfusion the heart was perfused with 4°C cold PBS with glucose (10 mM) and Sulfo-NHS-LC-biotin (1 mg/ml, Thermo Fisher Scientific) for biotin labelling for 25 min at constant flow. Finally, the heart was perfused with 4°C cold PBS and glycine (15 mM) for 5 min at constant flow to quench the biotinylation. The heart was removed from the canula, snap frozen and stored at -80°C.

4 groups of n=4/group were perfused:
Group 1: Control (no biotin, no ouabain perfusion)
Group 2: Biotin control (biotin but no ouabain perfusion)
Group 3: Low ouabain (biotin and 10 nm ouabain perfusion)
Group 4: High ouabain (biotin and 50 µM ouabain perfusion)

4.2.2.14 Neutravidin affinity purification with rat heart tissue

Neutravidin affinity purifications protocols were done with ouabain stimulated rat hearts. First, membranes and cytosol were separated from the ouabain stimulated hearts as described in section 4.2.2.9. Briefly, the hearts were mechanically disrupted, cytosol and membranes were separated due to different high speed centrifugation steps. Protein concentrations were measured with Bradford and 100 µg aliquots from cytosol and membranes were prepared in tissue homogenization buffer (320 mM Sucrose, 50 mM NaCl, 2 mM EDTA, 20 mM HEPES pH 7.4) with protease and phosphatase inhibitors and stored at -80°C. For a neutravidin affinity enrichment experiment one aliquot of separated membranes or cytosol from each animal was defrosted and centrifuged at 100.000 g for 15 min to collect the membranes. After centrifugation the membranes were solubilized in ComplexioLyte48 solubilization buffer as already described in section 4.2.2.9. Solubilized heart membranes were diluted 1:5 with ComplexioLyte48 dilution buffer. The cytosol samples were diluted 1:4 with ComplexioLyte48 dilution buffer and 1 volume ComplexioLyte48 solubilization buffer, that both fractions contain the same amount of detergent. 10% input samples from membrane and cytosol samples were removed, TCA precipitated (section 4.2.2.7) and stored at -20°C. For 100 µg cytosol or membrane sample 50 µl neutravidin bead slurry (Thermo Fisher Scientific) was washed twice in

ComplexioLyte 48 dilution buffer with one volume ComplexioLyte 48 solubilization buffer. The washed neutravidin beads were added to the prepared membrane or cytosol heart samples and incubated overnight at 4°C under rotation. The beads were collected and washed three times in ComplexioLyte48 dilution buffer. Finally, the samples were eluted with SDS samples buffer (2% SDS, 0.1% Bromophenol blue, 10% glycerol, 50 mM Tris-HCl pH 6.8) supplemented with 100 mM DTT and 10 mM biotin. The sample buffer was headed up to 70°C, added to the washed beads, incubated for 5 min at RT and the elution was collected by centrifugation.

4.2.2.15 Wheat germ agglutinin affinity purification with rat heart tissue

Wheat germ agglutinin (WGA) affinity purification experiments were done with separated membranes and cytosol from ouabain treated rat hearts. The membrane and cytosol inputs were prepared as described (section 4.2.2.9). The solubilization of membranes was done as described in section 4.2.2.9, the only difference was the solubilization buffer. For WGA affinity purification experiments the detergent TritonX-100 was used (10 mM NaCl, 1.5% TritonX-100, 50 mM Tris-HCl, pH 7.35). After cytosol and membrane preparation 10% of each input was removed, TCA precipitated (section 4.2.2.7) and stored at -20°C. For 100 µg cytosol or membrane sample 12.5 µl WGA bead slurry (Tagarose conjugated with Triticum vulgaris lectin, Sigma Aldrich) was incubated for 5 min in wash buffer I (150 mM NaCl, 2 mM EDTA, 20 mM HEPES pH 6.8) followed by washing 4 times in equilibration buffer (10 mM NaCl, 5 mM $MnCl_2$, 5 mM $CaCl_2$, 20 mM Tris HCl, pH 7.35) and a final washing step in solubilization buffer. Solubilized membranes or cytosol were added to the prepared wheat germ agglutinin resin and incubated for 5h at 4°C under rotation. Afterwards, the resin was collected and washed 6 times in wash buffer II (150 mM NaCl, 2.5 mM $MnCl_2$, 2.5 mM $MgCl_2$, 2.5 mM $CaCl_2$, 50 mM Tris HCl, pH 7.35). The bound proteins were eluted from the resin with SDS sample buffer supplemented with 100 nM DTT. For elution, samples were incubated for 5 min at RT and finally collected by centrifugation.

4.2.2.16 Binding assay with recombinant purified TASK constructs

15 µg of the recombinant purified GST-MST27-TASK-1 mutants were immobilized and phosphorylated as described in section 4.2.2.8. The phosphorylated and immobilized bait proteins were washed and resuspended in GST buffer pH 7.4 (20 mM HEPES pH 7.4m 150 mM KOAc, 5 mM $Mg(OAc)_2$, 1 mM EDTA, 1mM DTT 1 x phosphatase inhibitor, 0.1% TritonX-100). Equimolar amounts of the potential binding partners (PDZ domain containing proteins) were added to the GST buffer pH 7.4 and incubated for 1h at 4°C under gentle rotation. After binding, the samples were washed 4 times and eluted in elution buffer supplemented with 1mM DTT. Binding assays were analysed by Western blotting and Coomassie stained Phos-tag and SDS-PAGE gels.

Table 10. Plasmids generated and used in chapter IV.

Plasmid name	Description	Restriction enzymes	Source
pGEX6P-1	Bacterial expression vector for N-terminal GST-tagged proteins	ClaI - XhoI	M. Kilisch
pGEX6P-1 KKXX	Bacterial expression vector for GST-MST27-KKXX control protein	Insert at ClaI-XhoI	J. Menzel
pGEX-6P-1 TASK-1 C15 WT	Bacterial expression vector for GST-MST27-TASK-1 C15 WT	Insert at ClaI-XhoI	J. Menzel
pGEX-6P-1 TASK-1 C15 S392A	Bacterial expression vector for GST-MST27-TASK-1 C15 S392A	Insert at ClaI-XhoI	J. Menzel
pGEX-6P-1 TASK-1 C15 S393A	Bacterial expression vector for GST-MST27-TASK-1 C15 S393A	Insert at ClaI-XhoI	J. Menzel
pGEX-6P-1 TASK-1 C15 S392A/S393A	Bacterial expression vector for GST-MST27-TASK-1 C15 S292A/S293A	Insert at ClaI-XhoI	J. Menzel
pGEX-6P-1 TASK-1 C15 dV394	Bacterial expression vector for GST-MST27-TASK-1 C15 dV394	Insert at ClaI-XhoI	J. Menzel
pGEX-6P-1 TASK-3 C15 WT	Bacterial expression vector for GST-MST27-TASK-3 C15 WT	Insert at ClaI-XhoI	J. Menzel
pGEX-6P-1 TASK-3 C15 S373A	Bacterial expression vector for GST-MST27-TASK-3 C15 S373A	Insert at ClaI-XhoI	J. Menzel
pGEX-6P-1 TASK-3 C15 dV374	Bacterial expression vector for GST-MST27-TASK-3 C15 dV374	Insert at ClaI-XhoI	J. Menzel
pMal2CX	Bacterial expression vector for N-terminal MBP-tagged proteins	Insert at EcoRI - HindIII	New England BioLabs
pMal2CX Dlg1	Bacterial expression vector for MBP-Dlg1	Insert at SalI-HindIII	J. Menzel

pMal2CX Dlg1 - V5	Bacterial expression vector for MBP-FXa-Dlg1-V5	Insert at EcoRI - SalI	J. Menzel
pMal2CX Dlg1-ΔPDZ1- V5	Bacterial expression vector for MBP-FXa-Dlg1-ΔPDZ1-V5	Insert at EcoRI - SalI	J. Menzel
pMal2CX Dlg1 ΔPDZ2- V5	Bacterial expression vector for MBP-FXa-Dlg1-ΔPDZ2-V5	Insert at EcoRI - SalI	J. Menzel
pMal2CX Dlg1 ΔPDZ3- V5	Bacterial expression vector for MBP-FXa-Dlg1-ΔPDZ3-V5	Insert at EcoRI - SalI	J. Menzel
pMal2CX Dlg1 ΔPDZ1,2- V5	Bacterial expression vector for MBP-FXa-Dlg1-ΔPDZ1,2-V5	Insert at EcoRI - SalI	J. Menzel
pMal2CX Dlg1 ΔPDZ1,3- V5	Bacterial expression vector for MBP-FXa-Dlg1-ΔPDZ1,3-V5	Insert at EcoRI - SalI	J. Menzel
pMal2CX Dlg1 ΔPDZ1,2,3- V5	Bacterial expression vector for MBP-FXa-Dlg1-ΔPDZ1,2,3-V5	Insert at EcoRI - SalI	J. Menzel
pMal2CX Dlg1 ΔPDZ2,3- V5	Bacterial expression vector for MBP-FXa-Dlg1-ΔPDZ2,3-V5	Insert at EcoRI - SalI	J. Menzel
pMal2CX Dlg4	Bacterial expression vector for MBP-Dlg4	Insert at SalI-HindIII	J. Menzel

Table 11. Oligonucleotides used for PCR's.

Name	Description	Sequence (5'-3')
Dlg-1-FP	Used to generate Dlg1 from rat cDNA template, forward primer	CCG CCG GAA TTC ATG CCG GTC CGG AAG CAA GAT ACC CAG
Dlg-1- V5-Rev	Used to generate Dlg1 from rat cDNA template, reverse primer	ACG CAC GCG TCG ACT TAC GTA GAA TCG AGA CCG AGG AGA GGG TTA GGG ATA GGC TTA CCG CTG CCG CCG CCT AAT TTT TCT TTT GCT GGG ACC CAG ATG TAA GGA CCA GAC TGC
TEV-Dlg-1 FP (short)	Used to generate tev-cleavable Dlg1 protein, forward primer	GGG AAA ACC TGT ATT TTC AGG GCA TTT CAG AAA TGC CGG TCC GGA AGC AAG ATA CC
TEV-Dlg-1 FP long	Used to generate tev-cleavable Dlg1 protein, forward primer	GCT CGA ACA ACA ACA ACA ATA ACA ATA ACA ACA ACC TCG GGG AAA ACC TGT ATT TTC AGG GCA TTT CAG AAA TGC CGG TCC GGA AGC AAG ATA CCC AGA GAG C
Dlg-1-V5-Rev shorter	Used to generate tev-cleavable Dlg1 protein, reverse primer	CCA GTG CCA AGC TTG CCT GCA GGT CGA CTT ACG TAG AAT CGA GAC CGA GGA GAG GG
Dlg1 For (new ECORI)	Used to generate Dlg-1 truncations in the PDZ domains, forward primer	CAA CAA CAA CAA TAA CAA TAA CAA CAA CCT CGG GGA AAA CCT GTA TTT TCA GGG CGA ATT CAT GCC GGT CCG GAA GCA AGA TAC C
Dlg-1 V5 longer Rev	Used to generate Dlg-1 truncations in the PDZ domains, forward primer	CGA CGT TGT AAA ACG ACG GCC AGT GCC AAG CTT GCC TGC AGG TCG ACT TAC GTA GAA TCG AGA CCG AGG AGA GGG
PDZ1 For	Used to generate Dlg-1 truncations in the PDZ domains, forward primer	TAC TGA TGC AGA TTA TGA ATA TGA GAG GCG GAA GCC AGC C
PDZ1 Rev	Used to generate Dlg-1 truncations in the PDZ domains, reverse primer	TTT TTT CTG AGG CTG GCT TCC GCC TCT CAT ATT CAT AAT CTG CAT CAG TAC CAT TAA CAT AAG T
PDZ2 For	Used to generate Dlg-1 truncations in the PDZ domains, forward primer	GAA GCC AGC CTC AGA AAA AAT CAT GAC AAG TAT GTA TAT AAA TGA TGG CTA TGC ACC

PDZ2 Rev	Used to generate Dlg-1 truncations in the PDZ domains, reverse primer	AGC CAT CAT TTA TAT ACA TAC TTG TCA TGA TTT TTT CTG AGG CTG GCT TCC
PDZ3 For	Used to generate Dlg-1 truncations in the PDZ domains, forward primer	TGA TGA GAT CAC TAG GGA ACC TAG ACC TGA AGA GTA CAG TCG TTT TGA AGC
PDZ3 Rev	Used to generate Dlg-1 truncations in the PDZ domains, reverse primer	CTT CAA AAC GAC TGT ACT CTT CAG GTC TAG GTT CCC TAG TGA TCT CAT CAT CTC CA
PDZ 1,2 For	Used to generate Dlg-1 truncations in the PDZ domains, forward primer	TAC TGA TGC AGA TTA TGA ATA TGA GAC AAG TAT GTA TAT AAA TGA TGG CTA TGC ACC
PDZ 1,2 Rev	Used to generate Dlg-1 truncations in the PDZ domains, reverse primer	AGC CAT CAT TTA TAT ACA TAC TTG TCT CAT ATT CAT AAT CTG CAT CAG TAC CAT TAA CAT AAG T
PDZ23 For	Used to generate Dlg-1 truncations in the PDZ domains, forward primer	GAA GCC AGC CTC AGA AAA AAT CAT GAC AAG TAT GTA TAT AAA TGA TGG CTA TGC ACC
PDZ 2,3 Rev	Used to generate Dlg-1 truncations in the PDZ domains, reverse primer	AGC CAT CAT TTA TAT ACA TAC TTG TCA TGA TTT TTT CTG AGG CTG GCT TCC
PDZ 2,3 For	Used to generate Dlg-1 truncations in the PDZ domains, forward primer	TGA TGA GAT CAC TAG GGA ACC TAG ACC TGA AGA GTA CAG TCG TTT TGA AGC
PDZ2,3 Rev	Used to generate Dlg-1 truncations in the PDZ domains, reverse primer	CTT CAA AAC GAC TGT ACT CTT CAG GTC TAG GTT CCC TAG TGA TCT CAT CAT CTC CA
PDZ 1,3 For	Used to generate Dlg-1 truncations in the PDZ domains, forward primer	TAC TGA TGC AGA TTA TGA ATA TGA GAG GCG GAA GCC AGC C
PDZ1,3 Rev	Used to generate Dlg-1 truncations in the PDZ domains, reverse primer	TTT TTT CTG AGG CTG GCT TCC GCC TCT CAT ATT CAT AAT CTG CAT CAG TAC CAT TAA CAT AAG T
PDZ-1 For	Used to generate Dlg-1 truncations in the PDZ domains, forward primer	TGA TGA GAT CAC TAG GGA ACC TAG ACC TGA AGA GTA CAG TCG TTT TGA AGC
PDZ13 Rev	Used to generate Dlg-1 truncations in the PDZ domains, reverse primer	CTT CAA AAC GAC TGT ACT CTT CAG GTC TAG GTT CCC TAG TGA TCT CAT CAT CTC CA

PDZ1,2,3 For	Used to generate Dlg-1 truncations in the PDZ domains, forward primer	TAC TGA TGC AGA TTA TGA ATA TGA GCC TGA AGA GTA CAG TCG TTT TGA A
PDZ1,2,3 Rev	Used to generate Dlg-1 truncations in the PDZ domains, reverse primer	CTT CAA AAC GAC TGT ACT CTT CAG GCT CAT ATT CAT AAT CTG CAT CAG TAC CAT TAA CAT AAG T
Dlg-4 For	Used to generate Dlg4 from rat cDNA template, forward primer	CCG CCG GAA TTC ATG GAC TGT CTC TGT ATA GTG ACA ACC
Dlg-4 V5 Rev	Used to generate Dlg4 from rat cDNA template, reverse primer	CCC CCC AAG CTT TTA CGT AGA ATC GAG ACC GAG GAG AGG GTT AGG GAT AGG CTT ACC GCT GCC GCC GCC GAG TCT CTC TCG GGC TGG GAC CC

Table 12. Phosphorylated oligonucleotides.

Name	Description	Sequence (5'-3')
GST-MST27-TASK-1-WT-FP	Last 15 AA of TASK-1 C-terminus	CGAT GGC GGC GGC GGC TCG GGC GGC GGC GGC TCT CAC AGT TTA TCG ACA TTT CGA GGT CTC ATG AAG CGA AGA AGC TCA GTG TAA C
GST-MST27-TASK-1-WT-RP	Last 15 AA of TASK-1 C-terminus	TCGAG TTA CAC TGA GCT TCT TCG CTT CAT GAG ACC TCG AAA TGT CGA TAA ACT GTG AGA GCC GCC GCC GCC CGA GCC GCC GCC GCC AT
GST-MST27-TASK-1-S392A-FP	Last 15 AA of TASK-1 C-terminus, include S392A mutation	CGAT GGC GGC GGC GGC TCG GGC GGC GGC GGC TCT CAC AGT TTA TCG ACA TTT CGA GGT CTC ATG AAG CGA AGA GCC TCA GTG TAA C
GST-MST27-TASK-1-S392A-RP	Last 15 AA of TASK-1 C-terminus, include S392A mutation	TCGAG TTA CAC TGA GGC TCT TCG CTT CAT GAG ACC TCG AAA TGT CGA TAA ACT GTG AGA GCC GCC GCC GCC CGA GCC GCC GCC GCC AT
GST-MST27-TASK-1-S393A-FP	Last 15 AA of TASK-1 C-terminus, include S393A mutation	CGAT GGC GGC GGC GGC TCG GGC GGC GGC GGC TCT CAC AGT TTA TCG ACA TTT CGA GGT CTC ATG AAG CGA AGA AGC GCA GTG TAA C
GST-MST27-TASK-1-S393A-RP	Last 15 AA of TASK-1 C-terminus, include S393A mutation	TCGAG TTA CAC TGC GCT TCT TCG CTT CAT GAG ACC TCG AAA TGT CGA TAA ACT GTG AGA GCC GCC GCC GCC CGA GCC GCC GCC GCC AT
GST-MST27-TASK-1-S392A/S393A-FP	Last 15 AA of TASK-1 C-terminus, include S392A/S393A mutation	CGAT GGC GGC GGC GGC TCG GGC GGC GGC GGC TCT CAC AGT TTA TCG ACA TTT CGA GGT CTC ATG AAG CGA AGA GCC GCA GTG TAA C
GST-MST27-TASK-1-S392A/S393A-RP	Last 15 AA of TASK-1 C-terminus, include S392A/S393A mutation	TCGAG TTA CAC TGC GGC TCT TCG CTT CAT GAG ACC TCG AAA TGT CGA TAA ACT GTG AGA GCC GCC GCC GCC CGA GCC GCC GCC GCC AT

GST-MST27-TASK-1-dV394-FP	Last 15 AA of TASK-1 C-terminus, include deletion of V394	CGAT GGC GGC GGC GGC TCG GGC GGC GGC GGC TCT CAC AGT TTA TCG ACA TTT CGA GGT CTC ATG AAG CGA AGA AGC TCA TAA C
GST-MST27-TASK-1-dV394-RP	Last 15 AA of TASK-1 C-terminus, include deletion of V394	TCGAG TTA TGA GCT TCT TCG CTT CAT GAG ACC TCG AAA TGT CGA TAA ACT GTG AGA GCC GCC GCC GCC CGA GCC GCC GCC GCC
GST-MST27-TASK-3-WT-FP	Last 15 AA of TASK-3 C-terminus	CGA TGG CGG CGG CGG CTC GGG CGG CGG CGG CTC TAG CTT TAC CGA CCA CCA GAG GCT GAT GAA ACG CCG GAA GTC CGT TTA AC
GST-MST27-TASK-3-WT-RP	Last 15 AA of TASK-3 C-terminus	TCG AGT TAA ACG GAC TTC CGG CGT TTC ATC AGC CTC TGG TGG TCG GTA AAG CTA GAG CCG CCG CCG CCC GAG CCG CCG CCG CCA T
GST-MST27-TASK-3-S373A-FP	Last 15 AA of TASK-3 C-terminus, include S373A mutation	CGAT GGC GGC GGC GGC TCG GGC GGC GGC GGC TCT AGC TTT ACC GAC CAC CAG AGG CTG ATG AAA CGC CGG AAG GCC GTT TAA C
GST-MST27-TASK-3-S373A-RP	Last 15 AA of TASK-3 C-terminus, include S373A mutation	TCGAG TTA AAC GGC CTT CCG GCG TTT CAT CAG CCT CTG GTG GTC GGT AAA GCT AGA GCC GCC GCC GCC CGA GCC GCC GCC GCC AT
GST-MST27-TASK-3-dV374-FP	Last 15 AA of TASK-3 C-terminus, include deletion of V374	CGAT GGC GGC GGC GGC TCG GGC GGC GGC GGC TCT AGC TTT ACC GAC CAC CAG AGG CTG ATG AAA CGC CGG AAG TCC TAA C
GST-MST27-TASK-3-dV374-RP	Last 15 AA of TASK-3 C-terminus, include deletion of V374	TCGAG TTA GGA CTT CCG GCG TTT CAT CAG CCT CTG GTG GTC GGT AAA GCT AGA GCC GCC GCC GCC CGA GCC GCC GCC GCC AT-

Table 13. Antibodies used in chapter IV.

Name	Supplier	Cat. No.	Dilution	Technique	Clonality
14-3-3 pan (H8)	Santa Cruz	Sc-1657	1:1000	WB	polyclonal
GAPDH	NeoBiotech	NB-29-00852	1:5000	WB	polyclonal
MAGUK pan	NeuroMab	75-029	1:100	WB	monoclonal
Na/K ATPase alpha	Santa Cruz	Sc-21712	1:1000	WB	monoclonal
Dlg1 (SAP97)	Abcam	Ab3437	1:1000	WB	polyclonal
Dlg2 (PSD93)	Abcam	Ab2930	1:1000	WB	polyclonal
Dlg4 (PSD95)	Abcam	Ab18258	1:1000	WB	polyclonal
Streptavidin-HRP	Thermo Fisher Scientific	N100	1:5000	WB	-
TASK-1	-	-	1:500	WB	polyclonal
pTASK-1	-	-	1:500	WB	polyclonal

4.3 Results

4.3.1 Identification of novel cardiac interaction partners of the TASK-3 C-terminus

The K_2P channel TASK-3 exhibits a background leak current of K^+ ions in neurons and other electrically excitable tissues as cardiomyocytes. Surface expression of TASK channels is tightly regulated by 14-3-3 and COPI interaction (Zuzarte et al., 2009). Phosphorylation of the S373 residue in the extreme C-terminus of TASK-3 allows high affinity binding of 14-3-3 proteins, which promotes forward trafficking of the channel to the cell surface. However, COPI binds to the unphosphorylated C-terminus of TASK-3 which leads to the retrieval of the channel to early compartments of the secretory pathway (Kilisch et al., 2016). For the TASK-1 channel additional interaction partners and regulators were identified which are not interacting with TASK-3 (e.g. p11, syntaxin 8) (Kilisch et al., 2015). This indicates differences in TASK-1 and TASK-3 channel regulation.

I set out to further investigate the role of TASK-3 in the heart by analyzing the cardiac phosphorylation-dependent interactome of the TASK-3 trafficking control region, located in the extreme C-terminus.

4.3.1.1 Recombinant expression of TASK-3 fusion proteins

In order to identify novel interaction partners for TASK-3, pull-down experiments with the phosphorylated or unphosphorylated distal C-terminus of TASK-3 were performed with total rat heart lysate and analysed by mass spectrometry (MS). Therefore, TASK-3 fusion proteins were designed using the last 15 aa from the C-terminus fused to a GST-tag (Table 14). In order to avoid steric impediment, a long linker separating GST and the TASK-3 peptide was added. This linker is based on the MST27 protein, which has a high affinity to COPI (Sandmann et al., 2003), and will help to identify novel cardiac interaction partners beside 14-3-3 and COPI. To study the effect of phosphorylation of the TASK-3 C-terminus on potential novel interaction partners a phospho-dead mutant (S373A) was created as well (Table 14).

Table 14. Sequence of recombinant TASK-3 fusion proteins used to identify novel interaction partners.

The last 15 AA of TASK-3 were fused with a GST-tag and a MST27 linker. The ER-retrieval sequence (COPI binding site) is highlighted in blue. The phosphorylatable serine residue (part of mode II 14-3-3 binding motif) is shown in red and a serine to alanine mutation is depicted in green.

Peptide name	Detailed C-terminal sequence
TASK-3 WT	GST-MST27-CSFTDHQRLMKRRKSV-COOH
TASK-3 S373A	GST-MST27-CSFTDHQRLMKRRKAV-COOH

Recombinant GST-MST27-TASK-3 protein variants were expressed and affinity purified from *E. coli* and analysed by Coomassie stained SDS-PAGE gels. The purified TASK-3 proteins migrated at the expected size of approximated 38 kDa. Lower molecular weight (MW) bands were attributed to degradation products of the GST-MST27-fusion protein (Figure 31A). After purification, the TASK-3 C-terminal protein variants were recombinantly phosphorylated with the catalytic subunit of PKA and analysed on Coomassie stained Phos-tag-PAGE. A shift was visible for the PKA phosphorylated TASK-3 WT protein after treatment with PKA and energy mix (EM) indicating phosphorylation (Figure 31B). The Phos-tag-acrylamide compound and $MnCl_2$ incorporated into the gel mixture during casting, caused the retardation of phosphorylated protein on the gel by forming a complex with phosphate groups. Thus, I was able to distinguish between phosphorylated and unphosphorylated proteins. The migration of the TASK-3 S373A mutant was not altered upon incubation with the kinase, indicating that this protein was not phosphorylated by PKA (Figure 31B). Furthermore, the MST27-linker introduced into the TASK-3 fusion construct did not alter the ability to be phosphorylated.

This experiment confirmed, that the S373 residue in TASK-3 can be recombinantly phosphorylated by PKA (Kilisch et al., 2016) and allowed further experimentation. The C-terminal TASK-3 constructs were employed in pull-down experiments with cardiac tissue.

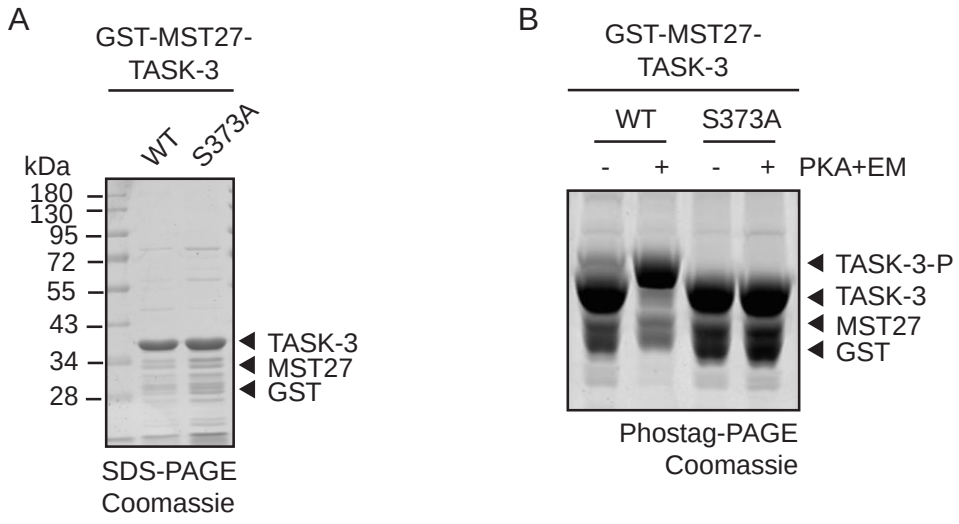

Figure 31. Recombinant purification and *in-vitro* phosphorylation of TASK-3 proteins.

(A) Different GST-MST27-TASK-3 mutant proteins were purified to address the different possible phosphorylation states of the TASK-3 C-termini. The proteins migrated at the expected size of 38 kDa, lower molecular weight species were attributed to degradation products of the GST-MST27-fusion protein. **(B)** Recombinant phosphorylation of TASK-3 protein variants with PKA. Phosphorylation was analysed on Phos-tag-PAGE and indicated by a shift. For each TASK-3 protein variant treatment with PKA and EM was compared with no treatment.

4.3.1.2 Phosphorylation dependent enrichment of novel interaction partners of the TASK-3 C-terminus

The purified and phosphorylated TASK-3 protein variants were incubated with total rat heart lysate to identify novel cardiac interaction partners. In order to avoid masking of the TASK-3 C-terminus endogenous 14-3-3 and COPI proteins were blocked or removed from the heart lysate prior the start of the experiment. Endogenous 14-3-3 proteins were blocked with the R18 peptide, a high affinity inhibitor of all 14-3-3 protein isoforms which binds very efficiently the 14-3-3 binding groove (Petosa et al., 1998). Endogenous COPI protein was removed by passing the rat heart lysate over beads containing GST-MST27-KKXX. The MST27 linker in combination with the KKXX motif represents a high-affinity COPI binding motif. This experimental set up allowed to enrich other interactors binding the TASK-3 C-terminus, even those with lower affinity than 14-3-3 and the COPI vesicular coat. After the pull-down experiment the TASK-3 bait proteins were eluted and analysed on Coomassie stained Phos-tag-PAGE (Figure 32A) to monitor the phosphorylation state of the recombinant proteins since it could have been altered by kinases or phosphatases present in the lysate. The elutions were further analysed on SDS-PAGE (Figure 32B), to confirm that similar amounts of bait proteins were used for each experiment. Gels were stained with Coomassie solution and weaker appearing protein bands migrating above 55 kDa were considered as potential interaction partners, which could be enriched from total rat heart lysate (Figure 32B). To increase the resolution of the weak bands identified in Figure 32, the elution samples were resolved on a big SDS-PAGE gel followed by silver staining (Figure 32C). Silver staining has a 100 fold higher sensitivity then Coomassie staining (Chevallet et al., 2006). The silver-stained gel showed differential protein patterns depending on the phosphorylation state of TASK-3 (Figure 32C, marked with asterisks). The different enriched cardiac proteins identified with the TASK-3 mutant proteins were analysed using LC-MS/MS in collaboration with Dr. Christoph Lenz from the MS core facility (UMG Göttingen).

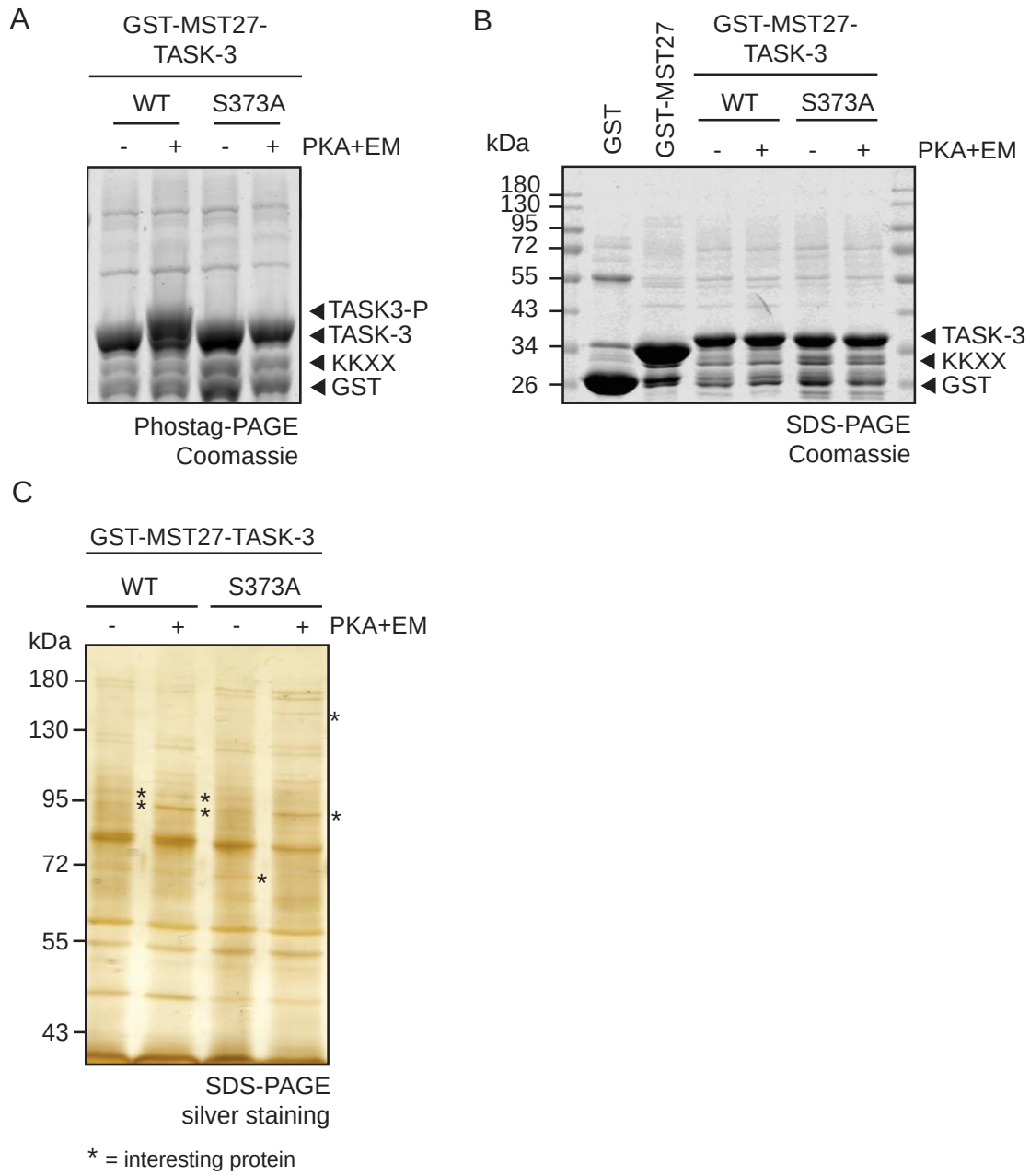

Figure 32. Novel cardiac TASK-3 interaction partners were enriched dependent on its phosphorylation state.

(**A**) The phosphorylation state of eluted TASK-3 C-terminal bait proteins were analysed on Coomassie stained Phos-tag-PAGE. (**B**) Eluted samples of the TASK-3 pull-down with rat heart lysate were analysed on Coomassie stained SDS-PAGE. (**C**) Elution of affinity purification of TASK-3 constructs after incubation with heart lysate were analysed on silver-stained SDS-PAGE. Protein bands, which seemed to change upon *in-vitro* phosphorylation of the bait proteins are highlighted with an asterisk.

The LC-MS/MS analysis identified new cardiac interaction partners which were enriched with the C-terminus of TASK-3 in a phosphorylation dependent manner. The obtained MS analysis was quantified by calculating and plotting the log_2-fold changes of ratios of TASK WT +/- phosphorylation and the TASK-3 S373A mutant +/- phosphorylation. Proteins which were enriched over the cut-off of each measurement (defined as 2σ, where σ is the standard abbreviation over all values) were assumed to be significantly enriched and highlighted in orange (Figure 33). I was especially interested in proteins which were specifically enriched to the TASK-3 C-terminus dependent on its phosphorylation status, because these proteins will be most likely involved in trafficking and regulation of TASK-3. Already known TASK-3 interaction partners like different 14-3-3 proteins were identified with phosphorylated TASK-3 WT C-terminus (Figure 33A; highlighted in pink). Among the main hits the Na/K ATPase alpha 1 subunit, several isoforms of the adaptor protein AP-2 and dynamin were identified (Figure 33A, highlighted in blue). All mentioned proteins were specifically enriched with the phosphorylated TASK-3 C-terminus and absent in the analysis of the TASK-3 phospho-dead mutant S373A (Figure 33B). The enrichment of known TASK-3 interaction partners serves as a positive control for the experiment. It should be mentioned that different 14-3-3 isoforms were identified in the MS analysis although endogenous 14-3-3 was blocked with the R18 peptide. This is likely the result of pre-existent interactions that I was unable to block by the use of the inhibitor peptide R18. This fact most may indicate that 14-3-3 was involved in protein-protein interactions with the enriched novel cardiac protein interactors of TASK-3.

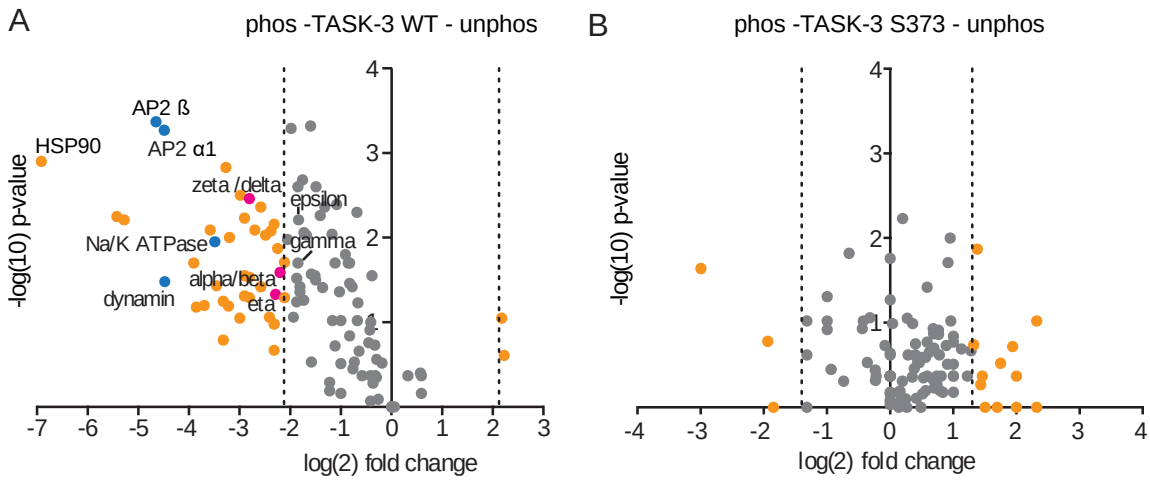

Figure 33. Na/K ATPase and endocytic regulatory proteins were identified as novel TASK-3 interaction partners in cardiac lysate.

Dot plots analysing the MS results of affinity purification experiments with rat heart lysate and TASK-3 protein variants. The log_2-fold changes of ratios of (**A**) TASK-3 WT +/- phosphorylation (phos) and (**B**) TASK-3 S373A +/- phosphorylation were calculated. Proteins which were enriched

over the cut-off of each measurement, defined as 2σ, where σ is the standard abbreviation over all values, were assumed to be significantly enriched and highlighted in orange. Identified 14-3-3 proteins are highlighted in pink. The enriched Na/K ATPase and endocytic regulatory proteins are highlighted in blue.

4.3.1.3 Analysis of a co-endocytosis of Na/K ATPase with TASK-3 via biotin labelling of surface proteins in rat hearts using Langendorff perfusion

The Na/K ATPase was identified for the phosphorylated TASK-3 C-terminus from cardiac tissue by MS analysis. In addition, proteins which are involved in endocytosis processes were identified for the phosphorylated TASK-3 C-terminus as well as different 14-3-3 isoforms (Figure 33). Efendiev et al., published that 14-3-3 is important to recruit phosphoinositide 3-kinase to the Na/K ATPase during clathrin-dependent endocytosis (Efendiev et al., 2005). This prompted the idea, that 14-3-3 dimers may bring phosphorylated TASK-3 and the Na/K ATPase in close proximity for a potential co-endocytosis mediated by AP-1 and dynamin. To further investigate this hypothesis, I performed an affinity purification experiment from rat heart lysate in a similar fashion to the one for subjected to MS. The affinity purification experiment was performed without 14-3-3 inhibition followed by incubation of phosphorylated TASK-3 protein variants and Western blotting analysis with 14-3-3 and Na/K ATPase antibodies (Figure 34). 14-3-3 was strongly enriched with the phosphorylated TASK-3 WT protein but not with the unphosphorylated controls (Figure 34). However, no Na/K ATPase was detected with any of the TASK-3 mutant proteins (Figure 34). Altogether, I was unable to confirm an interaction between the phosphorylated TASK-3 C-terminus and Na/K ATPase by Western blot. This indicates that the binding affinity between TASK-3 and Na/K ATPase is below the affinity of Western blot quantification and shows that MS analysis has a much higher sensitivity than Western blotting (Bass et al., 2017).

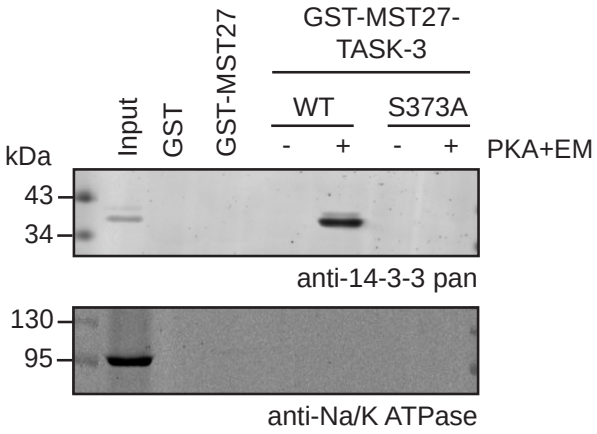

Figure 34. Western blot detection of the Na/K ATPase in samples obtained by TASK-3 pull-down experiments with heart lysate.

Analysis of affinity purification of TASK-3 protein variants with rat heart lysate and no R18 inhibitor treatment. The interaction between TASK-3 and 14-3-3 as well as with the Na/K ATPase were analysed (lower panel) by Western blot.

Verification of a potential Na/K ATPase interaction with TASK-3 was not possible with pull-down experiment followed by Western blot analysis. To further investigate the hypothesis of a potential co-endocytosis between TASK-3 and the Na/K-ATPase, the endocytosis rate of the Na/K ATPase was stimulated in rats. Therefore, whole rat hearts were stimulated with the putative endocytosis enhancing drug ouabain. Ouabain is a cardiac glycoside, which inhibits the Na/K-ATPase pump and was proposed to induce endocytosis in the heart (Liu, 2005). Internalization of endocytosed surface proteins was monitored by subsequent surface biotinylation of the hearts. The described treatment was performed in the context of Langendorff perfusion experiments. Rat hearts were perfused with different concentrations of ouabain followed by biotinylation with non-cell-permeable biotin to label proteins which are exposed at the cell surface (Figure 35A). Biotin-perfusion was performed at 4°C to stop intracellular trafficking during the labelling. Rat hearts were used since the TASK-3 Na/K ATPase interaction was identified in rat. However, the Na/K ATPase has a reduced sensitivity towards ouabain in rats (Cherniavsky-Lev et al., 2014). To ensure, that ouabain induces endocytosis in rat hearts a low dose of 100 nM and a high dose of 50 µM were used. To control the experiment and monitor background biotinylation the hearts were perfused in 4 different groups: (1) No ouabain and no biotin treatment during perfusion, (2) no ouabain but biotin treatment, (3) 100 nM ouabain and biotin treatment and (4) 50 µM ouabain and biotin treatment.

After the heart treatment using Langendorff perfusion, membranes and cytosol were fractionated and analysed for the amount of biotinylated proteins by Western blotting with streptavidin coupled to a fluorophore (Figure 35B). In the sample that was not treated with

ouabain and biotin, no enrichment of biotinylated proteins was visible for membranes or cytosol (Figure 35B). Biotinylated proteins were detected in membranes from heart samples which were perfused with biotin, but no differences were visible due to ouabain treatment (Figure 35B).

Surprisingly, biotinylated proteins were also enriched from the cytosol fraction, even though the amount of enriched proteins was reduced in comparison with the membrane fractions analysed (Figure 35B).

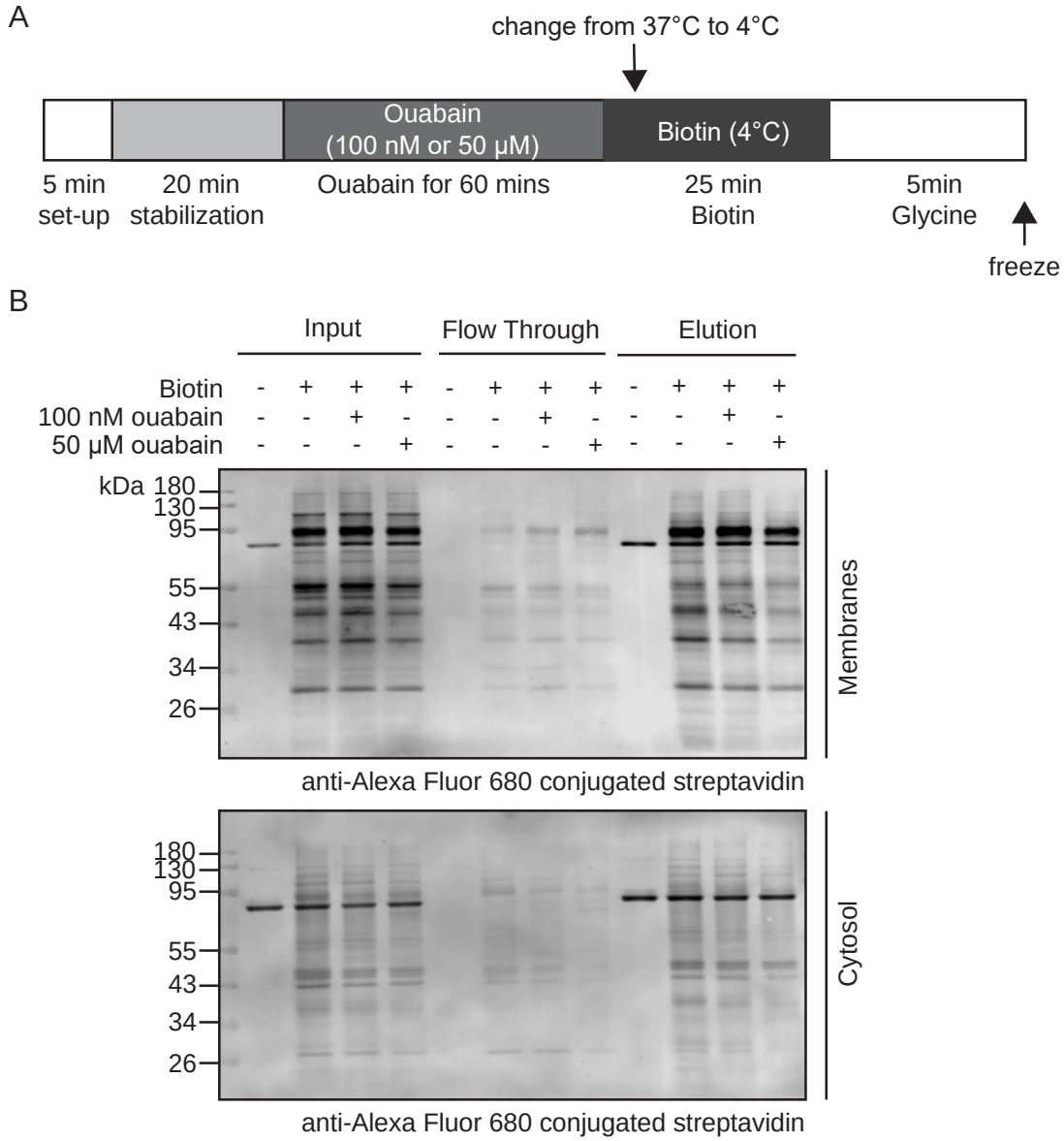

Figure 35. Enrichment of biotinylated proteins from rat hearts treated with ouabain.

(**A**) Rat hearts were treated in a Langendorff perfusion with ouabain (100 nM or 50 µM) followed by surface biotinylation with non-membrane permeable Sulfo-NHS-LC-biotin at 4°C. (**B**) Membranes or cytosol separated from the Langendorff perfused hearts were analysed for the enrichment of biotinylated proteins. Inputs, flow throughs and elutions were analysed by Western blotting with fluorophore-conjugated streptavidin.

Biotinylated proteins were enriched from the cytosolic fraction of hearts which were treated with biotin and ouabain (Figure 36). To exclude cross-contamination of the sample during the subcellular fractionation, cytosolic and membrane protein markers were analysed by Western blot using GAPDH and Na/K ATPase antibodies respectively. The cytosolic protein GAPDH was only detected in cytosol samples whereas Na/K ATPase was only detected in the membrane fraction samples (Figure 36). This indicates that the separated fractions of membrane or cytosol were clean, but it does not exclude that small amounts of biotin were introduced into the cytosol during sample preparation.

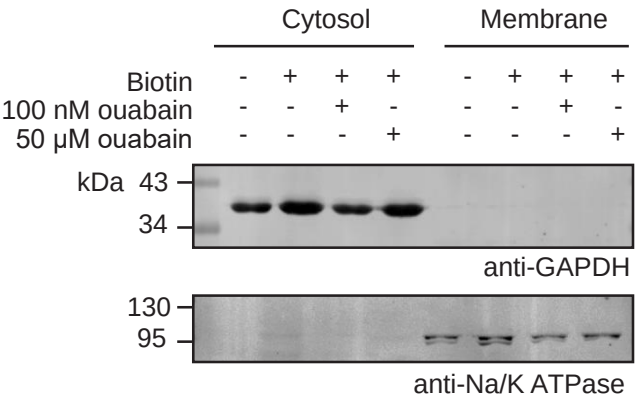

Figure 36. Probing for different marker proteins in ouabain treated heart membrane and cytosol.

The purity of the separated membrane or cytosolic fraction was confirmed by Western blotting and the detection of the cytosolic marker protein GAPDH (upper panel) or the membrane protein Na/K ATPase (lower panel).

4.3.1.4 Enrichment of Na/K ATPase and 14-3-3 in biotinylated heart membranes

I was able to show that membrane proteins expressed at the cell surface can be visualized with biotin surface labeling. Next, I wanted to analyse the behavior of biotinylated Na/K ATPase with or without ouabain induced endocytosis. Therefore, enriched biotinylated proteins from the membrane fraction were probed for the amount of Na/K ATPase under different ouabain concentrations. Ouabain has been shown to initiate Na/K ATPase endocytosis (Cherniavsky-Lev et al., 2014) and therefore ouabain-treated heart membranes should show less biotinylated Na/K ATPase after enrichment with neutravidin pull-downs. In the elution of the neutravidin pull-down, no biotinylated proteins were detected in the control sample which was not treated with biotin or ouabain. Biotinylated Na/K ATPase was enriched in all samples perfused with biotin, but no systematic difference was detectable compared to the control sample and the samples that were treated with different ouabain concentrations (Figure 37A,B). Also, no difference was

visible among the different ouabain concentrations (Figure 37A,B). Altogether, the enrichment of proteins which are expressed at the cell surface from complete rat hearts was possible with the help of neutravidin enrichment, but no significant difference was visible for the amounts of Na/K ATPase present at the cell surface after ouabain treatment.

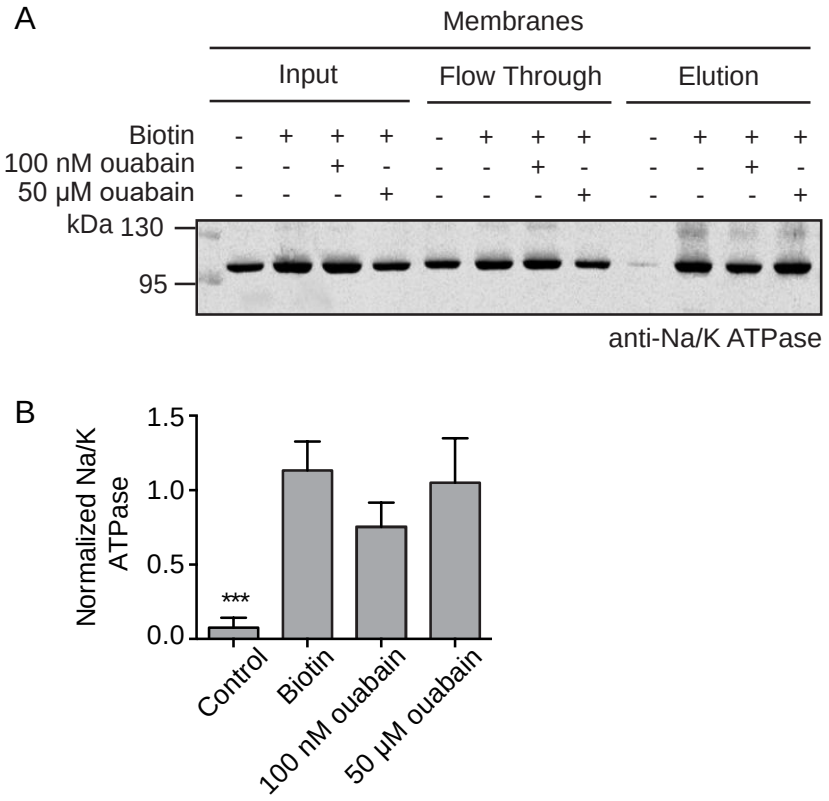

Figure 37. Biotinylated Na/K ATPase protein was enriched in biotinylated heart membranes. (**A)** Na/K ATPase protein levels in perfused heart samples treated with different concentrations of ouabain and biotin were analysed. Biotinylated proteins were purified with neutravidin resin and analysed by Western blot with a Na/K-ATPase antibody. (**B**) Quantification of experiment shown in (A) using values of the Na/K ATPase intensity normalized to the sample perfused with biotin but without ouabain. The data of three independent experiments are presented as mean ± SEM. An unpaired t-test showed significant differences between control versus biotin (***p=0.0003), but not between biotin versus ouabain treated samples.

Ouabain treatment did not influence the surface expression of Na/K ATPase in membranes. A potential co-endocytosis of the Na/K- ATPase with TASK-3 may require 14-3-3 which clamps the proteins in close proximity. To further investigate the role of 14-3-3, enriched biotinylated membrane proteins from neutravidin affinity experiments of the ouabain treated hearts were analysed regarding the presence of 14-3-3 proteins by Western blot. In the input samples used for the neutravidin enrichment experiment no 14-3-3 was detected at all. However, after neutravidin enrichment weak signals for 14-3-3

were detected (Figure 38). These 14-3-3 proteins were bound to biotinylated membrane proteins. In line, no 14-3-3 was detected in the control sample which was not treated with biotin (Figure 38). The amount of 14-3-3 proteins detected from biotinylated membranes did not vary between hearts treated with different doses of ouabain (Figure 38).

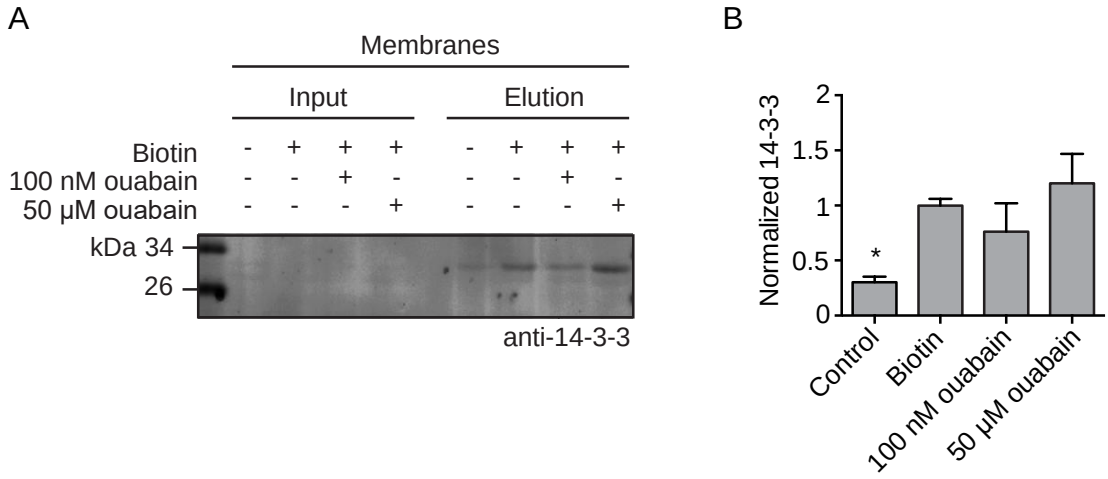

Figure 38. 14-3-3 was enriched in biotinylated heart membranes.

(**A**) Analysis of 14-3-3 protein levels in heart membranes treated with different concentrations of ouabain. Biotinylated proteins from perfused rat hearts were purified with neutravidin and analysed with Western blot and a 14-3-3 antibody. (**B**) Quantification of experiment shown in (A) using values of the 14-3-3 intensity normalized to the sample just perfused with biotin but without ouabain. The data of three independent experiments are presented as mean ± SEM. An unpaired t-test showed significant differences between control versus biotin (*p=0.0122), but not between biotin and ouabain treated samples.

4.3.1.5 Enrichment of glycosylated Na/K ATPase in rat heart membranes

Glycosylation is one of various post-translational modifications to ensure correct trafficking of proteins within the cell. Glycosylated proteins are transported to the plasma membrane (Bas et al., 2011). For presenting the membrane proteins to the extracellular matrix glycosylation is required as well (Hart, 1992). In addition, it was reported that glycosylation protects proteins from degradation resulting in a reduced rate of endocytosis (Altschuler et al., 2000; Russell et al., 2009). Ouabain treatment showed no influence on the amount of Na/K ATPase present in the plasma membrane or the amounts of 14-3-3 interacting with cell surface proteins. Another method to test whether ouabain influences the amount of cell-surface expressed membrane proteins is the analysis of glycosylated proteins. In order to test the effect of ouabain on Na/K ATPase endocytosis I analysed the glycosylation status of the Na/K ATPase with wheat germ agglutinin (WGA) enrichment experiments. WGA resin efficiently binds glycosylated proteins (Goldstein et al., 1997). Therefore, WGA resin was incubated with ouabain-treated heart membranes and the elutions were

analysed with Coomassie stained SDS-PAGE (Figure 39). For heart membranes the amount of glycosylated proteins in the elution is reduced in comparison with the input or flow-through fraction. Moreover, slightly less glycosylated proteins were eluted after WGA affinity enrichment from the ouabain treated membrane samples. But no difference between low and high ouabain concentrations were observed.

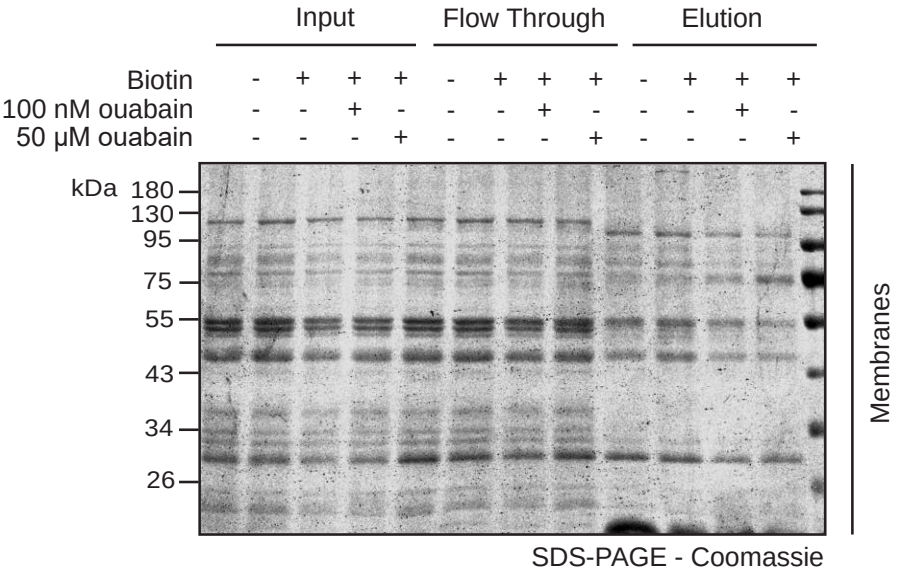

Figure 39. Glycosylated proteins were enriched from rat heart membranes.

Affinity enrichment of glycosylated proteins from ouabain treated cardiac membranes with WGA resin. Enrichment of glycosylated proteins was analysed on Coomassie stained SDS-PAGE. Inputs, flow throughs and elutions of the purification were analysed.

The analysis of the amount of glycosylated proteins in ouabain treated heart samples showed slightly less glycosylated proteins enriched from heart membranes after ouabain treatment. This result indicates that less membrane proteins are exposed to the extracellular matrix after ouabain treatment and may allow the conclusion that the endocytosis rate was increased in these samples. However, this effect should be also visible for the Na/K ATPase. Therefore, the samples were probed for specific amounts of glycosylated Na/K ATPase by Western blot with a Na/K ATPase antibody (Figure 40A). Input samples from solubilized membranes for the different ouabain and biotin treatments were compared with flow throughs and elutions after WGA affinity purification (Figure 40A). Glycosylated Na/K ATPase was massively enriched with the WGA affinity purification (Figure 40A). No statistical differences for Na/K ATPase protein levels were detected for the control heart samples in comparison with the different ouabain treated samples (Figure 40B).

Altogether, the Na/K ATPase pump was strongly enriched in membranes after WGA enrichment purification, indicating that – as expected – Na/K ATPase is a major cardiac membrane glycoprotein, but no differences were detected for the ouabain treatment.

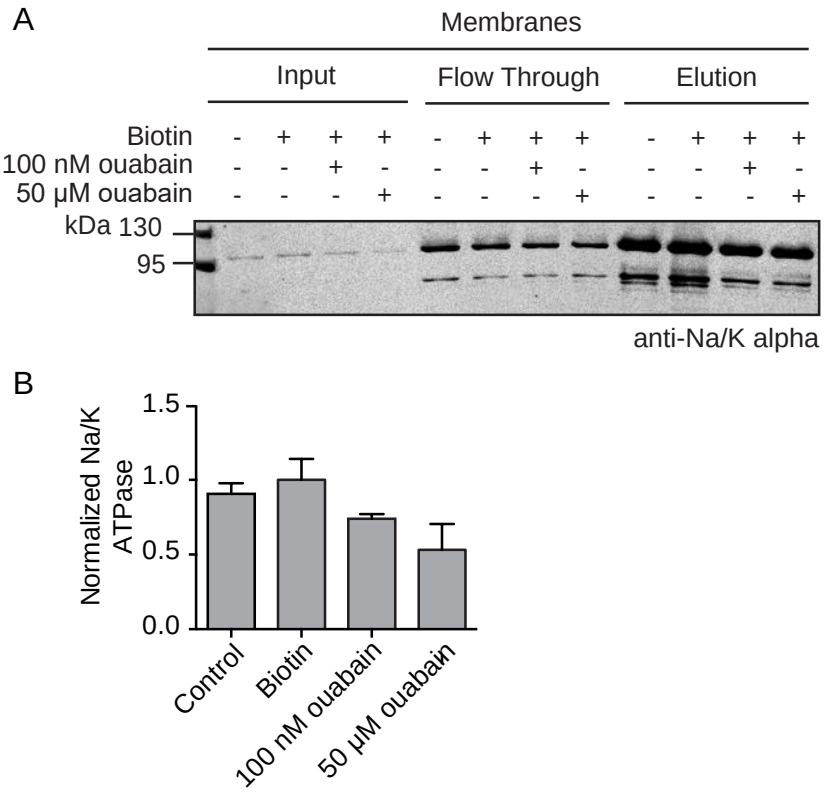

Figure 40. The Na/K ATPase was glycosylated in ouabain treated and control heart membranes.

(**A**) Glycosylated proteins were affinity purified with WGA, the elution was analysed by Western blotting with a Na/K ATPase antibody. Different levels of ouabain and different time points of the affinity purification were compared. (**B**) Quantification of experiment shown in (A) using values of the Na/K ATPase intensity normalized to the control sample which was not perfused with biotin or ouabain. The data of three independent experiments are presented as mean ± SEM. An unpaired t-test showed no significant differences between the samples.

4.3.1.6 Na/K ATPase and many other membrane proteins were biotinylated and glycosylated at the same time in rat hearts

To test the hypothesis of a 14-3-3 mediated co-endocytosis of the Na/K ATPase and TASK-3, I treated hearts with biotin, or biotin and ouabain to stimulate endocytosis. Consequently, the effect of ouabain treatment on exposed membrane proteins in the heart was analysed. Therefore, the amount of biotinylated and glycosylated Na/K ATPase was analysed with different affinity enrichment purifications. Neither the amount of biotinylated nor of glycosylated Na/K ATPase was altered due to ouabain treatment. Both methods indicated that no Na/K ATPase internalization is induced due to ouabain treatment.

However, to further understand trafficking of the Na/K ATPase after ouabain treatment, I compared how many glycosylated proteins are also biotinylated at the same time. Elutions of the two different affinity purifications were analysed for the amount of biotinylated proteins with fluorophore-conjugated streptavidin by Western blotting (Figure 41). Indeed, many glycosylated proteins were identified in the elution of the WGA affinity enrichment, indicating that a lot of glycosylated proteins were also biotinylated at the same time (Figure 41).

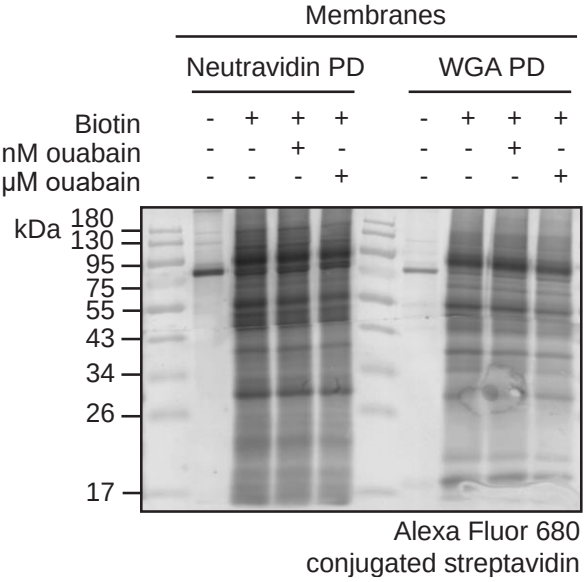

Figure 41. Glycosylated membrane proteins were also biotinylated in ouabain treated and control heart membranes.

Glycosylated proteins were affinity purified from ouabain treated heart membranes with WGA pull-downs (PD), biotinylated proteins were affinity enriched from the glycosylated protein fraction with neutravidin. The amount of enriched biotinylated proteins from both affinity enrichment experiments was analyzed by Western blotting with Alexa Fluor 680 conjugated streptavidin.

Subsequently, I analysed the amount of glycosylated and biotinylated Na/K ATPase or 14-3-3 proteins dependent on ouabain treatment. Therefore, biotinylated or glycosylated proteins enriched from heart membranes after ouabain treatment were analysed by Western blot. I probed for the Na/K ATPase and also assessed the 14-3-3 protein levels using a 14-3-3 antibody (Figure 42A). This experiment demonstrated that much more Na/K ATPase was glycosylated than biotinylated (Figure 42A,B). The reduced amount of biotinylated Na/K ATPase indicate that in general a large pool of Na/K ATPase was not exposed to the extracellular matrix during perfusion experiments performed with rat hearts. Overall, ouabain treatment did not have a significant effect on surface expressed and biotinylated Na/K ATPase levels in rat hearts.

14-3-3 proteins were present in the elutions from biotinylated enriched samples and reduced from glycosylated samples (Figure 42A). This result shows that 14-3 3 proteins were interacting with membrane proteins exposed at the cell surface, but reduced interaction with glycosylated membrane proteins was detected (Figure 42C). Indeed, there is a membrane bound fraction of 14-3-3 present, explaining why 14-3-3 was enriched in the MS analysis of the pull-down experiment performed with rat heart membranes.

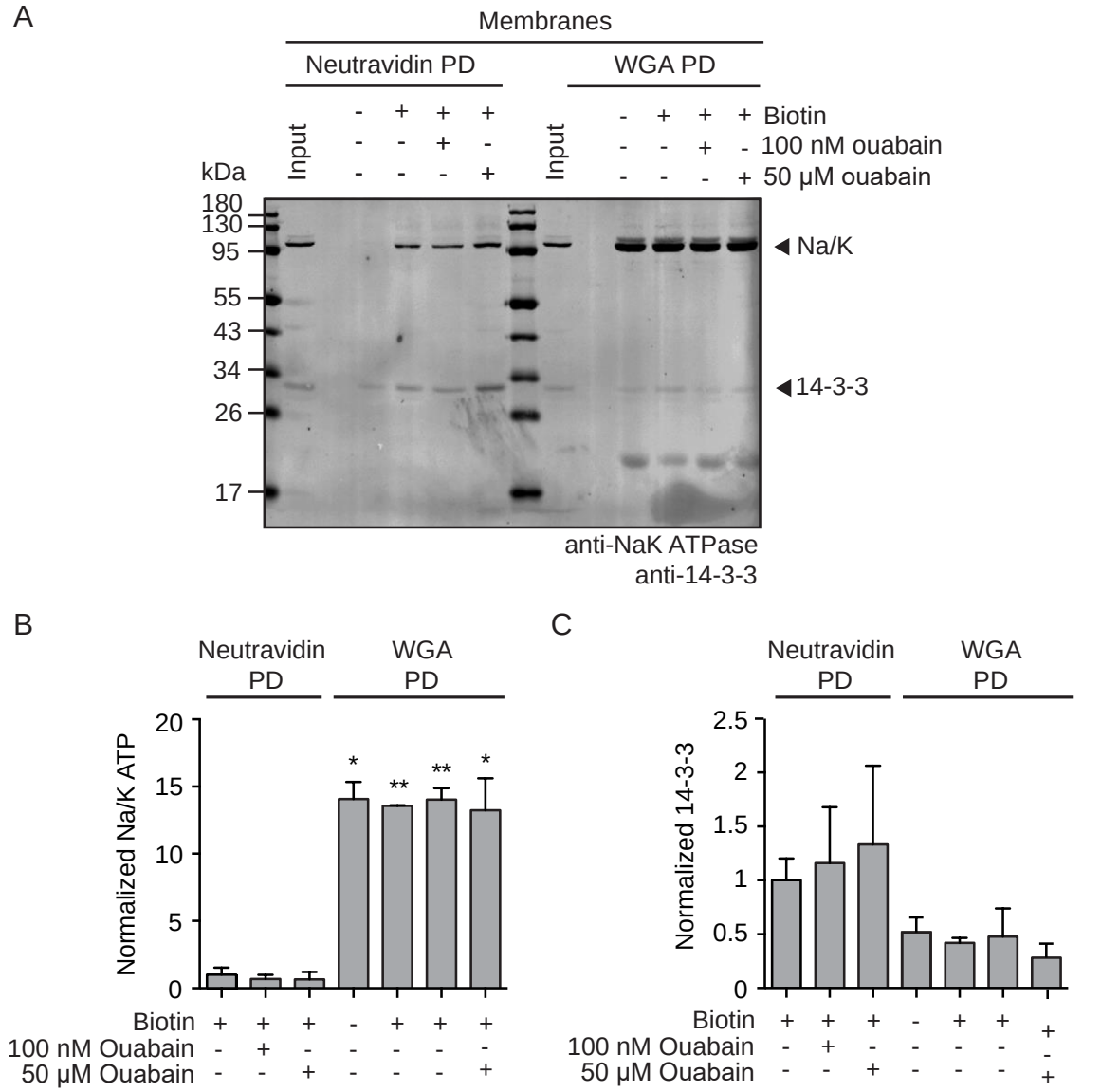

Figure 42. Comparison of biotinylated and glycosylated Na/K ATPase and 14-3-3 proteins enriched from ouabain treated hearts.

(**A**) Biotinylated proteins were affinity purified from ouabain treated cardiac membranes with neutravidin pull-downs (PD) meanwhile glycosylated proteins were enriched with WGA resin. Samples were analyzed by Western blot and detected for Na/K ATPase and 14-3-3 pan antibodies. **(B)** Na/K ATPase protein levels enriched with neutravidin or WGA pull-down experiments were normalized to the biotin control sample from neutravidin PD. The data of three independent experiments are presented as mean ± SEM. An unpaired t-test showed significant differences

between biotin control from the neutravidin PD and the samples enriched from WGA PD (*p=0.0109 or 0.0372, **p=0.0019 or 0.0060). **(C)** 14-3-3 protein levels enriched with neutravidin or WGA pull-down experiments were normalized to the biotin control sample from neutravidin PD. The data of three independent experiments are presented as mean ± SEM. An unpaired t-test showed no significant differences between biotin control sample from neutravidin PD and the samples enriched from WGA PD.

4.3.2 Identification of novel cardiac interaction partners of the TASK-1 C-terminus

After I analysed the interactome of heart proteins which interact with the extreme C-terminus of TASK-3, I was also interested in potential novel cardiac interaction partners for the TASK-1 C-terminus. In comparison with TASK-3, the TASK-1 C-terminus has two PKA phosphorylatable serine residues (S392 and S393) in the trafficking control region. It is already known that 14-3-3 binds the phosphorylated S393 with high binding affinities in the micromolar range (Kilisch et al., 2016). The two different serine residues in the trafficking control of TASK1, which are absent in TASK-3, indicate that trafficking of TASK-1 is regulated in a more complex manner (Kilisch et al., 2016). To further understand the function of both serine residues in TASK-1 and identify novel interaction partners which are involved in TASK-1 trafficking and regulation pull-down experiments with rat heart tissue were performed and analysed by MS.

4.3.2.1 Recombinant expression of TASK-1 fusion proteins

To analyse the potential cardiac interactome depend on the phosphorylation status of TASK-1, recombinant proteins were designed and cloned in a similar manner as already described for TASK-3. The last 15 aa of the TASK-1 C-termini were fused to a GST-tag and a MST27-linker. In order to investigate the role of TASK-1 C-terminus phosphorylation state regulating the binding of interaction partners, I used serine phospho-dead mutants for the single serine residues and the combination of both (Table 15).

Table 15. Sequence of recombinant purified TASK-1 proteins used to identify new cardiac interaction partners.

The last 15 AA of TASK-1 were fused with a GST-tag and a MST27 linker. The ER-retrieval sequence is highlighted in blue. The phosphorylatable serine residues are shown in red and the serine to alanine mutations are depicted in green.

Peptide name	Amino acid sequence
TASK- 1 WT	GST-MST27-CSLSTFRGLMKRRSSV-COOH
TASK- 1 S392A	GST-MST27-CSLSTFRGLMKRRASV-COOH
TASK- 1 S393A	GST-MST27-CSLSTFRGLMKRRSAV-COOH
TASK- 1 S392A/S393A	GST-MST27-CSLSTFRGLMKRRAAV-COOH

The first step for the analysis of novel cardiac interaction partners for TASK-1 was the recombinant overexpression and purification of TASK-1 mutants, which addresses different possible phosphorylation states of TASK-1 from *E. coli.* The recombinant purified TASK-1 proteins were analysed on Coomassie stained SDS-PAGE (Figure 43A). The

GST-MST27-TASK-1 mutants have a size of approximated 38 kDa, which was confirmed on a SDS-PAGE (Figure 43A). The bands below likely reflect degradation products of the MST27 linker or the GST-tag. For the identification of novel cardiac interaction partners the different phosphorylation states of the TASK-1 C-terminus were considered to be important. Therefore, the purified TASK-1 mutant proteins were recombinant phosphorylated with PKA in presence of an ATP regeneration system. Phosphorylation was confirmed on Coomassie stained Phos-tag-PAGE. All purified TASK-1 constructs were compared in its unphosphorylated or phosphorylated state. The TASK-1 WT protein has two potential PKA phosphorylation sites (S392 and S393). After phosphorylation, two slower-migrating bands were visible on a Phos-tag-PAGE, which indicates that both residues were phosphorylated (Figure 43B). TASK-1 S392A and S393A mutants just showed one slower-migrating band on the gel (Figure 43B), indicating single phosphorylation. As expected, no phosphorylation was detected in the case of double phospho-dead mutant TASK-1 S392A/S393A (Figure 43B). Altogether, this experiment confirms that the TASK-1 WT can be *in-vitro* phosphorylated by PKA on both serine residues S392 and S393 simultaneously but also individually.

This experiment confirmed, that both serine residues in TASK-1 can be recombinantly phosphorylated by PKA (Kilisch et al., 2016) and allowed further experimentation.

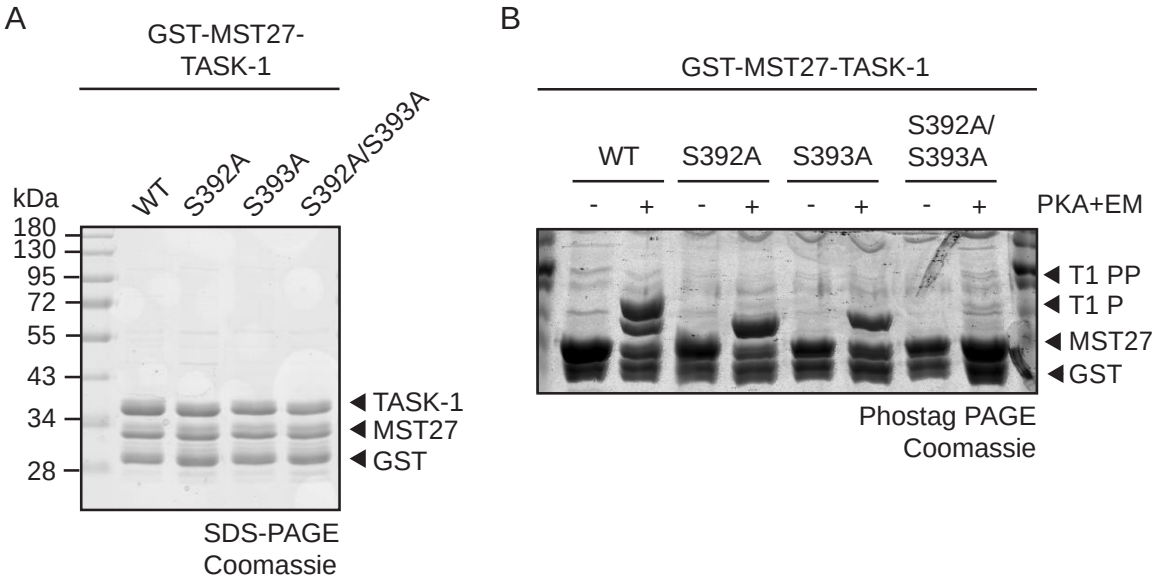

Figure 43. TASK-1 protein is phosphorylatable by PKA at S392 and S393 residues at the same time and individually *in-vitro*.

(**A**) Different GST-MST27-TASK-1 mutant proteins were purified to address the different possible phosphorylation states of the TASK-1 C-terminus. All proteins were purified from *E.coli* and confirmed on Coomassie stained SDS-PAGE. (**B**). Recombinant TASK-1 constructs were phosphorylated with PKA. Phosphorylation is indicated as a shift on a Coomassie stained Phos-tag-PAGE.

4.3.2.2 Phosphorylation dependent enrichment of novel cardiac interaction partners of the TASK-1 C-terminus

With affinity purification experiments from cardiac tissue novel interaction partners for TASK-1 were identified. During the analysis of the affinity purification experiments with the TASK-3 C-terminus (section 4.3.1), I realized that separation of rat heart membranes and cytosol will be an additional control to exclude unspecific interaction. Moreover, I expected to gain more information about trafficking processes in cardiac membranes or cytosol. First, I separated membranes and cytosol and analyzed them by Western blot, detecting for GAPDH and Na/K ATPase antibodies (Figure 44A). Na/K ATPase protein levels were detected in the membrane fraction but absent in the cytosol (Figure 44A) and GAPDH protein levels were detected in the cytosol but just very low levels in the membrane fraction (Figure 44A).

The already performed affinity purification experiments with TASK-3 showed that the TASK-3 bait proteins masks proteins with a molecular mass between 26-40 kDa size in a SDS-PAGE analysis. High-salt elution (NaCl) elution is another possibility to elute the bait proteins after a pull-down experiment. NaCl just elutes enriched proteins bound to the GST-bait protein without eluting the bait protein itself from the affinity resin. First, L-Gluthathione elution was compared with 1 M NaCl elution (Figure 44B) on silver-stained SDS-PAGE. Recombinant purified TASK-1 WT C-terminal proteins were used as bait protein and incubated with rat heart membranes or cytosol which were again pre-cleared from native 14-3-3 and COPI. GST and a GST-MST27 control proteins were included to distinguish unspecific interactions (Figure 44B). The NaCl elution was cleaner, allowed the analysis of novel interaction partners which have similar sizes than the bait protein already on a SDS-PAGE (Figure 44B). Moreover, different bands were identified on the silver gel dependent on the phosphorylation state of the TASK-1 bait protein (Figure 44B, marked with asterisks), indicating novel cardiac interaction partners enriched with the phosphorylated TASK-1 C-terminus. Based on this optimization, I decided to use NaCl elution for the TASK-1 pull-down experiment with rat heart membranes and cytosol.

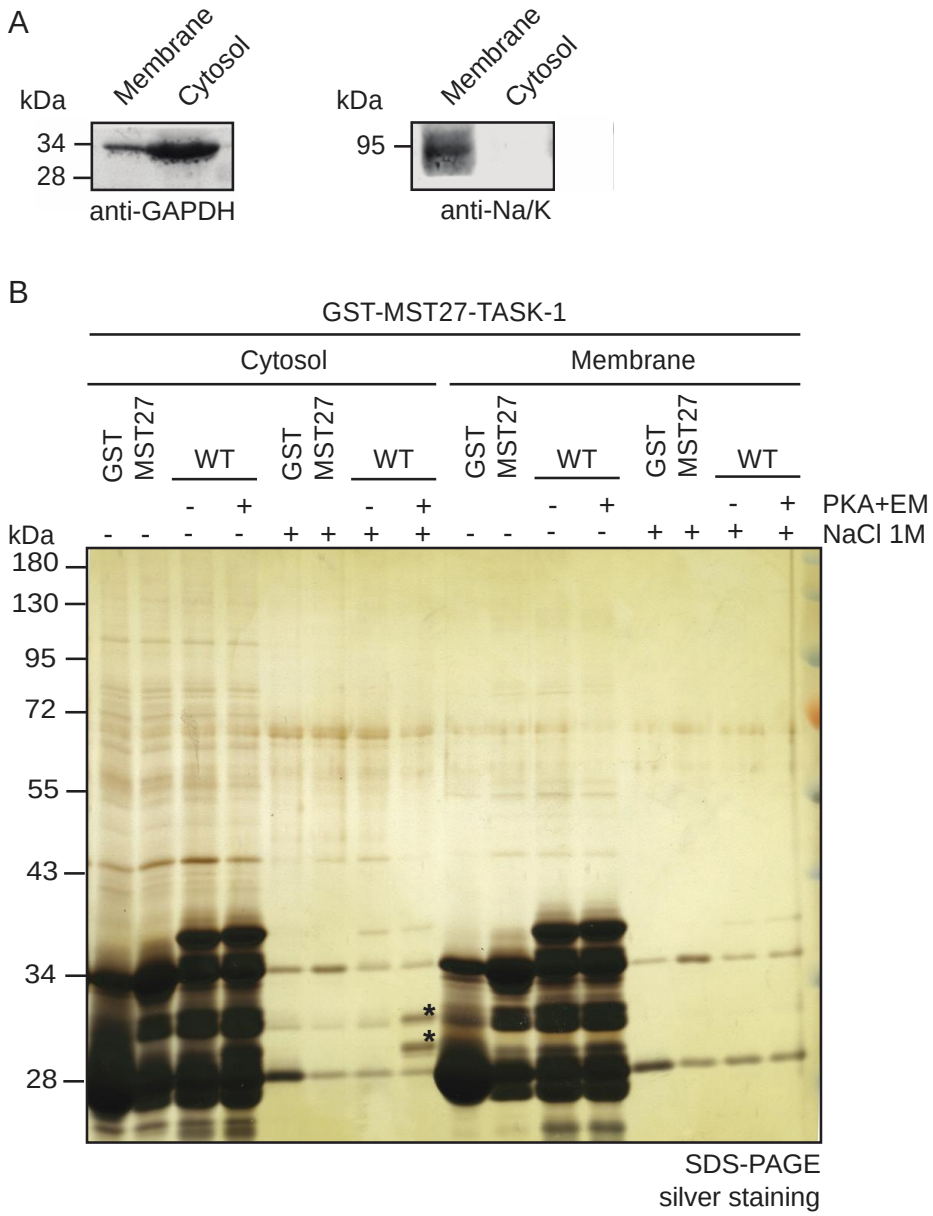

Figure 44. Compared L-glutathione and high salt elution of TASK-1 pull-downs with separated heart membranes and cytosol.

(**A**)The purity of the separated membrane or cytosolic fraction was confirmed by Western blotting and the detection of the cytosolic marker protein GAPDH or the membrane marker Na/K ATPase. (**B**) Comparison of L-Gluthathione and NaCl elution after a pull-down experiment with GST-MST27-TASK-1 WT unphosphorylated or phosphorylated and rat heart cytosol or membranes. GST or GST-MST27 (MST27) constructs were used as negative controls. Elutions were analysed on a silver-stained SDS-PAGE. Interestingly differences are highlighted with an asterisk.

The purified and phosphorylated TASK-1 C-terminal fusion proteins (GST-MST27-TASK-1 WT,- S392A,- S393A,- S392/S393A) were used for the TASK-1 pull-down experiment with cardiac tissue optimized as indicated. In order to avoid masking of the TASK-1 C-terminus endogenous 14-3-3 and COPI were removed from the separated heart cytosol and membranes. The elution of the TASK-1 pull-down experiments was analysed on Phos-tag SDS-PAGE to confirm the phosphorylation states of the TASK-1 bait proteins after the pull-down from membranes (Figure 45A) and cytosol (Figure 45B). Therefore, the bait proteins were eluted with L-Glutathione after NaCl elution and analysed on SDS-PAGE. In both affinity purification experiments the TASK-1 WT protein was phosphorylated at both serine residues, meanwhile the single serine to alanine mutant proteins were single phosphorylated and the double serine to alanine mutant was not phosphorylated at all (Figure 45 A,B). Phosphorylation states were also confirmed with Western blotting with a TASK-1 antibody (Figure 45 A,B) and phospho-specific TASK-1 antibody (Figure 45 A,B).

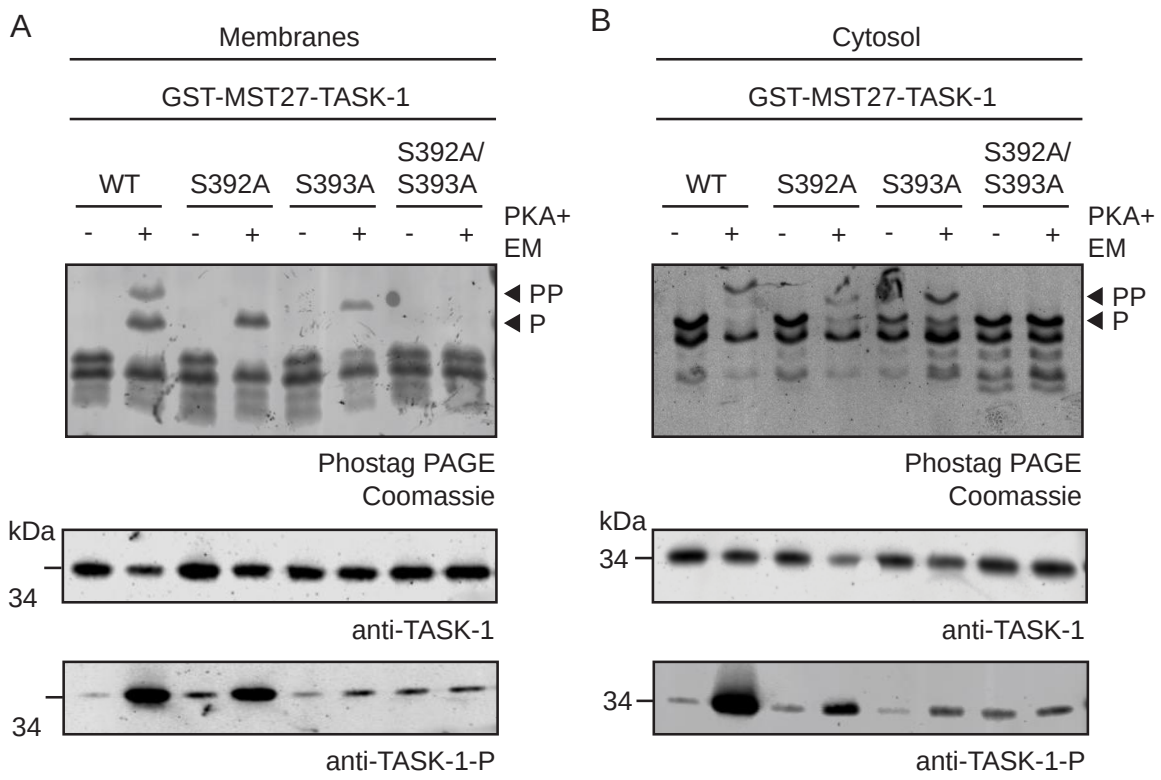

Figure 45. Analysis of phosphorylation state GST-MST27-TASK-1 protein variants after the affinity purification experiment with membranes or cytosol.

The phosphorylation state of eluted TASK-1 C-terminal bait proteins were analysed after a pull-down experiment from membranes (**A**) or cytosol (**B**) on Coomassie stained Phos-tag-PAGE. Phosphorylation is indicated as a shift on the Phos-tag-PAGE (highest panel) and was confirmed by Western blot and detection with an antibody which binds TASK-1 (middle panel) or the phosphorylated form of TASK-1 (lower panel).

After confirmation of the phosphorylation status of the TASK-1 bait proteins the elutions obtained from the TASK-1 pull-down experiment were analysed on a silver-stained SDS-PAGE (Figure 46). I focused on those bands that were differentially present depending on the phosphorylation state of TASK-1 C-terminus (Figure 46, marked with asterisks). These differential bands indicate enrichment of cardiac proteins due to the phosphorylation state of the TASK-1 C-terminus. The eluted samples were subjected to LC-MS/MS analysis which was performed in collaboration with Dr. Christoph Lenz (UMG Göttingen).

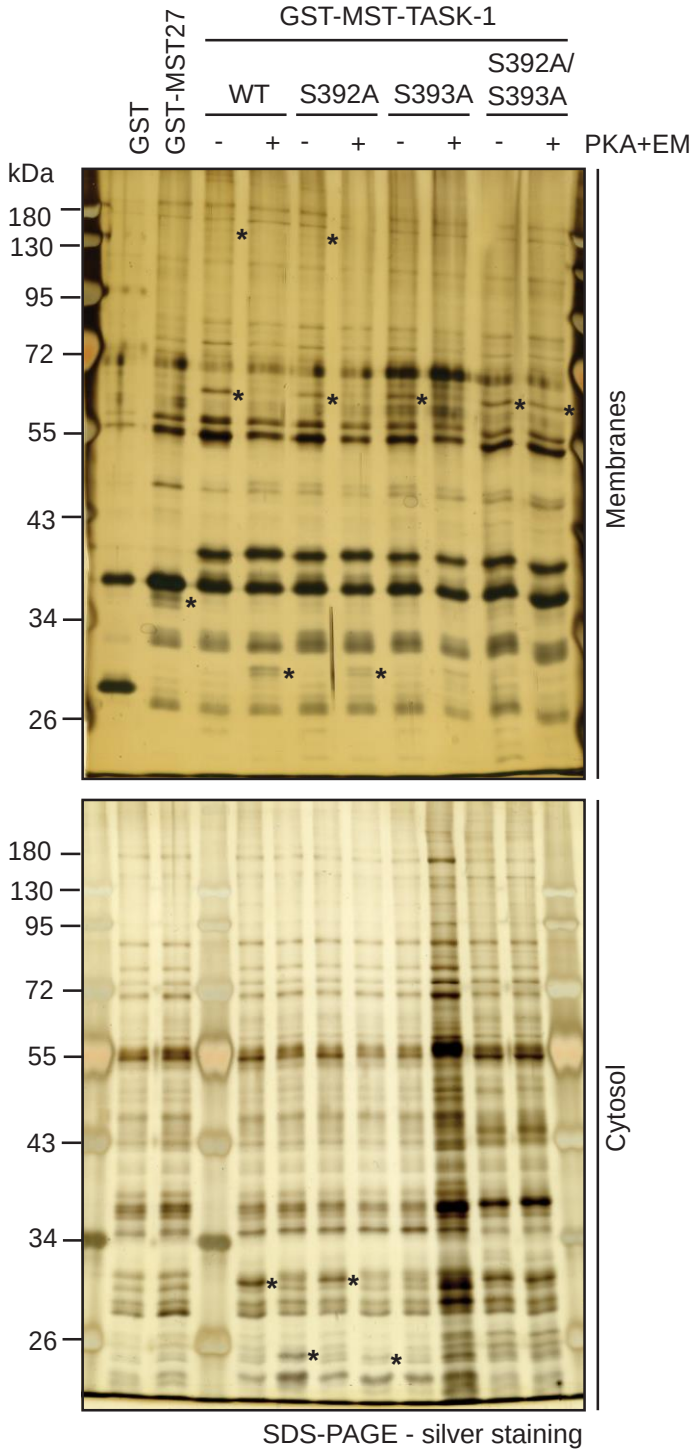

Figure 46. Affinity purification with recombinant phosphorylated GST-MST27-TASK-1 proteins and solubilized rat heart membranes or cytosol.

Elutions of TASK-1 pull-down samples were analyzed on big SDS-PAGE prior to be sent for MS analysis. GST and GST-MST27 proteins were used as controls to monitor background binding. Interestingly differences are highlighted with an asterisk.

The LC-MS/MS analysis revealed new cardiac interaction partners which bind to the C-terminal trafficking control region of TASK-1 depending on its phosphorylation state. The MS analysis was quantified by calculation and plotting the log_2 fold changes of ratios of TASK-1 WT-/+ phosphorylation, TASK-1 S392A-/+ phosphorylation, TASK-1 S393A-/+ phosphorylation and TASK-1 S392A/S393A-/+ phosphorylation. Proteins which were enriched over the cut-off of each measurement (defined as 2σ, where σ is the standard abbreviation over all values) were assumed to be significantly enriched and highlighted in orange (Figure 47 A-D). The protein with the highest log_2-fold change identified in the MS analysis was disk large homolog 1 (Dg1, Figure 47A). Dlg1 belongs to the PDZ domain containing protein family. Beside Dlg1, more PDZ domain containing proteins were identified such as disk large homolog 4 (Dlg4) or membrane-associated guanylate kinase, WW and PDZ domain-containing protein 3 (Magi-3). All PDZ domain containing proteins are depicted in red (Figure 47A-D). Interestingly, the PDZ domain proteins were exclusively enriched with the unphosphorylated TASK-1 WT protein (Figure 47A) from cardiac membranes. However, none of the PDZ domain containing proteins were identified with the TASK-1 phospho-dead mutants regardless of their phosphorylation state (Figure 47A-D). Furthermore, no PDZ domain containing protein was enriched with different TASK-1 mutants from rat heart cytosol (Figure 48).

Moreover, already known interaction partners like different 14-3-3 isoforms were enriched exclusively with phosphorylated TASK-1 C-terminus in both affinity purification experiments as well and highlighted in pink (Figure 47, 48), although the cardiac membrane and cytosol were treated with an inhibitor beforehand. Kilisch et al reported that phosphorylation of both serine residues in parallel abolish 14-3-3 interaction. In line with this notion, none of the 14-3-3 isoforms were enriched in the PKA phosphorylated TASK-1 S392A/S393A mutant (Figure 47D).

Interestingly, several different PDZ domain containing proteins were exclusively enriched in the affinity purification experiment with rat heart membranes with the unphosphorylated TASK-1 C-terminus. Among them just Dlg1 and Magi-3 were enriched over the cut-off.

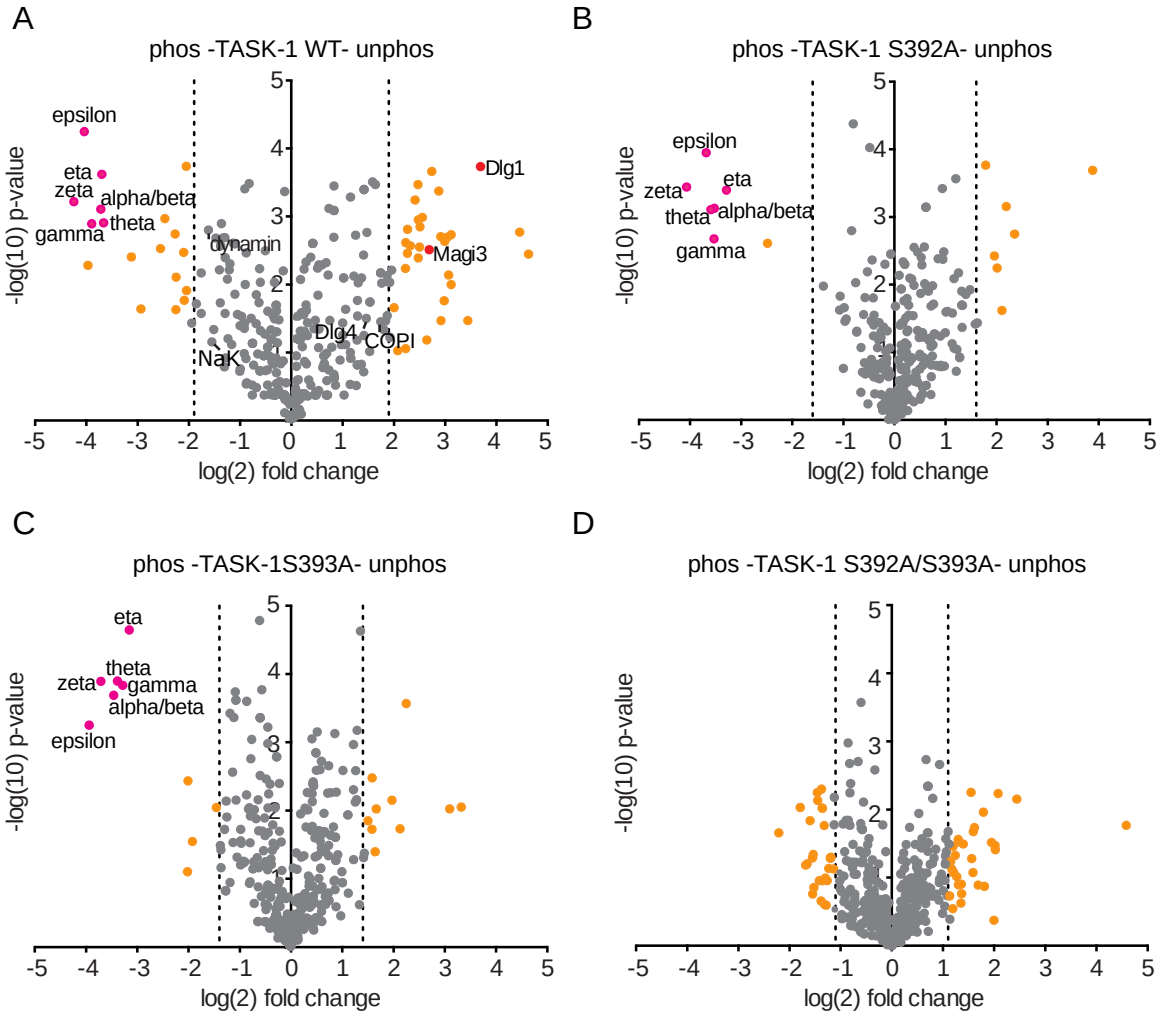

Figure 47. PDZ domain containing proteins were identified as novel TASK-1 interaction partners in cardiac membranes.

Dot plots analysing the MS results of affinity purification experiments with rat heart membranes and TASK-1 C-terminal protein variants. The log_2-fold changes of ratios of (**A**) TASK-1 WT +/- phosphorylation (phos), (**B**) TASK-1 S392A +/- phosphorylation, (**C**) TASK-1 S393A +/- phosphorylation, (**D**) TASK-1 S392A/S393A +/- phosphorylation were calculated. The cut-off of each measurement was calculated corresponding to 2σ, where σ is the standard abbreviation over all values. Proteins which were enriched over the cut-off are highlighted in orange. Identified PDZ domain containing proteins are labelled in red and 14-3-3 isoforms in pink.

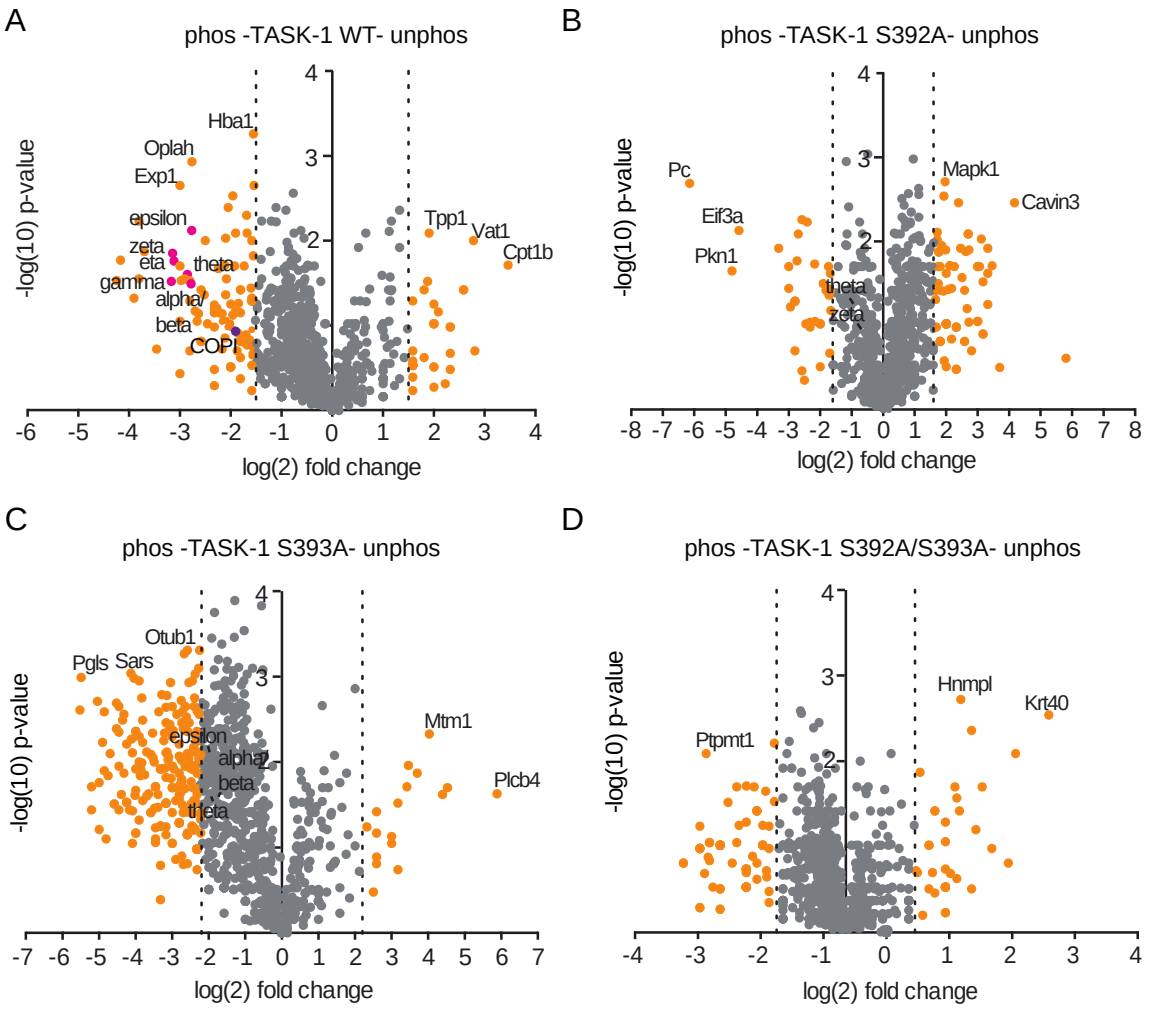

Figure 48. PDZ domain containing proteins were absent as TASK-1 interaction partners in cardiac cytosol.

Dot plots analysing the MS results of affinity purification experiments with rat heart cytosol and TASK-1 C-terminal protein variants. The log_2-fold changes of ratios of (**A**) TASK-1 WT +/- phosphorylation (phos), (**B**) TASK-1 S392A +/- phosphorylation, (**C**) TASK-1 S393A +/- phosphorylation, (**D**) TASK-1 S392A/S393A +/- phosphorylation were calculated and plotted. The cut-off of each measurement was calculated corresponding to 2σ, where σ is the standard abbreviation over all values. Proteins which were enriched over the cut-off are highlighted in orange. Identified 14-3-3 isoforms are labelled in pink, COPI is depicted in purple.

4.3.2.3 PDZ domain containing proteins were identified as novel TASK-1 interaction partners in the heart by MS analysis

The analysis of the cardiac interactome of TASK-1 revealed PDZ domain containing proteins as the most prominent novel interaction partners. Interestingly, the last four amino acids of TASK-1 C-terminus contain a conserved PDZ-binding motif (X-S/T-X-V/I), which is absent in TASK-3 (Rajan, et al., 2002). This implicates that the unphosphorylated S392

is required for the PDZ protein interaction. In line, Dlg1 binding was abolished with the TASK-1 S392A protein in the MS approach (Figure 47B). However, also no PDZ domain protein was identified with the TASK-1 S393A protein (Figure 47C), although the PDZ binding site is intact in this TASK-1 mutant. To confirm the interaction of PDZ domain containing proteins in the predicted PDZ-binding motif of TASK-1 and to clarify the issue with the TASK-1 S393A protein the MS approach was repeated. Therefore, TASK-1 mutant proteins addressing the predicted PDZ binding motif were used. This includes the V394 residue in TASK-1, which is also predicted to be required for PDZ protein interaction according to the PDZ-binding motif in TASK-1 (Rajan et al., 2002). Consequently, the C-terminal TASK-1 dV394 protein was included as another control and a GST-MST27-TASK-1 dV394 protein was recombinantly purified (Figure 49A) and phosphorylated with PKA (Figure 49B) as already shown for the other TASK proteins used in this study.

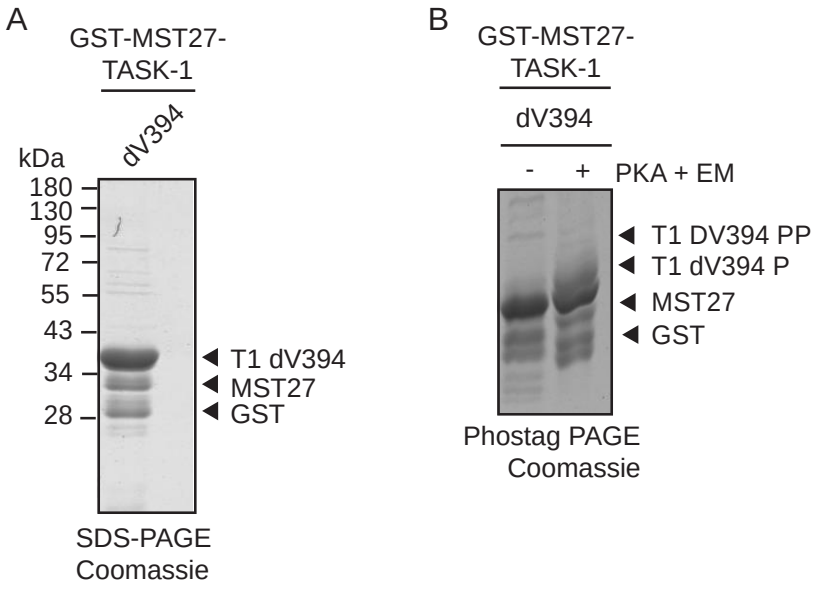

Figure 49. Purification of TASK-1 dV394 protein variant.

(**A**) The recombinant C-terminal GST-MST27-TASK-1 dV394 protein was used as an additional control. The purified GST-MST27-TASK-1 dV394 protein has an expected size of 38 kDa on a SDS-PAGE. (**B**) Phosphorylation with PKA was confirmed on a Coomassie stained Phos-tag-PAGE.

For the repetition of the MS approach C-terminal TASK-1 WT, single phospho-dead TASK-1 S393A, double phospho-dead TASK-1 S392A/S393A and TASK-1 dV394 were incubated in rat heart membranes. The membranes were again pre-cleared from native 14-3-3 and COPI coat. Elutions were analysed on Coomassie stained Phos-tag-PAGE to confirm the right phosphorylation status of the different TASK-1 mutant proteins after the affinity purification experiment (Figure 50A). Besides, the eluted samples were analysed on a silver-stained SDS-PAGE (Figure 50B) for enriched novel proteins. Finally, the

samples were sent for LC-MS/MS analysis which was performed in collaboration with Dr. Christoph Lenz (UMG Göttingen).

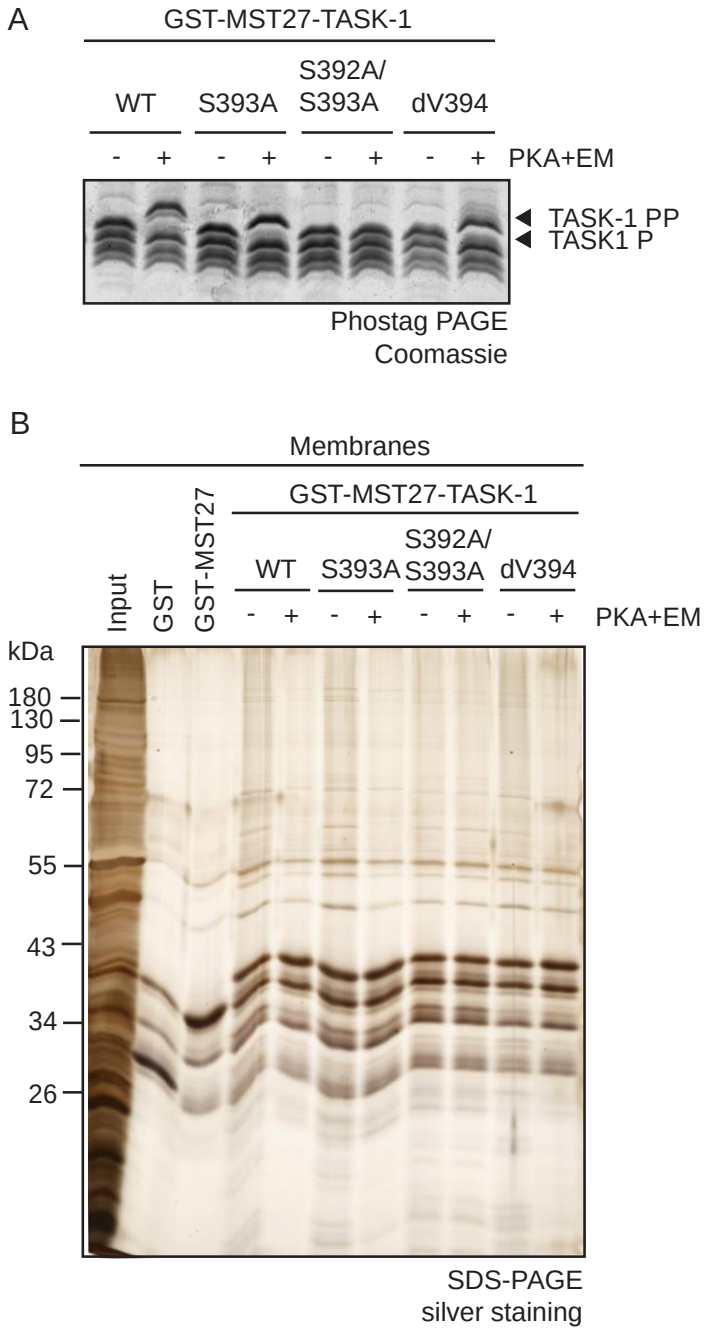

Figure 50. Analysis of affinity purification with TASK-1 proteins and rat heart membranes. (**A**) Phosphorylation status of TASK-1 bait mutant proteins after the affinity purification experiment was confirmed on Coomassie stained Phos-tag-PAGE. (**B**) Analysis of potential interaction partners after a TASK-1 affinity purification experiment with heart membranes. A specified set of C-terminal mutants was used to confirm interactions with PDZ domain containing proteins.

The biological replicate of the affinity purification experiment of different C-terminal TASK-1 mutant proteins with rat heart membranes identified again several PDZ domain proteins in

the MS analysis (Figure 51A-D). Especially, Dlg1 and Dlg4 were again significantly enriched. All PDZ domain proteins were enriched with the unphosphorylated TASK-1 WT protein and the S393A mutant variant (Figure 51A,B). As expected, the serine 392A/393A TASK-1 and as well as the TASK-1 dV394 mutant proteins disrupted the putative PDZ-binding motif in the TASK-1 C-terminus and no PDZ protein was identified with one of these two mutant variants in the MS analysis (Figure 51A-D).

Altogether, PDZ domain proteins were identified as the most promising novel TASK-1 interaction partners in two independent MS analysis. The set of TASK-1 mutant proteins confirmed the suggested putative PDZ-binding motif X-S/T-X-V/I in the extreme C-terminus of TASK-1 and showed that the S392 is relevant for the interaction.

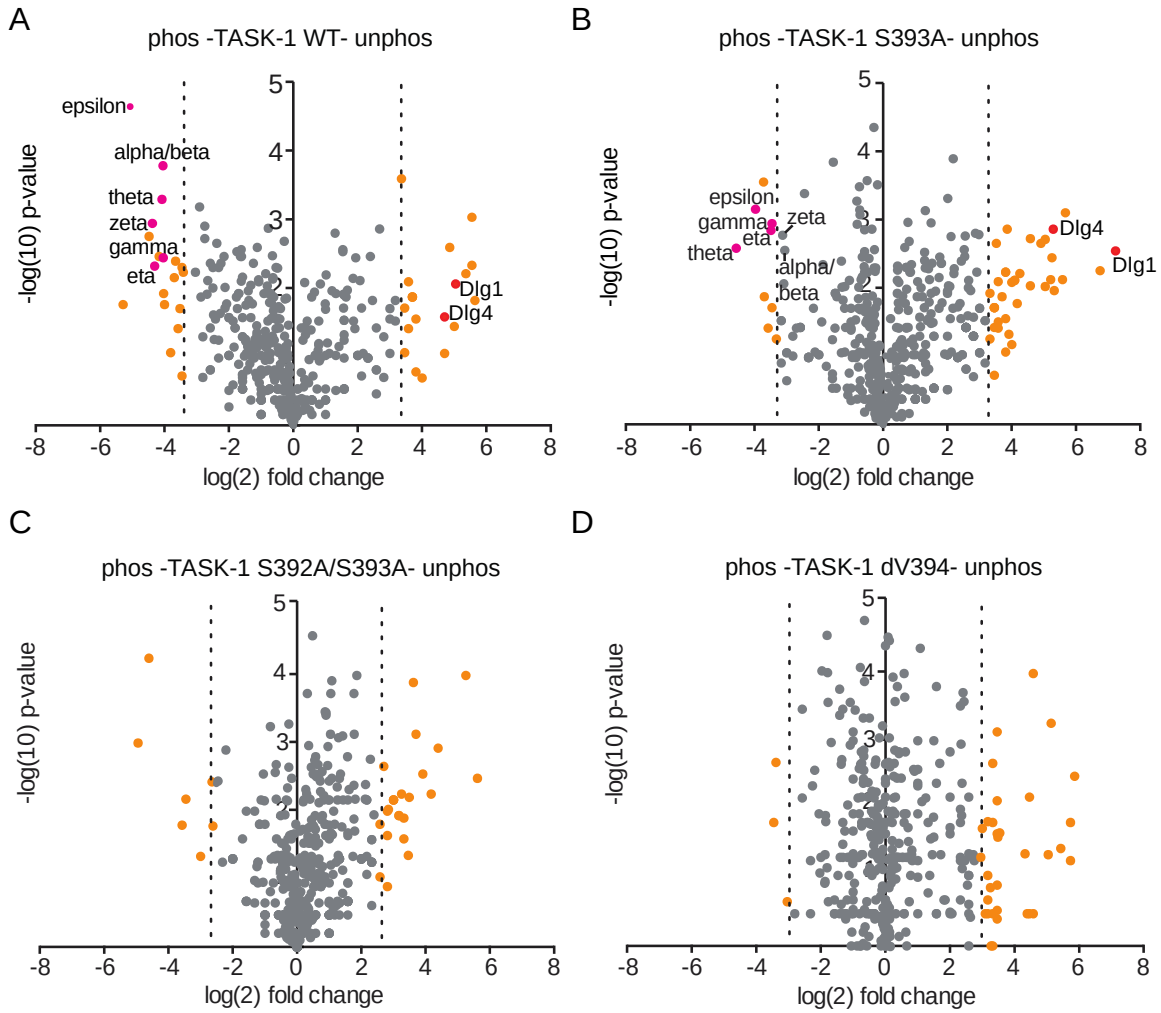

Figure 51. PDZ domain containing proteins were identified as TASK-1 interaction partners in cardiac membranes.

Dot plot analysis of MS results after affinity purification of rat heart membranes with GST-MST27-TASK-1 constructs. The $\log_2$-fold changes of ratios of (**A**) TASK-1 WT +/- phosphorylation (phos), (**B**) TASK-1 S393A +/- phosphorylation, (**C**) TASK-1 S392A/S393A +/- phosphorylation, (**D**) TASK-1 dV394 +/- phosphorylation were calculated. The cut-off of each measurement was calculated corresponding to 2σ, where σ is the standard abbreviation over all values. Proteins which were

enriched over the cut-off are highlighted in orange. Identified 14-3-3 isoforms are highlighted in pink and PDZ domain containing proteins are depicted in red.

Several different MS analyses of the extreme C-terminus of the TASK-1 or TASK-3 channel were performed with either heart membranes, cytosol or total lysate and summarized in table 16. Already known binding partners like several 14-3-3 isoforms as well COPI were identified and serve as positive controls. Interestingly, the Na/K ATPase protein was identified in the TASK-1 and TASK-3 MS analysis, although the enrichment in the TASK-1 PD was reduced. The same was true for the endocytosis adaptor proteins like dynamin. However, PDZ domain proteins were specifically enriched in the TASK-1 affinity purification experiment with heart membranes. Unlike TASK-1, TASK-3 was unable to enrich PDZ domain proteins since it lacks a PDZ-binding motif.

Table 16. Summary MS analysis performed with TASK-1 and TASK-3 C-termini constructs in affinity purification experiments carried out with cardiac tissue.

	Identified interaction partners	TASK-1 Membrane	TASK-1 Cytosol	TASK-3
Known TASK binding partners	14-3-3 epsilon	✓	✓	(✓)
	14-3-3 eta	✓	✓	✓
	14-3-3 zeta/delta	✓	✓	✓
	14-3-3 beta/alpha	✓	✓	✓
	14-3-3 theta	✓	✓	✖
	14-3-3 gamma	✓	✓	(✓)
	COPI	(✓)	✓	✖
Na/K ATPase alpha		(✓)	✖	✓
Involved in endocytosis	AP-2 complex	✖	✖	✓
	Dynamin-like-protein 1	(✓)	✖	✓
PDZ domain containing proteins	Disk large homolog 1	✓	✖	✖
	Disk large homolog 4	✓	✖	✖
	Membrane associated guanylate kinase protein-3	✓	✖	✖

✓	detected (significant)	(✓)	detected (at limit of significance)	✖	not detected

4.3.2.4 PDZ domain containing proteins Dlg1 and Dlg4 are direct interaction partners of the unphosphorylated TASK-1 channel

Intriguingly, I could identify several PDZ domain containing proteins as novel interaction partners of the TASK-1 C-terminus. This confirms a previously hypothesized but never demonstrated interaction of TASK-1 with PDZ domain containing proteins (Rajan et al., 2002). To confirm the identified hits from the MS analysis binding assays using recombinant purified proteins were performed. From the several identified PDZ domain containing proteins, I focused on the top hits Dlg1 and Dlg4. The remaining PDZ domain containing proteins present in the list of hits were hardly expressed in hearts or the size was too big for an optimal recombinant expression *in vitro* (i.e. Magi-3). Full length MBP-Dlg1 and MBP-Dlg4 were recombinant expressed, purified and confirmed on Coomassie stained SDS-PAGE (Figure 52).

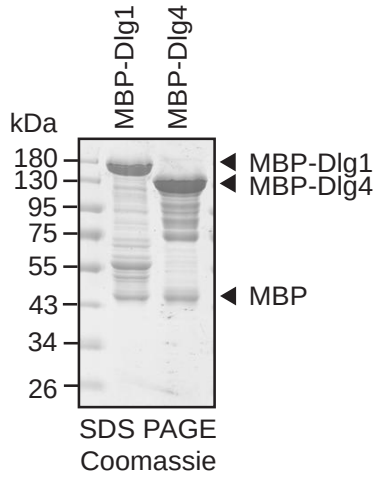

Figure 52. Recombinant purification of the PDZ domain containing proteins MBP-Dlg1 and MBP-Dlg4.

Both proteins were expressed in *E. coli* and affinity purified**.** Results were analyzed on Coomassie stained SDS-PAGE.

The binding assay allowed confirmation of the novel interaction between PDZ domain containing proteins and TASK-1 and allows simultaneously characterization of the binding site in TASK-1. Purified MBP-tagged PDZ proteins were used for binding experiments with recombinant purified GST-tagged TASK-1 C-terminus mutants either phosphorylated or unphosphorylated. TASK-1 WT and TASK-1 S393A proteins are both proteins containing an intact PDZ binding motif. Besides, TASK-1 S392A/S393A, TASK-1 dV394 and TASK-3 proteins were used as negative controls because in these mutants the PDZ-binding motif in TASK-1 is disrupted. The C-terminal TASK bait proteins were recombinant phosphorylated, immobilized to an affinity resin and offered to equimolar amounts of MBP-Dlg1 (Figure 53) and MBP-Dlg4 (Figure 54). The experiment was analysed on Coomassie

stained SDS-PAGE gels. Along the same line as the MS results, both MBP-Dlg1 and MBP-Dlg4 interact with unphosphorylated TASK-1 WT protein and unphosphorylated TASK-1 S393A protein (Figure 53, 54). Phosphorylation disrupts the interaction in both cases (Figure 53, 54). The double mutation of both phosphorylatable serine residues in the TASK-1 C-terminus (S392A/S393A) disrupts the interaction with Dlg1 and Dlg4 (Figure 53, 54), indicating that the unphosphorylated serine 392 in TASK-1 is important for the interaction. Besides, neither Dlg1 nor Dlg4 interact with TASK-1 dV394 or TASK-3 independent of the phosphorylation status (Figure 53, 54). The binding was confirmed by Western blot and detection with anti-Dlg1 and anti-Dlg4 antibodies (Figure 53, 54). Phosphorylation of C-terminal GST-TASK-1 and GST-TASK-3 proteins was probed by Coomassie stained Phos-tag SDS-PAGE (Figure 53, 54).

Altogether, Dlg1 and Dlg4 were confirmed as novel and direct interaction partners of the TASK-1 channel with MS analysis and reconstitution experiments using recombinant proteins. It was also shown that the interaction is phosphorylation independent and that the S392 and V394 in the TASK-1 C-terminus are required for the interaction. These findings confirm the predicted PDZ interacting motif in the extreme TASK-1 C-terminus as a functionally relevant motif and indicate a novel function for the S292 as the target site for regulating the interaction with the PDZ domain.

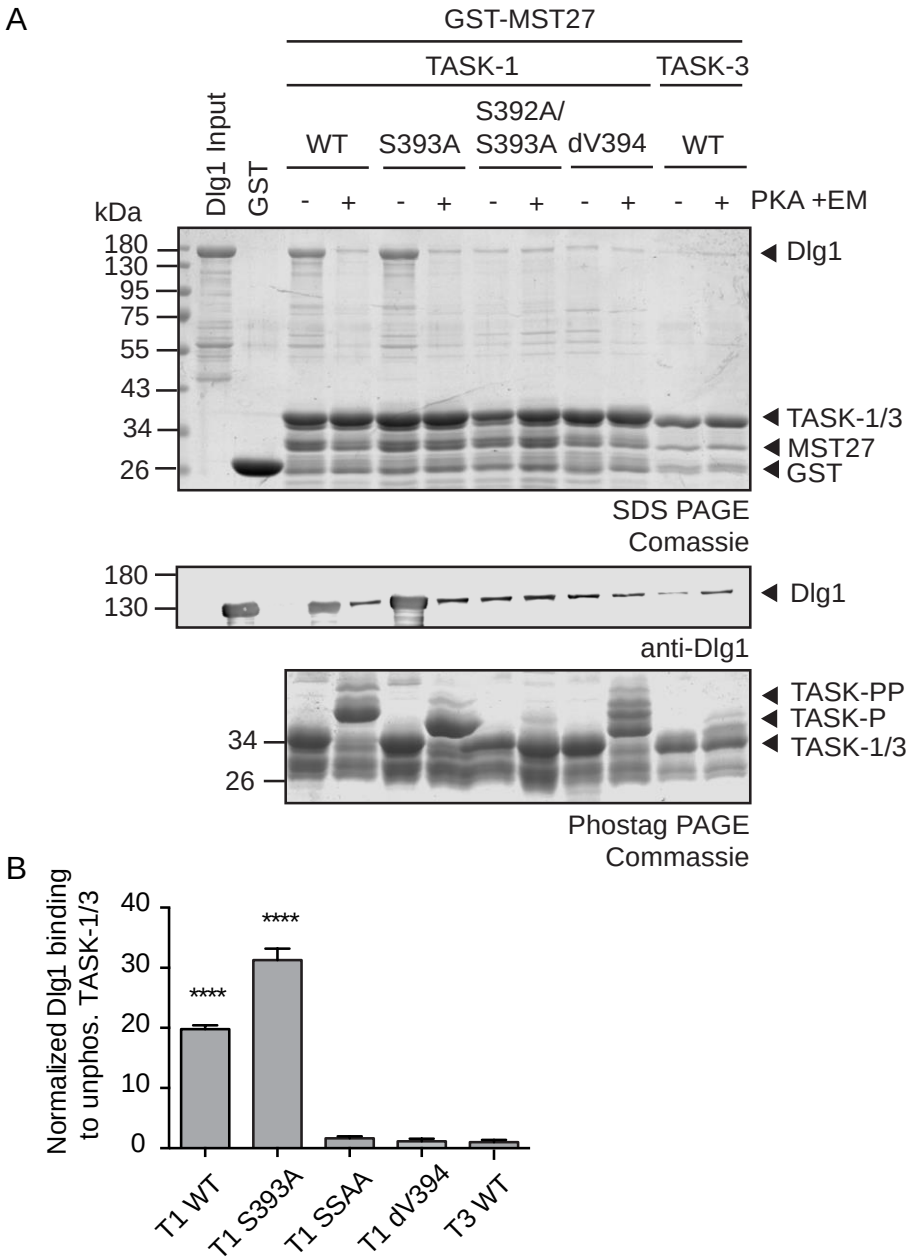

Figure 53. Dlg1 binds *in-vitro* to the unphosphorylated TASK-1 C-terminus.

(A) Recombinant purified MBP-Dlg1 binds to the unphosphorylated TASK-1 WT and S393A protein variants. Phosphorylation disrupted the interaction (upper panel). Binding was confirmed by Western blotting with a Dlg1 antibody (middle panel). The phosphorylation state of the bait protein was analyzed on Phos-tag-PAGE (lower panel). **(B)** Quantification of Dlg1 binding to different unphosphorylated TASK-1 and TASK-3 protein variants. Dlg1 protein levels were normalized to the TASK-3 WT control sample. The data of three independent experiments is presented as mean ± SEM. A one-way ANOVA analysis showed significant differences between the groups presented in (B) (p=<0.0001), followed by a Tukey test revealing significant differences between T1 WT versus T3 WT (**** p=<0.0001) and T1 S393A versus T3 WT (**** p=<0.0001).

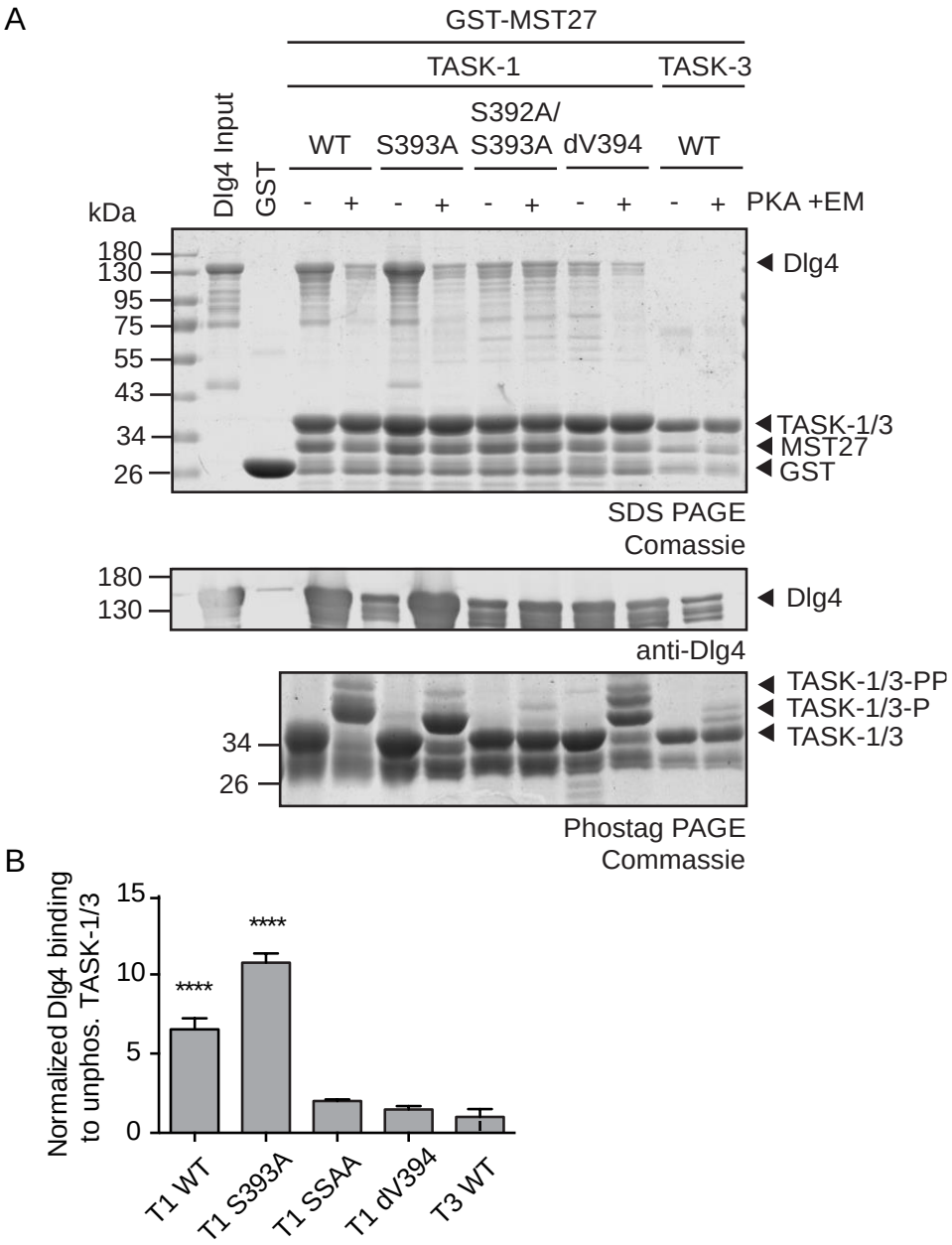

Figure 54. Dlg4 binds *in-vitro* to the unphosphorylated TASK-1 C-terminus.

(A) Recombinant purified MBP-Dlg4 binds to the unphosphorylated TASK-1 WT and S393A protein variants. Phosphorylation disrupted the interaction (upper panel). Binding was confirmed by Western blotting with a Dlg4 antibody (middle panel). The phosphorylation state of the bait protein was analyzed on Phos-tag-PAGE (lower panel). **(B)** Quantification of experiment shown in (A). Dlg4 protein levels binding to the different TASK proteins were normalized to the TASK-3 WT control sample. The data of three independent experiments is presented as mean ± SEM. A one-way ANOVA analysis showed significant differences between the groups presented in (B) (p=<0.0001), followed by a Tukey test revealing significant differences between T1 WT versus T3 WT (**** p=<0.0001) and T1 S393A versus T3 WT (**** p=<0.0001).

I could demonstrate that Dlg1 and Dlg4, enriched in binding experiments, bind directly to PDZ binding motif in the TASK-1 C-terminus. Dlg1 and Dlg4 belong to membrane-associated guanylate kinase homologs family (MAGUK) and contain three PDZ domains, a Src-homology 3 (SH_3) domain and a guanylate kinase-like domain which is enzymatically inactive (McGee et al., 2001). Dlg1 is strongly expressed in the heart and involved in the regulation and trafficking of several cardiac ion channels (Gillet et al., 2015a). Consequently, I decided to characterize the binding of Dlg1 to the distal C-terminus of TASK-1 potassium channel in detail. It was already shown, that Dlg1 interacts via its PDZ domains with other potassium ion channels (El-Haou et al., 2009; Kim et al., 1995). Here, I analysed which of the three PDZ domains in Dlg1 are required for the Dlg-1/TASK-1 interaction. In addition to a MBP-tagged full-length Dlg1 fusion protein construct, different truncation constructs covering all possible combinations of the three PDZ domain ablations were designed (Figure 55A), recombinantly expressed and affinity purified from *E. coli* (Figure 55B).

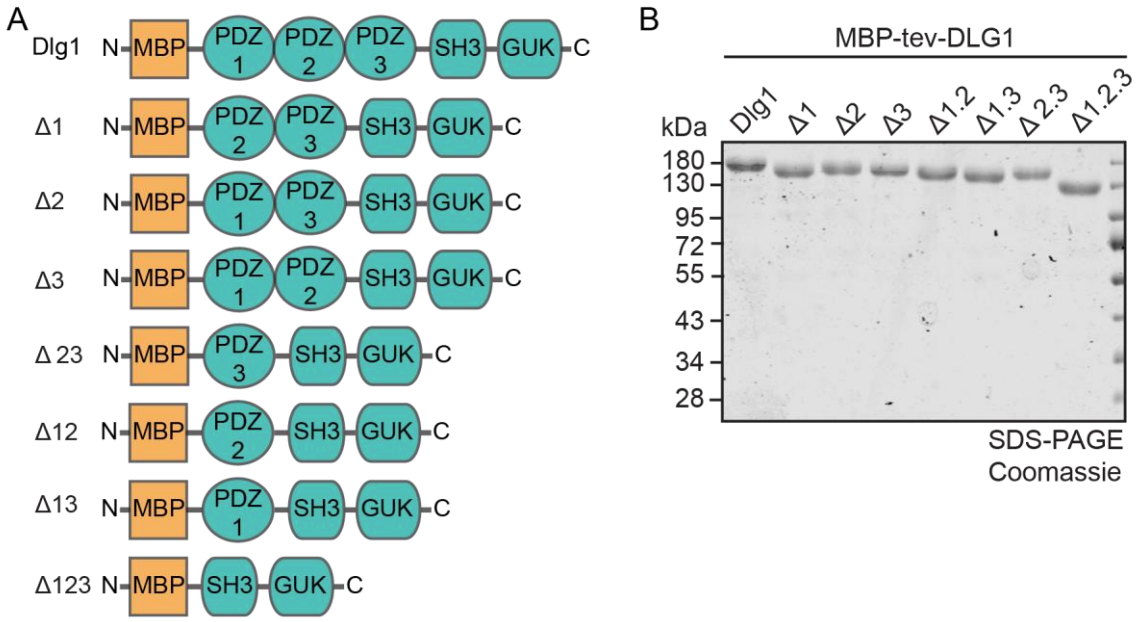

Figure 55. Design and expression of recombinant Dlg1 PDZ truncation proteins to identify the TASK-1 interaction site in Dlg1.

(**A**) MBP-Dlg1 full-length protein and several MBP-tagged Dlg1 PDZ truncation proteins were designed to cover all possible combinations of the three PDZ domain ablations. (**B**) The recombinant proteins were expressed in *E. coli* and affinity purified. Purified MBP-Dlg1 PDZ truncation proteins were analyzed on a Coomassie stained SDS-PAGE.

Purified truncated Dlg1 proteins employed in binding assays with the unphosphorylated TASK-1 C-terminus. The TASK-1 C-terminal protein was immobilized and equimolar amounts of the different truncated MBP-Dlg-1 proteins were offered. The experiment was analysed by Western blot and probed for Dlg1 and MBP with corresponding antibodies. The Dlg1 antibody does not bind to the PDZ domains in Dlg1 but to confirm that the Dlg-1 antibody is still able to bind the truncated versions of Dlg1 with similar affinities, an anti-MBP antibody was used in parallel (Figure 56A). Equal loading of the TASK-1 protein was confirmed by detection with a GST antibody (Figure 56A) and equal input of PDZ-1 truncation proteins offered in the binding assay was shown Coomassie stained SDS-PAGE (56C).

The TASK-3 C-terminus was used as a negative control. Full-length MBP-Dlg1 with all three PDZ domains was used as a positive control. Recombinant MBP was incubated with immobilized GST-MST27-TASK-1 to exclude unspecific interactions between the tag of the Dlg1 or Dlg4 constructs and the TASK-1 construct. The truncation of PDZ domain 2, either alone or in combination with other PDZ domains, was enough to abolish the interaction with TASK-1 C-terminus (Figure 56A,B). The binding of TASK-1 remained unaltered, compared to full-length Dlg1, when other Dlg1 PDZ truncations were present. This experiment indicated that the PDZ domain 2 is the preferred TASK-1 binding site in Dlg1.

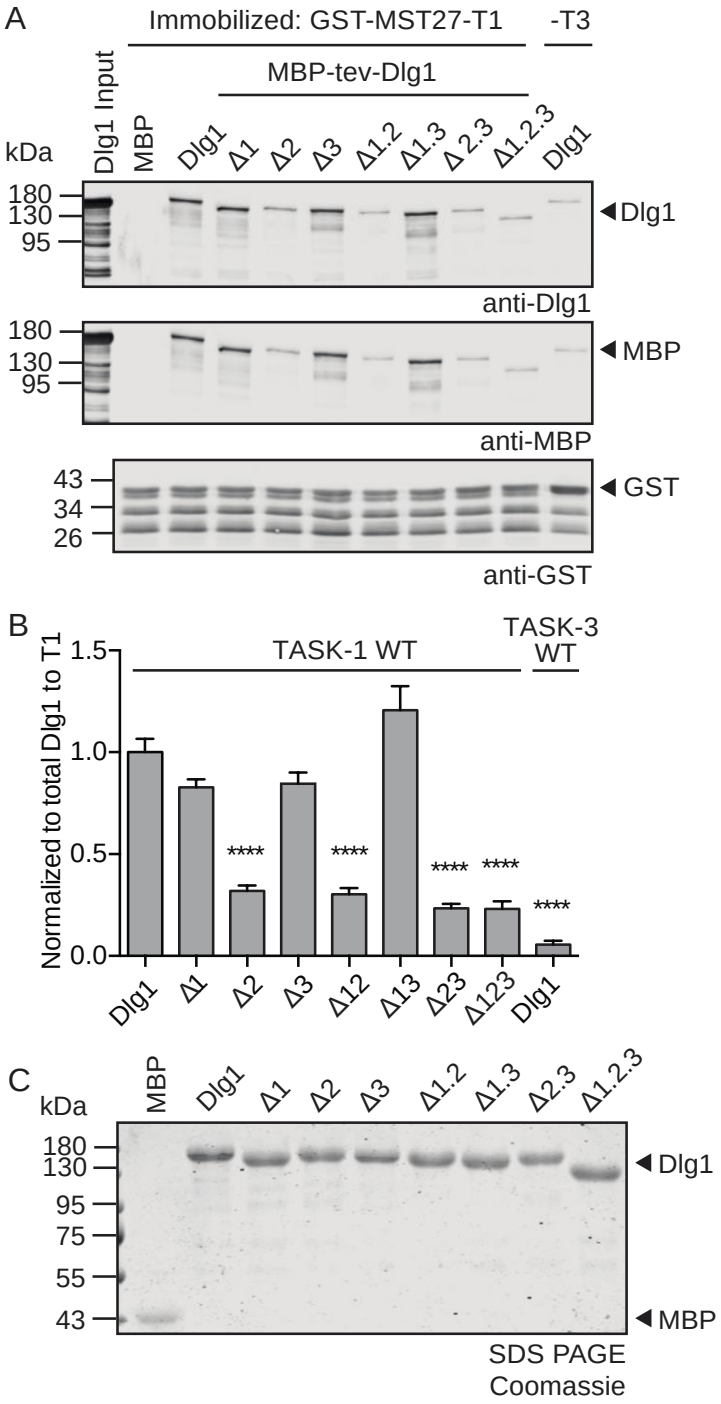

Figure 56. PDZ-2 domain of Dlg1 is preferentially bound by the TASK-1 C-terminus.

(A) Recombinant binding assays were performed with immobilized TASK-1 or TASK-3 protein and Dlg1 PDZ truncation proteins. Dlg1 was used as a positive control, immobilized TASK-3 with Dlg1 was a negative control. Binding assays were analysed by Western blotting with a Dlg1 (upper panel) and MBP (middle panel) antibody. Equal loading was confirmed with a GST antibody (lower panel). **(B)** Binding of the Dlg1 PDZ truncations proteins to TASK-1 was normalized to full-length Dlg1 bound to TASK-1. The data of six independent experiments are presented as mean ± SEM. A one-way ANOVA analysis showed significant differences between the groups presented in (B) (p=<0.0001), followed by a Tukey test revealing significant differences between T1 with bound full

length Dlg1 versus T1 Δ2 (**** p=<0.0001), or versus T1 Δ1,2 (**** p=<0.0001), or versus Δ2,3 (**** p=<0.0001), or versus Δ1,2,3 (**** p=<0.0001), or versus T3 full length Dlg1 (**** p=<0.0001). (**C**) Equal offered inputs were confirmed on Coomassie stained SDS-PAGE.

4.4 Discussion

K_2P channels are so called open-leak channels, meaning once expressed at the cell surface they contribute substantially to the leak current of K^+-ions measured in cells such as neurons, or cardiac myocytes (Renigunta et al., 2015). Therefore, trafficking and insertion of these channels into membranes require careful regulation. It is already well established, that trafficking of the TASK channels is regulated via phosphorylation dependent binding of 14-3-3 and COPI (Kilisch et al., 2016). To further understand the regulation and trafficking of TASK channels especially in the cardiovascular system, cardiac interaction partners for TASK-3 and TASK-1 were investigated in this chapter.

4.4.1 TASK-3 and the Na/K ATPase are potentially co-endocytosed by clathrin-mediated endocytosis

Affinity purification experiments using recombinant TASK-3 proteins and heart lysate were performed and analysed by MS. The Na/K ATPase was identified as a potential interaction partner of TASK-3. Because phosphorylation is an important aspect of TASK trafficking the affinity purification experiments were performed with phosphorylated and unphosphorylated TASK-3 bait proteins. Interestingly, Na/K ATPase was exclusively enriched in samples obtained from PD experiments performed with phosphorylated GST-MST27-TASK-3 fusion protein (Figure 33). This indicates specific interaction between the phosphorylated TASK-3 protein and Na/K ATPase but leaves open whether this is a direct or an indirect interaction. Besides Na/K ATPase, proteins involved in clathrin-mediated endocytosis (i.e. AP-2 or dynamin-1) were enriched with phosphorylated TASK-3 (Figure 33). Interestingly, MS analysis revealed that also known TASK-3 binding partners, such as different 14-3-3 isoforms, were enriched, indicating either that inhibition of 14-3-3 did not completely prevent these proteins from binding or that the enriched proteins were already bound to later enriched TASK-3 interaction partners during the inhibitor treatment and therefore not addressable. The fact, that several 14-3-3 isoforms were significantly enriched in several independent pull-down experiments (Figure 33,47,51), suggests that the 14-3-3 proteins were tightly bound to interaction partners which were later purified in the pull-down experiments.

Efendiev et al published in 2011, that Na/K ATPase is endocytosed together with phosphoinositide-3 kinase mediated by 14-3-3 after phosphorylation of Na/K ATPase. They could show that dopamine enhances the interaction between 14-3-3 and Na/K ATPase and that 14-3-3 recruits the phosphoinositide-3 kinase, followed by clathrin-mediated endocytosis of the complex (Efendiev et al., 2005). Taken together with the results from the MS analysis of TASK-3, I developed the hypothesis that 14-3-3 dimers

scaffold phosphorylated TASK-3 and phosphorylated Na/K ATPase which recruits the mediators of clathrin-based endocytosis like AP2 or dynamin (Figure 57).

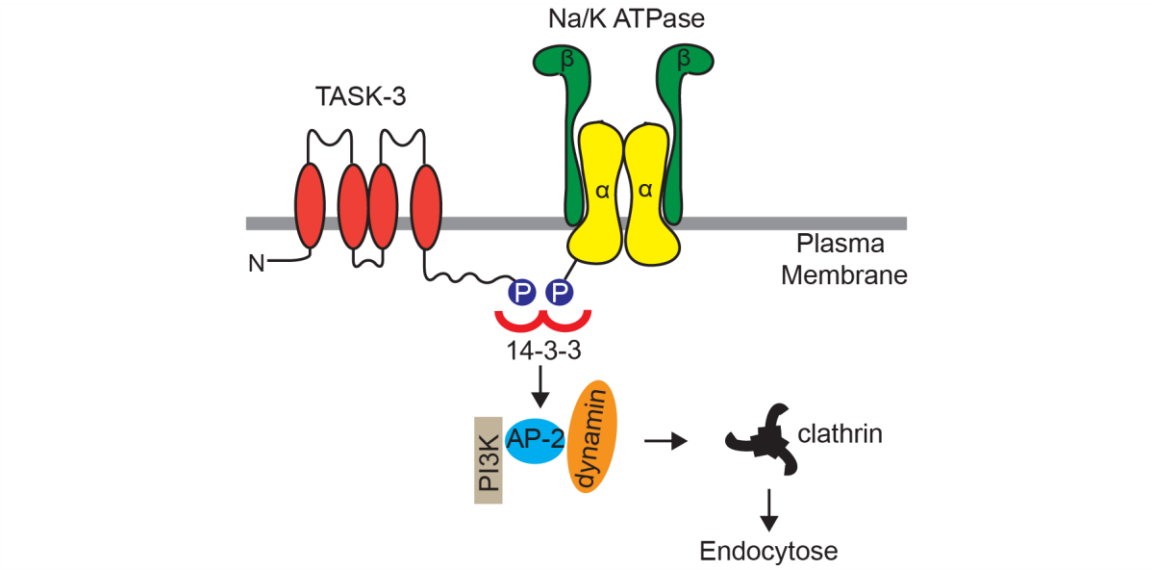

Figure 57. Model for a potential 14-3-3 mediated co-endocytosis of TASK-3 and Na/K ATPase. The phosphoadaptor-protein 14-3-3 binds the C-terminus of TASK-1 and the N-terminus of the Na/K ATPase and bring both proteins in close proximity for AP-1 and dynamin mediated co-endocytosis.

Co-localization between TASK-3 and clathrin was identified, indicating that TASK-3 endocytosis is regulated by clathrin-dependent endocytosis (Mant et al., 2013). In line with this notion, Mant et al showed with surface biotinylation assays in mammalian cells that TASK-3 is endocytosed via dynamin mediated endocytosis within 60 min (Mant et al., 2013). Based on my MS results, I obtained further confirmation that clathrin-mediated endocytosis is responsible for TASK-3 endocytosis. AP-2 and dynamin were enriched with the phosphorylated TASK-3 C-terminus. For the TASK-1 channel it was already shown that phosphorylation plays a role during endocytosis. It was found that PKC phosphorylation of TASK-1 recruits 14-3-3 which initiates endocytosis (Gabriel et al., 2012). Also Efendiev et al showed that endocytosis of the Na/K ATPase is initiated upon phosphorylation and 14-3-3 interaction (Efendiev et al., 2005). Therefore, it is plausible that a potential co-endocytosis of TASK-3 and Na/K ATPase is regulated by phosphorylation and 14-3-3.

However, I was unable to confirm the presumably indirect interaction via 14-3-3 proteins between phosphorylated TASK-3 and Na/K ATPase by Western blot of the pull-down experiment (Figure 34). A possible explanation could be that MS analysis has a higher sensitivity then Western blot detection (Bass et al., 2017). It is possible that the interaction between TASK-3 and Na/K ATPase requires mediators or is regulated in the context of a bigger protein complex. Therefore, the potential co-endocytosis of TASK-3 and Na/K

ATPase was analysed in rat hearts that were treated with ouabain (Figure 35). Ouabain induces Na/K ATPase endocytosis which was monitored by surface glycosylation in hearts. Affinity enrichment assays for biotinylated proteins showed that the Na/K ATPase was expressed at the plasma membrane, but the amount of present Na/K ATPase remained unaltered upon ouabain treatment (Figure 37). This raises the question whether ouabain initiates Na/K ATPase endocytosis in rat hearts and if the concentrations suggested by one publication were sufficient (Cherniavsky-Lev et al., 2014). The Na/K ATPase is a receptor for cardiac glycosides such as ouabain. Almost all mammalian species are very sensitive for ouabain beside rats (Cherniavsky-Lev et al., 2014; Hansen, 2003). The Na/K ATPase consist of a hydrolytic alpha-peptide responsible for the transport of Na^+ and K^+ ions and a small alpha-glycoprotein. Four different isoforms have been identified for the alpha-peptide. In rats the alpha-1 form of the Na/K ATPase has a very reduced sensitivity to ouabain (Hansen, 2003). However, cardiac rat tissue express a mixture of different Na/K ATPase alpha-isoforms, but the ratio between the insensitive alpha-1 isoforms and the sensitive isoforms is not well known (Hansen, 2003). Overall, with surface biotinylation I could not confirm the effect of ouabain on the Na/K ATPase internalization. Glycosylation is a post-translational modification involved in intracellular forward trafficking to the plasma membrane (Bas et al., 2011). With a WGA pull-down experiment, I could analyse the total amount of mature, glycosylated Na/K ATPase in the rat membranes (Figure 40). Consequently, the ratio between glycosylated and biotinylated Na/K ATPase can be compared, which allows to differentiate between the total amount of Na/K ATPase and the exposed Na/K ATPase pool (Figure 42). The Na/K ATPase was found to be strongly glycosylated in all heart samples but the amount of glycosylated proteins was not influenced by ouabain treatment (Figure 40,42).

Overall, neither the surface pool nor the intracellular amount of the Na/K ATPase was altered upon ouabain treatment implying that no endocytosis of the Na/K ATPase was induced by ouabain. This indicates that not the right ouabain concertation was used to induce endocytosis in rat or that ouabain does not trigger endocytosis as proposed. A possibility would the repetition of the experiment with mice heart. Mice do not have the ouabain insensitive Na/K ATPase alpha1 isoform and therefore show a high sensitivity (Hansen, 2003).

In addition to the analysis of the Na/K ATPase also 14-3-3 proteins, enriched from biotinylated membranes, were analysed (38,42). 14-3-3 proteins are located in the cytosol (Fu et al., 2000). The used biotin was non-cell permeable, suggesting that the enriched 14-3-3 proteins were co-purified together with biotinylated cell surface exposed membrane proteins such as Na/K ATPase. This also explains why 14-3-3 proteins were enriched in the TASK-3 MS analysis.

However, MS analysis with TASK-1 also identified the Na/K ATPase as a novel TASK-1 interaction partner, although with less efficiency (Figure 47). Likewise, phosphorylation of TASK-1 channel was required in order to interact with Na/K ATPase. Even though in the absence of biochemical confirmation, two independent MS analysis identified the Na/K ATPase as a binding partner for TASK channels. The lack of a commercially-available TASK-3 antibody makes the analysis of TASK-3-Na/K ATPase interaction difficult. To further investigate this interaction, *in vitro* binding assays with recombinant proteins could be an option. Besides, a tagged TASK-3 construct could be overexpressed in mammalian cells in order to overcome the lacking TASK-3 antibody. Subsequent immunostaining experiments would further provide information about co-localization TASK-3 and Na/K ATPase. Immunostaining experiments could be also performed after stimulation of endocytosis in mammalian cells to further investigate this aspect.

4.4.2 PDZ domain containing proteins Dlg1 and Dlg4 are novel TASK-1 interaction partners in heart

Further analysis of the MS data obtained from TASK-1 affinity enrichment experiments identified several PDZ domain containing proteins exclusively enriched with the distal, unphosphorylated C-terminus (Figure 47). Especially, Dlg1 and Dlg4 were identified as main hits. These proteins are known as important scaffolds, involved in variety cellular functions such as trafficking, ion channel regulation and signaling processes. In many cases PDZ domains were identified to bind short C-terminal motifs in their ligands (Espejo et al., 2017). Rajan et al reported in 2002, that the last five amino acids of the extreme C-terminus constitute a PDZ-binding motif (X-S/T-X-V/I) which overlaps the already known COPI and 14-3-3 binding motifs and is absent in TASK-3 (Figure 58). Interestingly, the PDZ binding domain in TASK-1 requires the first serine residue (S392) in the trafficking control region of TASK1 (Figure 58). There was no PDZ domain containing protein identified as TASK-1 interactor in literature (Rajan et al., 2002; Mathie et al., 2010). My MS analysis of TASK-1 with heart membranes identified several PDZ domain containing proteins and all interacting with the unphosphorylated TASK-1 channel exclusively in cardiac membranes (Figure 47, 51). With binding assays with recombinant purified proteins, I confirmed direct interaction with Dlg1 and Dlg4 (Figure 53,54). Phosphorylation of S392 in TASK-1 disrupted the interaction between TASK-1 and PDZ domain containing proteins Dlg1 and Dlg4, indicating that this serine residue is required for the interaction and confirms the suggested PDZ motif.

The sequence of the C-terminal PDZ domain binding motifs is divided into three main classes depending on the aa in the third last position of the motif. In case of the identified TASK-1 PDZ domain binding motif a serine residue is located in this position defining this

motif as a class 1 motif (Gogl et al., 2020). Consequently, the S392 residue in the TASK-1 C-terminus is a target side for PDZ domain containing proteins. The S392 residue is located within the 14-3-3-binding site of TASK-1 (Figure 58). No competition will occur between 14-3-3 and PDZ domain proteins (Figure 58) because 14-3-3 binding requires phosphorylation meanwhile PDZ domain containing proteins bind to the unphosphorylated TASK-1 C-terminus. Phosphorylation of PDZ domain binding motifs have been identified to be common resulting in an abolished interaction between the PDZ domain containing proteins and the corresponding motif (Gogl et al., 2020). An overlapping 14-3-3/PDZ domain binding motif regulated as a “switch” by phosphorylation was already identified in other ion channels such as Kir2.1 (Espejo et al., 2017). However, the PDZ-binding motif in TASK-1 is also neighboring the COPI-binding site (KKR) (Figure 58). Curiously, PDZ domain containing proteins and COPI bind to the unphosphorylated TASK-1 trafficking control domain. Therefore, it could be hypothesized that COPI and PDZ domain containing proteins compete for binding to the TASK-1 C-terminus. Consequently, the binding of one of these two proteins will mask the binding site for the other one. This can be tested, with competition binding experiments with recombinant proteins and alternating ratios of the two binding partners offered to unphosphorylated TASK-1 protein.

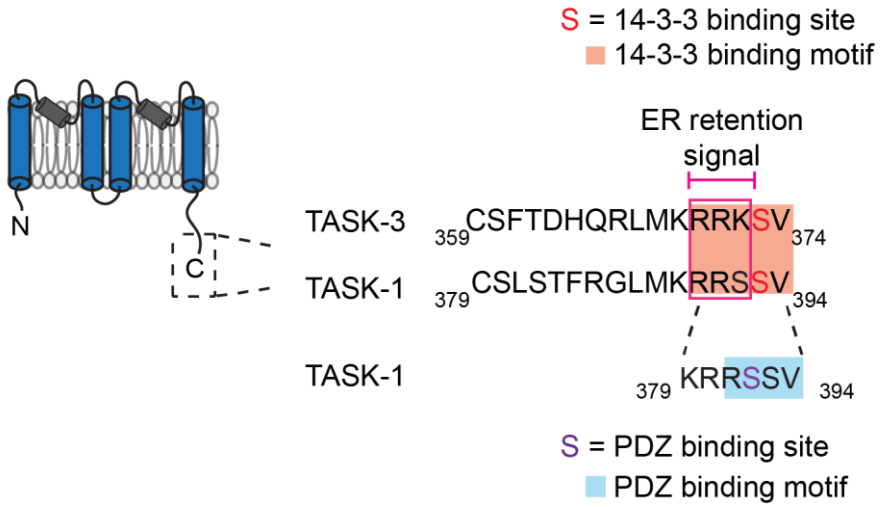

Figure 58. Overlapping 14-3-3, COPI and PDZ motifs in the C-terminus of TASK-1.

The last 5 aa of TASK-1 and TASK-3 contain an overlapping 14-3-3 motif (orange) with an ER retention motif (pink). 14-3-3 binds upon phosphorylation to the serine residues depicted in red (S393 in TASK1, S373 in TASK-3). TASK-1 has an additional PDZ domain motif (light blue) localized within the last 5 aa of the C-terminus. This motif is absent in TASK-3. PDZ domain containing proteins bind to the unphosphorylated serine depicted in purple (S392).

4.4.3 Potential functional consequences of the Dlg1/TASK-1 interaction

From all identified PDZ domain containing proteins, Dlg1 is the most abundant in heart tissue (Godreau et al., 2002). Dlg1 has been reported to regulate assembly, trafficking and localization of several ion channels like K_v (1.5, 4.2, 4.3) or K_{ir} (2.1, 2.2, 2.3, 4.1) (Leonoudakis et al., 2004; Gillet et al., 2015). In many cases Dlg1 regulates membrane ion channels as a scaffold by forming multi-protein complexes, bringing required interaction partners together or by anchoring them in a specific cellular localization (Fourie et al., 2014). It was already shown that Dlg1 is involved in trafficking of K_v1 and other potassium channels from the ER to the Golgi (Walch, 2013). As a consequence, down-regulation of Dlg1 in ventricular cardiomyocytes reduces the inward rectifier potassium current (Vaidyanathan et al., 2010). Moreover, Dlg1 and different ion channels showed that both co-localize at the plasma membrane and the intercalated disc (Eichel et al., 2016). TASK-1 is expressed in these two subcellular localizations as well. This allow to speculate whether, a potential *in vivo* interaction between TASK-1 and Dlg1 could regulate trafficking and stabilization TASK-1 at the membrane in a similar fashion as reported for other ion channels. In line, the interaction between TASK-1 C-terminus and Dlg1 was exclusively identified in affinity purification experiments from heat membranes and absent in the experiment performed in cytosol (Figure 47,48). It is well investigated that upon phosphorylation of the TASK-1 C-terminus 14-3-3 binding initiates forward trafficking by masking the COPI motif (Kilisch et al., 2016), but it is not investigated so far whether 14-3-3 dissociates upon TASK-1 insertion in the plasma membrane. Based on the reported function of Dlg1 on other ion channels and the specific enrichment in cardiac membranes, it seems plausible that 14-3-3 dissociates upon TASK-1 insertion in the plasma membrane. This allows dephosphorylation of the TASK-1 C-terminus by cellular phosphatases and Dlg1 binding which anchor TASK-1 at the plasma membrane.

Moreover, it is well established that Dlg1 directly interacts with the beta-adrenergic receptor and recruits the PKA-anchoring protein-79 (AKAP 79) which in turn recruits PKA. It has also been reported that the Dlg1/AKAP-79 complex targets PKA to the AMPA receptor and calcium sensitive channels (Walch, 2013). Demonstrating the essential role of Dlg1 in many cellular processes. So far it is not known which AKAP's recruit PKA to the TASK channels. Interestingly, AKAP79 is also expressed in the heart (Diviani et al., 2011). No AKAP protein was identified in the MS analysis for TASK-1, but the recombinant proteins used for the MS analysis were already phosphorylated before incubation in the heart lysate and membranes and cytosol were separated for this experiment. Another speculation about a potential function of the Dlg1 TASK-1 interaction could be the recruitment of the required AKAP's and PKA to the C-terminus of TASK-1. However, TASK-3 is missing the PDZ binding domain in the extreme C-terminus but is also

phosphorylated by PKA and regulated by 14-3-3 and COPI. TASK-1 protein levels are more abundant in the heart than TASK-3 protein levels (Gurney & Manoury, 2009). Furthermore, TASK-1 and TASK-3 show specific regulatory characteristics, such as different affinities for 14-3-3 (Kilisch et al., 2016) or different interaction partners. Additional regulatory sites in the trafficking control domain of TASK-1 further indicate that TASK-1 require an enhanced regulation. Besides, the formation of a TASK-1/TASK-3 heterodimer channel was found in cardiac tissue (Rinné et al., 2015).

Furthermore, Dlg1 was found in a complex with clathrin and a subunit of AP-1 in endothelia cells (Philippe et al., 2013). In this study the complex of Dlg1 with clathrin and AP-1 was shown in the formation of Weibel bodies, which is a specific form to store the von Willebrand factor protein. In addition, Dlg1 has been reported to be involved in the regulation of 3-hydroxy-5-methyl-4-isoxazolepropionic acid (AMPA) receptor endocytosis by identifying a complex of AMPA receptors, AP-2, Dlg1 and myosin-VI in neurons. It was found that Dlg1 recruits myosin-VI to endocytotic vesicles containing AMPA receptors resulting in clathrin-mediated endocytosis (Osterweil et al., 2005). The mentioned examples are the only hint of a relationship between Dlg1 and clathrin-dependent protein transport. Further research is required to test whether Dlg1 could be the missing link between TASK channels and the Na/K ATPase identified in the MS analysis. Such a hypothesis raises again the question how a potential co-endocytosis of Na/K ATPase and TASK-3 is regulated. The circumstance that the Na/K ATPase was identified in several MS analysis for TASK-1 and TASK-3 well speaks for an additional adaptor protein which is involved in this interaction and brings TASK channels and Na/K ATPase together. In addition to the function of a Dlg1 TASK-1 interaction, it is of course an interesting question whether TASK-1 can also interact with Dlg1 in neurons. This should be analysed by affinity purification experiments from brain lysate. Moreover, the idea that TASK-1 may form a potential complex between TASK-1, Dlg1, AKAP79 and PKA should be further analysed, for example with APEX labeling or complexome profiling from total heart lysate.

Altogether, several novel cardiac interaction partners were identified for the C-terminus of TASK-1 and TASK-3. MS analysis revealed an alteration of the interaction with the Na/K ATPase depending on the phosphorylation state of the bait proteins involved. Identification of components of the endocytosis machinery indicated that TASK-1 and TASK-3 may be co-endocytosed together with other membrane proteins such the Na/K ATPase. I was not able to confirm a direct interaction between the TASK channels and the Na/K ATPase. Since either the Na/K ATPase or TASK-1 and TASK-3 bind 14-3-3 I hypothesize that 14-3-3 or other adaptor proteins might influence the spatial organization of these proteins during endocytosis.

In addition, my binding experiments yielded strong evidence that the distal C-terminus of TASK-1 indeed contains a PDZ binding motif. I could show that this PDZ binding motif preferentially bind to PDZ domain two of Dlg1. These findings expand the knowledge of the TASK-1 /TASK-3 interactome in hearts, although many of these interactions require confirmation *in vivo* and further characterization regarding their physiological functions.

Data File S2-S5. All detected proteins in the MS approach using GST-MST27-TASK-3 or GST-MST27-TASK-1 and different preparations of total heart lysate and separated membranes and cytosol can be found under this link:
https://owncloud.gwdg.de/index.php/s/v18RVghJqu0uE5w

5 Chapter V: Discussion

This work identified the phospho-adaptor protein 14-3-3 as a novel interaction partner of the cardiac protein PLN, an inhibitor of the Ca^{2+} pump SERCA (Tada et al., 1975). A regulatory mechanism of PLN was uncovered where different kinases create different 14-3-3 binding sites allowing a fine-tuned regulation of PLN. 14-3-3 binding to phosphorylated PLN resulted in protection from phosphatases and prolonged SERCA activity under physiological conditions.

In addition, the cardiac interactome of TASK channels was analysed. 14-3-3 is also an interactor of TASK channels and responsible for the stable expression of the channels at the plasma membrane (Kilisch et al., 2016; Rajan et al., 2002). Here, I identified a direct interaction between TASK-1 and the PDZ domain containing protein Dlg1.

Both novel interactions uncover new regulatory mechanisms and functions of PLN and the K^+ ion channel TASK-1.

5.1 14-3-3 is a novel interactor of the cardiac protein PLN

PLN is a small tail-anchored protein containing a cytosolic domain, a small loop and a transmembrane domain (Ablorh & Thomas, 2015) (Figure 59). Interaction between PLN and SERCA, as well as the oligomerization of PLN pentamers, are regulated by different functional motifs present in the transmembrane domain of PLN (Ablorh & Thomas, 2015). The regulatory cytosolic domain of PLN includes a di-arginine signal (R13, R14) followed by two phosphorylatable residues (S16, T17) (Figure 59).

Di-arginine based signals (xRRx) bind the vesicle coat complex COPI and in many cases also the phospho-adaptor protein 14-3-3 (Michelsen et al., 2005; Nufer & Hauri, 2003). Closer observation of the PLN N-terminus revealed a putative 14-3-3 binding motif overlapping with the di-arginine xRRx signal and the two phospho-residues (Arakel et al., 2014; Figure 59). Consequently, the overlapping dibasic COPI interaction site with a 14-3-3 binding motif in PLN was analysed for the possibility of 14-3-3 interaction.

Figure 59. Schematic representation of the N-terminal domain of PLN.

The cytosolic domain Ia contains a di-arginine motif (XRRX, highlighted in orange) and two phosphorylatable residues (depicted in green). The putative 14-3-3 binding motif is marked in red.

The putative 14-3-3 interaction site in PLN was analysed by pull-down experiments with recombinant 14-3-3 proteins and solubilized mice heart membranes. A strong enrichment of a protein migrating at 28 kDa on a SDS-PAGE gel was observed and identified to be pentameric PLN (chapter 2, figure 1E). This result was the first indicator that 14-3-3 and PLN physically interact with each other. Based on these findings, I further investigated whether 14-3-3 and PLN interact *in-vitro* and *in-vivo*. The 14-3-3 binding motif present in PLN includes the two phospho-residues S16 and T17 which are either phosphorylated by PKA or CaMKII kinases. In many cases, 14-3-3 binds to the phosphorylated residue present in the 14-3-3-binding motifs but not always (Fu et al., 2000). Further dissection of the 14-3-3 binding site in PLN showed that 14-3-3 is able to bind either phospho-residue (S16 and T17) present in PLN (chapter 2, figure 3). This confirmed that PLN includes a 14-3-3 binding motif in the N-terminus, which is very similar to a mode II type 14-3-3 binding motif (RXY/FX(pS/pT)XP) and overlaps with a dibasic COPI retention signal (Figure 59).

The potential COPI interaction site in PLN had been investigated (Sharma et al., 2010). The authors found that COPI and PLN co-localized in the ER and verified direct binding with different co-immunoprecipitation experiments (Sharma et al., 2010). These findings suggest that PLN is retrieved from the Golgi to the ER by COPI via the di-arginine motif in the N-terminus of PLN. However, Sharma et al did not discuss why a protein located in the sarcoplasmic reticulum, such as PLN, should traffic to the Golgi. Another study performed by Stenoien et al found that Golgi-mediated trafficking of PLN to the plasma membrane is important for muscle cell maturation (Stenoien et al., 2007). In contrast, it was reported that PLN is confined to the SR by retrieval from the ERGIC without any further trafficking of PLN in the cellular periphery (Butler et al., 2007). In line with the findings of a direct PLN/COPI interaction (Sharma et al., 2010), Butler et al suggested that retrieval of PLN from the ERGIC to the ER is mediated by COPI vesicular retrograde trafficking (Butler et al., 2007).

I also investigated the localization of PLN by co-localization experiments staining mammalian cells transfected with different PLN mutants for ER localization and various subcellular markers. I observed that PLN is localized in the ER, but no robust co-localization was identified with the early endosomal marker EEA1 or the late endosomal marker Rab7 (Figure 26-28). These findings suggest, that PLN is confined to the ER in mammalian cells and does not escape to other secretory compartments or the cell periphery as previously reported (Butler et al., 2007). Overall, the possibility of intracellular PLN trafficking has been barely investigated so far. The few studies, which analysed PLN trafficking and localization used different cellular model systems ranging from different mammalian cells over muscle cells until cardiomyocytes.

Several K^+ ion channels such as K_{ATP} channels or the K_2P channels TASK-1 and TASK-3 also present di-arginine (xRRx) signals, often with overlapping 14-3-3 motifs, very similar to the ones identified in PLN (Figure 60 A,B). For TASK channels it was shown that phosphorylation dependent binding of 14-3-3 sterically masks COPI binding allowing anterograde trafficking and cell surface expression (Kilisch et al., 2016). Consequently, the presence of trafficking signals of COPI or 14-3-3 in PLN raises the questions if PLN traffic within the cell or whether these motives are involved in maintaining PLN in the ER as already suggested (Butler et al., 2007) or fulfill other physiological functions. Further research is required to investigate the raised questions, as well as the functional consequence of the COPI interaction.

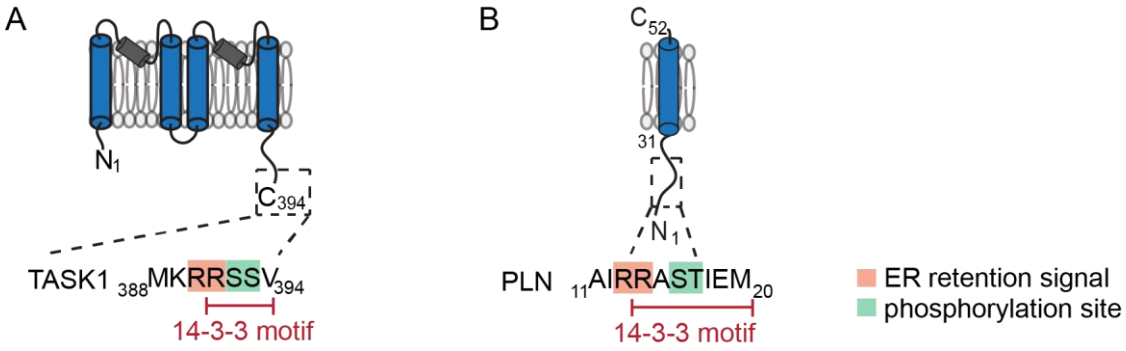

Figure 60. Schematic representation of di-arginine ER retention signal and 14-3-3 motif present in (A) TASK-1 channel and (B) PLN.

The di-arginine motif is highlighted in orange, the putative 14-3-3 binding domain is shown in red and phospho-residues are depicted in green.

5.2 14-3-3 binds to different binding motifs in PLN and TASK-1

Even though, the overlapping di-arginine ER retention and 14-3-3 motives are quite similar in PLN and TASK-1 (Figure 60A,B), there are differences in 14-3-3 binding.

TASK-1 contains a mode III 14-3-3 binding motif which is characterized by the localization at the distal C-terminus and by the position of the phosphorylated residue as a penultimate residue (Coblitz the al. 2005). Analysis of the 14-3-3 motif in the C-terminus of TASK showed that 14-3-3 is able to recognize and bind the S393 residue upon phosphorylation (Kilisch et al., 2016). 14-3-3 binding requires an arginine residue in position -3 or -4 relative to the phospho-residue to stabilize the phospho-peptide in the 14-3-3 binding groove by hydrogen bonds and intramolecular salt bridges (Gouw et al., 2018, Rittinger et al., 1999). The two phospho-residues in TASK-1 are located adjacent to the arginine residues (Figure 61A). Consequently, the arginine residues are required in position -3 or -2 relative to the phosphorylated S393 residue to form a canonical mode III 14-3-3 binding site. The S392 residue in TASK-1 cannot fulfill the requirement for a 14-3-3 phospho-residue due to the

position of the phosphorylated residue at position -3 from the distal C-terminus and the direct positioning of arginine residues.

Like TASK-1, PLN contains two adjacent phospho-serine residues in the 14-3-3 motif in adjacent to the di-arginine motif (Figure 61B). The two phospho-residues in PLN are separated by one alanine residue from the di-arginine motif (Figure 61B). Consequently, the 14-3-3 binding site is shifted in PLN by one residue which allows a different positioning of the di-arginine motif in the 14-3-3 binding pocket and consequently both phospho-residues create a 14-3-3 binding site (Figure 61B). Further analysis of both 14-3-3 interaction sites in PLN showed different 14-3-3 binding affinities. Recombinant binding assays identified the phosphorylated S16 residue as a low affinity binding site and the phosphorylated T17 residue as a high affinity binding site (chapter 2, figure 3C,G,S4). Molecular dynamic simulations showed that 14-3-3 is able to bind PLN in two different manners depending on their phosphorylation and this results in different placements of the two arginine residues in the 14-3-3 binding groove (chapter 2, figure 4A,B). Furthermore, the polar side chain of the T17 residue adjacent to the phosphorylated S16 residue provides an energetically less favored placement of the peptide in the 14-3-3 binding groove (Figure 61B).

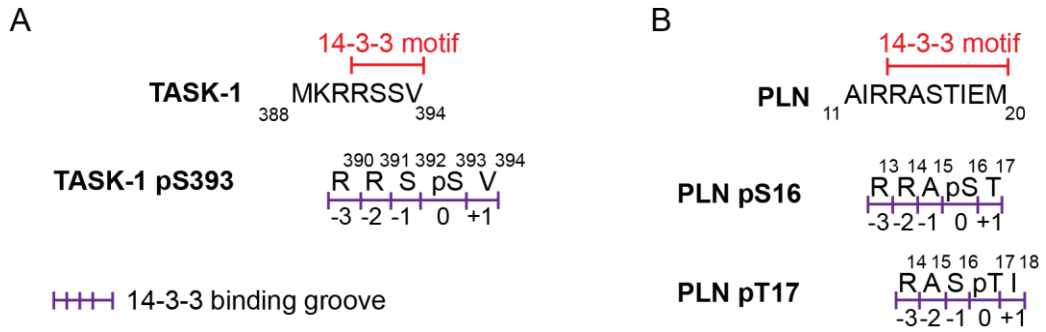

Figure 61. Schematic representation of TASK-1 or PLN placed in the 14-3-3 binding groove. For the TASK-1 channel (**A**), the solely phosphorylated S393 residue binds the 14-3-3 binding groove. In PLN (**B**) either phospho-residue, S16 and T17, can bind to the 14-3-3 binding groove but different orientations of the phospho-peptide inside the 14-3-3 binding groove explain different binding affinities. The 14-3-3 binding motif in (A) TASK-1 and (B) PLN is highlighted in red, the 14-3-3 binding groove is shown in purple.

Altogether, molecular dynamic simulations showed that 14-3-3 binds both PLN phospho-residues in the canonical binding groove consistent with a mode II binding motif, but does so with different affinities. However, different 14-3-3 binding affinities are not exclusively explained by the placement of the phospho-residues in the canonical binding motif. Although the canonical binding groove is highly conserved among the different 14-3-3

isoforms present in humans, many targets bind different isoforms with different affinities (Fu et al., 2000). This was also shown for TASK-1, where binding affinities of the seven different 14-3-3 isoforms were measured with SPR experiments and ranged about 7 fold (Kilisch et al., 2016).

5.3 14-3-3 interaction with PLN depends on kinase interplay in cardiomyocytes

PLN can be present in a monomeric or pentameric form in cardiomyocytes (Kimura et al., 1997). 14-3-3 proteins are dimeric and hence beside affinity also avidity influences the apparent binding affinity resulting in a higher 14-3-3 affinity towards PLN oligomers (chapter 2, figure 3A,E). Functionally, the 14-3-3/PLN interaction was found to protect phosphorylated PLN from cellular phosphatases in recombinant dephosphorylation assays (chapter 2, figure 5,S7). Consistently, 14-3-3 prolonged SERCA activity in living cardiomyocytes upon beta-adrenergic stimulation (chapter 2, figure 7).
Under basal conditions, as well as in stress situations, the balance between kinases and phosphatases determines the precise features of PLN and 14-3-3 regulation and consequently will influence SERCA regulation (Cerra & Imbrogno, 2012).

The S16 residue of PLN is phosphorylated by PKA upon beta-adrenergic stimulation as previously shown (Coyler, 1998). Phosphorylation of S16 in PLN was found to be sufficient for maximal cardiac output (Vincent 2008; Chu et al., 2000). Exclusive S16 phosphorylation in PLN occurs either at baseline phosphorylation of PLN in resting organisms or under high beta-adrenergic stimulation with low Ca^{2+} concentrations (Wittmann et al., 2015).
With recombinant binding assays I determined phosphorylated S16 in PLN as the low 14-3-3 affinity site (chapter 2, figure 3C). However, PLN pentamers containing phosphorylated S16 residues bound to 14-3-3 from heart tissue indicating that beside affinity also avidity influences the apparent 14-3-3 binding affinity (chapter 2, figure 1G, 3A). Based on these results, I conclude that 14-3-3 does not bind monomeric PLN phosphorylated at S16, but PLN pentamers phosphorylated at S16.
Time course experiments showed that PKA phosphorylation of S16 happens within 30 sec, meanwhile CaMKII phosphorylation of T17 takes 1-3 min (Grimm & Brown, 2010). Consequently, the S16 phosphorylation site in PLN is regulated faster than T17 phosphorylation. The cardiac contraction cycle occurs within seconds and the PLN/SERCA interaction exchanges every few seconds (Robia et al., 2007). However, 14-3-3 binds the phosphorylated S16 residue in PLN and stabilizes the phosphorylated form by sterically protection from phosphatases (chapter 2, figure S7). Consequently, a monomeric PLN pool phosphorylated at S16, which cannot bind to 14-3-3, maintains the

PLN/SERCA interaction within the rapid cycle of the cardiac contraction and contributes to cardiac relaxation.

On the other hand, CaMKII kinase phosphorylates the T17 residue in PLN (Coyler, 1998). Higher Ca^{2+} levels are required for CaMKII activation, therefore initial findings suggested that prior phosphorylation of S16 and beta-adrenergic stimulation are required for T17 phosphorylation in PLN (Mattiazzi & Kranias, 2014). Mundiña-Weilenmann et al demonstrated that PLN can be phosphorylated by CaMKII at T17 without prior S16 phosphorylation under high Ca^{2+} concentrations and simultaneously suppression of the phosphatase PP1 (Mundiña-Weilenmann et al., 1996). Based on these observations, it was suggested that PKA and CaMKII can phosphorylate PLN individually and independently from each other. Intriguingly, the conditions under which the authors showed an independent T17 PLN phosphorylation did not occur physiologically because PP1 is not suppressed without beta-adrenergic stimulation or high cAMP levels (Mundiña-Weilenmann et al., 1996). Physiologically, such conditions are happening during frequency stimulation resulting in exclusive phosphorylation of T17 by CaMKII (Hagemann et al., 2000, Valverde et al., 2005). CaMKII was found to translate Ca^{2+} spikes in kinase activity (De Konick et al., 1998), resulting in phosphorylation of T17 in PLN in the absence of beta-adrenergic stimulation and the use of phosphatase inhibitors (Mattiazzi & Kranias 2014).
I determined binding affinities for PLN phosphorylated at S16 and T17 and observed that T17 results in the generation of a high affinity 14-3-3 binding site, able to interact with monomeric and pentameric PLN (chapter 2, figure 3,G). Furthermore, I performed dephosphorylation assays and in line with the different 14-3-3 affinity sites in PLN, 14-3-3 protected the phosphorylated T17 residue much longer from phosphatases than 14-3-3 bound to phosphorylated S16 (chapter 2, figure 5,S7). Grimm and Brown previously described that CaMKII kinase activation and phosphorylation occurs slower compared to activation and phosphorylation of PKA (Grimm & Brown, 2010). This indicates that 14-3-3 binding to phosphorylated T17 of PLN traps this slowly phosphorylated protein population of PLN longer in its inactivated phosphorylated state, thus prolonging SERCA activity.
My findings, of the CaMKII induced high affinity 14-3-3 binding site in PLN could contribute to the further understanding of PLN phosphorylation by CaMKII under frequency stimulation without inhibition of PP1. While many publications support the involvement of CaMKII in frequency stimulated cardiac relaxation, this mechanism is not widely accepted (Mattizzia & Kranias 2014). The involvement of 14-3-3 in this mechanism stays elusive and should be further investigated.
In physiological conditions under full beta-adrenergic stimulation, both kinases PKA and CaMKII are active and have an additive effect resulting in double phosphorylation of PLN

(Mundiña-Weilenmann et al., 1996). In turn, active PKA additionally phosphorylates the protein phosphatase PP1 resulting in its inactivation (Mattiazzi et al., 2005). However, in my binding experiments with recombinant monomeric PLN, I observed that 14-3-3 binding to doubly phosphorylated PLN is abolished *in vitro* (Figure 17). A similar effect was previously observed for 14-3-3 binding to the C-terminus of the K^+-ion channel TASK-1, which also has two adjacent phospho-residues within the 14-3-3 binding motif (Kilisch et al., 2016). With 14-3-3 pull-down experiments with separated PLN monomers and pentamers I showed an increased affinity of 14-3-3 for PLN pentamers (chapter 2, figure 1). Subsequently, I conclude that 14-3-3 preferentially binds and stabilizes adjacent phosphorylated PLN proteins in the pentamer rather than the two closely phospho-sites in a monomer. These findings suggest that under full adrenergic stimulation 14-3-3 does not bind to double phosphorylated PLN monomers, allowing for a distinct pool of PLN able to regulate SERCA during fast contraction cycles. In addition, PLN pentamers phosphorylated at S16, or T17 are stabilized by 14-3-3 binding, allowing for a fine-tuned modulation of the ratio between PLN monomers and PLN oligomers during cardiac action. In conclusion, different 14-3-3 binding affinities towards PLN were identified based on the number and kind of phosphorylation present in PLN monomers or pentamers. This suggests a model where the abundance of pS16 or pT17 in PLN pentamers determine the 14-3-3 occupancy (Figure 62).

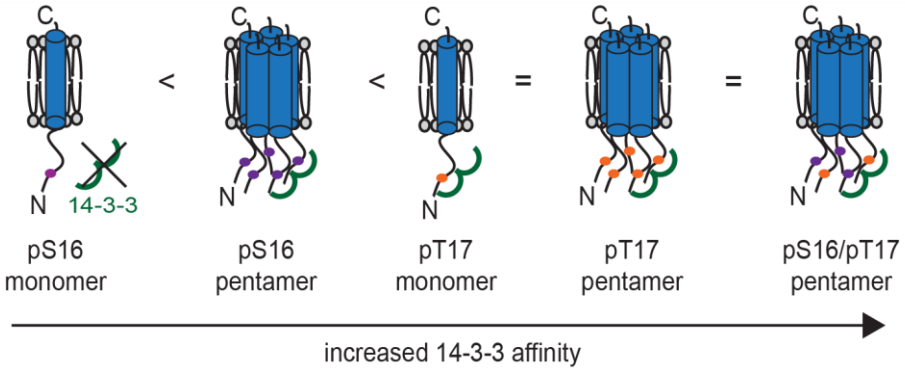

Figure 62. Schematic representation of 14-3-3 binding affinities to PLN dependent on phosphorylation and oligomerization.

14-3-3 binding affinities dependent on the phosphorylation and oligomerization status of PLN. The T17 phospho-site in PLN is the high affinity 14-3-3 binding site. PLN pentamers containing a single T17 phosphorylated residue have an increased 14-3-3 affinity than pentamers exclusively phosphorylated at S16. 14-3-3 dimer is shown in green, S16 phosphorylation is depicted in purple and T17 phosphorylation is indicated in orange.

5.4 The physiological role of the PLN pentamer

In cardiac tissue PLN can be found in its monomeric or oligomeric form, whereby the majority of PLN (70-80%) is present as a pentamer which is in a dynamic equilibrium with a small fraction of monomer (Glaves et al., 2019; Kimura et al., 1997; Reddy et al., 1999). Several publications suggest a shifted monomer/pentamer configuration based on the phosphorylation status of PLN, resulting in an increased pentameric population upon phosphorylation and a reduced amount of monomers (Cornea et al., 2000; Hou et al., 2008; Robia et al., 2007). In contrast, unaltered PLN pentamer populations upon phosphorylation were observed on SDS-PAGEs in several other studies (Cornea et al., 1997; Wittmann et al., 2015). Interestingly, a shift in the pentamer/monomer ratio of PLN upon phosphorylation would be further stabilized by the interaction with 14-3-3. SDS-PAGE studies here clearly show an increased steady-state level of PLN pentamers phosphorylated at S16 upon isoprenaline stimulation in cardiomyocytes and suggests an increased PLN oligomerization upon phosphorylation (chapter 2, figure 6C). However, it was reported that the exchange of PLN pentamers was found to be slow and occurs on a minute time scale (Robia et al., 2007). A very slow pentamer formation or dissociation is in contrast to the fast cardiac cycle, which would require that the increased pentamer population of PLN dissociates rapidly (within seconds) in every cardiac cycle to provide a pool of inhibitory PLN monomers. In addition, the postulated subunit inhibitory model in which PLN inhibits SERCA by structural remolding without dissociation from SERCA contradicts an increased PLN pentamer population upon phosphorylation as well (Bidwell et al., 2011; Gustavsson et al., 2013; Mueller et al., 2004). It is still under discussion, whether phosphorylation of PLN influences the pentamer/monomer equilibrium (Wittmann et al., 2015) as well as the different models of PLN/SERCA inhibitory interaction.

Initially, it was assumed that phosphorylated pentamers are a consequence of oligomerized phosphorylated monomers (Kimura et al., 1997, Kimura et al., 1998). In contrast, Wittmann et al found that PLN pentamers can also be phosphorylated directly by PKA (Wittmann et al., 2015). Furthermore, the authors reported that the PLN pentamer has a higher affinity towards PKA than the monomer (Wittmann et al., 2015). Based on these findings, Wittmann et al proposed a model where the SERCA/PLN interaction is prolonged after beta-adrenergic stimulation by first phosphorylating the pentamer (Wittmann et al., 2015). CaMKII phosphorylation of PLN pentamers was not analysed in this study, but it can be assumed that full beta-adrenergic stimulation also activates CaMKII which phosphorylates the PLN pentamer as well. In line, 14-3-3 has a higher affinity for pentameric PLN and further stabilizes the pentamer in the phosphorylated state upon beta-adrenergic stimulation. Furthermore, I could show that 14-3-3 protects PLN after

isoprenaline stimulation in cardiomyocytes with patch clamp measurements resulting in prolonged SERCA activity (chapter 2, figure 7). The 14-3-3/PLN interaction supports the idea of Wittmann et al that regulation of the PLN pentamer can influence the interaction between SERCA and PLN.

Disassembly of the PLN pentamer plays an important role for the SERCA/PLN inhibition (Kimura et al., 1998) and is also interesting with respect to the 14-3-3 interaction. Surprisingly, not much is reported in the literature about PLN pentamer disassembly. The pentamer is stabilized by an isoleucine zipper in the transmembrane domain of PLN (Kimura et al., 1997). PLN is primarily present as an oligomer in membranes, but when labeled PLN was reconstituted with purified SERCA, the monomeric fraction of PLN was strongly increased by 30-40% in FRET experiments (Reddy et al., 1999). From this experiment, it was concluded that the PLN/SERCA ratio influences the PLN disassembly into monomers (Reddy et al., 1999). However, I found that 14-3-3 preferentially binds and stabilizes phosphorylated PLN pentamers. This finding elucidates a novel aspect into PLN pentamer disassembly because dissociation of 14-3-3 is an additional requirement for PLN de-oligomerization and subsequent SERCA inhibition. With recombinant dephosphorylation assays and with Ca^{2+} measurements in living cardiomyocytes I observed that 14-3-3 dissociates slower from T17 phosphorylated PLN than from S16 phosphorylated PLN (chapter 2, figure 5,7,S7). Consequently, PLN oligomer dissociation may also depend on the number and kind of phosphorylation residues present in the pentamer and the resulting strength of 14-3-3 interaction.

A recent study, compared the dissociation constants of several oligomeric SERCA interaction partners like PLN, DWORF or SLN with FRET experiments in human embryonic kidney cells (Singh et al., 2019). A surprisingly low dissociation constant for oligomeric PLN was measured in comparison with the other oligomeric proteins (Singh et al., 2019). Since 14-3-3 and beta-adrenergic receptors are expressed in human embryonic kidney cells one can speculate, that 14-3-3 was bound to phosphorylated PLN pentamers in the FRET analysis influencing the low dissociation constant. The impact of 14-3-3 binding on PLN oligomer association and dissociation should be further addressed.

5.5 PKA and CaMKII kinase activity under pathophysiological conditions

Pathophysiological conditions such as acidosis, myocardial stunning or HF influence the balance between kinases and phosphatases activity involved in PLN regulation (Cerra & Imbrogno, 2012). Especially, CaMKII activity was found to be significantly elevated under several pathophysiological or stress conditions (Grimm & Brown, 2010; Mattiazzi & Kranias, 2014). Acidosis occurs during ischemia, resulting in decreased cardiac contractions, due to a decreased Ca^{2+} sensitivity of myofilaments, impaired with a

depressant effect on SERCA function (Mattiazzi & Kranias, 2014). The initial decreased contractility and relaxation is followed by a spontaneous mechanical recovery in which CaMKII plays an important role (Vittone et al., 2008). Acidosis is associated with an increase of CaMKII activity and at the same time inhibition of PP1. This mode of action leads to the phosphorylation of T17 of PLN and was found to be responsible for 50% of early cardiac relaxation recovery (Mattiazzi et al., 2007). During acidosis, PLN phosphorylation at S16 is significantly reduced (Vittone et al., 1996), underlining the importance of CaMKII activity (Mattiazzi & Kranias 2014). The role of 14-3-3 binding to PLN under stress conditions stays elusive and would require further investigation. My findings may, however, suggest that phosphorylated T17 is the 14-3-3 high affinity binding site, that 14-3-3 is involved in the recovery of acidosis by stabilizing phosphorylated T17 residues. It should be analysed whether 14-3-3 is recruited to phosphorylated PLN under such pathophysiological conditions in ischemic mice models where ischemia is induced by surgical processes (Traystman 2003).

Interestingly, the K^+ channel TASK-1 is inhibited by acidosis and has been described to contribute to the net outward current during the cardiac action potential plateau phase (Putzke et al., 2007). Functional TASK-1 expression at the cell surface is mediated by PKA phosphorylation followed by 14-3-3 binding (Kilisch et al., 2016). Thus, reduced PKA activation during acidosis could further contribute to reduced TASK-1 expression in addition to the inhibitory effect of acidosis. The general reduced contractility during acidosis suggest that more than a single population of K^+-channels with different pH sensitivity are involved (Putzke et al., 2007), but the mentioned TASK-1 characteristics suggest a potential involvement of TASK-1 channels in cardiac acidosis, which should be further addressed.

Beside the involvement in the recovery of acidosis, CaMKII activity was also found to be altered in HF (Mattiazzi et al., 2005). HF is associated with decreased intracellular Ca2+ transients and diminished SR Ca2+ load causing altered contractility (Mattiazzi et al., 2005). Consistently, with diminished Ca2+ load also SERCA expression is decreased in HF. In many HF models beta-adrenergic stimulation was found to be down-regulated (Bristow et al., 1986; de Lucia et al., 2018), whereas PP1 activity was identified to be increased (Gupta et al., 2003). Consistently, phosphorylation of both residues S16 and T17 in PLN were determined to be decreased in HF (Schwinger et al., 1999; Munch et al., 2002). This downregulation of PLN phosphorylation in HF models further inhibit SERCA and contributes to a reduced Ca^{2+} uptake (Vittone et al., 2008). Interestingly, the decrease in S16 and T17 phosphorylation in PLN was observed despite an increase in CaMKII activity, which is also an characteristic of HF (Anderson et al., 2011; Grimm & Brown,

2010). Excessive CaMKII activity in combination with PLN ablation was found to be disadvantageous on overall cardiac function due to accelerating Ca^{2+} uptake in the SR and increased SR Ca^{2+} load (Mattiazzi & Kranias, 2014; T. Zhang et al., 2010). Altering SERCA and PLN protein levels or activity are potential strategies to restore Ca^{2+} handling and treat HF (Vittone et al., 2008). Under such conditions, the 14-3-3/PLN interaction could also play a role as a stabilizer of phosphorylated PLN. Therefore, the function of PLN phosphorylation and 14-3-3 binding in HF should be further investigated. I was able to show that 14-3-3 binds T17 phosphorylated PLN pentamers and monomers with high affinities in pull-down experiments and recombinant binding assays (chapter 2, figure 3E,G). Followed recombinant dephosphorylation assays showed that 14-3-3 binding stabilizes phosphorylated, monomeric PLN and protects from phosphatases (chapter 2, figure 5). Based on these results, 14-3-3 presumably protects PLN monomers and pentamers upon CaMKII phosphorylation from dephosphorylation by cellular phosphatases and potentially helps to balance the overall reduced PLN phosphorylation during reduced beta-adrenergic stimulation in HF. A starting point would be the analysis of 14-3-3 steady-state levels in fractionated cardiac membranes from different HF disease mouse models.

5.6 The 14-3-3/PLN interaction in PLN disease mutations

Different mutations in the PLN gene occur naturally in humans, such as R9C, R14del and L39Stop mutations (Young et al., 2015). All of them are associated with DCM and HF (Young et al., 2015). The R9C and the R14del mutation are interesting with respect to their 14-3-3 interaction, since in both mutations PKA phosphorylation is abolished (Haghighi et al., 2006; Schmitt et al., 2003). Both mutations were only identified in heterozygous patients so far (Haghighi et al., 2006; Young et al., 2015).

Haghighi et al analysed the functional consequences of the R14del mutation by co-expression of the R14del PLN mutant with or without WT PLN in mammalian cells mimicking homozygous and heterozygous disease backgrounds. In the absence of endogenous WT PLN, the PLN R14del mutant is mislocated to the plasma membrane after expression (Haghighi et al., 2012). Co-expression of the R14del PLN mutant and WT PLN resulted in an PLN protein which strongly inhibits SERCA. This inhibition was not reversible upon phosphorylation (Haghighi et al., 2014). Consequently, the authors assumed that the heterozygous R14del PLN mutation leads to persistent interaction with SERCA. The consequences of a non-interrupted PLN SERCA interaction will be reduced back-transport of Ca^{2+} ions in the SR after contraction and cardiac relaxation.

The R14del mutation disrupts the PKA target motif in PLN and abolishes PKA phosphorylation at S16 (Haghighi et al., 2006). As a consequence, CaMKII phosphorylation is the only remaining mechanism to phosphorylate the PLN R14del mutant, which makes the potential 14-3-3 interaction interesting. First, it was questioned whether 14-3-3 can bind this mutant, because the R14 residue was found to be a stabilizing residue in the 14-3-3 binding groove in molecular dynamic simulations. To address this question, I phosphorylated recombinant PLN R14del protein with recombinant PKA and CaMKII kinases and analysed the result on Phos-tag-PAGE gels (chapter 2, figure S6). This experiment confirmed that PKA phosphorylation is abolished, but also that CaMKII kinase phosphorylation is possible *in vitro* (Haghighi et al., 2006, te Rijdt et al., 2016). After phosphorylation, I performed a recombinant binding assay with 14-3-3 and CaMKII phosphorylated PLN R14del protein revealing that the 14-3-3 interaction is still possible (chapter 2, figure 4D). Molecular dynamic simulations showed that R14 is stabilized by the 14-3-3 interaction directly to the phosphorylated T17 residue in PLN and in addition revealed that the R13 residue is not placed in the canonical binding groove of 14-3-3 (chapter 2, figure 4B). This indicates that the missing R14 residue is replaced by the R13 residue and therefore stabilize the 14-3-3 interaction. *In-vitro* binding assays showed that 14-3-3 is able to physically interact with PLN carrying the R14del mutation upon CaMKII phosphorylation. Based on the functional analysis of the 14-3-3/PLN interaction it seems plausible that 14-3-3 stabilizes R14del PLN in its phosphorylated state and thus enhances SERCA activity. To further investigate the 14-3-3 interaction with the PLN R14del mutation I analysed homozygous and heterozygous PLN R14del mouse disease models.

The steady-state levels of PLN R14del and 14-3-3 were analysed by Western blotting of separated membranes and cytosol from both R14del mouse models (Figure 18,19,21,22). In both R14del mouse models the PLN R14del mutant protein was decreased (Figure 18,21,24). The reduced steady-state levels of R14del PLN complicate the intended analysis of investigating whether membrane-associated 14-3-3 protein levels vary with the presence of PLN R14del. This approach was based on the hypothesis that PLN recruits a substantial amount of 14-3-3 to cardiac membranes. 14-3-3 levels were not altered either in the homozygous nor in the heterozygous mice model (Figure 19,22), which is hard to interpret because of the decreased R14del PLN levels. The observation of reduced R14del PLN protein level is consistent with findings made in cardiomyocytes from R14del heterozygous patients where PLN aggregates were identified by immunohistochemistry (te Rijdt et al., 2016). My observations and te Rijdt et al suggest that the R14del mutation leads to the formation of cellular PLN aggregates. The potential formation of PLN R14del aggregates contradict the hypothesis that the R14del mutation represents a super-inhibitory form of PLN (Haghighi et al., 2006; te Rijdt et al., 2016). This discrepancy also

questions the functional consequences of the R14del PLN mutation in heterozygous patients. The formation of PLN R14del aggregates in heterozygous patients suggests that exclusively the “healthy” PLN population is able to regulate SERCA in patients. My observations in R14del disease mouse models support the proposed aggregation model. To further clarify this issue, isolated cardiomyocytes from both disease models should be subjected to staining protocols that may reveal such aggregates and would allow to test the presence of 14-3-3 proteins in them.

Further studies are required to understand the functional consequences of the R14del PLN mutation on cardiac action and during beta adrenergic stimulation. To this end, mice disease models or corresponding induced pluripotent stem cell-derived cardiomyocytes can be used. Using such a model, one could further analyse the physiological effects of the 14-3-3/PLN R14del interaction and clarify whether the regulation of this interaction could be a putative target to increase cardiac performance in these patients.

The PLN R9C mutation was identified in 2003 by sequencing unrelated patients suffering DCM (Schmitt et al., 2003). Initially, the R9C mutation was identified as a loss-of-function mutation because it was found that PKA strongly bound to the PLN R9C mutation. Consequently, traps PKA blocked the S16 phosphorylation site in PLN and prevents SERCA inhibition (Schmitt et al., 2003). Later studies showed that the R9C mutants are clustered together in pentamers stabilized by disulfide bridges (Ha et al., 2011, Abrol et al., 2015). These stable pentamers were reported to be less accessible for the catalytic subunit of PKA (Ha et al., 2011). Furthermore, the PLN R9C pentamers are not able to interact with SERCA because of the disability to dissociate into monomers (Ha et al., 2011).

However, the cellular localization of this mutant was reported to be unaltered (Abrol et al., 2015) and I confirmed this finding with IF experiments after expression of a recombinant PLN R9C construct in mammalian cells (Figure 26-28).

The R9C mutation is not located in the identified 14-3-3 interaction site in PLN. Consequently, I predict that the R9C mutation in PLN will not affect 14-3-3 binding resulting in a low affinity 14-3-3 binding site upon S16 phosphorylation and a high 14-3-3 binding ability upon CaMKII phosphorylation. With recombinant phosphorylation assays I showed that the monomeric PLN R9C protein was phosphorylated by PKA, indicating that the reported reduced PKA accessibility (Ha et al., 2011) is caused due to the formation of very stable pentamers (chapter 2, figure S6). With recombinant phosphorylation assays, I also showed that CaMKII phosphorylation is not affected by the R9C mutation. Further, I tested 14-3-3 binding with a recombinant binding assay indicating that 14-3-3 is able to bind the PLN R9C protein upon CaMKII phosphorylation (chapter 2, figure 4D). With recombinant

de-phosphorylation assays and Ca^{2+} measurements in cardiomyocytes, I investigated the function of 14-3-3 binding implying that 14-3-3 protects PLN from phosphatases and prolongs PLN phosphorylation and SERCA activity (chapter 2, figure 5,S7,7). Due to the avidity effect 14-3-3 clamps and stabilizes pentamers with high affinities. Consequently, one can assume that 14-3-3 further stabilizes the strong pentamer formation in the PLN R9C mutation. Notably, the R9C mutation was also found to enhance PLN WT oligomerization and increases the stability of these pentamers (Abrol et al., 2015). However, it is still in question whether CaMKII phosphorylation is also affected in the stable PLN R9C pentamers and whether homo- or heteropentamers are formed in heterozygous patients. The role of CaMKII phosphorylation and 14-3-3 interaction in this mutation should be further evaluated by using a corresponding disease mouse model. Such analysis would also help to clarify whether regulation of 14-3-3 could potentially help to weaken the stable pentamers of the PLN R9C mutants as a therapeutic strategy.

Overall, CaMKII activity was found to be important for several pathophysiological conditions in the heart. Currently, CaMKII inhibitors are of general interest to increase cardiac performance and to treat heart diseases (Beauverger et al., 2019). CaMKII inhibition results in a reduction of T17 phosphorylation of PLN in disease mouse models (Beauverger et al., 2019). The CaMKII inhibitors, should be administered with caution regarding the various PLN mutations, since in the PLN R14del mutation PKA phosphorylation is abolished. Consequently, CaMKII kinase phosphorylation is important for PLN regulation in these patients and reduced phosphorylation of PLN could be detrimental. From recombinant binding assays, I have evidence that 14-3-3 binds PLN R14del and R9C mutants upon CaMKII phosphorylation (chapter 2, figure 4D) resulting in stabilization of pentamers and protection from phosphatases. Inhibition of CaMKII will lead to a reduced 14-3-3 binding to these proteins with unknown potential effects. *In vivo* this action would affect the regulation of SERCA by PLN through further decrease of PLN phosphorylation resulting in decreased SERCA function. In general, the administration of CaMKII inhibitors might cause dangerous side effects due to the number of potential client proteins phosphorylated by CaMKII.

Overall, the newly discovered 14-3-3/PLN interaction requires additional characterization especially in the light of the various disease-causing mutations (in both PLN and 14-3-3) and pathophysiological conditions. The 14-3-3 interaction regulates PLN phosphorylation in a fine-tuned manner. Further understanding of PLN regulation may help to improve cardiac performance under disease or pathophysiological conditions.

5.7 Involvement of regulatory proteins like Dlg1 or 14-3-3 in cardiac function

Regulatory proteins like Dlg1 or 14-3-3 are involved in several distinct cellular functions in various tissues (Balse & Eichel, 2017; Godreau et al., 2003; Walch, 2013). Dlg1 was reported to be altered in different forms of cardiomyopathy (Asimaki et al., 2014). Consequently, Dlg1 was analysed in the PLN R14del mutation, which is associated with DCM or ACM. In 88% of analysed heart samples from PLN R14del patients, Dlg1 was found to be mislocated to the sarcomere (te Rijdt et al., 2019).

In healthy hearts, Dlg1 is located at the intercalated disc and lateral membranes, and is responsible for signal transduction and ion channel activity (Eichel et al., 2016). It is well established that altered potassium ion channel expression can cause arrhythmia and contribute to HF (Mustroph et al., 2014). In cardiomyocytes complexes of $K_v4.2/K_v4.3$ channels with Dlg1 and CaMKII were identified (El-Haou et al., 2009). Interestingly, in different cardiomyopathies CaMKII was found to be upregulated, whereas Dlg1 was downregulated or mislocated changing the outward current of $K_v4.2/K_v4.3$ channels (Mustroph et al., 2014).

The K_2P channel TASK-1 was found to contribute to arrhythmogenic effects and HF (Schmidt et al., 2011, Schmidt at el., 2019). The exclusive atrial expression turns TASK-1 into an interesting target to treat AF specifically (Limberg et al., 2011; Schmidt et al., 2014). Dlg1 was identified as a novel cardiac interaction partner of TASK-1 in this thesis (Figure 47,51). Dlg1 was identified as a direct interaction partner of TASK-1 binding via its PDZ domain to the unphosphorylated TASK-1 channel (Figure 53,56). Based on the already known function of Dlg1 on other ion channels, it is conceivable that Dlg1 stabilizes the TASK-1 channel at the plasma membrane surface (Hong et al., 2015). The physiological function of the Dlg1/TASK-1 interaction needs to be further investigated and could help to clarify the involvement of TASK-1 channels in arrhythmias (Ma et al., 2013) or other cardiac pathophysiological conditions.

Overall, the involvement of regulatory proteins like 14-3-3 and Dlg1 in main pathways of excitation-contraction coupling mechanism illustrates their importance in cardiac function.

5.8 14-3-3 proteins as a potential drug target – possible treatments in various diseases

Pathophysiological cardiac conditions or PLN human disease mutations result in many cases in increased CaMKII activity or/and in abolished beta-adrenergic signaling (Grimm & Brown 2010; Anderson et al., 2011; Najafi et al., 2016). Although, the function of 14-3-3 under this pathophysiological condition has not been well investigated so far, it is conceivable that 14-3-3 could be used to stabilize phosphorylated PLN under pathophysiological conditions modulating SERCA activity and recover cardiac function. 14-3-3 proteins are involved in numerous protein-protein interactions and are prevalent in several human diseases, such as cancer, neurodegenerative or reproductive disorders, which points to a general interest as valuable drug targets (Aghazadeh & Papadopoulos, 2016; Stevers et al., 2018). 14-3-3 proteins serve as adaptor proteins and have a broad spectrum of phosphorylated and non-phosphorylated ligands, a compound against 14-3-3 alone could impact several 14-3-3 interactions and lead to unwanted pharmacologically side effects (Stevers et al., 2018). Consequently, the drug has to specifically target the complex formation between 14-3-3 and a specific ligand by either inhibition or stabilization (Thiel et al., 2012, Stevers et al., 2018). Therefore, a series of small molecules was already identified and is under further evaluation (Study et al., 2012, Stevers et al., 2019). With regard to the 14-3-3/PLN interaction, stabilization and inhibition could both be potential strategies for modulating the pool of phosphorylated PLN and the SERCA/PLN inhibitory interaction according to different pathophysiological conditions. The identification of protein stabilizers is more complex than the identification of specific inhibitors (Study et al., 2012). Such a stabilizer must be able to stabilize a ternary complex by simultaneously contacting two partner proteins (Study et al., 2012). An example for a 14-3-3 stabilizer is fusicoccin A, a diterpene glycoside from the fungus *Phomopsis amygdali*. Fusicoccin A was found to bind the rim of the interface of the 14-3-3 interaction with the plasma membrane H^+-ATPase and to increase the affinity of 14-3-3 for the H^+-ATPase about 90-fold (Study et al., 2012). Remarkably, fusicoccin A binds exclusively to the complex and not the two individual interaction partners (Study et al., 2012). Several stabilizers and inhibitors have been identified so far for several 14-3-3 interactions (Study et al., 2012, Stevers et al., 2018), but the presence of seven 14-3-3 isoforms in mammals further complicates the identification of specific compounds targeting such interactions. Regarding, the 14-3-3 PLN interaction, I found with recombinant bindings assays that all 14-3-3 isoforms can bind phosphorylated PLN (chapter 2, figure S3). In addition, an APEX affinity proteomic approach identified six out of seven 14-3-3 isoforms in close proximity with PLN in cardiomyocytes (chapter 2, figure 2). The binding grooves of the different 14-3-3 isoforms are conserved and in many cases all 14-3-3 isoforms are able to bind the phosphoresidue-

containing motif of a ligand (Yaffe et al., 1997) but the affinities may vary among them (Kilisch et al., 2016). Consequently, differences in the PLN binding affinities for the seven 14-3-3 isoforms should be further evaluated, for example with surface plasmon resonance or isothermal titration experiments.

14-3-3 as a drug target could also be interesting for the regulation of TASK channels. Especially, TASK-1 was found to be associated with AF (Schmidt et al., 2019). 14-3-3 was identified to regulate forward trafficking and thereby surface expression of TASK-1 and TASK-3 channels (Kilisch et al., 2006). A semi-synthetic fusicoccin THF analogue was already tested for stabilization of the TASK-3/14-3-3 interaction by binding the interface of the two interaction partners (Anders et al., 2013). Transfection of TASK-3 in *Xenopus* oocytes and treatment with 10 µM fusicoccin THF showed a 45% increased TASK-3 expression at the plasma membrane (Anders et al., 2013). However, fusicoccin THF was identified to stabilize the complex between 14-3-3 and a protein presenting a 14-3-3 mode III motif (Stever at al., 2018). Consequently, fusicoccin THF was also found to modulate surface expression of TASK-1 with a comparable efficiency as identified for TASK-3 (Anders et al., 2013). Fusicoccin THF was identified as a specific 14-3-3 mode III stabilizer. So far only six 14-3-3 ligands are known to present a 14-3-3 mode III binding motif (Anders et al., 2013). The bulky tetrahydrofuran substitution in fusicoccin THF is responsible for the specificity between 14-3-3 and a mode III motif (Anders et al., 2013). It can be assumed, that fusicoccin THF stabilizes all six known 14-3-3 target proteins with a mode III motif. Further studies are required to diminish unwanted pharmacological effects and strategies to enhance specificity for the 14-3-3/TASK channel interaction.

In general, 14-3-3 might represent a drug target protein but due to the number of potential 14-3-3 target proteins and the involvement in various cellular processes the risk of unwanted pharmacologically side-effects are high. Targeting 14-3-3 in a cellular context would prove to be challenging, if not impossible. Current studies attempt to target 14-3-3 protein-protein interactions individually to identify specific compounds which stabilize or disrupt a specific 14-3-3-protein interaction. A first step to target the PLN/14-3-3 interaction would be the determination of a crystal structure between 14-3-3 and the two different phospho-target sites in PLN. This would allow a better understanding of the interaction and could contribute to a successful high throughput screen for potential small molecules which may either stabilize or interrupt the 14-3-3/PLN interaction. Therefore, the generation of such a structure should be a priority for further investigation of 14-3-3 as a drug target to overcome regulatory problems of PLN associated with PLN disease mutations or pathophysiological conditions.

6 Bibliography

1. Ablorh, N. A. D., & Thomas, D. D. (2015). Phospholamban phosphorylation, mutation, and structural dynamics: a biophysical approach to understanding and treating cardiomyopathy. *Biophysical Reviews*, *7*(1), 63–76.
2. Abrol, N., de Tombe, P. P., & Robia, S. L. (2015). Acute Inotropic and Lusitropic Effects of Cardiomyopathic R9C Mutation of Phospholamban. *The Journal of Biological Chemistry*, *290*(11), 7130–7140.
3. Afara, M. R., Trieber, C. A., Glaves, J. P., & Young, H. S. (2006). Rational design of peptide inhibitors of the sarcoplasmic reticulum calcium pump. *Biochemistry*, *45*(28), 8617–8627.
4. Aggarwal, S. K., & MacKinnon, R. (1996). Contribution of the S4 segment to gating charge in the Shaker K+ channel. *Neuron*, *16*(6), 1169–1177.
5. Aghazadeh, Y., & Papadopoulos, V. (2016). The role of the 14-3-3 protein family in health, disease, and drug development. *Drug Discovery Today*, *21*(2), 278–287.
6. Aitken, A., Collinge, D. B., van Heusden, B. P. H., Isobe, T., Roseboom, P. H., Rosenfeld, G., & Soll, J. (1992). 14-3-3 Proteins: a Highly Conserved, Widespread Family of Eukaryotic Proteins. *Trends in Biochemical Sciences*, *17*(12), 498–501.
7. Akin, B. L., Hurley, T. D., Chen, Z., & Jones, L. R. (2013). The structural basis for phospholamban inhibition of the calcium pump in sarcoplasmic reticulum. *Journal of Biological Chemistry*, *288*(42), 30181–30191.
8. Altschuler, Y., Kinlough, C. L., Poland, P. A., Bruns, J. B., Apodaca, G., Weisz, O. A., & Hughey, R. P. (2000). Clathrin-mediated endocytosis of MUC1 is modulated by its glycosylation state. *Molecular Biology of the Cell*, *11*(3), 819–831.
9. Anders, C., Higuchi, Y., Koschinsky, K., Bartel, M., Schumacher, B., Thiel, P., Nitta, H., Preisig-Müller, R., Schlichthörl, G., Renigunta, V., Ohkanda, J., Daut, J., Kato, N., & Ottmann, C. (2013). A semisynthetic fusicoccane stabilizes a protein-protein interaction and enhances the expression of K+ channels at the cell surface. *Chemistry and Biology*, *20*(4), 583–593.
10. Anderson, M. E., Brown, J. H., & Bers, D. M. (2011). CaMKII in myocardial hypertrophy and heart failure. *J Mol Cell Cardiol*, *23*(1), 468–473.
11. Arakel, E. C., Brandenburg, S., Uchida, K., Zhang, H., Lin, Y.-W., Kohl, T., Schrul, B., Sulkin, M. S., Efimov, I. R., Nichols, C. G., Lehnart, S. E., & Schwappach, B. (2014). Tuning the electrical properties of the heart by differential trafficking of KATP ion channel complexes. *Journal of Cell Science*, *127*(9), 2106–2119.
12. Asahi, M., Green, N. M., Kurzydlowski, K., Tada, M., & MacLennan, D. H. (2001). Phospholamban domain IB forms an interaction site with the loop between transmembrane helices M6 and M7 of sarco(endo)plasmic reticulum Ca2+ ATPases. *Proceedings of the National Academy of Sciences of the United States of America*, *98*(18), 10061–10066.
13. Ashmole, I., Goodwin, P. A., & Stanfield, P. R. (2001). TASK-5, a novel member of the tandem pore K+ channel family. *Pflugers Archiv European Journal of Physiology*, *442*(6), 828–833.
14. Asimaki, A., Kapoor, S., Plovie, E., Arndt, A. K., Adams, E., Liu, Z., James, C. A., Judge, D. P., Calkins, H., Churko, J., Wu, J. C., MacRae, C. A., Kléber, A. G., & Saffitz, J. E. (2014). Identification of a New Modulator of the Intercalated Disc in a Zebrafish Model of Arrhythmogenic Cardiomyopathy. *Science Translational Medicine*, *6*(261), 1–15.
15. Balse, E., & Eichel, C. (2017). The Cardiac Sodium Channel and Its Protein Partners. *Handbook of Experimental Pharmacology*, *246*(January), 73–99.
16. Barth, A. S., Merk, S., Arnoldi, E., Zwermann, L., Kloos, P., Gebauer, M., Steinmeyer, K., Bleich, M., Kääb, S., Hinterseer, M., Kartmann, H., Kreuzer, E., Dugas, M., Steinbeck, G., & Nabauer, M. (2005). Reprogramming of the human atrial transcriptome in permanent atrial fibrillation: Expression of a ventricular-like

genomic signature. *Circulation Research*, *96*(9), 1022–1029.
17. Bartos, D. C., Grandi, E., & Ripplinger, C. M. (2015). Ion channels in the heart. *Comprehensive Physiology*, *5*(3), 1423–1464.
18. Bas, T., Gao, G. Y., Lvov, A., Chandrasekhar, K. D., Gilmore, R., & Kobertz, W. R. (2011). Post-translational N-glycosylation of type I transmembrane KCNE1 peptides: Implications for membrane protein biogenesis and disease. *Journal of Biological Chemistry*, *286*(32), 28150–28159.
19. Bass, J. J., Wilkinson, D. J., Rankin, D., Phillips, B. E., Szewczyk, N. J., Smith, K., & Atherton, P. J. (2017). An overview of technical considerations for Western blotting applications to physiological research. *Scandinavian Journal of Medicine and Science in Sports*, *27*(1), 4–25.
20. Baukrowitz, T., Schulte, U., Oliver, D., Herlitze, S., Krauter, T., Tucker, S. J., Ruppersberg, J. P., & Fakler, B. (1998). PIP2 and PIP as determinants for ATP inhibition of K(ATP) channels. *Science*, *282*(5391), 1141–1144.
21. Becker, R., Merkely, B., Bauer, A., Geller, L., Fazekas, L., Freigang, K. D., Voss, F., Senges, J. C., Kuebler, W., & Schoels, W. (2000). Ventricular arrhythmias induced by endothelin-1 or by acute ischemia: A comparative analysis using three dimensional mapping. *Cardiovascular Research*, *46*(3), 604–607.
22. Becucci, L., Cembran, A., Karim, C. B., Thomas, D. D., Guidelli, R., Gao, J., & Veglia, G. (2009). On the function of pentameric phospholamban: Ion channel or storage form? *Biophysical Journal*, *96*(10).
23. Benzinger, A., Popowicz, G. M., Joy, J. K., Majumdar, S., Holak, T. A., & Hermeking, H. (2005). The crystal structure of the non-liganded 14-3-3σ protein: Insights into determinants of isoform specific ligand binding and dimerization. *Cell Research*, *15*(4), 219–227.
24. Bidwell, P., Blackwell, D. J., Hou, Z., Zima, A. V., & Robia, S. L. (2011). Phospholamban binds with differential affinity to calcium pump conformers. *Journal of Biological Chemistry*, *286*(40), 35044–35050.
25. Bilezikjian, L. M., Kranias, E. G., Potter, J. D., & Schwartz, A. (1981). Studies on phosphorylation of canine cardiac sarcoplasmic reticulum by calmodulin-dependent protein kinase. *Circulation Research*, *49*(6), 1356–1362.
26. Blin, S., Chatelain, F. C., Feliciangeli, S., Kang, D., Lesage, F., & Bichet, D. (2014). Tandem pore domain halothane-inhibited K+channel subunits THIK1 and THIK2 assemble and form active channels. *Journal of Biological Chemistry*, *289*(41), 28202–28212.
27. Bocksteins, E., Labro, A. J., Mayeur, E., Bruyns, T., Timmermans, J. P., Adriaensen, D., & Snyders, D. J. (2009). Conserved negative charges in the N-terminal tetramerization domain mediate efficient assembly of Kv2.1 and Kv2.1/Kv6.4 channels. *Journal of Biological Chemistry*, *284*(46), 31625–31634.
28. Bristow, M. R., Ginsburg, R., Umans, V., Fowler, M., Minobe, W., Rasmussen, R., Zera, P., Menlove, R., Shah, P. I. R., Jamieson, S., & Stinson, E. B. (1986). Beta1- and Beta2-Adrenergic-Receptor Subpopulations in Nonfailing and Failing Human Ventricular Myocardium: Coupling of Both Receptor Subtypes to Muscle Contraction and Selective /3i-Receptor Down-Regulation in Heart Failure. *Circulation Research*, *59*(3), 297–309.
29. Buentzel, J., & Thoms, S. (2017). The Use of Glycosylation Tags as Reporters for Protein Entry into the Endoplasmic Reticulum in Yeast and Mammalian Cells. *Peroxisomes*, *1595*, 243–248.
30. Bulbarelli, A., Sprocati, T., Barberi, M., Pedrazzini, E., & Borgese, N. (2002). Trafficking of tail-anchored proteins: Transport from the endoplasmic reticulum to the plasma membrane and sorting between surface domains in polarised epithelial cells. *Journal of Cell Science*, *115*(8), 1689–1702.
31. Butler, J., Lee, A. G., Wilson, D. I., Spalluto, C., Hanley, N. A., & East, J. M. (2007). Phospholamban and sarcolipin are maintained in the endoplasmic reticulum by retrieval from the ER-Golgi intermediate compartment. *Cardiovascular Research*,

74(1), 114–123.
32. Calderón, J. C., Bolaños, P., & Caputo, C. (2014). The excitation-contraction coupling mechanism in skeletal muscle. *Biophysical Reviews*, *6*(1), 133–160.
33. Callahan, R., Labunskiy, D. A., Logvinova, A., Abdallah, M., Liu, C., Cotten, J. F., & Yost, C. S. (2004). Immunolocalization of TASK-3 (KCNK9) to a subset of cortical neurons in the rat CNS. *Biochemical and Biophysical Research Communications*, *319*(2), 525–530.
34. Cau, Y., Valensin, D., Mori, M., Draghi, S., & Botta, M. (2018). Structure, Function, Involvement in Diseases and Targeting of 14-3-3 Proteins: An Update. *Current Medicinal Chemistry*, *25*(1), 5–21.
35. Ceholski, D. K., Trieber, C. A., Holmes, C. F. B., & Young, H. S. (2012). Lethal , Hereditary Mutants of Phospholamban Elude Phosphorylation by Protein Kinase A. *Journal of Biological Chemistry*, *287*(32), 26596–26605.
36. Cerra, M. C., & Imbrogno, S. (2012). Phospholamban and cardiac function: a comparative perspective in vertebrates. *Acta Physiologica*, *205(1)*, 9–25.
37. Chen, X., Talley, E. M., Patel, N., Gomis, A., McIntire, W. E., Dong, B., Viana, F., Garrison, J. C., & Bayliss, D. A. (2006). Inhibition of a background potassium channel by Gq protein α-subunits. *Proceedings of the National Academy of Sciences of the United States of America*, *103*(9), 3422–3427.
38. Chen, Z., Akin, B. L., & Jones, L. R. (2010). Ca2+ binding to site I of the cardiac Ca2+ pump is sufficient to dissociate phospholamban. *Journal of Biological Chemistry*, *285*(5), 3253–3260.
39. Chen, Z., Stokes, D. L., Rice, W. J., & Jones, L. R. (2003). Spatial and Dynamic Interactions between Phospholamban and the Canine Cardiac Ca2+ Pump Revealed with Use of Heterobifunctional Cross-linking Agents. *Journal of Biological Chemistry*, *278*(48), 48348–48356.
40. Cherniavsky-Lev, M., Golani, O., Karlish, S. J. D., & Garty, H. (2014a). Ouabain-induced internalization and lysosomal degradation of the Na +/K+-ATPase. *Journal of Biological Chemistry*, *289*(2), 1049–1059.
41. Chevallet, M., Luche, S., & Rabilloud, T. (2006). Silver staining of proteins in polyacrylamide gels. *Nature Protocols*, *1*(4), 1852–1858.
42. Choudhary, C., Kumar, C., Gnad, F., Nielsen, M. L., Rehman, M., Walther, T. C., Olsen, J. V., & Mann, M. (2009). Lysine acetylation targets protein complexes and co-regulates major cellular functions. *Science*, *325*(5942), 834–840.
43. Chu, G., Lester, J. W., Young, K. B., Luo, W., Zhai, J., & Kranias, E. G. (2000). A Single Site (Ser 16) Phosphorylation in Phospholamban Is ␣ -Agonists. *Journal of Biological Chemistry*, *275*(49), 38938–38943.
44. Chu, G., Li, L., Sato, Y., Harrer, J. M., Kadambi, V. J., Hoit, B. D., Bers, D. M., & Kranias, E. G. (1998). Pentameric assembly of phospholamban facilitates inhibition of cardiac function in vivo. *Journal of Biological Chemistry*, *273*(50), 33674–33680.
45. Coblitz, B., Wu, M., Shikano, S., & Li, M. (2006). C-terminal binding: An expanded repertoire and function of 14-3-3 proteins. *FEBS Letters*, *580*(6), 1531–1535.
46. Cornea, Răzvan L., Jones, L. R., Autry, J. M., & Thomas, D. D. (1997). Mutation and phosphorylation change the oligomeric structure of phospholamban in lipid bilayers. *Biochemistry*, *36*(10), 2960–2967.
47. Cornea, Razvan L, Autry, J. M., Chen, Z., & Jones, L. R. (2000). Reexamination of the Role of the Leucine/Isoleucine Zipper Residues of Phospholamban in Inhibition of the Ca2+ Pump of Cardiac Sarcoplasmic Reticulum. *Journal of Biological Chemistry*, *275*(52), 41487–41494.
48. Cotten, J. F., Keshavaprasad, B., Laster, M. J., Eger, E. I., & Yost, C. S. (2006). The ventilatory stimulant doxapram inhibits TASK tandem pore (K 2P) potassium channel function but does not affect minimum alveolar anesthetic concentration. *Anesthesia and Analgesia*, *102*(3), 779–785.
49. Coyler, J. (1998). Phosphorylation States of Phospholamban. *Ann N Y Acad Sci*, 79–91.

50. Cyganek, L., Tiburcy, M., Sekeres, K., Gerstenberg, K., Bohnenberger, H., Lenz, C., Henze, S., Stauske, M., Salinas, G., Zimmermann, W. H., Hasenfuss, G., & Guan, K. (2018). Deep phenotyping of human induced pluripotent stem cell-derived atrial and ventricular cardiomyocytes. *JCI Insight*, *3*(12), 1–17.
51. Czirják, G., & Enyedi, P. (2002). Formation of functional heterodimers between the TASK-1 and TASK-3 two-pore domain potassium channel subunits. *Journal of Biological Chemistry*, *277*(7), 5426–5432.
52. Czirják, G., Tóth, Z. E., & Enyedi, P. (2004). The Two-pore Domain K+ Channel, TRESK, Is Activated by the Cytoplasmic Calcium Signal through Calcineurin. *Journal of Biological Chemistry*, *279*(18), 18550–18558.
53. Davis, B. A., Edes, I., Gupta, R. C., Young, E. F., Kim, H. W., Steenaart, N. A. E., Szymanska, G., & Kranias, E. G. (1990). The role of phospholamban in the regulation of calcium transport by cardiac sarcoplasmic reticulum. *Molecular and Cellular Biochemistry*, *99*(2), 83–88.
54. de Lucia, C., Eguchi, A., & Koch, W. J. (2018). New insights in cardiac β-Adrenergic signaling during heart failure and aging. *Frontiers in Pharmacology*, *9*, 1–14.
55. De Simone, A., Gustavsson, M., Montalvao, R. W., Shi, L., Veglia, G., & Vendruscolo, M. (2013). Structures of the excited states of phospholamban and shifts in their populations upon phosphorylation. *Biochemistry*, *52*(38), 6684–6694.
56. Decher, N., Kiper, A. K., Rolfes, C., Schulze-Bahr, E., & Rinné, S. (2014). The role of acid-sensitive two-pore domain potassium channels in cardiac electrophysiology: Focus on arrhythmias. *Pflugers Archiv European Journal of Physiology*, *467*(5), 1055–1067.
57. Decher, N., Wemhöner, K., Rinné, S., Netter, M. F., Zuzarte, M., Aller, M. I., Kaufmann, S. G., Li, X. T., Meuth, S. G., Daut, J., Sachse, F. B., & Maier, S. K. G. (2011). Knock-out of the potassium channel TASK-1 leads to a prolonged qt interval and a disturbed QRS complex. *Cellular Physiology and Biochemistry*, *28*(1), 77–86.
58. Diviani, D., Dodge-Kafka, K. L., Li, J., & Kapiloff, M. S. (2011). A-kinase anchoring proteins: scaffolding proteins in the heart. *AJP: Heart and Circulatory Physiology*, *301*(5), 1742–1753.
59. Dong, X., & Thomas, D. D. (2014). Time-resolved FRET reveals the structural mechanism of SERCA-PLB regulation. *Biochemical and Biophysical Research Communications*, *449*(2), 196–201.
60. Donner, B. C., Schullenberg, M., Geduldig, N., Hüning, A., Mersmann, J., Zacharowski, K., Kovacevic, A., Decking, U., Aller, M. I., & Schmidt, K. G. (2011). Functional role of TASK-1 in the heart: Studies in TASK-1-deficient mice show prolonged cardiac repolarization and reduced heart rate variability. *Basic Research in Cardiology*, *106*(1), 75–87.
61. Duprat, F., Lauritzen, I., Patel, A., & Honoré, E. (2007). The TASK background K2P channels: chemo- and nutrient sensors. *Trends in Neurosciences*, *30*(11), 573–580.
62. Duprat, F., Lesage, F., Fink, M., Reyes, R., Heurteaux, C., & Lazdunski, M. (1997). TASK, a human background K+ channel to sense external pH variations near physiological pH. *EMBO Journal*, *16*(17), 5464–5471.
63. Edes, I., & Kranias, E. G. (1990). Phospholamban and troponin I are substrates for protein kinase C in vitro but not in intact beating guinea pig hearts. *Circulation Research*, *67*(2), 394–400.
64. Efendiev, R., Chen, Z., Krmar, R. T., Uhles, S., Katz, A. I., Pedemonte, C. H., & Bertorello, A. M. (2005). The 14-3-3 protein translates the NA+,K+-ATPase α1-subunit phosphorylation signal into binding and activation of phosphoinositide 3-kinase during endocytosis. *Journal of Biological Chemistry*, *280*(16), 16272–16277.
65. Eichel, C. A., Beuriot, A., Chevalier, M. Y. E., Rougier, J., Louault, F., Dilanian, G., Amour, J., Coulombe, A., Abriel, H., Hatem, S. N., & Balse, E. (2016). Lateral Membrane-Specific MAGUK CASK Down-Regulates NaV 1.5 Channel in Cardiac

Myocytesgy. *Circulation Research*, *119*, 544–556.
66. Eijgenraam, T. R., Boukens B. J., Boogerd, C. J., Schouten E. M., van de Kolk, C. W. A., Stege, N. M., te Rijdt, W. P., Hoorntje, E. T., van der Zwaag, P. A., van Rooji, E., van Tintelen, J. P., van den Berg, M.P., van der Meer, P., van der Velden, J., Silljé, H. H. W., & de Boer, R. (2020). The phospholamban p.(Arg14del) pathogenic variant leads to cardiomyopathy with heart failure and is unreponsive to standard heart failure therapy. *Scientific Reports*, 10 (1).
67. Eisner, D. A., Caldwell, J. L., Kistamás, K., & Trafford, A. W. (2017). Calcium and Excitation-Contraction Coupling in the Heart. *Circulation Research*, *121*(2), 181–195.
68. El-Haou, S., Balse, E., Neyroud, N., Dilanian, G., Gavillet, B., Abriel, H., Coulombe, A., Jeromin, A., & Hatem, S. N. (2009). Kv4 potassium channels form a tripartite complex with the anchoring protein SAP97 and CaMKII in cardiac myocytes. *Circulation Research*, *104*(6), 758–769.
69. Enyedi, P., & Czirják, G. (2010). Molecular Background of Leak K+ Currents : Two-Pore Domain Potassium Channels. *Physiol Rev*, 559–605.
70. Espejo, A. B., Gao, G., Black, K., Gayatri, S., Veland, N., Kim, J., Chen, T., Sudol, M., Walker, C., & Bedford, M. T. (2017). PRMT5 C-terminal phosphorylation modulates a 14-3-3/PDZ interaction switch. *Journal of Biological Chemistry*, *292*(6), 2255–2265.
71. Fearnley, C. J., Llewelyn Roderick, H., & Bootman, M. D. (2011). Calcium signaling in cardiac myocytes. *Cold Spring Harbor Perspectives in Biology*, *3*(11), 1–20.
72. Feliciangeli, S., Chatelain, F. C., Bichet, D., & Lesage, F. (2015). The family of K2P channels: Salient structural and functional properties. *Journal of Physiology*, *593*(12), 2587–2603.
73. Filgueiras-Rama, D., & Jalife, J. (2016). Structural and functional bases of cardiac fibrillation differences and similarities between atria and ventricles. *JACC: Clinical Electrophysiology*, *2*(1), 1–3.
74. Fourie, C., Li, D., & Montgomery, J. M. (2014). The anchoring protein SAP97 influences the trafficking and localisation of multiple membrane channels. *Biochimica et Biophysica Acta - Biomembranes*, *1838*(2), 589–594.
75. Fu, H., Subramanian, R. R., & Masters, S. C. (2000). 14-3-3 Proteins: Structure , Function , and Regulation. *Annu Rev Phar,a Toxicol*, *40*, 617–647.
76. Gabriel, L., Lvov, A., Orthodoxou, D., Rittenhouse, A. R., Kobertz, W. R., & Melikian, H. E. (2012). The acid-sensitive, anesthetic-activated potassium leak channel, KCNK3, is regulated by 14-3-3β-dependent, protein kinase C (PKC)-mediated endocytic trafficking. *Journal of Biological Chemistry*, *287*(39), 32354–32366.
77. Gardino, A. K., Smerdon, S. J., & Yaffe, M. B. (2006). Structural determinants of 14-3-3 binding specificities and regulation of subcellular localization of 14-3-3-ligand complexes: A comparison of the X-ray crystal structures of all human 14-3-3 isoforms. In *Seminars in Cancer Biology*, 16 (3), 173–182.
78. Gillet, L., Rougier, J.-S., Shy, D., Sonntag, S., Mougenot, N., Essers, M., Shmerling, D., Balse, E., Hatem, S. N., & Abriel, H. (2015). Cardiac-specific ablation of synapse-associated protein SAP97 in mice decreases potassium currents but not sodium current. *Heart Rhythm*, *12*(1), 181–192.
79. Glaves, J. P., Primeau, J. O., Espinoza-Fonseca, L. M., Lemieux, M. J., & Young, H. S. (2019). The Phospholamban Pentamer Alters Function of the Sarcoplasmic Reticulum Calcium Pump SERCA. *Biophysical Journal*, *116*(4), 633–647.
80. Glaves, J. P., Trieber, C. A., Ceholski, D. K., Stokes, D. L., & Young, H. S. (2011). Phosphorylation and mutation of phospholamban alter physical interactions with the sarcoplasmic reticulum calcium pump. *J Mol Biol*, *23*(1), 1–7.
81. Godreau, D., Vranckx, R., Maguy, A., Goyenvalle, C., & Hatem, S. N. (2003). Different Isoforms of Synapse-associated Protein, SAP97, Are Expressed in the Heart and Have Distinct Effects on the Voltage-gated K+ Channel Kv1.5. *Journal*

of Biological Chemistry, *278*(47), 47046–47052.
82. Godreau, D., Vranckx, R., Maguy, A., Rücker-Martin, C., Goyenvalle, C., Abdelshafy, S., Tessier, S., Couétil, J. P., & Hatem, S. N. (2002). Expression, regulation and role of the MAGUK protein SAP-97 in human atrial myocardium. *Cardiovascular Research*, *56*(3), 433–442.
83. Gogl, G., Jane, P., Caillet-Saguy, C., Kostmann, C., Bich, G., Cousido-Siah, A., Nyitray, L., Vincentelli, R., Wolff, N., Nomine, Y., Sluchanko, N. N., & Trave, G. (2020). Dual Specificity PDZ- and 14-3-3-Binding Motifs: A Structural and Interactomics Study. *Structure*, 1–13.
84. Goldstein, I. J., Winter, H. C., & Poretz, R. D. (1997). Chapter 12 Plant Lectins: tools for the Study of Complex Carbohydrates. In *New Comprehensive Biochemistry*, 29, 403–474.
85. Goldstein, S. A. N., Bayliss, D. A., Kim, D., Lesage, F., & Plant, L. D. (2005). Nomenclature and Molecular Relationships of Two-P Potassium Channels. *Pharmacological Reviews*, *57*(4), 527–540.
86. Goldstein, S. A. N., Bockenhauer, D., O'Kelly, I., & Zilberberg, N. (2001). Potassium leak channels and the KCNK family of two-p-domain subunits. *Nature Reviews Neuroscience*, *2*(3), 175–184.
87. Gomes, A. V, Potter, J. D., & Szczesna-Cordary, D. (2002). The Role of Troponins in Muscle Contraction. *IUBMB Life*, *54*(10), 323–333.
88. Grimm, M., & Brown, J. H. (2010). β-Adrenergic receptor signaling in the heart: Role of CaMKII. *Journal of Molecular and Cellular Cardiology*, *48*(2), 322–330.
89. Gupta, R. C., Mishra, S., Rastogi, S., Imai, M., Habib, O., & Sabbah, H. N. (2003). Cardiac SR-coupled PP1 activity and expression are increased and inhibitor I protein expression is decreased in failing hearts. *American Journal of Physiology - Heart and Circulatory Physiology*, *285*(6 54-6), 2373–2381.
90. Gurney, A. M., Osipenko, O. N., MacMillan, D., McFarlane, K. M., Tate, R. J., & Kempsill, F. E. J. (2003). Two-Pore Domain K Channel, TASK-1, in Pulmonary Artery Smooth Muscle Cells. *Circulation Research*, *93*(10), 957–964.
91. Gurney, A., & Manoury, B. (2009). Two-pore potassium channels in the cardiovascular system. *European Biophysics Journal*, *38*(3), 305–318.
92. Gustavsson, M., Traaseth, N., & Veglia, G. (2011). Activating and deactivating rolesof lipid bilayers on the Ca2+-ATPase/Phospholamban complex. *Biochemistry*, *50*(47), 10367–10374.
93. Gustavsson, M., Verardi, R., Mullen, D. G., Mote, K. R., Traaseth, N. J., Gopinath, T., & Veglia, G. (2013). Allosteric regulation of SERCA by phosphorylationmediated conformational shift of phospholamban. *Proceedings of the National Academy of Sciences of the United States of America*, *110*(43), 17338–17343.
94. Gutman, G. A., Chandy, K. G., Grissmer, S., Lazdunski, M., McKinnon, D., Pardo, L. A., Robertson, G. A., Rudy, B., Sanguinetti, M. C., Stühmer, W., & Wang, X. (2005). Nomenclature and molecular relationships of voltage-gated potassium channels. *Pharmacological Reviews*, *57*(4), 473–508.
95. Ha, K. N., Gustavsson, M., & Veglia, G. (2012). Tuning the structural coupling between the transmembrane and cytoplasmic domains of phospholamban to control sarcoplasmic reticulum Ca 2+-ATPase (SERCA) function. *Journal of Muscle Research and Cell Motility*, *33*(6), 485–492.
96. Ha, K. N., Mastersona, L. R., Hou, Z., Verardi, R., Walsh, N., Veglia, G., & Robia, S. L. (2011). Lethal Arg9Cys phospholamban mutation hinders Ca2+-ATPase regulation and phosphorylation by protein kinase A. *Proceedings of the National Academy of Sciences of the United States of America*, *108*(7), 2735–2740.
97. Haghighi, K., Kolokathis, F., Gramolini, A. O., Waggoner, J. R., Pater, L., Lynch, R. A., Fan, G., Tsiapras, D., Parekh, R. R., Li, G. W. D., Maclennan, D. H., Kremastinos, D. T., & Kranias, E. G. (2006). A mutation in the human phospholamban gene , deleting arginine 14 , results in lethal , hereditary cardiomyopathy. *PNAS*, *103*, 1388–1393.

98. Haghighi, K., Kolokathis, F., Pater, L., Lynch, R. A., Asahi, M., Gramolini, A. O., Fan, G. C., Tsiapras, D., Hahn, H. S., Adamopoulos, S., Liggett, S. B., Dorn, G. W., MacLennan, D. H., Kremastinos, D. T., & Kranias, E. G. (2003). Human phospholamban null results in lethal dilated cardiomyopathy revealing a critical difference between mouse and human. *Journal of Clinical Investigation*, *111*(6), 869–876.
99. Haghighi, K., Pritchard, T., Bossuyt, J., Waggoner, J. R., Yuan, Q., Fan, G. C., Osinska, H., Anjak, A., Rubinstein, J., Robbins, J., Bers, D. M., & Kranias, E. G. (2012). The human phospholamban Arg14-deletion mutant localizes to plasma membrane and interacts with the Na/K-ATPase. *Journal of Molecular and Cellular Cardiology*, *52*(3), 773–782.
100. Han, S. K., Kim, D., Lee, H., Kim, I., & Kim, S. (2018). Divergence of noncoding regulatory elements explains gene-phenotype differences between human and mouse orthologous genes. *Molecular Biology and Evolution*, *35*(7),
101. Hancox, J. C., James, A. F., Marrion, N. V, Zhang, H., & Thomas, D. (2016). Novel ion channel targets in atrial fibrillation. *Expert Opinion on Therapeutic Targets*, *8222*(April), 1–12.
102. Hansen, O. (2003). No evidence for a role in signal-transduction of Na+/K+-ATPase interaction with putative endogenous ouabain. *European Journal of Biochemistry*, *270*(9), 1916–1919.
103. Hart, G. W. (1992). Glycosylation. *Current Opinion in Cell Biology*, *4*(6), 1017–1023.
104. Hermeking, H. (2003). The 14-3-3 cancer connection. *Nature Reviews Cancer*, *3*(12), 931–943.
105. Hibino, H., Inanobe, A., Furutani, K., Murakami, S., Findlay, I., & Kurachi, Y. (2010). Inwardly rectifying potassium channels: Their structure, function, and physiological roles. *Physiological Reviews*, *90*(1), 291–366.
106. Hof, I. E., van der Heijden, J. F., Kranias, E. G., Sanoudou, D., de Boer, R. A., van Tintelen, J. P., van der Zwaag, P. A., & Doevendans, P. A. (2019). Prevalence and cardiac phenotype of patients with a phospholamban mutation. *Netherlands Heart Journal*, *27*(2), 64–69.
107. Hoit, B. D., Khoury, S. F., Kranias, E. G., Ball, N., & Walsh, R. A. (1995). In vivo echocardiographic detection of enhanced left ventricular function in gene-targeted mice with phospholamban deficiency. *Circulation Research*, *77*(3), 632–637.
108. Hong, X., Avetisyan, M., Ronilo, M., & Standley, S. (2015). SAP97 blocks the RXR ER retention signal of NMDA receptor subunit GluN1-3 through its SH3 domain. *Biochimica et Biophysica Acta - Molecular Cell Research*, *1853*(2), 489–499.
109. Hopwood, S. E., & Trapp, S. (2005). TASK-like K+ channels mediate effects of 5-HT and extracellular pH in rat dorsal vagal neurones in vitro. *Journal of Physiology*, *568*(1), 145–154.
110. Hou, Z., Kelly, E. M., & Robia, S. L. (2008). Phosphomimetic mutations increase phospholamban oligomerization and alter the structure of its regulatory complex. *Journal of Biological Chemistry*, *283*(43), 28996–29003.
111. Huang, C. L., Feng, S., & Hilgemann, D. W. (1998). Direct activation of inward rectifier potassium channels by PIP2 and its stabilization by Gβγ. *Nature*, *391*(6669), 803–806.
112. Hughes, S., Foster, R. G., Peirson, S. N., & Hankins, M. W. (2017). Expression and localisation of two-pore domain (K2P) background leak potassium ion channels in the mouse retina. *Scientific Reports*, *7*, 1–14.
113. Humphries, E. S. A., & Dart, C. (2015). Neuronal and cardiovascular potassium channels as therapeutic drug targets: Promise and pitfalls. *Journal of Biomolecular Screening*, *20*(9), 1055–1073.
114. Huotari, J., & Helenius, A. (2011). Endosome maturation. *EMBO Journal*,

30(17), 3481–3500.
115. Ichimura, T., Isobe, T., Okuyama, T., Takahashi, N., Araki, K., Kuwano, R., & Takahashi, Y. (1988). Molecular cloning of cDNA coding for brain-specific 14-3-3 protein, a protein kinase-dependent activator of tyrosine and tryptophan hydroxylases. *Proceedings of the National Academy of Sciences*, *85*(19), 7084–7088.
116. James, A. F., Ramsey, J. E., Reynolds, A. M., Hendry, B. M., & Shattock, M. J. (2001). Effects of endothelin-1 on K+ currents from rat ventricular myocytes. *Biochemical and Biophysical Research Communications*, *284*(4), 1048–1055.
117. James, P., Inui, M., Tada, M., Chiesi, M., & Carafoli, E. (1989). Nature and site of phospholamban regulation of the Ca2+ pump of sarcoplasmic reticulum. *Nature*, *342*(6245), 90–92.
118. Jeevaratnam, K., Chadda, K. R., Huang, C. L. H., & Camm, A. J. (2018). Cardiac Potassium Channels: Physiological Insights for Targeted Therapy. *Journal of Cardiovascular Pharmacology and Therapeutics*, *23*(2), 119–129.
119. Johnson, C., Crowther, S., Stafford, M. J., Campbell, D. G., Toth, R., & MacKintosh, C. (2010). Bioinformatic and experimental survey of 14-3-3-binding sites. *Biochemical Journal*, *427*(1), 69–78.
120. Jones, D. H., Ley, S., & Aitken, A. (1995). Isoforms of 14-3-3 protein can form homo- and heterodimers in vivo and in vitro: implications for function as adapter proteins. *FEBS Letters*, *368*(1), 55–58.
121. Jones, L. R., Simmerman, H. K. B., William, W. W., Gurd, F. R. N., & Wegener, A. D. (1985). Purification and characterization of phospholamban from canine cardiac sarcoplasmic reticulum. *Journal of Biological Chemistry*, *260*(6), 3708–3715.
122. Jones, S. A., Morton, M. J., Hunter, M., & Boyett, M. R. (2002). Expression of TASK-1, a pH-sensitive twin-pore domain K+ channel, in rat myocytes. *American Journal of Physiology - Heart and Circulatory Physiology*, *283*(1 52-1), 181–185.
123. Jovic, M., Sharma, M., Rahajeng, J., & Caplan, S. (2010). The early endosome: A busy sorting station for proteins at the crossroads. *Histology and Histopathology*, *25*(1), 99–112.
124. Karim, C. B., Stamm, J. D., Karim, J., Jones, L. R., & Thomas, D. D. (1998). Cysteine reactivity and oligomeric structures of phospholamban and its mutants. *Biochemistry*, *37*(35), 12074–12081.
125. Karim, C. B., Zhang, Z., Howard, E. C., Torgersen, K. D., & Thomas, D. D. (2006). Phosphorylation-dependent Conformational Switch in Spin-labeled Phospholamban Bound to SERCA. *Journal of Molecular Biology*, *358*(4), 1032–1040.
126. Kilisch, M., Lytovchenko, O., Arakel, E. C., & Bertinetti, D. (2016). A dual phosphorylation switch controls 14-3-3-dependent cell surface expression of TASK-1. *Journal of Cell Science*, *January*, 831–842.
127. Kilisch, M., Lytovchenko, O., Schwappach, B., Renigunta, V., & Daut, J. (2015). The role of protein-protein interactions in the intracellular traffic of the potassium channels TASK-1 and TASK-3. *Pflugers Archiv European Journal of Physiology*, 1105–1120.
128. Kim, D., & Gnatenco, C. (2001). TASK-5, a new member of the tandem-pore K+ channel family. *Biochemical and Biophysical Research Communications*, *284*(4), 923–930.
129. Kim, D. M., & Nimigean, C. M. (2016). Voltage-gated potassium channels: A structural examination of selectivity and gating. *Cold Spring Harbor Perspectives in Biology*, *8*(5), 1–19.
130. Kim, E., Niethammer, M., Rothschild, A., Nung Jan, Y., & Sheng, M. (1995). Clustering of Shaker-type K+ channels by interaction with a family of membrane-associated guanylate kinases. *Nature*, *378*(6552), 85–88.
131. Kim, Y., Bang, H., & Kim, D. (1999). TBAK-1 and TASK-1, two-pore K+

channel subunits: Kinetic properties and expression in rat heart. *American Journal of Physiology - Heart and Circulatory Physiology*, *277*(5 46-5).

132. Kimura, Y., Asahi, M., Kurzydlowski, K., Tada, M., & MacLennan, D. H. (1998). Phospholamban domain Ib mutations influence functional interactions with the Ca2+-ATPase isoform of cardiac sarcoplasmic reticulum. *Journal of Biological Chemistry*, *273*(23), 14238–14241.
133. Kimura, Y., Kurzydlowski, K., Tada, M., & Maclennan, D. H. (1997). Phospholamban Inhibitory Function Is Activated by Depolymerization. *Journal of Biological Chemistry*, *272*, 15061–15065.
134. Kimura, Y., Kurzydlowski, K., Tada, M., & MacLennan, D. H. (1996). Phospholamban regulates the Ca2+-ATPase through intramembrane interactions. *Journal of Biological Chemistry*, *271*(36), 21726–21731.
135. Kiriazis, H., Sato, Y., Kadambi, V. J., Schmidt, A., Gerst, M. J., Hoit B. H., & Kranias, E. G. (2002). Hypertrophy and functional alteration in hyperdynamic phospholamban-knockout mouse hearts under chronic aortic stenosis. *Cardiovascular Research,* 53(2), 372-381.
136. Kranias, E. G., & Hajjar, R. J. (2012). Modulation of cardiac contractility by the phopholamban/SERCA2a regulatome. *Circulation Research*, *110*(12), 1646–1660.
137. Kuang, Q., Purhonen, P., & Hebert, H. (2015). Structure of potassium channels. *Cellular and Molecular Life Sciences*, *72*(19), 3677–3693.
138. Kumar, G., (2018). A simple method for detecting phosphorylation of proteins by using Zn2+-Phos-Tag SDS-PAGE at neutral pH. *Methods Mol Biol*, 1853, 223-229.
139. Kurata, H. T., Soon, G. S., Eldstrom, J. R., Lu, G. W. K., Steele, D. F., & Fedida, D. (2002). Amino-terminal determinants of U-type inactivation of voltage-gated K+ channels. *The Journal of Biological Chemistry*, *277*(32), 29045–29053.
140. Kuschel, M., Karczewski, P., Hempel, P., Schlegel, W.-P., Krause, E.-G., & Bartel, S. (1999). Ser 16 prevails over Thr 17 phospholamban phosphorylation in the beta -adrenergic regulation of cardiac relaxation. *Am J Physiol*, *276*(5), 1625–1633.
141. Lafer, E. M. (2002). Clathrin - Protein interactions. *Traffic*, *3*(8), 513–520.
142. Landstrom, A. P., Adekola, B. A., Bos, J. M., Ommen, S. R., & Ackerman, M. J. (2011). PLN-encoded Phospholamban Mutation in a Large Cohort of Hypertrophic Cardiomyopathy Cases: Summary of the Literature and Implications for Genetic Testing Andrew. *Am J Physiol Regulatory Integrative Comp Physiol*, *176*(1), 165–171.
143. Laver, D. R. (2007). Ca2+ stores regulate ryanodine receptor Ca2+ release channels via luminal and cytosolic Ca2+ sites. *Biophysical Journal*, *92*(10), 3541–3555.
144. Leonoudakis, D., Conti, L. R., Anderson, S., Radeke, C. M., McGuire, L. M. M., Adams, M. E., Froehner, S. C., Yates, J. R., & Vandenberg, C. A. (2004). Protein trafficking and anchoring complexes revealed by proteomic analysis of inward rectifier potassium channel (Kir2.x)-associated Proteins. *Journal of Biological Chemistry*, *279*(21), 22331–22346.
145. Lesage, F., Guillemare, E., Fink, M., Duprat, F., Lazdunski, M., Romey, G., & Barhanin, J. (1996). TWIK-1, a ubiquitous human weakly inward rectifying K+ channel with a novel structure. *The EMBO Journal*, *15*(5), 1004–1011.
146. Lesage, F., (2003). Pharmacology of neuronal background potassium channels. *Neuropharmacology*, *44*(1), 1–7.
147. Li, X. T., Dyachenko, V., Zuzarte, M., Putzke, C., Preisig-Müller, R., Isenberg, G., & Daut, J. (2006). The stretch-activated potassium channel TREK-1 in rat cardiac ventricular muscle. *Cardiovascular Research*, *69*(1), 86–97.
148. Li, Z., Liu, J. Y., & Zhang, J. T. (2009). 14-3-3Σ, the Double-Edged Sword of Human Cancers. *American Journal of Translational Research*, *1*(4), 326–340.

149. Liang, B., Soka, M., Christensen, A. H., Olesen, M. S., Larsen, A. P., Knop, F. K., Wang, F., Nielsen, J. B., Andersen, M. N., Humphreys, D., Mann, S. A., Huttner, I. G., Vandenberg, J. I., Svendsen, J. H., Haunsø, S., Preiss, T., Seebohm, G., Olesen, S. P., Schmitt, N., & Fatkin, D. (2014). Genetic variation in the two-pore domain potassium channel, TASK-1, may contribute to an atrial substrate for arrhythmogenesis. *Journal of Molecular and Cellular Cardiology*, *67*, 69–76.
150. Limberg, S. H., Netter, M. F., Rolfes, C., Rinné, S., Schlichthörl, G., Zuzarte, M., Vassiliou, T., Moosdorf, R., Wulf, H., Daut, J., Sachse, F. B., & Decher, N. (2011). TASK-1 channels may modulate action potential duration of human atrial cardiomyocytes. *Cellular Physiology and Biochemistry*, *28*(4), 613–624.
151. Lindemann, J. P., Jones, L. R., Hathaway, D. R., Henry, B. G., & Watanabe, A. M. (1983). β-Adrenergic stimulation of phospholamban phosphorylation and Ca 2+-ATPase activity in guinea pig ventricles. *Journal of Biological Chemistry*, *258*(1), 464–471.
152. Lindner, M., Leitner, M. G., Halaszovich, C. R., Hammond, G. R. V., & Oliver, D. (2011). Probing the regulation of TASK potassium channels by PI(4,5)P 2 with switchable phosphoinositide phosphatases. *Journal of Physiology*, *589*(13), 3149–3162.
153. Liu, D., Bienkowska, J., Petosa, C., Collier, R. J., Fu, H., & Liddington, R. (1995). Crystal structure of the zeta isoform of the 14-3-3 protein. In *Nature* (Vol. 376, Issue 6536, pp. 191–194).
154. Liu, J. (2005). Ouabain-induced endocytosis and signal transduction of the NA/K-ATPase. *Frontiers in Bioscience*, *10*(1), 2056–2063.
155. Liu, W., & Saint, D. A. (2004). Heterogeneous expression of tandem-pore K+ channel genes in adult and embryonic rat heart quantified by real-time polymerase chain reaction. *Clinical and Experimental Pharmacology and Physiology*, *31*(3), 174–178.
156. Lopes, C. M. B., Rohács, T., Czirják, G., Balla, T., Enyedi, P., & Logothetis, D. E. (2005). PIP2 hydrolysis underlies agonist-induced inhibition and regulates voltage gating of two-pore domain K+ channels. *Journal of Physiology*, *564*(1), 117–129.
157. Luo, W., Grupp, I. L., Harrer, J., Ponniah, S., Grupp, G., Duffy, J. J., Doetschman, T., & Kranias, E. G. (1994). Targeted ablation of the phospholamban gene is associated with markedly enhanced myocardial contractility and loss of β-agonist stimulation. *Circulation Research*, *75*(3), 401–409.
158. Luo, Wusheng, Chu, G., Sato, Y., Zhou, Z., Kadambi, V. J., & Kranias, E. G. (1998). Transgenic approaches to define the functional role of dual site phospholamban phosphorylation. *Journal of Biological Chemistry*, *273*(8), 4734–4739.
159. Ma, L., Roman-Campos, D., Austin, E. D., Eyries, M., Sampson, K. S., Soubrier, F., Germain, M., Trégouët, D.-A., Borczuk, A., Rosenzweig, E. B., Girerd, B., Montani, D., Humbert, M., Loyd, J. E., Kass, R. S., & Chung, W. K. (2013). A Novel Channelopathy in Pulmonary Arterial Hypertension. *N Engl J Med*, *369*(4), 351–361.
160. MacDougall, L. K., Jones, L. R., & Cohen, P. (1991). Identification of the major protein phosphatases in mammalian cardiac muscle which dephosphorylate phospholamban. *European Journal of Biochemistry*, *196*(3), 725–734.
161. MacKinnon, R. (2003). Potassium channels. *FEBS Letters*, *555*(1), 62–65.
162. MacLennan, D. H., Kimura, Y., & Toyofuku, T. (1998). Sites of regulatory interaction between calcium ATPases and phospholamban. *Annals of the New York Academy of Sciences*, *853*(26), 31–42.
163. MacLennan, D. H., & Kranias, E. G., (2003). Phospholamban: A crucial regulator of cardiac contractility. *Nature Reviews*, *4*(July), 566–577.
164. Makino, T., Skretas, G., & Georgiou, G. (2011). Strain engineering for improved expression of recombinant proteins in bacteria. *Microbial Cell Factories*,

10(1), 32.
165. Mant, A., Elliott, D., Eyers, P. A., & O'Kelly, I. M. (2011). Protein kinase A is central for forward transport of two-pore domain potassium channels K2P3.1 and K2P9.1. *Journal of Biological Chemistry*, *286*(16), 14110–14119.
166. Mant, A., Williams, S., & O'Kelly, I. (2013). Acid sensitive background potassium channels K2P3.1 and K 2P9.1 undergo rapid dynamin-dependent endocytosis. *Channels*, *7*(4), 288–292.
167. Marasciulo, F., Montagnani, M., & Potenza, M. (2006). Endothelin-1: The Yin and Yang on Vascular Function. *Current Medicinal Chemistry*, *13*(14), 1655–1665.
168. Mathie, A. (2007). Neuronal two-pore-domain potassium channels and their regulation by G protein-coupled receptors. *The Journal of Physiology*, *578*(2), 377–385.
169. Mathie, A., Al-Moubarak, E., & Veale, E. L. (2010). Gating of two-pore domain potassium channels. *Journal of Physiology*, *588*(17), 3149–3156.
170. Mathie, A., Rees, K. A., Hachmane, M. F. El, & Veale, E. L. (2010). Trafficking of Neuronal Two-pore Domain Potassium Channels. *Current Neuropharmacology*, 276–286.
171. Mattiazzi, A., & Kranias, E. G. (2014). The role of CaMKII regulation of phospholamban activity in heart disease. *Frontiers in Pharmacology*, *5*, 1–11.
172. Mattiazzi, A., Mundin, C., Vittone, L., & Kranias, E. (2005). Role of phospholamban phosphorylation on Thr 17 in cardiac physiological and pathological conditions. *Cardiovascular Research*, *68*, 366–375.
173. Mattiazzi, A., Mundiña-Weilenmann, C., Guoxiang, C., Vittone, L., & Kranias, E. (2005). Role of phospholamban phosphorylation on Thr17 in cardiac physiological and pathological conditions. *Cardiovascular Research*, *68*(3), 366–375.
174. McGee, A. W., Dakoji, S. R., Olsen, O., Bredt, D. S., Lim, W. A., & Prehoda, K. E. (2001). Structure of the SH3-guanylate kinase module from PSD-95 suggests a mechanism for regulated assembly of MAGUK scaffolding proteins. *Molecular Cell*, *8*(6), 1291–1301.
175. McLaughlin, S., Wang, J., Gambhir, A., & Murray, D. (2002). PIP2 and proteins: Interactions, organization, and information flow. *Annual Review of Biophysics and Biomolecular Structure*, *31*, 151–175.
176. McTiernan, C. F., Frye, C. S., Lemster, B. H., Kinder, E. A., Ogletree-Hughes, M. L., Moravec, C. S., & Feldman, A. M. (1999). The human phospholamban gene: Structure and expression. *Journal of Molecular and Cellular Cardiology*, *31*(3), 679–692.
177. Medhurst, A. D., Rennie, G., Chapman, C. G., Meadows, H., Duckworth, M. D., Kelsell, R. E., Gloger, I. I., & Pangalos, M. N. (2001). Distribution analysis of human two-pore domain potassium channels in tissues of the central nervous system and periphery. *Molecular Brain Research*, *86*(1–2), 101–114.
178. Meller, N., Liu, Y. C., Collins, T. L., Bonnefoy-Bérard, N., Baier, G., Isakov, N., & Altman, A. (1996). Direct interaction between protein kinase C theta (PKC theta) and 14-3-3 tau in T cells: 14-3-3 overexpression results in inhibition of PKC theta translocation and function. *Molecular and Cellular Biology*, *16*(10), 5782–5791.
179. Metcalfe, E. E., Traaseth, N. J., & Veglia, G. (2005). Serine 16 phosphorylation induces an order-to-disorder transition in monomeric phospholamban. *Biochemistry*, *44*(11), 4386–4396.
180. Metcalfe, E. E., Zamoon, J., Thomas, D. D., & Veglia, G. (2004). 1H/15N heteronuclear NMR spectroscopy shows four dynamic domains for phospholamban reconstituted in dodecylphosphocholine micelles. *Biophysical Journal*, *87*(2), 1205–1214.
181. Mhawech, P. (2005). 14-3-3 proteins — an update. *Cell Research*, *15*(4),

228–236.
182. Mi Hwang, E., Kim, E., Yarishkin, O., Ho Woo, D., Han, K. S., Park, N., Bae, Y., Woo, J., Kim, D., Park, M., Lee, C. J., & Park, J. Y. (2014). A disulphide-linked heterodimer of TWIK-1 and TREK-1 mediates passive conductance in astrocytes. *Nature Communications*, *5*.
183. Michelsen, K., Yuan, H., & Schwappach, B. (2005). Disputation. *EMBO Reports*, *6*(8), 717–722.
184. Mueller, B., Karim, C. B., Negrashov, I. V., Kutchai, H., & Thomas, D. D. (2004). Direct detection of phospholamban and sarcoplasmic reticulum Ca-ATPase interaction in membranes using fluorescence resonance energy transfer. *Biochemistry*, *43*(27), 8754–8765.
185. Mundiña-Weilenmann, C., Vittone, L., Ortale, M., De Cingolani, G. C., & Mattiazzi, A. (1996). Immunodetection of phosphorylation sites gives new insights into the mechanisms underlying phospholamban phosphorylation in the intact heart. *Journal of Biological Chemistry*, *271*(52), 33561–33567.
186. Muslin, A. J., Tanner, J. W., Allen, P. M., & Shaw, A. S. (1996). Interaction of 14-3-3 with signaling proteins is mediated by the recognition of phosphoserine. *Cell*, *84*(6), 889–897.
187. Mustroph, J., Maier, L. S., & Wagner, S. (2014). CaMKII regulation of cardiac K channels. *Frontiers in Pharmacology*, *5*, 1–12.
188. Najafi, A., Sequeira, V., Kuster, D. W., & van der Velden, J. (2016). B-Adrenergic Receptor Signalling and Its Functional Consequences in the Diseased Heart. *European Journal of Clinical Investigation*, *46*(4), 362–374.
189. Neal, C. L., Yao, J., Yang, W., Zhou, X., Nguyen, N. T., Lu, J., Danes, C. G., Guo, H., Lan, K. H., Ensor, J., Hittelman, W., Hung, M. C., & Yu, D. (2009). 14-3-3Z Overexpression Defines High Risk for Breast Cancer Recurrence and Promotes Cancer Cell Survival. *Cancer Research*, *69*(8), 3425–3432.
190. Niemeyer, M. I., Cid, L. P., González, W., & Sepúlveda, F. V. (2016). Gating, Regulation, and structure in K2P K+ Channels: In varietate concordia? *Molecular Pharmacology*, *90*(3), 309–317.
191. Nufer, O., & Hauri, H. P. (2003). ER export: Call 14-3-3. *Current Biology*, *13*(10), 391–393.
192. Obsil, T., Ghirlando, R., Anderson, D. E., Hickman, A. B., & Dyda, F. (2003). Two 14-3-3 Binding Motifs Are Required for Stable Association of Forkhead Transcription Factor FOXO4 with 14-3-3 Proteins and Inhibition of DNA Binding. *Biochemistry*, *42*(51), 15264–15272.
193. Obsil, T., & Obsilova, V. (2011). Structural basis of 14-3-3 protein functions. *Seminars in Cell and Developmental Biology*, *22*(7), 663–672.
194. Osterweil, E., Wells, D. G., & Mooseker, M. S. (2005). A role for myosin VI in postsynaptic structure and glutamate receptor endocytosis. *Journal of Cell Biology*, *168*(2), 329–338.
195. Oxenoid, K., & Chou, J. J. (2005). The structure of phospholamban pentamer reveals a channel-like architecture in membranes. *Proceedings of the National Academy of Sciences of the United States of America*, *102*(31), 10870–10875.
196. Periasamy, M., & Kalyanasundaram, A. (2007). SERCA pump isoforms: Their role in calcium transport and disease. *Muscle and Nerve*, *35*(4), 430–442.
197. Petosa, C., Masters, S. C., Bankston, L. A., Pohl, J., Wang, B., Fu, H., & Liddington, R. C. (1998). 14-3-3Z Binds a Phosphorylated Raf Peptide and an Unphosphorylated Peptide Via Its Conserved Amphiphatic Groove. *Journal of Biological Chemistry*, *273*(26), 16305–16310.
198. Peuch, C. J. L., Haiech, J., & Demaille, J. G. (1979). Concerted Regulation of Cardiac Sarcoplasmic Reticulum Calcium Transport by Cyclic Adenosine Monophosphate Dependent and Calcium-Calmodulin-Dependent Phosphorylations. *Biochemistry*, *18*(23), 5150–5157.

199. Pfeiffer, E. R., Tangney, J. R., Omens, J. H., & McCulloch, A. D. (2014). Biomechanics of cardiac electromechanical coupling and mechanoelectric feedback. *Journal of Biomechanical Engineering*, *136*(2), 1–11.
200. Philippe, M., Leǵer, T., Desvaux, R., & Walch, L. (2013). Discs large 1 (Dlg1) scaffolding protein participates with clathrin and adaptator protein complex 1 (AP-1) in forming weibel-palade bodies of endothelial cells. *Journal of Biological Chemistry*, *288*(18), 13046–13056.
201. Plant, L. D., Zuniga, L., Araki, D., Marks, J. D., & Goldstein, S. A. N. (2012). SUMOylation silences heterodimeric TASK potassium channels containing K2P1 subunits in cerebellar granule neurons. *Science Signaling*, *5*(251).
202. Potter, J. D., & Gergely, J. (1974). Troponin, tripomyosin, and actin interactions in the Ca2+ ion regulation of muscle contraction. *Biochemistry*, *13*(13), 2697–2703.
203. Putzke, C., Wemhöner, K., Sachse, F. B., Rinné, S., Schlichthörl, G., Li, X. T., Jaé, L., Eckhardt, I., Wischmeyer, E., Wulf, H., Preisig-Müller, R., Daut, J., & Decher, N. (2007). The acid-sensitive potassium channel TASK-1 in rat cardiac muscle. *Cardiovascular Research*, *75*(1), 59–68.
204. Rajan, S., Preisig-Müller, R., Wischmeyer, E., Nehring, R., Hanley, P. J., Renigunta, V., Musset, B., Schlichthörl, G., Derst, C., Karschin, A., & Daut, J. (2002). *Interaction with 14-3-3 proteins promotes functional expression of the potassium channels TASK-1 and TASK-3*. 13–26.
205. Ratte, A., Wiedmann, F., Kraft, M., Katus, H. A., & Schmidt, C. (2019). Antiarrhythmic properties of ranolazine: Inhibition of atrial fibrillation associated TASK-1 potassium channels. *Frontiers in Pharmacology*, *10*, 1.
206. Ravens, U., Wang, X. L., & Wettwer, E. (1989). Alpha adrenoceptor stimulation reduces outward currents in rat ventricular myocytes. *Journal of Pharmacology and Experimental Therapeutics*, *250*(1), 364–370.
207. Reddy, L. G., Jones, L. R., & Thomas, D. D. (1999). Depolymerization of phospholamban in the presence of calcium pump: A fluorescence energy transfer study. *Biochemistry*, *38*(13), 3954–3962.
208. Reimann, F., & Ashcroft, F. (1999). Inwardly rectifying potassium channels Frank Reimann and Frances M Ashcroft. *Current Opinion in Cell Biology*, *11*, 503–508.
209. Renigunta, V., Fischer, T., Zuzarte, M., Kling, S., Zou, X., Siebert, K., Limberg, M. M., Rinné, S., Decher, N., Schlichthörl, G., & Daut, J. (2014). Cooperative endocytosis of the endosomal SNARE protein syntaxin-8 and the potassium channel TASK-1. *Molecular Biology of the Cell*, *25*(12), 1877–1891.
210. Renigunta, V., Schlichthörl, G., & Daut, J. (2015). Much more than a leak: structure and function of K2P-channels. *Pflugers Archiv European Journal of Physiology*, 867–894.
211. Renigunta, V., Yuan, H., Zuzarte, M., Rinné, S., Koch, A., Wischmeyer, E., Schlichthörl, G., Gao, Y., Karschin, A., Jacob, R., Schwappach, B., Daut, J., & Preisig-Müller, R. (2006). The retention factor p11 confers an endoplasmic reticulum-localization signal to the potassium channel TASK-1. *Traffic*, *7*(2), 168–181.
212. Rinné, S., Kiper, A. K., Schlichthörl, G., Dittmann, S., Netter, M. F., Limberg, S. H., Silbernagel, N., Zuzarte, M., Moosdorf, R., Wulf, H., Schulze-Bahr, E., Rolfes, C., & Decher, N. (2015a). TASK-1 and TASK-3 may form heterodimers in human atrial cardiomyocytes. *Journal of Molecular and Cellular Cardiology*, *81*, 71–80.
213. Rittinger, K., Budman, J., Xu, J., Volinia, S., Cantley, L. C., Smerdon, S. J., Gamblin, S. J., & Yaffe, M. B. (1999). Structural analysis of 14-3-3 phosphopeptide complexes identifies a dual role for the nuclear export signal of 14-3-3 in ligand binding. *Molecular Cell*, *4*(2), 153–166.
214. Robia, S. L., Campbell, K. S., Kelly, E. M., Hou, Z., Winters, D. L., &

Thomas, D. D. (2007). Förster transfer recovery reveals that phospholamban exchanges slowly from pentamers but rapidly from the SERCA regulatory complex. *Circulation Research*, *101*(11), 1123–1129.

215. Rosenquist, M., Sehnke, P., Ferl, R. J., Sommarin, M., & Larsson, C. (2000). Evolution of the 14-3-3 protein family: Does the large number of isoforms in multicellular organisms reflect functional specificity? *Journal of Molecular Evolution*, *51*(5), 446–458.
216. Rougier, J. S., & Abriel, H. (2016). Cardiac voltage-gated calcium channel macromolecular complexes. *Biochimica et Biophysica Acta - Molecular Cell Research*, *1863*(7), 1806–1812.
217. Russell, D., Oldham, N. J., & Davis, B. G. (2009). Site-selective chemical protein glycosylation protects from autolysis and proteolytic degradation. *Carbohydrate Research*, *344*(12), 1508–1514.
218. Said, M., Mundiña-Weilenmann, C., Vittone, L., & Mattiazzi, A. (2002). The relative relevance of phosphorylation of the Thr17 residue of phospholamban is different at different levels of β-adrenergic stimulation. *Pflugers Archiv European Journal of Physiology*, *444*(6), 801–809.
219. Sandmann, T., Herrmann, J. M., Dengjel, J., Schwarz, H., & Spang, A. (2003). Suppression of coatomer mutants by a new protein family with COPI and COPII binding motifs in Saccharomyces cerevisiae. *Molecular Biology of the Cell*, *14*, 2372–2384.
220. Sansom, M. S. P., Shrivastava, I. H., Bright, J. N., Tate, J., Capener, C. E., & Biggin, P. C. (2002). Potassium channels: structures, models, simulations. *Biochimica et Biophysica Acta*, *1565*, 294–307.
221. Schewe, M., Nematian-Ardestani, E., Sun, H., Musinszki, M., Cordeiro, S., Bucci, G., De Groot, B. L., Tucker, S. J., Rapedius, M., & Baukrowitz, T. (2016). A Non-canonical Voltage-Sensing Mechanism Controls Gating in K2P K+ Channels. *Cell*, *164*(5), 937–949.
222. Schiekel, J., Lindner, M., Hetzel, A., Wemhöner, K., Renigunta, V., Schlichthörl, G., Decher, N., Oliver, D., & Daut, J. (2013). The inhibition of the potassium channel TASK-1 in rat cardiac muscle by endothelin-1 is mediated by phospholipase C. *Cardiovascular Research*, *97*(1), 97–105.
223. Schmidt, C., Kisselbach, J., Schweizer, P. A., Katus, H. A., & Thomas, D. (2011). The pathology and treatment of cardiac arrhythmias: Focus on atrial fibrillation. *Vascular Health and Risk Management*, *7*(1), 193–202.
224. Schmidt, C., Wiedmann, F., Beyersdorf, C., Zhao, Z., El-Battrawy, I., Lan, H., Szabo, G., Li, X., Lang, S., Korkmaz-Icöz, S., Rapti, K., Jungmann, A., Ratte, A., Müller, O. J., Karck, M., Seemann, G., Akin, I., Borggrefe, M., Zhou, X. B., … Thomas, D. (2019). Genetic Ablation of TASK-1 (Tandem of P Domains in a Weak Inward Rectifying K+ Channel-Related Acid-Sensitive K+ Channel-1) (K2P3.1) K+ Channels Suppresses Atrial Fibrillation and Prevents Electrical Remodeling. *Circulation: Arrhythmia and Electrophysiology*, *12*(9), 1–10.
225. Schmidt, C., Wiedmann, F., Langer, C., Tristram, F., Anand, P., Wenzel, W., Lugenbiel, P., Schweizer, P. A., Katus, H. A., & Thomas, D. (2014). Cloning, functional characterization, and remodeling of K2P3.1 (TASK-1) potassium channels in a porcine model of atrial fibrillation and heart failure. *Heart Rhythm*, *11*(10), 1798–1805.
226. Schmidt, C., Wiedmann, F., Schweizer, P. A., Katus, H. A., & Thomas, D. (2014). Inhibition of cardiac two-pore-domain K+ (K2P) channels - An emerging antiarrhythmic concept. *European Journal of Pharmacology*, *738*, 250–255.
227. Schmidt, C., Wiedmann, F., Voigt, N., Zhou, X. B., Heijman, J., Lang, S., Albert, V., Kallenberger, S., Ruhparwar, A., Szabó, G., Kallenbach, K., Karck, M., Borggrefe, M., Biliczki, P., Ehrlich, J. R., Baczkó, I., Lugenbiel, P., Schweizer, P. A., Donner, B. C., … Thomas, D. (2015). Upregulation of K2P 3.1 K + Current Causes Action Potential Shortening in Patients with Chronic Atrial Fibrillation.

Circulation, *132*(2), 82–92.
228. Schmitt, J. P., Kamisago, M., & Asahi, M. (2003). Dilated Cardiomyopathy and Heart Failure Caused by a Mutation in Phospholamban. *Science*, *299*, 1410–1413.
229. Schwappach, B. (2008). An overview of trafficking and assembly of neurotransmitter receptors and ion channels (Review). *Molecular Membrane Biology*, *25*(4), 270–278.
230. Scott, C. C., Vacca, F., & Gruenberg, J. (2014). Endosome maturation, transport and functions. *Seminars in Cell and Developmental Biology*, *31*, 2–10.
231. Sharma, P., Ignatchenko, V., Grace, K., Ursprung, C., Kislinger, T., & Gramolini, A. O. (2010). Endoplasmic Reticulum Protein Targeting of Phospholamban : A Common Role for an N-Terminal Di-Arginine Motif in ER Retention ? *PLoS Biology*, *5*(7).
232. Shaw, R. M., & Colecraft, H. M. (2013). L-type calcium channel targeting and local signalling in cardiac myocytes. *Cardiovascular Research*, *98*(2), 177–186.
233. Shrivastava, I. H., Tieleman, D. P., Biggin, P. C., & Sansom, M. S. P. (2002). K+ versus Na+ ions in a K channel selectivity filter: A simulation study. *Biophysical Journal*, *83*(2), 633–645.
234. Sierra, A., Zhu, Z., Sapay, N., Sharotri, V., Kline, C. F., Luczak, E. D., Subbotina, E., Sivaprasadarao, A., Snyder, P. M., Mohler, P. J., Anderson, M. E., Vivaudou, M., Zingman, L. V., & Hodgson-Zingman, D. M. (2013). Regulation of cardiac ATP-sensitive potassium channel surface expression by calcium/calmodulin-dependent protein kinase II. *Journal of Biological Chemistry*, *288*(3), 1568–1581.
235. Silver, I. A., & Erecinska, M. (1990). Intracellular and Extracellular Changes of Ca2+ in Hypoxia and Ischemia in Rat Brain In Vivo. *Journal Of General Physiology*, *95*.
236. Simmerman, H. K. B., Kobayashi, Y. M., Autry, J. M., & Jones, L. R. (1996). A leucine zipper stabilizes the pentameric membrane domain of phospholamban and forms a coiled-coil pore structure. *Journal of Biological Chemistry*, *271*(10), 5941–5946.
237. Singh, D. R., Dalton, M. P., Cho, E. E., Pribadi, M. P., Zak, T. J., Šeflová, J., Makarewich, C. A., Olson, E. N., & Robia, S. L. (2019). Newly Discovered Micropeptide Regulators of SERCA Form Oligomers but Bind to the Pump as Monomers. *Journal of Molecular Biology*, *431*(22), 4429–4443.
238. Sluchanko, N. N. (2018). Association of Multiple Phosphorylated Proteins with the 14-3-3 Regulatory Hubs: Problems and Perspectives. *Journal of Molecular Biology*, *430*(1), 20–26.
239. Sluchanko, N. N., & Bustos, D. M. (2019). Intrinsic disorder associated with 14-3-3 proteins and their partners. *Molecular Biology and Translational Science*, 166, 19–61.
240. Sluchanko, N. N., & Gusev, N. B. (2016). Moonlighting chaperone-like activity of the universal regulatory 14-3-3 proteins. *The FEBS Journal*, *284*(9), 1279–1295.
241. Smeazzetto, S., Saponaro, A., Young, H. S., Moncelli, M. R., & Thiel, G. (2013). Structure-Function Relation of Phospholamban: Modulation of Channel Activity as a Potential Regulator of SERCA Activity. *PLoS ONE*, *8*(1), 2–8.
242. Smith, A. J., Daut, J., & Schwappach, B. (2011). Membrane proteins as 14-3-3 clients in functional regulation and intracellular transport. *Physiology*, *26*(3), 181–191.
243. Song, Y., Yang, Z., Ke, Z., Yao, Y., Hu, X., Sun, Y., Li, H., Yin, J., & Zeng, C. (2012). Expression of 14-3-3γ in patients with breast cancer: Correlation with clinicopathological features and prognosis. *Cancer Epidemiology*, *36*(6), 533–536.
244. Stauffer, T. P., Ahn, S., & Meyer, T. (1998). Receptor-induced transient

reduction in plasma membrane Ptdlns(4,5)P2 concentration monitored in living cells. *Current Biology*, *8*(6), 343–346.

245. Steele, D. F., Eldstrom, J., & Fedida, D. (2007). Mechanisms of cardiac potassium channel trafficking. *Journal of Physiology*, *582*(1), 17–26.
246. Stenoien, D. L., Knyushko, T. V, Londono, M. P., Opresko, L. K., Mayer, M. U., Brady, S. T., Squier, T. C., & Bigelow, D. J. (2007). Cellular trafficking of phospholamban and formation of functional sarcoplasmic reticulum during myocyte differentiation. *American Journal of Physiology, 99352*, 2084–2094.
247. Şterbuleac, D. (2019). Molecular determinants of chemical modulation of two-pore domain potassium channels. *Chemical Biology and Drug Design*, *94*(3), 1596–1614.
248. Stevers, L. M., Sijbesma, E., Botta, M., Mackintosh, C., Obsil, T., Landrieu, I., Cau, Y., Wilson, A. J., Karawajczyk, A., Eickhoff, J., Davis, J., Hann, M., O'Mahony, G., Doveston, R. G., Brunsveld, L., & Ottmann, C. (2018). Modulators of 14-3-3 Protein-Protein Interactions. *Journal of Medicinal Chemistry*, *61*(9), 3755–3778.
249. Streit, A. K., Netter, M. F., Kempf, F., Walecki, M., Rinne, S., Bollepalli, M. K., Preisig-Muller, R., Renigunta, V., Daut, J., Baukrowitz, T., Sansom, M. S. P., Stansfeld, P. J., & Decher, N. (2011). A specific two-pore domain potassium channel blocker defines the structure of the TASK-1 open pore. *Journal of Biological Chemistry*, *286*(16), 13977–13984.
250. Suzuki, Y., Tsutsumi, K., Miyamoto, T., Yamamura, H., & Imaizumi, Y. (2017). *Heterodimerization of two-pore domain K + channel TASK1 and TALK2 in living heterologous expression systems*. 1–17.
251. Sweadner, J., & Donnet, C. (2001). Structural similarities of Na,K-ATPase and SERCA, the Ca2+-ATPase of the sarcoplasmic reticulum. *Biochemical Journal*, *356*, 694–704.
252. Tada, M., Kirchberger, M. A., & Katz, A. M. (1975). Phosphorylation of a 22,000 dalton component of the cardiac sarcoplasmic reticulum by adenosine 3',5' monophosphate dependent protein kinase. *Journal of Biological Chemistry*, *250*(7), 2640–2647.
253. Talley, E. M., & Bayliss, D. A. (2002). Modulation of TASK-1 (Kcnk3) and TASK-3 (Kcnk9) potassium channels. Volatile anesthetics and neurotransmitters share a molecular site of action. *Journal of Biological Chemistry*, *277*(20), 17733–17742.
254. Talley, E. M., Lei, Q., Sirois, J. E., & Bayliss, D. A. (2000). TASK-1, a two-pore domain K+ channel, is modulated by multiple neurotransmitters in motoneurons. *Neuron*, *25*(2), 399–410.
255. te Rijdt, W. P., Asimaki, A., Jongbloed, J. D. H., Hoorntje, E. T., Lazzarini, E., van der Zwaag, P. A., de Boer, R. A., van Tintelen, J. P., Saffitz, J. E., van den Berg, M. P., & Suurmeijer, A. J. H. (2019). Distinct molecular signature of phospholamban p.Arg14del arrhythmogenic cardiomyopathy. *Cardiovascular Pathology*, *40*, 2–6.
256. te Rijdt, W. P., van Tintelen, J. P., Vink, A., van der Wal, A. C., de Boer, R. A., van den Berg, M. P., & Suurmeijer, A. J. H. (2016). Phospholamban p.Arg14del cardiomyopathy is characterized by phospholamban aggregates, aggresomes, and autophagic degradation. *Histopathology*, *69*(4), 542–550.
257. Thiel, P., Kaiser, M., & Ottmann, C. (2012). Small-molecule stabilization of protein-protein interactions: An underestimated concept in drug discovery? *Angewandte Chemie - International Edition*, *51*(9), 2012–2018.
258. Thomas, D., & Goldstein, S. A. N. (2009). Two-P-Domain (K 2P) Potassium Channels: Leak Conductance Regulators of Excitability. *Encyclopedia of Neuroscience*, *December 2009*, 1207–1220.
259. Thomas, K., Goudy, J., Henley, T., Bressan, M. (2018). Optical Electrophysiology in the Developing Heart. *J Cardiovasc Dev Dis*, 5(2), 28.

260. Toyofuku, T., Kurzydlowski, K., Tada, M., & MacLennan, D. H. (1994). Amino acids Glu2 to Ile18 in the cytoplasmic domain of phospholamban are essential for functional association with the Ca2+-ATPase of sarcoplasmic reticulum. *Journal of Biological Chemistry*, *269*(4), 3088–3094.
261. Traaseth, N. J., Thomas, D. D., & Veglia, G. (2006). Effects of Ser16 Phosphorylation on the Allosteric Transitions of Phospholamban/Ca2+-ATPase Complex. *Journal of Molecular Biology*, *358*(4), 1041–1050.
262. Traaseth, N.J., Ha, K. M., Verardi, R., Shi, L., Buffy, J. J., Masterson, L. R., & Veglia, G. (2008). Structural and Dynamic Basis of Phospholamban and Sarcolipin Inhibition of Ca2+ -ATPase. *Biochemistry*, *47*(1), 1–7.
263. Traaseth, N. J., & Veglia, G. (2010). Probing excited states and activation energy for the integral membrane protein phospholamban by NMR CPMG relaxation dispersion experiments. *Biochimica et Biophysica Acta - Biomembranes*, *1798*(2), 77–81.
264. Traaseth, N. J., Verardi, R., Torgersen, K. D., Karim, C. B., Thomas, D. D., & Veglia, G. (2007). Spectroscopic validation of the pentameric structure of phospholamban. *Proceedings of the National Academy of Sciences of the United States of America*, *104*(37), 14676–14681.
265. Vafiadaki, E., Arvanitis, D. A., Sanoudou, D., & Kranias, E. G. (2013). Identification of a Protein Phosphatase-1/Phospholamban Complex That Is Regulated by cAMP- Dependent Phosphorylation. *PLoS ONE, 8*(11).
266. Vaidyanathan, R., Taffet, S. M., Vikstrom, K. L., & Anumonwo, J. M. B. (2010). Regulation of cardiac inward rectifier potassium current (IK1) by synapse-associated protein-97. *Journal of Biological Chemistry*, *285*(36), 28000–28009.
267. van der Zwaag, P. A., van Rijsingen, I. A. W., de Ruiter, R., Nannenberg, E. A., Groeneweg, J. A., Post, J. G., Hauer, R. N. W., van Gelder, I. C., van den Berg, M. P., van der Harst, P., Wilde, A. A. M., & van Tintelen, J. P. (2013). Recurrent and founder mutations in the Netherlands-Phospholamban p.Arg14del mutation causes arrhythmogenic cardiomyopathy. *Netherlands Heart Journal*, *21*(6), 286–293.
268. van der Zwaag, P. A., van Rijsingen, I. A. W., Asimaki, A., Jongbloed, J. D. H., van Veldhuisen, D. J., Wiesfeld, A. C. P., Cox, M. G. P. J., van Lochem, L. T., de Boer, R. A., Hofstra, R. M. W., Christiaans, I., van Spaendonck-Zwarts, K. Y., Deprez, R. H. L. D., Judge, D. P., Calkins, H., Suurmeijer, A. J. H., Hauer, R. N. W., Saffitz, J. E., Wilde, A. A. M., … van Tintelen, J. P. (2012). Phospholamban R14del mutation in patients diagnosed with dilated cardiomyopathy or arrhythmogenic right ventricular cardiomyopathy: Evidence supporting the concept of arrhythmogenic cardiomyopathy. *European Journal of Heart Failure*, *14*(11).
269. van Heusden, G. P. H. (2005). 14-3-3 Proteins: Regulators of numerous eukaryotic proteins. *IUBMB Life*, *57*(9), 623–629.
270. van Opbergen, C. J. M., Delmar, M., & van Veen, T. A. B. (2017). Potential new mechanisms of pro-arrhythmia in arrhythmogenic cardiomyopathy : focus on calcium sensitive pathways. *Netherlands Heart Journal*, *25*, 157–169.
271. Vandecaetsbeek, I., Vangheluwe, P., Raeymaekers, L., Wuytack, F., & Vanoevelen, J. (2011). The Ca2+ Pumps of the Endoplasmic Reticulum and Golgi Apparatus. *Cold Spring Harbor Perspectives in Biology*, *3*(5), 1–24.
272. Vincent, J. L. (2008). Understanding cardiac output. *Critical Care*, *12*(4), 12.
273. Vincenz, C., & Dixit, V. M. (1996). 14-3-3 proteins associate with A20 in an isoform-specific manner and function both as chaperone and adapter molecules. *Journal of Biological Chemistry*, *271*(33), 20029–20034.
274. Vittone, L., Mundina-Weilenmann, C., & Mattiazzi, A. (2008). Phospholamban phosphorylation by CaMKII under pathophysiological conditions. *Frontiers in Bioscience*, *13*(15), 5988–6005.
275. Walch, L. (2013). Emerging role of the scaffolding protein Dlg1 in vesicle trafficking. *Traffic*, *14*(9), 964–973.

276. Walker, C. A., & Spinale, F. G. (1999). The structure and function of the cardiac myocyte: A review of fundamental concepts. *Journal of Thoracic and Cardiovascular Surgery*, *118*(2), 375–382.
277. Wang, B., Yang, H., Liu, Y. C., Jelinek, T., Zhang, L., Ruoslahti, E., & Fu, H. (1999). Isolation of high-affinity peptide antagonists of 14-3-3 proteins by phage display. *Biochemistry*, *38*(38), 12499–12504.
278. Wang, W., & Shakes, D. C. (1996). Molecular Evolution of the 14-3-3 Protein Family. *Journal of Molecular Evolution*, *43*(4), 384–398.
279. Watanabe, M., Isobe, T., Ichimura, T., Kuwano, R., Takahashi, Y., & Kondo, H. (1993). Molecular cloning of rat cDNAs for β and γ subtypes of 14-3-3 protein and developmental changes in expression of their mRNAs in the nervous system. *Molecular Brain Research*, *17*(1–2), 135–146.
280. Wegener, A. D., Simmerman, H. K. B., Liepnieks, J., & Jones, L. R. (1986). Proteolytic cleavage of phospholamban purified from canine cardiac sarcoplasmic reticulum vesicles. Generation of a low resolution model of phospholamban structure. *Journal of Biological Chemistry*, *261*(11), 5154–5159.
281. Wiedmann, F., Schmidt, C., Lugenbiel, P., Staudacher, I., Rahm, A. K., Seyler, C., Schweizer, P. A., Katus, H. A., & Thomas, D. (2016). Therapeutic targeting of two-pore-domain potassium (K2P) channels in the cardiovascular system. *Clinical Science*, *130*(9), 643–650.
282. Wittmann, T., Lohse, M. J., & Schmitt, J. P. (2015). Phospholamban pentamers attenuate PKA-dependent phosphorylation of monomers. *Journal of Molecular and Cellular Cardiology*, *80*, 90–97.
283. Xiao, B., Smerdon, S. J., Jones, D. H., Dodson, G. G., Soneji, Y., Aitken, A., & Gamblin, S. J. (1995). Structure of a 14-3-3 protein and implications for coordination of multiple signalling pathways. *Nature* 376,188–191.
284. Yaffe, M. B., Rittinger, K., Volinia, S., Caron, P. R., Aitken, A., Leffers, H., Gamblin, S. J., Smerdon, S. J., & Cantley, L. C. (1997). The Structural Basis for 14-3-3: Phosphopeptide Binding Specificity. *Cell*, *91*(7), 961–971.
285. Young, H. S., Ceholski, D. K., & Trieber, C. A. (2015). Deception in simplicity : Hereditary phospholamban mutations in dilated cardiomyopathy. *Biochem. Cell Biol.*, *93*, 1–7.
286. Yu, X., & Lorigan, G. A. (2014). Secondary structure, backbone dynamics, and structural topology of phospholamban and its phosphorylated and Arg9Cys-mutated forms in phospholipid bilayers utilizing 13C and 15N solid-state NMR spectroscopy. *Journal of Physical Chemistry B*, *118*(8), 2124–2133.
287. Zamoon, J., Mascioni, A., Thomas, D. D., & Veglia, G. (2003). NMR solution structure and topological orientation of monomeric phospholamban in dodecylphosphocholine micelles. *Biophysical Journal*, *85*(4), 2589–2598.
288. Zhang, H., Craciun, L. C., Mirshahi, T., Rohács, T., Lopes, C. M. B., Jin, T., & Logothetis, D. E. (2003). PIP2 activates KCNQ channels, and its hydrolysis underlies receptor-mediated inhibition of M currents. *Neuron*, *37*(6), 963–975.
289. Zhang, T., Guo, T., Mishra, S., Dalton, N. D., Kranias, E. G., Peterson, K. L., Bers, D. M., & Brown, J. H. (2010). Phospholamban ablation rescues sarcoplasmic reticulum Ca2+ handling but exacerbates cardiac dysfunction in CaMKIIδC transgenic mice. *Circulation Research*, *106*(2), 354–362.
290. Zhao, W., Uehara, Y., Chu, G., Song, Q., Qian, J., Young, K., & Kranias, E. G. (2004). Threonine-17 phosphorylation of phospholamban: A key determinant of frequency-dependent increase of cardiac contractility. *Journal of Molecular and Cellular Cardiology*, *37*(2), 607–612.
291. Zuzarte, M., Heusser, K., Renigunta, V., Wischmeyer, E., Schwappach, B., & Preisig-m, R. (2009). Intracellular traffic of the K + channels TASK-1 and TASK-3 : role of N- and C-terminal sorting signals and interaction with 14-3-3 proteins. *The Journal of Physiology*, *5*, 929–952.

7 Acknowledgements

Foremost, I would like to take this opportunity to sincere my gratitude to Prof. Dr. Blanche Schwappach-Pignataro for her excellent supervision and support. Her enthusiasm about science and engagement motivated me and where very helpful during my entire time as a PhD student. Beside her tight schedules, she always took time for scientific discussions and support.

I further would like to thank my thesis committee members, Prof. Dr. Dörthe Katschinski und Prof. Dr. Stephan Lehnart. I am very grateful for the fruitful discussions and the guidance during my PhD studies. Further I would like to thank Prof. Dr. Stephan Lehnart for inviting me in the CurePlan network, which gave me the opportunity to discuss my research in the PLN field and also to meet patients suffering the R14del PLN mutation. Furthermore, I would like to thank Prof. Dr. Michael Shattock, for being my supervisor on the London side, for inspiring discussions and for hosting me two times in his lab. The close communication during my entire PhD helped me to expand my scientific experiences. I would also like to thank the extended committee members Prof. Dr. Michael Meinecke, Prof. Dr. Jürgen Wienands.

I further would like to thank the IRTG1819 for providing a nice and helpful network. Furthermore, I would like to thank Dr. Christina Würtz and Fulya Ören for support and help with organizational questions.

I extend my sincere thanks to Prof. Dr. Herman Silljé and Tim Eijgenraam for providing the *Pln*$^{\Delta R14/\Delta R14}$ and *Pln*$^{+/\Delta R14}$ mouse models as well as to Prof. Dr. Niels Voigt for providing the right atrial appendages from normal sinus rhythm patients.

I thank Dr. Markus Kilisch, for helping me in the starting phase of my PhD and also later with SPR experiments and the data analysis even after leaving the lab. Further, I would like to thank Dr. Eric Arakel, Dr. Jhon Rivera Monroy and Dr. Javier Coy Vergara for a lot of scientific discussions, honest opinions and support during my PhD studies.

To the members of the Schwappach lab, former and recent, I am thankful for the nice working environment, their support and discussion during our group meetings. I would especially thank Dr. Evelina De Laurentiis, Dr. Venkat Ramnarayan, Dr. Javier Coy Vergara and Dr. Markus Kilisch for their honest and helpful opinions on this thesis and polishing my writing style.

I am thankful for the nice colleges in the Department of Molecular Biology who make this institute a nice place to work.

Thanks to Jhon, Javi, Eric, Markus and Jimena for the warm welcome in the institute for coffee and lunch breaks, I never wanted to take. Thanks for the support, your patience and all the fun inside or outside the lab.

I really like to thank Katha, Becci and Lena for being my friends and kind of family since the first day I arrived in Göttingen. Thanks for always listening to me, always supporting me and all the fun at the stable.
A special thanks to Patrick, Katharina, Constantin, Florian and Marcel for being my family-friends. Without you my life would be boring, once we are spread in the world, I will miss you a lot.
I heartfully like to thank my boyfriend Marcel for his patience and understanding. For tolerating long working days and supporting me wherever possible.
Finally, I am forever thankful to my family for open doors and open ears, for their support, patience and believe in me. Without you I would not have made it.